



ScuDo
Scuola di Dottorato ~ Doctoral School
WHAT YOU ARE, TAKES YOU FAR



Doctoral Dissertation
Doctoral Program in Materials Science and Technology (31st Cycle)

Design, Process and Characterization of Innovative Smart Coatings for Harsh Environments

By

Cristian Marro Bellot

Supervisors

Prof. Marco Sangermano, Supervisor
Prof. Milena Salvo, Co-Supervisor
Dr Massimo Olivero, Co-Supervisor

Doctoral Examination Committee:

Prof. Alberto Frache, Politecnico di Torino, Italy
Prof. Angels Serra, University of Rovira i Virgili, Spain
Prof. Daniel Milanese, University of Parma, Italy
Prof. Federico Smeacetto, Politecnico di Torino, Italy
Prof. Galder Kortaberria, University of the Basque Country, Spain

Politecnico di Torino
July 15th, 2019

Declaration

I hereby declare that, the contents and organisation of this dissertation constitute my own original work and does not compromise in any way the rights of third parties, including those relating to the security of personal data.

Cristian Marro Bellot

Turin, July 15th, 2019

* This dissertation is presented in partial fulfilment of the requirements for Ph.D. degree in the Graduate School of Politecnico di Torino (ScuDo).

Summary

The presented PhD dissertation refers, as summarized in the title, to the study and design of innovative “smart” coatings for devised applications in harsh environments, such as oil & gas industries, aerospace and marine. The “smart” feature relies on the fact that the coatings are equipped with sensors and sensing materials to foresee their degradation at an early stage. The coating materials investigated in this work have been Glass Fibre Reinforced Polymers (GFRPs), whereas optical fibre sensors (OFSs) have been the main type of sensor analysed, experimentally developed and tested.

The experimental activity carried out during has followed five research lines: (i) epoxy preparation and characterization (for subsequent fabrication of GFRPs), (ii) fabrication of optical fibre sensors (OFSs), (iii) degradation tests of epoxy and GFRPs samples containing embedded OFSs, (iv) study of chalcogenide optical fibre sensors, and (v) study of Carbon Nanotubes (CNTs) electrical-based sensors.

The thesis begins with a chapter (chapter 2) about the state-of-art on GFRP composites in oil & gas industries and the use of OFSs to detect the moisture diffusion in GFRPs. The state-of-art remarks the main features that sensors for GRFP must have. In particular, they must be non-destructive, and they must be able to operate remotely and in real-time. These requirements support the idea of developing new low-cost OFSs for monitoring the ageing of composites. The main features of OFSs, such as their immunity to radiofrequency interferences and intrinsic fire safety, are put into the context of oil & gas, where conventional electric-based sensors may give remarkable limitations in terms of remote operation, embedding and reliable operation in harsh environments.

Chapter 3 reports the details (materials, setups and methods) on the experimental activity on the different research lines. Subsequently, chapter 4 reports and summarize the outcome of several experiments that were performed for each research line.

In a material engineering science framework, epoxy samples were fabricated and characterized to develop and optimum curing procedure and asses mechanical/thermal/chemical properties. Meanwhile, novel OFSs were designed, fabricated and embedded in epoxy and GFRP samples. The OFSs were produced from commercial multimode fibres by etching the cladding -to make the fibre

sensitive through the evanescent field and depositing a reflective silver surface on the fibre tip –to make the sensors working in reflection, so that they could be used as probes and reduce failures during the embedding process.

One issue of the OFSs based on silica is their employment at infrared wavelengths, which are a range of the electromagnetic spectrum very interesting for chemical sensing. Therefore, chalcogenide fibre sensors were investigated to overcome the limitations of silica glass fibres. Chalcogenide optical fibres were manufactured and used as sensors to monitor epoxy-curing reactions as well as diffusion of water and ethanol. This research has highlighted interesting features on the process of total polymer conversion.

Another activity focused on carbon nanotubes (CNTs), which were used as an alternative to OFSs to monitor the diffusion of water in epoxy and epoxy composites. As a proof-of-concept, the combined sensors were used to detect in situ and in real-time the diffusion of water in composites. Proof-of-concept experiments demonstrated that both types of sensors (CNTs and OFSs) were successfully able to detect the water diffusion through the epoxy matrix.

The last technical section, chapter 5, reports an outlook of the possible technology transfer of this research toward a commercial product or service. Market analysis, economical estimations and a tentative business plan for the industrialization and commercialization of OFSs and “smart” GFRPs are discussed.

In summary, this PhD thesis provides experimental hints on three different sensors that can be embedded in a GFRP composite to monitor its degradation caused by the diffusion of chemicals. This study opens up to the realization of “smart” composites structures, such as pipelines and storage tanks used in the oil and gas sector, for effective and efficient maintenance routines.

Acknowledgements

I would like to express my deepest gratitude to my supervisor Prof. Marco Sangermano and my co-supervisors Dr Massimo Olivero and Prof. Milena Salvo, whose advice, support, and guidance have been fundamental and inspiring for my academic research. They taught and guided me in the laboratories from the very beginning with great patience and provided me with all the resources necessary to develop the optical fibre sensors.

I wish to thank Dr Nadia Boetti, who lent me her optical microscope to measure the fibres; Dr Sergio Perero, Prof. Daniel Milanese and Prof. Davide Janner, who guided me in the optical fibres etching and sputtering tricks; Prof. Monica Ferraris, who worked with me on developing a new polymeric coating for harsh environments and on the elaboration of poster presentations to be presented during the European Researchers' Night. I would also like to thank the students of the Ferraris Disat Laboratory for their support, time sharing and teaching me how to speak Italian.

I am grateful to Dr Stefanos Gianis and Dr Barry Thomson for their advice and help at Element Technology, Hitchin. My special thanks to Dr Keyur Somani, who stayed with me for long hours in the Element Technology laboratories working on the samples under pressure. Thanks too to Dr M. Cavasin, Dr S. Ivan and Element Materials Technology Ltd. for their support with the sample preparation and the mechanical tests.

I would like to acknowledge Prof. Emiliano Bilotti, who supervised me during my secondment in Nanoforce Ltd., London, UK, where the electrical-based sensors were developed and tested. Thanks to the Nanoforce Ltd. laboratory team, who have taught me how to use the laboratory instrumentation. My special thanks to Mrs. Giulia De Leo, who worked with me performing the tests. Thanks to Mr. Arnaud Kerin, Dr Han Zhang, Dr Minmin Yu and Dr Francesco Gucci for letting me share their office and their software guidance.

I wish to acknowledge Dr Catherine Boussard, who helped me with the manufacture and testing of the chalcogenide fibre sensors. Thanks to her laboratory team, who were very kind and helpful during my secondment tenure in Rennes.

I would like to acknowledge Dr Alessandra D’Anna and Dr Nicolas Klikovits for their work carried out during their master projects. Thanks to Dr Damian Rodriguez Sartori for his time in the Politecnico di Torino polymer laboratories.

My thanks to my chemistry and hometown friends and their support is this PhD adventure, in particular Dr Alba Maceira Torrents, Mrs Gemma Rius Painous, Mrs. Patricia Celades Altés, Mr. Alexandre Asensio Turné, Dr Pablo Solis Muñana, and the Sant Hilaris, specially to Mr. Joaquim Mauri Ferré. My thanks to the “Centro Linguistico di Ateneo” (CLA), the language centre of Politecnico di Torino, who helped me with the English revisions. In particular, thanks to Mrs. Marta Serrano, Mrs. Margaret Pate, Mrs. Mary McIntosh and Mr. Ian Lister.

I have been fortunate enough to be recruited in the CoACH-ETN program. I am grateful to all the team management and consortium members, and extend my sincerest thanks to the chief coordinator, Prof. Milena Salvo. Sincere thanks also to all the CoACH fellows. We, the Coachitos, have been a close-knit team who successfully came through the training courses, workshops, conferences, and leisure trips. Thanks to Dr Pablo Lopez Iscoa, Dr Hassan Javed, Dr Francesca Elisa Ciraldo, Dr Nicoletta Tonolia, Dr Bhuvanesh Srinivasan, Dr Acacio Rincon, Dr Alessia Masino, Dr Gianmarco Taveri, Dr Silviu Ivan, Dr Rocio Tejido, Dr Francesco Gucci, Dr Minmin Yu, and Dr Katarzyna Placha.

I would like to acknowledge the Fullcomp-ETN and HeyMedPoly-ETN projects, who have shared their courses and workshops with CoACH-ETN. Thanks to their coordinators and their fellows, in particular Dr Ibrahim Kaleel, Dr Guohong Li, Dr Alberto Garcia de Miguel, Mrs. Florencia Obilinovic, Dr Manish Nagaraj, and Dr Subha Purkayastha.

I wish to acknowledge all those people who helped make my three years in Turin a fantastic and unforgettable time. Thanks to Dr Federico Conrado, Mr. Joan Baseda, and Mr. James Larson for the climbing time. My special thanks to Mr. Marco Mandara, and Mr. Jan Konecny for the house sharing. These years are going to remain in my heart forever.



Finally, my biggest recognition is dedicated to my family for their constant support and encouragement.

*To my lovely parents
and my little sister*

List of Tables

Chapter 2: State-of-Art

Table 2. 1. General classification of polymer matrixes.	- 32 -
Table 2. 2. Selected properties of reinforced fibres [18], [23], [24], and [25].	- 34 -
Table 2. 3. Comparison of selected glass fibre properties of the silica, phosphate tellurite, fluoride ZBLAN, and chalcogenide glasses [43], [51], [52], [53], [54], [55], [56], and [57]. These values may vary with changing the glass chemical compositions.	- 52 -
Table 2. 4. Comparison of piezoelectric sensors.	- 78 -
Table 2. 5. Overview of fibre humidity-based sensors using different chemical doping for humidity detection.....	- 89 -
Table 2. 6. Overview of fibre humidity EW based sensors using different chemicals doping for humidity detection.....	- 93 -
Table 2. 7. Overview of fibre humidity grating based sensors using different chemical doping for humidity detection.	- 99 -
Table 2. 8. Overview of fibre humidity interferometric based sensors using different chemical doping for humidity detection.	- 101 -
Table 2. 9. Current commercially available smart composites.	- 102 -

Chapter 4: Results & Discussion

Table 4. 1. FT-IR conversion results at 60, 80, and 100 °C for 3 and 5 hours.	- 128 -
Table 4. 2. DMTA data results at 60, 80, and 100 °C for 3 and 5 hours.	- 129 -
Table 4. 3. Diffusion coefficients calculated from Figure 4. 9. ASW = artificial sea water.....	- 134 -
Table 4. 4. Diffusion coefficients calculated from Figure 4. 10.	- 136 -
Table 4. 5. Diffusion coefficients calculated from Figure 4. 10.	- 136 -
Table 4. 6. The RI of the epoxy after curing, the epoxy after being treated in artificial salty water and hydrochloric acid for two weeks.	- 137 -
Table 4. 7. Mechanical test results of the tensile test and three-point bending test of GFRPs with and without embedded OFSs.	- 146 -
Table 4. 8. Calculated and measured diffusion heights.	- 153 -
Table 4. 9. Calculated and measured diffusion heights.	- 154 -

Table 4. 10. Summarized drop signals of the embedded optical fibre sensors and the spread CNTs on the plies in the H-GFRP..... - 179 -

Chapter 5: Exploitation Plan

Table 5. 1. Criteria and Alternatives in strategic choices: in yellow the strategic choices that concern for the companies in terms of intellectual property / spin-off / start-up. - 186 -

Table 5. 2. Cost item table. - 191 -

Table 5. 3. R&D activities budget. - 192 -

Table 5. 4. Technical solution implementation budget..... - 193 -

Table 5. 5. Exploitation Plan budget..... - 194 -

Table 5. 6. Implementation plan for two years. - 194 -

Table 5. 7. Business Plan Model of the economic and financial plan for five years. - 202 -

List of Figures

Chapter 2: State-of-Art

Figure 2. 1. Types of composite materials [18].	- 31 -
Figure 2. 2. Types of fibres composites.	- 31 -
Figure 2. 3. Scheme of the bag moulding process [26].	- 35 -
Figure 2. 4. Scheme of the resin fluxing through the plies in order to obtain the composite.	- 36 -
Figure 2. 5. Scheme of compressing moulding.	- 37 -
Figure 2. 6. Scheme of the compression moulding of the composite.	- 37 -
Figure 2. 7. Scheme of the pultrusion process.	- 38 -
Figure 2. 8. Scheme of the full electromagnetic frequencies, where the light spectrum is found.	- 53 -
Figure 2. 9. Scheme of the refraction, critical angle, and reflection principles. The incoming ray is found in water, with a refractive index n_1 , and the out-coming ray in air with refractive index n_2 .	- 57 -
Figure 2. 10. Scheme of the refraction, critical angle, and reflection principles. The incoming ray is found in water, with a refractive index n_1 , and the out-coming ray in air with refractive index n_2 .	- 58 -
Figure 2. 11. Optical fibre scheme.	- 59 -
Figure 2. 12. Acceptance angle of an optical fibre where the light ray that accomplish the conditions of the $\alpha < \alpha_{\max}$ is propagate by TIR.	- 60 -
Figure 2. 13. Scheme of the numerical aperture of an optical fibre. Rays within the acceptance cone are guided by total internal reflection.	- 60 -
Figure 2. 14. a) Scheme of meridional rays, which travel along the fibre crossing the symmetry axis. b) Scheme of skew rays, which propagate in a helical path.	- 63 -
Figure 2. 15. Scheme of wavefront propagation along the fibre. In order to be propagated, the electromagnetic wave cannot be destructive.	- 64 -
Figure 2. 16. Transverse electric (TE) mode field patterns.	- 65 -
Figure 2. 17. Light pulse travelling in a waveguide optical structure where the initial signal is broken into various modes. The emerging signals is broadened [76].	- 66 -
Figure 2. 18. Light pulse travelling in a waveguide optical structure where the initial signal is broken into various modes. The emerging signals is broadened [80].	- 69 -
Figure 2. 19. V number graph example construction, (adapted from [76]).	- 70 -

Figure 2. 20. Scheme illustration of the light pulse travelling in different fibre step-index profiles.	- 71 -
Figure 2. 21. Scheme of the rod-tube-technique. On the right, ultra-pure rod of silica represented on blue. In the middle, tube of the ultra-pure silica with 1% of impurities added. On the left, the perform rod.	- 72 -
Figure 2. 22. Scheme of a drawing tower. 1: preform descent; 2: inert flux input; 3: ring furnace heater; 4: insulation air chamber protection; 5: specimen rod; 6: necked fibre; 7: diameter measurement; 8: polymer coating; 9: polymer heater; 10: coated fibre; 11: tension-meter; 12: drum	- 73 -
Figure 2. 23. Scheme representation of the Chilled Mirror Hygrometer (adapted from [83])......	- 74 -
Figure 2. 24. Two transmittance measurements necessary for determining the concentration of water vapour [85]......	- 75 -
Figure 2. 25. Scheme of E/M impedance method of an array of 4 piezoelectric active sensors where a structural crack or corrosion damage can be detected (adapted from [34]).	- 77 -
Figure 2. 26. Fabricated interdigital sensor (adapted from [34])......	- 77 -
Figure 2. 27. Scheme of the sample PI/MWNT film. (adapted from [92]).	- 79 -
Figure 2. 28. Basic modulating arrangement of a basic optic sensor system. ..	- 82 -
Figure 2. 29. Scheme of general optical glass fibre design of: (a) extrinsic sensor and (b) intrinsic sensor (adapted from [111]).	- 83 -
Figure 2. 30. Scheme of the basic modulation techniques.....	- 84 -
Figure 2. 31. Schematic diagram of the fibre setup used by Zhou et al. (adapted from [122])......	- 87 -
Figure 2. 32. Schematic diagram of the instrumentation used for Otsuki et al. (adapted from [118])......	- 87 -
Figure 2. 33. U-bent fibre optic configuration tailored with HEC and CoCl ₂ . (adapted from Kharaz et al. [126])......	- 90 -
Figure 2. 34. Attenuation of the intensity spectrum of light guided in the U-bent configuration sensor coated with sol-gel silica film (adapted from [128])......	- 92 -
Figure 2. 35. Illustration of FBG sensor working principle. FBGs work in transmitted spectrum (adapted from [134]).	- 94 -
Figure 2. 36. Illustration of LBG sensor working principle. FBGs work in reflected spectrum (adapted from [134]).	- 95 -
Figure 2. 37. FBG sensor tracks the evaporation rates for three souk moisture levels (adapted from [136])......	- 97 -
Figure 2. 38. LPG transmission spectrum on the refractive index of surrounding medium (adapted from [138])......	- 98 -

Figure 2. 39. LPG spectrum with %RH changes from 42.8 to 99 %RH (adapted from [140])..... - 98 -

Chapter 3: Materials & Methods

Figure 3. 1. Schematic of an epoxy sample with multiple optical fibre sensors (OFSs) with silver (Ag) coated tip that are embedded at different heights. ... - 110 -

Figure 3. 2. Schematic of a GFRP sample with an optical fibre sensor (OFS) with silver (Ag) coated tip that is embedded between glass fibre plies..... - 111 -

Figure 3. 3. Schematic of the interrogation setup for the OFSs..... - 112 -

Figure 3. 4. Picture of the interrogator setup. - 112 -

Figure 3. 5. Picture of the user interface of the custom LabView programme used to automatically control 16 OFSs. - 113 -

Figure 3. 6. Schematic of the interrogation setup where the samples were placed in another room. - 114 -

Figure 3. 7. Schematic of an embedded optical fibre sensor (OFS) and sputtered OFS with aluminium (Al-OFS) in an epoxy polymer matrix (adapted from [15]).
..... - 115 -

Figure 3. 8. Scheme of the vacuum sealing. 1: connection to the pump; 2: thermo to keep the liquid nitrogen and to hold the water trap inside; 3: water trap; 4: nitrogen; 5: valves; 6: glass connectors; 7: glass tube; 8: chalcogenide elements.
..... - 116 -

Figure 3. 9. Special distillation vacuum. 1; connection to the pump; 2: thermo beaker; 3: water trap; 4: nitrogen; 5: valve; 6: second sample holder; 7: first sample holder; 8: furnace; 9: sample insertion which was sealed by melting the silica glass.
..... - 117 -

Figure 3. 10. Furnace pre-purification set up. 1: first purification sample; 2: second sample holder; 3: third sample holder; 4: furnace. - 118 -

Figure 3. 11. Scheme of drawing tower. 1: preform descent; 2: He/Ar flux input; 3: ring furnace heater; 4: insulation air chamber protection; 5: TAS rod; 6: TAS necked fibre; 7: diameter measurement; 8: tension-meter; 9: drum. - 119 -

Figure 3. 12. Profile scheme of the TAS fibre embedded with the epoxy and with the water or ethanol on the top inside the mould. 1: distilled water or ethanol, 2: epoxy resin, 3 TAS fibre, 4: silicone custom mould. - 120 -

Figure 3. 13. Scheme of the principle of fibre wave spectroscopy (FEWS). 1: FTIR spectrometer, 2: chalcogenide fibre, 3: mould to hold the chemical to analyse, 4: MCT detector, 5: amplifier, 6: PC. - 121 -

Figure 3. 14. Schematic cross section representation of the SC-GFRP sample.
..... - 123 -

Figure 3. 15. Schematic of the interrogation set up of the combined sensors GFRP sample. - 124 -

Chapter 4: Results & Discussion

Figure 4. 1. DSC evaluation of the nonisothermal curve from 20 to 200 °C of the total ΔH study starting from 20 to 200 °C. The total ΔH is ($\Delta H_{Total} = 426 J/g$)..... - 126 -

Figure 4. 2. DSC isothermals analysis at 60, 80, and 100 °C for 3 hours..... - 126 -

Figure 4. 3. DSC isothermals analysis at 60, 80, and 100 °C for 5 hours..... - 127 -

Figure 4. 4. DSC results at 60, 80, and 100 °C for 3 and 5 hours..... - 127 -

Figure 4. 5. FT-IR spectra for uncured epoxy (black) resin versus cured resin (red). The epoxy was treated for 24 hours at room temperature and 5 hours at 80 °C. The strong epoxy band appears between 930 to 890 cm^{-1} . Conversion is around 90 %. - 128 -

Figure 4. 6. DMTA $\tan\delta$ curves for the crosslinked epoxy at 60, 80, and 100 °C for 3 and 5 hours..... - 130 -

Figure 4. 7. DMTA characterisation of the sectioned into 15 pieces of an epoxy sample of 110 x 80 x 50 mm..... - 131 -

Figure 4. 8. TGA graphic analysis. The $T_{5\%}$ value occurs at around 333 ± 5 °C. - 132 -

Figure 4. 9. Weight increment of the epoxy and GFRP samples immersed into artificial sea water (ASW at 80 °C, 80 °C under 50 bars of pressure and HCl at room temperature. - 133 -

Figure 4. 10. Gravimetric experiment results of epoxy specimens full immersed into distilled water at 80 °C and ethanol at room temperature, and Epoxy05 and GFRP05 samples full immersed into artificial salty water at 80 °C. All samples were tested up to 712 hours. - 135 -

Figure 4. 11. The RI average measurements at the wavelengths from 633 to 1533 nm. The epoxy RI average is 1.55 ± 0.01 - 137 -

Figure 4. 12. Etching graph relation where the etching rate follows the equation $y = 125.1 - 2.1 \cdot t$ at room temperature. - 138 -

Figure 4. 13. Microscopy cross-section images taken during the etching process; 1: Pristine optical fibre (i.e. before etching); 2: 10 min etching; 3: 20 min etching; 4: 30 min etching; A: longitudinal image; B: cross-section image (bright inner circle is the core where the light is guided). From 1B to 4B it can be observed that the diameter is almost reduced to the core. Scratches, due to poor cleaving, are observable in all cross-section pictures. - 139 -

Figure 4. 14. a) Uncoated optical fibre perfectly cleaved at 90°, b) optical fibre after silver deposition using Tollens' reagent.	- 140 -
Figure 4. 15. SEM image of the extreme tip coated using Tollen's reagent. .	- 141 -
Figure 4. 16. Sectional SEM image of the extreme tip coated using Tollen's reagent.	- 142 -
Figure 4. 17. Experimental optimization of the length of the optical fibre sensors embedded in an epoxy by comparing back-reflected spectrum with that of a reference fibre mirror.	- 143 -
Figure 4. 18. Standard deviation fluctuation of the recorded spectra for 24 hours.	- 145 -
Figure 4. 19. a) Picture of epoxy sample where two OFSs are embedded.	- 146 -
Figure 4. 20. Reflected spectra of an OFS embedded in the epoxy exposed to artificial salty water at 80 °C. Spectra were collected every 5 min, but only relevant curves are here reported.	- 148 -
Figure 4. 21. Reflected spectra of a Cu-OFS embedded into the epoxy exposed to expose to artificial salty water at 80 °C.	- 149 -
Figure 4. 22. Reflected spectrum before water diffusion (black) and after the water-diffused sample was dried at 80C for two weeks (red).	- 150 -
Figure 4. 23. Signal intensity, at wavelength of 1532 nm, from an optical glass sensor embedded in an epoxy sample at depth of 1.6 mm.	- 151 -
Figure 4. 24. Signal intensity at wavelength of 1532 nm from three embedded Cu-OFSs for 24 hours in continuous monitoring.	- 152 -
Figure 4. 25. Signal intensity, at a wavelength of 1532 nm, from three optical fibre sensors embedded in an epoxy at different depths. The sample was immersed in artificial sea water at 80 °C.	- 153 -
Figure 4. 26. Microscope image of the cut and polished epoxy sample section containing a cross-section cut of one OFS.	- 155 -
Figure 4. 27. SEM micrographs of the cross section of (a) an OFS and (b) a Cu-OFS embedded in the epoxy resin.	- 156 -
Figure 4. 28. Picture of epoxy sample where two OFSs are embedded. b) Picture of GFRP sample with one embedded OFS.	- 157 -
Figure 4. 29. Signal at intensity, at wavelength of 1532 nm, from an optical glass sensor embedded in an GFRP sample at depth of 1.6 mm. The sample was immersed in artificial sea water at 80 °C up to 48 hours.	- 158 -
Figure 4. 30. Signal intensity, at a wavelength of 1532 nm, from the five different optical glass sensors embedded in GFRP sample at similar depths of nearly 0.9 ± 0.1 mm from the surface.	- 159 -

Figure 4. 31. Cu sputtered optical fibre sensors (Cu-OFSs) were not able to detect the water diffusion through GFRP sample. - 159 -

Figure 4. 32. Cross-section optical microscope image of GFRP sample containing two embedded OFSs. - 160 -

Figure 4. 33. Total reflection of the transmitted light spectra between 1500 and 1600 nm at different selected pressures. The data was recorded in continuous mode. - 161 -

Figure 4. 34. Graph where on the left is represented the temperature and on the right is represented the pressure. Pressure agrees with the temperature. - 162 -

Figure 4. 35. Optical microscope image at (20 X) of the optical glass fibre after the pressure exposure test at 75 bars..... - 163 -

Figure 4. 36. Signal intensity at a wavelength of 1532 nm from an OFS embedded in an epoxy and in a GFRP at depths of 0.9 ± 0.1 mm and 0.8 ± 0.1 mm, respectively. The samples were immersed into artificial sea water at 80 °C and 50 bars.... - 164 -

Figure 4. 37. Signal intensity at a wavelength of 1532 nm from sensors embedded in the epoxy exposed to a) artificial sea water and b) HCl. The Al-OFS are sensitive to HCl, whereas they do not exhibit any response to artificial sea water (ASW). - 166 -

Figure 4. 38. Signal intensity at a wavelength of 1532 nm from sensors embedded in GFRP exposed to (a) artificial sea water and (b) HCl. The Al-OFS are sensitive to HCl, whereas they do not exhibit any response to artificial sea water. - 167 -

Figure 4. 39. FT-IR spectra where the epoxy groups conversion is zoomed. The registration was produced every half an hour and the selected: 0, 8, 16, 24, 29 hours, are represented. The first 24 hours corresponds to the cross-linking of the resin at room temperature and the last 5 hours corresponds to the thermal curing of the epoxy..... - 169 -

Figure 4. 40. FT-IR transmittance spectrum of the same epoxy where the registration was not in continuous and it is only represented the epoxy resin at 0 hours and the epoxy cured after 29 hours. The epoxy group conversion is zoomed. - 170 -

Figure 4. 41. FT-IR spectra of the detection of water using TAS fibre in a large mould. The sensitive part corresponded to only 200 mm. Water was detected by observing a drop in the spectra at ~ 2.7 μm and at ~ 6.25 μm - 171 -

Figure 4. 42. Transmittance spectra of the detection of ethanol using TAS fibre where the absorbance alcoholic groups are pointed out. - 172 -

Figure 4. 43. Optical microscope image (10x) of a TAS fibre in the middle embedded with an epoxy resin. It shows a good adhesion between the fibre and the epoxy..... - 173 -

Figure 4. 44. Electrical conductivity of epoxy samples with the different percentage of filler. - 174 -

Figure 4. 45. Electrical conductivity graph of 4 different epoxy samples with different concentrations of CNTs immersed in artificial sea water at 80 °C. Data was reordered every 24 hours (non-continuous monitoring)..... - 175 -

Figure 4. 46. Conductivity graph pristine GFRP composite and GFRP05 composites. Both immersed with in artificial sea water at 80 °C. - 176 -

Figure 4. 47. Signal intensities at a wavelength of 1532 nm from the OFSs in Continuous monitoring. The sample was immersed in artificial sea water at 80 °C for 7 days. - 178 -

Figure 4. 48. Conductivity signal of the spread CNT on the plies at depth of 2.2 ± 0.3 mm, signal increased after 48 h. All sensors embedded in the H-GFRP composite. - 178 -

Chapter 5: Exploitation Plan

Figure 5. 1. Pipeline Incidents: Count (1997-2017), (adapted graph from [193]). - 183 -

Figure 5. 2. Pipeline Incidents: Fatalities (1997-2017), (adapted graph from [193]). - 183 -

Figure 5. 3. Pipeline Incidents: Total costs (1997-2017), (adapted graph from [193]). - 183 -

Figure 5. 4. Project R&D WBS. - 191 -

Figure 5. 5. Financial Highlights. - 201 -

Table of Contents

Acknowledgments	6
List of tables.....	8
List of figures.....	10
1. Introduction.....	24
2. State-of-Art	28
2.1. Composites in oil and gas	28
2.1.1. Glass fibre reinforced polymers.....	28
2.1.2. Composite components.....	29
2.1.2.1. Types of matrixes.....	30
2.1.2.2. Types of fibres	32
2.1.3. Composites processing	34
2.1.3.1. Bag-moulding process	34
2.1.3.2. Compression moulding.....	35
2.1.3.3. Pultrusion moulding.....	36
2.2. GFRP composites in oil & gas.....	37
2.2.1. Pipes, tanks and vessels	39
2.2.2. Composite pipelines.....	41
2.2.2.1. Tanks and vessels.....	43
2.2.2.2. Reinforced thermoplastic pipework.....	43
2.2.2.3. Flexible thermosetting tube	43
2.2.2.4. Lined pipes.....	44
2.2.2.5. Rigid risers	44

2.2.2.6. Flexible risers.....	45
2.2.2.7. Fibre-reinforced composites for the rehabilitation of metal pipelines	45
2.3. Sensors for polymer composites	46
2.4. Optical fibres.....	46
2.5. Glass systems	47
2.5.1. Silica based glasses	47
2.5.2. Non-silicate oxide glasses.....	48
2.5.3. Fluoride ZBLAN.....	48
2.5.4. Chalcogenide	49
2.6. Introduction to optical fibres.....	52
2.6.1. Basic concepts about light propagating in optical fibres	52
2.6.2. Refraction, reflection, critical angle, and total internal reflection	55
2.6.3. Basic structure of an optical fibre	57
2.6.4. Acceptance angle and numerical aperture	58
2.7. Light propagation, the optical fibre communications basics	61
2.7.1. Ray theory.....	61
2.7.2. Mode theory.....	62
2.7.3. The single-mode SM fibres and the multi-mode MM fibres	66
2.7.4. Step-index and graded-index fibres	67
2.7.5. Optical fibres fabrication	70
2.8. Conventional humidity sensing techniques	73
2.8.1. The chilled mirror hygrometer.....	73
2.8.2. The infrared optical absorption hygrometer	74
2.8.3. Piezoelectric sensors	75
2.8.4. Self-diagnosing fibre reinforced composites	77
2.9. Optical fibre sensors (OFSs).....	78
2.9.1. Classification of OFSs	82
2.9.2. Modulation techniques.....	82
2.9.2.1. Intensity modulated OFSs.....	83
2.9.2.2. Phase modulated OFSs	83

2.9.2.3. Polarization modulated OFSs	84
2.9.2.4. Wavelength modulated OFSs	84
2.10. Fibre optic techniques for humidity sensing.....	85
2.10.1. Direct spectroscopy optical based humidity sensors	85
2.10.2. Evanescent wave spectroscopy optical based humidity sensors.....	88
2.11. Fibre grating based sensor	92
2.11.1. Fibre Bragg gratings (FBGs)	93
2.11.1.1. Long period gratings (LPGs)	94
2.11.1.2. Fibre bragg grating sensors-based humidity sensors	95
2.11.2. Interferometric sensors-based humidity sensors.....	99
2.12. Current available smart composites.....	100
2.13. Description of the work and partners objectives	102
3. Materials & methods.....	104
3.1. Epoxy preparation and characterization	104
3.2. Fabrication and optimization of the evanescent wave optical fibre sensors	107
3.3. Epoxy and glass reinforced fibre polymer fabrication.....	109
3.4. Characterization of epoxy and glass fibre reinforced polymer samples equipped with OFSs.....	110
3.5. Interrogation setup for samples subjected at 50 bars and 80 °C	112
3.6. Selective optical fibre sensors.....	113
3.7. Mechanical testing	114
3.8. Fabrication of chalcogenide TAS glass and fibre	115
3.8.1. Sample and instrumentation setup	118
3.9. Epoxy containing CNTs samples fabrication	120
3.9.1. GFRP samples containing spread CNTs on the plies (GFRP05).....	121
3.9.2. GFRP samples containing spread CNTs on the plies and embedded OFSs fabrication (SC-GFRP)	121
3.9.3. Optical fibre sensors fabrication and the interrogation setup	123

4. Results & discussion.....	124
4.1. Epoxy, preparation and characterization results	124
4.1.1. Evaluation of the best curing conditions.....	124
4.1.2. Evaluation of the epoxy viscoelastic characteristics.....	128
4.1.3. Evaluation of the thermal degradation temperature.....	130
4.1.4. Evaluation of the diffusion coefficients.....	131
4.1.5. Evaluation of the epoxy refractive index	135
4.2. Fabrication of the optical fibre sensors.....	136
4.2.1. Etching of the optical fibres.....	136
4.2.2. Silver coating deposition and fabrication of the optical glass fibre sensor	139
4.2.3. Optimization of the optical fibre sensor length	141
4.3. Mechanical tests.....	144
4.4. Characterization of the epoxy samples equipped with optical fibre sensors	145
4.4.1. Epoxy samples subjected to artificial salty water at 80 °C non- continuous monitoring	145
4.4.2. Epoxy samples subjected to artificial salty water at 80 °C continuous monitoring.....	149
4.4.3. Epoxy samples subjected to artificial salty water at 80 °C with OFSs embedded at different depths in the epoxy in continuous monitoring.....	151
4.4.4. Microscope analysis: Optical microscope and SEM	154
4.5. Characterization of GFRP samples equipped with optical fibre sensors results.....	155
4.5.1. GFRP samples equipped with embedded OFSs	155
4.6. Evaluation of samples subjected at harsh conditions of 50 bars and 80 °C	160
4.6.1. The vessel and the Conax adaptor for high pressure	160
4.6.2. Epoxy and GFRP samples equipped with OFSs tested in harsh conditions.....	162
4.7. Selective sensors	164
4.7.1. Epoxy and GFRP samples containing OFSs subjected to hydrochloric acid at room temperature in continuous monitoring.....	164
4.8. Chalcogenide fibre sensors	167

4.8.1. Cross-linking and diffusion monitoring using TAS fibre.....	167
4.8.2. Samples subjected to distilled water at 80 °C in continuous monitoring	169
4.8.3. Samples subjected to ethanol at room temperature in continuous monitoring.....	170
4.9. Electrical sensors using carbon nanotubes.....	172
4.9.1. Evaluation of the percolation curve	172
4.9.2. Conductivity evaluation of epoxy and GFRP samples containing embedded CNTs	173
4.9.3. Evaluation of the conductivity of GFRP05.....	174
4.9.4. Evaluation of the OFS and CNT	175
5. Exploitation plan.....	180
5.1. Relevant results after research activities.....	180
5.1.1. Target solutions.....	180
5.1.2. Main features	180
5.1.3. Benefits and fields of application	181
5.2. Main players	183
5.3. Most relevant costs for industrialization.....	183
5.4. Strategic choices	184
5.5. How the business model works	187
5.6. Operations	189
5.6.1. Implementation Plan	196
5.7. How much value can we obtain?	199
6. Conclusions.....	204
Appendix A: List of acronyms and symbols	208
Appendix B: Publications resulting from this thesis	214
References.....	216

Chapter 1

Introduction

Petroleum production compels the oil & gas industry to invest in developing new ways to explore, extract, refine, transport, and market petroleum derivatives. The main products of the petrochemical industries are fuel oil and gasoline [1]. Oil is the raw material for numerous chemical products, including pharmaceuticals, diluters, fertilisers, insecticides, synthetic perfumes and plastics [2]. For this reason, petroleum is known as black gold.

This black gold, a yellowish-black liquid, can be found in geological formations on the Earth's surface. Petroleum can be found in natural spring fountains, normally in rocks, or under the seawater in deep oceans. In all cases, the crude oil must be transported from the extracting point to the oil & gas industry. It is then that the petroleum is processed, and its derivatives are obtained.

Petrochemical industries use different strategies to convey crude oil. These includes ships, trains, trucks, aeroplanes, and pipelines. The most efficient and cheapest means of transportation of petroleum for long distances are pipelines. For this reason, the latest Pipeline & Gas Journal survey points out that around 200,000 km of new pipelines are planned to be constructed in 2019 [3].

The installation of subsea pipelines for oil and gas transportation is affected by economic, technical and environmental parameters [4]. The basis of a pipeline design consists of its functional requirements, for example the definition of the environment, the selection of the mechanical design, the installation method, and the pipe-soil interactions. Furthermore, pipelines have to withstand other vital parameters like pressure and temperature changes and corrosion.

Researchers such as Collberg et al. [5] expressed the fundamental principle to verify that design loads affect and do not exceed design resistances. However, these methods do not integrate sensors to monitor the integrity of the pipelines continuously because they are based on valid empirical data and predictions up to 20 years. For these reasons, when the oil and gas pipeline industry is considering innovation, it must act conservatively due to its large initial investment.

The implementation of innovative technologies is undertaken very carefully and executed only when it is vital or when it leads to a reduced loss of time or cost [6]. At present, ageing pipelines are the main application areas and open new opportunities to implement new technologies. Seabed pipelines are especially exposed to harsh environments, and hostile environment can produce leakage, corrosion, and cracks in them [7]. For this reason, the petrochemical industries are now focusing on improvements to the integrity of pipelines by monitoring their functionalities. New trends are making it possible to enhance the introduction of innovative sensing technologies in the oil and gas pipeline industry [8], [9]. These include operational intelligence composites, in situ and real-time infrastructure monitoring, easy and cheap reinforced composite development, market supply and demand, the utilisation of green materials and concept, and implementing new technologies [9]. Petrochemical companies are identifying new technologies, as well as transforming and devising new strategies to speed up the incorporation of novel sensing platforms. Their continuous innovation has led to new developments in sensing technologies. This opens up great opportunities for a project to develop new sensors.

Monitoring the integrity and durability of reinforced composites in the subsea environment is one of the most challenging areas for oil & gas companies. For example, Kassel et al. [10] explains the challenges of manufacturing the pipeline that will connect Russia and Germany in the Nord Stream 2 Project. This is especially the case when petrochemical companies must choose very carefully the components of their pipelines, which have to work perfectly in underwater conditions for more than 20 years. This project will place underwater a total length of one pipeline of 1,200 km, which have to withstand a pressure of 220 bars.

Numerous sensors like the current fibre Bragg gratings (FBGs) and interferometers, fail over time in high-pressure in seabed environments, causing costs related to the sensor replacement. Frequently, the maintenance service costs for substituting the sensor are higher than the cost of the sensor itself [11]. For this reason, many applications require sensors with a long operating life. Metal sensors are susceptible to seawater attacks. In fact, current metal sensors must withstand harsh conditions at varying water depths, which results in accelerated corrosion produced by the different oxygen levels, temperature, pH, salinity, biological activity, the imposed electrical conductivity, and velocity flow rates present in the seawater at various depths [12].

This work reports on the design and experimental testing of new, low-cost optical fibre sensors (OFSs). These novel OFSs have been developed to monitor the degradation through the thickness caused by the diffusion of corrosive media in epoxy and GFRP materials. The new OFSs are aimed at obtaining a turnkey monitoring system for composite structures.

The sensors were based on the best characteristics of evanescent wave sensors developed in the previous research carried out by Milsom et al. [13]. The optical glass fibre sensors were made by etching the cladding and the optical glass fibre to make it sensitive to the surrounding environment. The optical glass fibre used was a standard commercial multimode used in telecommunications. These optical glass fibre sensors are defined as evanescent wave optical sensors (EWOSs), since they rely upon light leaking from the fibre that interacts with the surrounding material. For sensing applications, optical fibres are very interesting because of the small form factor, immunity to electromagnetic interferences and intrinsic fire safety (they cannot start fires). These features are very interesting for the oil and gas industry, where electric-based sensors may have considerable limitations [14]. The sensors presented have been developed to detect the presence of moisture and hydrochloric acid (HCl), which makes them suitable for pipeline corrosion monitoring, as well as, remote long-distance, in situ, and real-time sensing [15].

Finally, thanks to the Marie Skłodowska-Curie grant and the related European Training Network, the possibility to fabricate alternative sensors to monitor the degradation of the reinforced composites was explored. The possibility to use chalcogenide glass fibre sensors, which were developed and tested in Université de Rennes 1, (Rennes, France), and sensors based on carbon nanotubes (CNTs) were studied at Nanoforce Ltd, (London, UK).

The experimental activity of this research was carried out by 1) the preparation of epoxy samples and their thermal and viscoelastic characterisation; 2) the development of optical fibre sensors based on evanescent field sensing that could work in reflection; 3) the evaluation of chemical diffusion coefficients through epoxy and GFRP samples; 4) the evaluation of the interrogation setup for target molecule diffusion; 5) the water diffusion evaluation of epoxy and GFRP samples at high-pressure in order to simulate harsh environment conditions; 6) the evaluation of the mechanical characterisation of the GFRP samples; 7) the development of optical glass fibre tailored sensors for acid detection; 8) the development of alternative sensors.

Chapter 2

State-of-Art

2.1. Composites in oil and gas

This technical state-of-art report gives a survey of the current capabilities and limitations of the glass fibre reinforced polymer (GFRP) composites in oil and gas companies for monitoring the composites degradation and prevent oil spills. This research includes the analysis of systems for use in offshore petrochemical operations. It includes an overall of fabrication and types of the current GFRPs, and the existing sensors, especially the optical glass fibre sensors (OFSs) including their operational principle and the OFSs overall classification. Furthermore, it considers a variety of working and experimental remote sensing systems that are at present in use and their applications in different oil spill scenarios. The assessment reflects the suitability for using sensors for chemical detection and their strengths and weaknesses. Operational requirements, implementation, and costs are also analysed.

2.1.1. Glass fibre reinforced polymers

During the last century, fibre reinforced polymers (FRP), also known as fibre reinforced plastic, have been increasingly used as alternatives for traditional metal structural materials [16]. These present attractive characteristics due to their particularly high strength, stiffness, and tailorable properties.

Composites are defined as materials which have one or more components that together have better properties than each component on its own. Normally, they are constituted by a matrix and by reinforcement component. However, they are not a human invention. Nature has already created its own composite materials. For example, we can find composite forms in wood, which has natural fibres embedded with natural resin, and bones, which have calcium structures filled with collagen. In the past, the first human colonies developed their own composites for building houses. These were the adobes, which consist of clay as a matrix and containing straw as reinforcement. These were improved over the centuries until the invention

of reinforced concrete, which has cement as a matrix to embed metals wires or other rod materials and the last invention of FRP.

The preliminary FRP composites incorporated glass fibres as a reinforced material embedded with a polymeric matrix. The combination of these materials greatly increased their mechanical properties improved to either of the materials on their own. The perfect combination of low-cost, high stiffness, high strength, easy manufacture and easy scalability made glass fibre reinforced polymer (GFRP) composites become one of the most used materials in current society. In addition, they present other properties such as environmental resistance, suitability for harsh environmental conditions, and playability with their stiffness and strength, as a result of the selection of high fibres such as glass, aramid and carbon, which dramatically increase their strength and stiffness. For example, GFRP composites have been a key part of the fast-increasing expansion of petrochemical companies. However, research on their particular modes of failure is lacking. They differ from metal composites because their ageing is difficult to predict. They can present matrix crazing, delamination, fibre failure and interfacial bound failure.

2.1.2. *Composite components*

Basically, all composites are formed by two phases, one phase of matrix and one phase of reinforcement, which is embedded by the first phase. Composites are classified in three main groups (Fig. 2. 1.), [17].

- a) Particulate composites, which have immersed spherical particles,
- b) Fibre composites, which have immersed fibres. Figure 2. 2. shows the different types of fibres,
 - a. unidirectional (long fibres),
 - b. alternate (short fibres),
 - c. orthogonal (fibre mesh),
 - d. layers.
- e. Laminate composites, which alternate the components phases in laminar form. The laminas can vary in thickness.

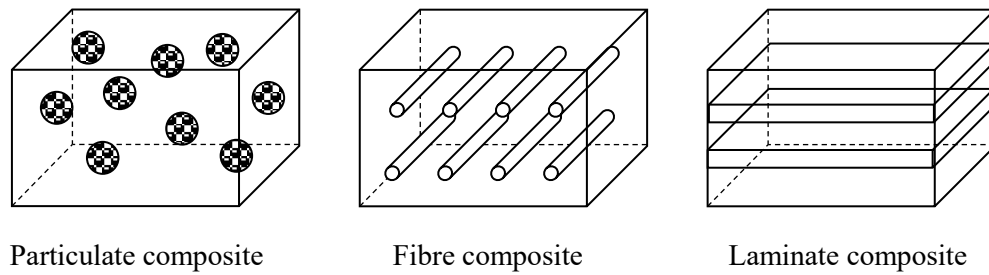


Figure 2. 1. Types of composite materials [18].

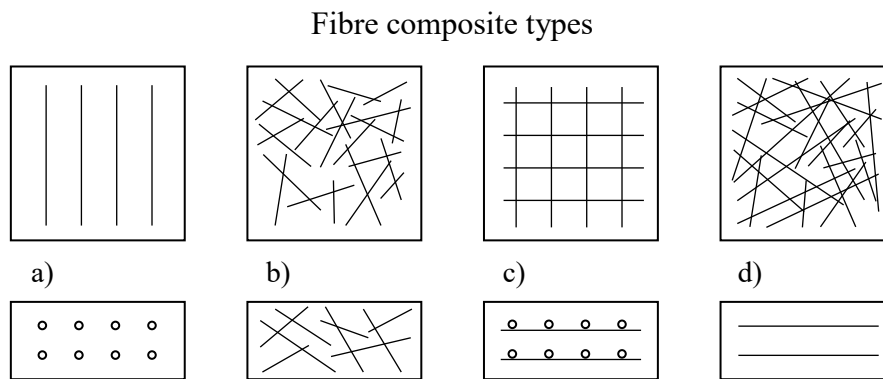


Figure 2. 2. Types of fibres composites.

2.1.2.1. Types of matrices

The matrix protects the fibres from being exposed to the surrounding atmospheric conditions. It also prevents the fibres from ageing and protects the fibres from being compressed to prevent buckling.

In general, matrixes can be classified in two main groups, thermoplastics and thermosetting. They basically differ for their behaviour in the presence of heat [18], [19]. Nevertheless, they are used indifferently for injection moulding process. Thermoplastic polymers can be re-melted and re-moulded whenever is necessary, while a thermoset remains solid until it burns. For this reason, thermosets bring great performances for high-heat applications [20]. Table 2. 1. summarise the most common polymer matrixes used in the market.

Table 2. 1. General classification of polymer matrixes.

Polymeric matrixes	
Thermoplastics	Thermosets
<p>Nylon</p> <p>polypropylene (PP)</p> <p>polyethylene (PE)</p> <p>Polystyrene (PS)</p> <p>Poly vinyl chloride (PVC)</p> <p>Poly carbonates (PC)</p> <p>Poly amides (PA)</p>	<p>Phenolic resins (PF)</p> <p>Epoxy resins (EP)</p> <p>Unsaturated polyesters (UP)</p> <p>Vinyl esters (VU)</p>
Elastomers	
<p>Polyurethanes (PU)</p> <p>Silicones (SI)</p>	

Thermoplastic materials are polymeric materials that become soft when they are heated and solidify again when they are cooled. This attribute leads them to be melted and re-formed multiple times, which allows the possibility of recycling them. For this reason, they are ideal materials for injection moulding technique, which is explained below. They can be amorphous, such as PS and PVC, or semi-crystalline, such as PE and PP. In general, they are cheap and present good chemical resistance, and strength comparable to rival metal materials. For example, they have applications in textile, building and medical engineering. They hold the 80% of the polymers market due to their extended applications.

Thermosets have independent molecules before hardening. Afterwards, they cross-link and form a three-dimensional structure. They represent the remaining 20 % of the total market consumption of polymers. They present good qualities for

infusion moulding technique. They do not drip when they are exposed against a fire, and in general they possess better creep behaviour. However, the crosslinking reaction is slow and takes a considerable time. Their processing is sometimes hard to monitor, and some of them release gases (in particular water vapour). Furthermore, they are not reusable, which leads to no green materials for the environment sustainability.

2.1.2.2. *Types of fibres*

Glass fibres, also known as fibre glass, are the most extensively used reinforcements in polymer composites. Table 2. 2. summarises the most common reinforced materials currently used. These are the glass fibres E- and S-glass, aramid, and carbon fibres [21], [22].

E-glass fibres refer to electrical insulation fibres. They are expensive but suitable for fabricating GFRP. S-glass fibres refer to high strength composites. These S-fibres are used for critical structural applications, such as aerospace and civil engineering. In comparison to E-glass fibres they are much more expensive.

Carbon fibres are used in high structural composites for aerospace applications. They possess a high stiffness (half of S-glass fibre), and low density. They are commonly less strong than glass fibres or aramid fibres, but their thermal properties are outstanding, because they can be stable until approximately 2000 °C. Furthermore, they show a very low coefficient of thermal expansion, and they are chemically inert to corrosion or oxidation until around 1000 °C. However, they cost double the price of S-glass fibres, and they are quite anisotropic [22], [23].

S-2 glass fibres are used to high strength applications. A-glass fibres are used for thermal insulation and C-Glass fibres which are used for chemical resistance applications [18], [23], [24]. Aramid fibres have an important relevance for reinforced materials and advanced composites. They have a very high strength, for example they have a strength five times higher than steel. The elongation is approximately above half of those S-glass fibres. They resist until approximately 175 °C and they are chemically stable. However, they are susceptible to acid or basic chemical attacks.

Table 2. 2. Selected properties of reinforced fibres [18], [23], [24], and [25].

Fibre	Use	Density (g/cm³)	Elongation (%)	Tensile strength (MPa)	Elastic modulus (GPa)
E-Glass	Electrical insulation	2.5	0.5	2000-3500	70
S-Glass	High strength composites	2.5	2.8	4570	86
S-2 Glass	High strength composites	2.5	5.7	3445	87
A	Thermal insulation	2.4	4.8	3300	72
C	Chemical applications	2.6	4.8	3300	69
Aramid (Std.)	High strength composites	1.4	3.3-3.7	3000-3100	63-67
Carbon (Std. PAN-based)	Chemical applications	1.4	1.4-1.8	4000	230-240

2.1.3. Composites processing

Since a composite material is made by a matrix and reinforcement, it was necessary to think in different ways to impregnate the reinforcement materials using the matrix. For this reason, different techniques were born to make a composite material. The most used and common techniques, among others [26], are the bag moulding process, the compression moulding, and the pultrusion.

2.1.3.1. Bag-moulding process

Figure 2. 3. shows a typical resin infusion process using a bag moulding technique, or liquid composite moulding. It is commonly used to fabricate composites by infusing the polymer matrix in the bag where the fibres are placed. The resin fluxes due to the vacuum and the fibres are impregnated with the resin [26].

Normally, fibre glass plies or other reinforcement materials are placed, as the product requires, on a metal or wood surface previously coated with a release agent, which can be a liquid or wax. This is done in order to avoid any possible attachment between the resin and the surface. Peel-ply is put on the glass fibres and a diffusion mesh on the peel–ply. A couple of tubes linked with a metal spring are placed on the extremes. One is used as input for the resin and the second as output. A plastic cover foil is put over everything and fixed with sealant tape and the vacuum bag is ready (Fig. 2.4.). Before infusing the resin, it is necessary to make a pre-vacuum in the bag-modelling to check possible failures in the sealant system.

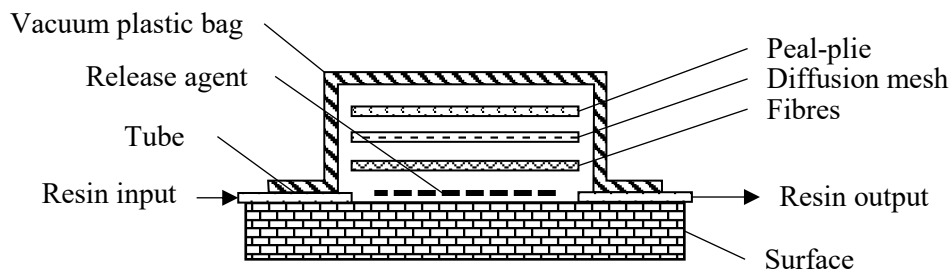


Figure 2. 3. Scheme of the bag moulding process [26].

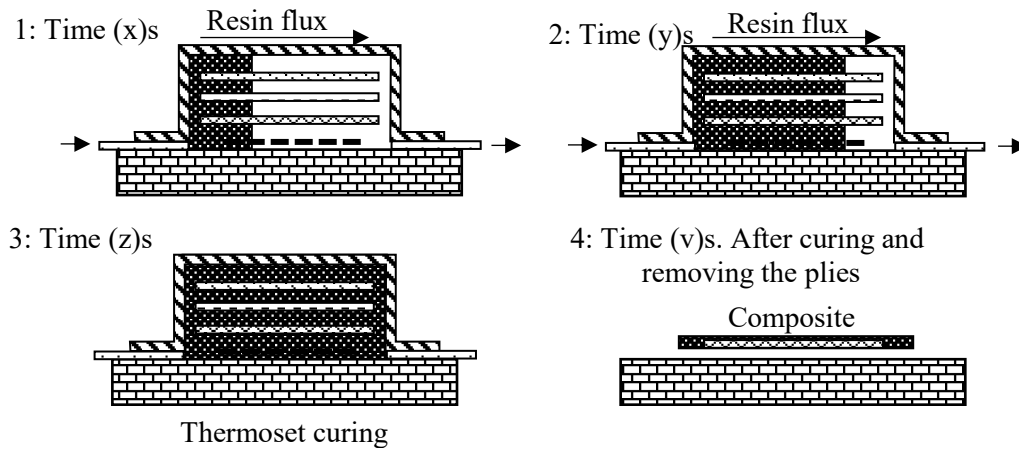


Figure 2. 4. Scheme of the resin fluxing through the plies in order to obtain the composite.

2.1.3.2. Compression moulding

In compression moulding thermoset or thermoplastic material can be used. Normally, this technique is commonly applied for manufacturing thermoplastic materials and composites. The reinforced material is placed between the matrix material, which has granules, sheets, or prepreg forms. These materials are placed between peel-ply which, at the same time, are placed between Teflon sheets (Fig. 2.5.). These thermoplastic materials are melted by applying heat and subsequently a load press [27]. After the curing, the materials are unloaded, and the composite is obtained. The mould where the materials are placed will define the composite shape (Fig. 2.6.). For example, Figure 6 shows the fabrication of a flat composite which is defined by the picture frames. If the mould has a bent shape the final product will have a curvature.

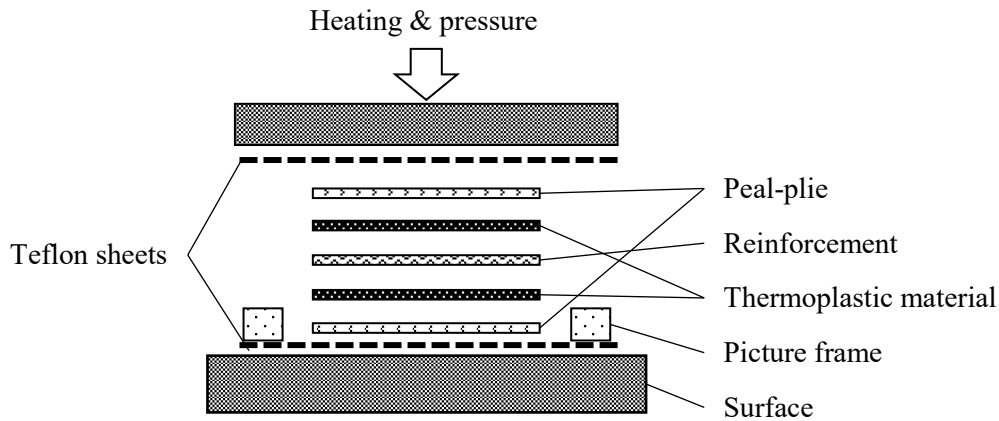


Figure 2. 5. Scheme of compressing moulding.

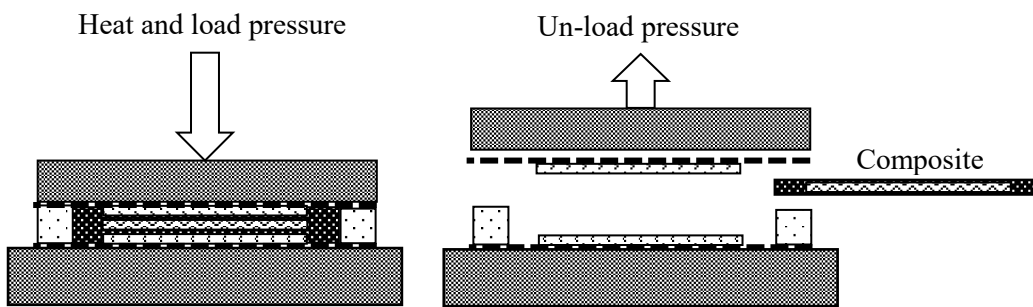


Figure 2. 6. Scheme of the compression moulding of the composite.

2.1.3.3. Pultrusion moulding

Figure 2. 7. shows the manufacturing of the pultrusion moulding technique. The fibre yarns are pulled to immerse them in a resin bath wetting the fibres. The impregnated fibres are passed through the holes of a mould plaque, which can possess different plaque forms, such as circumferential, elliptical, or any desired form. These are commonly called dies. For example, a circumferential form will produce a cylinder. The dies determine the finished profile and dimensions. Then the impregnated fibres are passed through a furnace, where they are heated, which quickly cures the resin. Finally, the composite is cut to the desired length.

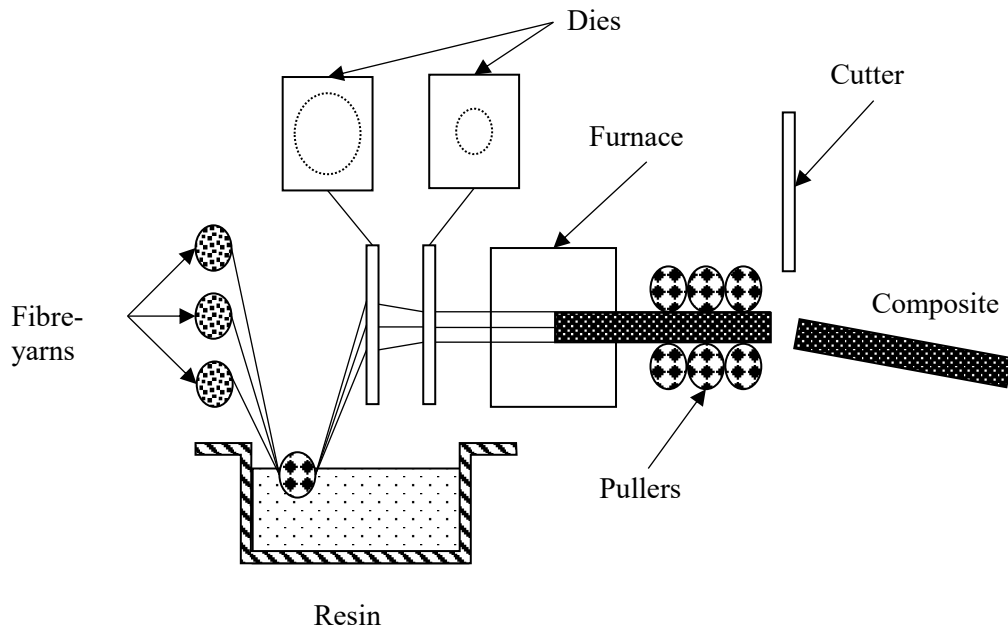


Figure 2. 7. Scheme of the pultrusion process.

2.2. *GFRP composites in oil & gas*

This section will discuss the most important areas where reinforced composites are being employed in oil and gas companies for fluid transport or storage. Today petrol and its derivatives, such as oil and gas, constitute the dominant source of energy worldwide. In recent decades, reinforced polymers have become one of the most interesting materials because they possess attractive properties for oil and gas companies. Among others, they are lightweight, easy to process and have low fabrication costs. For these reasons, not only oil and gas companies utilise polymer composites, in fact, they are much used in other sectors, such as aerospace, civil and energy engineering. Owing to their diverse industrial applications, several reinforced polymers have been developed using different reinforcement fibres, as explained in section 2.2.2. By changing the reinforcement fibres into a polymer, the mechanical properties can be improved.

The conveyance of petrol from the extraction point to the refinery requires huge pipelines [17]. These pipelines are typically exposed to high pressure and harsh conditions, particularly in the sub-seabed and underground environments. Currently, metal pipelines are the most efficient and safest and represent the most common fuel transport network. However, metal pipelines are expensive and are

susceptible to corrosion with sub-consequent cracks, dents and leaking [28], [14]. These pipelines which carry oil and gas fluids have a high probability of failure due to the deterioration produced by the surrounding environmental conditions or chemical attack from the fluids carried. Furthermore, the presence of salty water on the pipeline on the seabed and the presence of sulphur make these tubes vulnerable to corrosion and produce a failure in the system.

Interest in using pipelines made of glass fibre reinforced polymers for outer-continental-shelf fluid transport has increased in the oil and gas sectors due to their properties, such as cost-effectiveness. Over the last two decades, petrochemical companies have been studying the possibility of replacing metal pipes with GFRP pipes. However, the successful transport action of crude oil to refineries, and from these refineries to the user [28], requires new sensing methodologies but there is still a lack of knowledge about these.

Sometimes, the acquisition cost of reinforced composite components exceeds that of their metallic equivalents. However, because GFRP composites are relatively easy to manufacture and handle, the installation cost, particularly for pipelines systems, is often lower than for conventional steels [29]. Reinforced polymer composites present superior cost advantages when they substitute expensive corrosion-resistant metal components, such as copper-nickel alloys, duplex or super duplex stainless steel (duplex stainless steels have a two-phase microstructure that consists of grains of 50% austenitic and 50% ferritic stainless steel, and Super Duplex stainless steel has a higher chromium and molybdenum content, which provides it with increased corrosion resistance. [30]), or even titanium [31]. The capability of GFRP composites to resist corrosion also makes favourable them more reliable and leads to lower through-life costs.

In the 1980s several obstacles were identified to using reinforced composites in offshore platforms. These were [29]:

- a. Monitoring requests, particularly on combustibility;
- b. Lack of harsh environment offshore data (degradation, fatigue, cracks, sea flows at different depths);
- c. Lack of standard procedures for composite designs;
- d. Difficulty of scaling up the composite fabrication in industries.

The research carried out on reinforced composites in the last twenty years has made it possible to remove the presented obstacles 1, 3 and 4, especially as regards the standard procedures and the scaling up of their fabrication. However, there is still a lack of information about how the reinforced composites will behave over the next 30 years when exposed to harsh environments.

2.2.1. Pipes, tanks and vessels

The most common used composites for the oil and gas industry are made of epoxy, a phenolic polymer matrix combined with glass, carbon or aramid reinforced fibres [32]. They are currently being used for piping, tanks, and vessels [33], and they are also used for offshore drilling applications. Indeed, GFRP composites dominate the market of the fabrication of composites to be used in the oil and gas industry.

GFRP composites are ideal for the oil and gas industry because they provide desirable characteristics such as heat and corrosion resistance, strength, flexibility, durability, stability, as well as being lightweight. Epoxy resin-based composites are the most used because they have better performance at high temperature. They provide good adhesion strength and have lower styrene emissions than polyester resins. For these reasons, GFRP composites are often used to manufacture pipes which are slowly being introduced in some sections or integrated together with conventional metal pipes due to their excellent and unique properties of [33]:

- a. possessing good resistance to age and corrosion;
- b. not being electrically conductive;
- c. having high strength-to-weight ratio;
- d. providing improved fatigue endurance;
- e. having excellent dimensional stability;
- f. requiring little maintenance.

Focusing on pipes, a GFRP epoxy-based matrix provides excellent buoyancy modules for offshore drilling. These pipes have quickly found useful applications in the offshore drilling industry instead of metallic pipes due to:

- a. being cost-effective;
- b. being lightweight;
- c. needing low maintenance.

These characteristics make GFRP pipes, tanks, or vessels desirable for the oil and gas industries. The main benefits for using GFRP instead of conventional metallic alloys are:

a. GFRP has a high strength-to-weight ratio; so, represents a more cost-effective way of conveying equipment to drilling and production sites.

b. GFRP possesses good corrosion resistance, which reduces maintenance costs. Pipe corrosion is one of the most difficult and expensive problems to deal with among the current failure modes in metallic-alloy pipes used in oil and gas conveyance equipment.

c. GFRP provides good thermal insulation, excellent damping, and fatigue endurance.

d. However, GRFP pipes also present some disadvantages which sometimes make oil and gas companies decide to use metal pipes instead:

e. GFRP mechanisms for predicting long-term damage degradation or ageing and failure mechanisms of composite materials are not well understood. For this reason, sometimes it is necessary to use metal alloys for operations where structural failure cannot be predicted.

f. GFRP requires continuous in-service monitoring equipment, which provides a unique and excellent opportunity to develop new sensors for constant health diagnostic and integrity monitoring. The implementation of a sensor may be necessary to elevate the performance reliability of GFRP composites.

g. GFRP requires a high degree of manufacturing competence for their industrial fabrication.

h. Metallic alloys present better mechanical properties than GFRP composites. Furthermore, when GFRPs are manufactured, the induced heterogeneity and anisotropy make the structural integrity of the composite materials highly unpredictable.

One of the most common failures in structural composites is ageing. For example, moisture can trigger the degradation or ageing of reinforced composite pipelines in the oil and gas industries. For this reason, it is vital to monitor the integrity of the composites in an efficient way to quickly detection. The leak that take place over the mainland shelf have a direct impact on society, in its environmental and economic sectors. However, the spills are produced due to physical or chemical pipeline degradation. These factors are complicated to assess due to the harsh conditions that the pipelines have to withstand. This makes early detection and continuous monitoring with accurate analysis challenging. Furthermore, the invention of new sensor technologies is required, and an oil and gas company are now open to the introduction of new sensing methodologies such as optical glass fibre sensors.

2.2.2. *Composite pipelines*

Currently, epoxy polymers are one of the most used matrices to fabricate glass fibre reinforced epoxy (GRE), which is used inshore for low and high-pressure systems. Pipes made of GRE present an extensive range of applications, such as carrying different fluid gas typologies. In contrast, the main applications related to low-pressure aqueous services are carried out in the offshore.

The chemical and physical resistance of GRE depends on the resin and hardener employed. GRE pipes are mostly immune to the effects of hydrogen sulphide and carbon dioxide. However, they are susceptible to water rather than oil, especially to some highly aromatic chemical species such as toluene or xylene, which can produce severe damage. Standards for the use of composite piping, such as ISO/DIS 14692 (2000), and qualification procedures, such as ASTM 2992 and ISO 109281 (1997), facilitate their use.

GRE pipes present the best chemical resistance approaches. Nevertheless, other types of polymer resin can be used for specific purposes [29]:

- a. Isophthalic polyester, for general products;
- b. Vinyl ester, which also presents close corrosion resistance to epoxy;
- c. Phenolic, employed for fire-critical applications.

Typically, pipes containing fibreglass are manufactured by pultrusion moulding, as explained in section 2.5.

Its high strength and resistance to chemical corrosion make GRE ideal for petrochemical industries. On the onshore, they are used to transport oil, fresh water, seawater and other fluids. On the offshore, the use of GRE is limited to aqueous fluids.

The physical conditions related to the maximum temperature and pressure that GRE can withstand will depend on the typology of resin employed to manufacture the pipe. In applications where water is present, the main component is used amine-cured epoxy systems, which have been demonstrated to be suitable for temperatures up to 115 °C. Aromatic amine hardeners, such as menthane diamine (MDA), present around 15 °C of better temperature performance than aliphatic amines, such as isophorone diamine (IPD). Anhydride-cured epoxy systems usually operate at a maximum temperature of ~80 °C. However, while GFRP based on epoxy systems works well in liquid water, epoxy piping quickly sustains hydrolysis damage in steam. For these reasons, the applications where steam can be formed must avoid the use of GRE [29].

Epoxy and vinyl ester offer relative immunity to CO₂, H₂S, and the main components of crude oil attacks. However, they are susceptible to volatile aromatic liquids such as toluene and xylene.

The main competitor to epoxy is vinyl ester-based piping. It presents high corrosion applications and lower temperatures in water. However, epoxy vinyl ester is not as reliable as amine-cured epoxy pipes. The use of pipes in alkaline or acid application environments requires special treatment of the pipe, since the reinforced fibre can be attacked and degraded by liquid contact. Fortunately, the ionic species in corrosive liquids are insoluble with thermosetting resins. For this reason, these provide good resistance. However, the pipes will be vulnerable if a small crack occurs. Therefore, the ageing of GREs will have a direct effect on their mechanical, thermal and chemical properties. The material will then lead to failure due to plasticization of the polymers and the disruption of the chemical boundaries of the interface caused by the infused moisture [34]. Many non-destructive and non-invasive techniques have been developed to monitor local damage, such as cracks, and to prevent failures. However, a sensor able to monitor corrosive liquids such as acids is also needed, since the current pipes do not incorporate a sensor with these characteristics.

2.2.2.1. *Tanks and vessels*

Reinforced composites have been employed for some time for the manufacture of tanks to store water and diesel. There are effective and conservative standard preparations which enable the manufacture of tanks and vessels made of reinforced composites (BS4994, 1987 and ASME, 1992). These have also been designed for moderate pressures [29].

It is expected that in the near future, thermosetting resin systems will be more suitable for tank construction because they display improved levels of elongation before the composite breaks. Furthermore, they could have more extensive use in tanks, due their ability to operate at higher pressures. For this reason, the thermal and corrosion properties that GRE offers will be welcome for developing the new tanks and vessels.

2.2.2.2. *Reinforced thermoplastic pipework*

One of the most recent fabrications by oil and gas companies is Reinforced Thermoplastic Pipework (RTP). This is formed with three different parts: an inner thermoplastic (typically polyethylene), reinforced layers, and a thermoplastic cover.

Reinforced thermoplastic is of great interest to petrochemical companies because it presents higher flexibility, cost-effectiveness and easy fabrication. These systems employ non-impregnated aramids such as Kevlar or Twaron® [35] as reinforcements. The aramid fibre is wrapped directly onto the thermoplastic liner, and then the reinforcement fibre is covered with another thermoplastic. However, they present a lower temperature resistance (60 °C) in comparison to GRE (115 °C) in general. Furthermore, the outer coating is sometimes vulnerable to UV radiation which produces their degradation and abrasive effects [29].

2.2.2.3. *Flexible thermosetting tube*

The composite coil tube is a novel product that was born from the need for a non-metallic replacement for steel coil tubing. This composite is used for high-pressure applications (~500 bars). The coil tube can be easily transported using a

drum, uncoiled and forced into the well. After its use, it can be re-coiled and stored for future applications.

Composite coil tubes were also developed for the difficulties that metal tubes presented on long horizontal wells. They are extensively used in onshore applications. The tube is based on a thermoplastic liner such as polyethylene, cross-linked polyethylene or nylon to be englobed with an E-glass fibre or carbon, and over-wound with an epoxy-based structural thermosetting laminate. On coiling the matrix resin provides the flexural strain by cracking, but this does not damage either the load-bearing capability of the fibres or the fluid containment capability of the thermoplastic liner {Formatting Citation}. However, this coiled tube is restricted to a small diameter of 100 mm.

2.2.2.4. Lined pipes

Lining carbon steel pipes with polyethylene and PVC makes it possible to create a new composite resistant to corrosion and increases cost-effectiveness. Using this methodology, it is possible to place carbon steel pipes in corrosive environments. However, a serious issue is presented by the liner collapsing when the pipeline is depressurised, because when it is subjected to pressurised gas, this can permeate the liner and fill the interface between the liner and the carbon steel pipe. Furthermore, thermoset liners are susceptible to abrasion and damage from wire-lining operations [33].

2.2.2.5. Rigid risers

Rigid risers typically possess large diameters in comparison to coil tubes (between 250-500mm) and can withstand higher pressures (1000 bars). They employ a range of high strength and duplex steels. They are much used on offshore platforms in both shallow and deep water, especially over 1000 meters.

The introduction of rigid risers produced a few advantages such as cost-effectiveness through using synthetic foams, which also reduce the self-weight, and a reduction in riser external cross-section, leading to lower drag forces and reduced tension. The most advanced composite riser designs are based on a metallic or

elastomeric inner liner with a near-axial reinforcement (carbon fibre), and near-hoop reinforcement (S-glass or carbon) to support the high-pressure.

A large number of petrochemical companies have investigated rigid composite risers. Among others, these include Conoco, Petrobras, Shell and Statoil, Institut Français du Pétrole (IFP), Lincoln Composites, and Northrop Grumman [29].

2.2.2.6. Flexible risers

Flexible risers are used for high-performance products, and they are mainly produced by two companies, Coflixp and Wellstream. These present high-pressure resistances, and they are also flexible.

The pipe is made with inner stainless steel, such as carcass, to prevent buckling under external compressive load. Then, a polymeric liner is instead to avoid corrosion. Near-hoop and near-axial armour normally made of carbon are wrapped around the internal liner. Finally, everything is englobed with an outer polymeric coating for external environmental protection, which can be a thermoplastic or thermosetting.

2.2.2.7. Fibre-reinforced composites for the rehabilitation of metal pipelines

Traditionally, the most reliable repair solution when a pipe is damaged is to replace the entire section or cover it with a welded steel patch. However, welding pipelines underwater or underground is a highly cumbersome process due to the difficulty of accessing them. The buried pipelines are typically designed for operating in external pressure [36]. Therefore, service and safety become an expensive process because of their complex installation, inspection and maintenance requirements. An alternative is to use GFRP composites to repair metal pipelines [36]. For this reason, polymer composites are also increasingly being used as new alternative structural materials.

Numerous developments are being made many products are available in this domain. GFRP has been proven as a suitable material to repair metal structures. As a result of this, some commercial products have merged, such as the Clock Spring® [37], Sealxpert® [38], and RES-Q® [39]. For this reason, fibre-reinforced composites are often chosen as ideal materials for the rehabilitation of metal

pipelines. However, they still necessitate much research to perfectly understand their ageing behaviour when they are exposed to chemicals such as petrol derivatives. Indeed, a sensor capable of monitoring their structural degradation would allow their failure to be avoided, prevent environmental disasters, and provide greater safety in operating workstations. Nevertheless, repair techniques may be not necessary with effective health monitoring of the pipes with a sensor or may just be used when the sensor detects degradation or corrosion due to ageing produced by moisture infusion.

2.3. *Sensors for polymer composites*

This research project is highly motivated by the need for an innovative optical glass fibre sensor able to work in harsh conditions to monitor the degradation of glass fibre reinforced polymer composites such as pipelines used in oil and gas sectors. The sensor is aimed to possess low cost fabrication, easy to manufacture and easy to implement in composite structures such as the GRE composites explained before.

Currently, it exists different glassy systems which can be employed as sensors. Hereby, they are described because this project not only investigates the silica based optical glass fibre sensors. It had also explored to use a different glassy system, such as the chalcogenide glass, in order to create an alternative sensor.

2.4. *Optical fibres*

Nowadays, optical fibres (OFs) are the backbones of the current most advanced telecommunications networks and are assembled in optical cables. Optical glass fibres have become one of the most remarkable technologies of the last century. They link continents, cities and neighbourhoods around the world. Since then, there has been a huge development in optical fibres due to their proper and their wide applications for devices, such as aerospace, civil, mechanical, automotive, chemical sensing, biomedical engineering, and including optical fibre gratings devices [40]. Nearly two billion kilometres of OFs are placed around the world [41].

It was not until the invention of low-loss optical fibre in the 1970s, when the first fibre was fabricated and used for optical communication [34]. Therefore, the

award of the 2009 Nobel Prize in Physics was given to C.K. Kao and G.A. Hockham, for the ground-breaking achievements, which concerned the transmission of light in fibres for optical communications [42].

The secret of light transmission is found in the atomic structure of the material which allows the total internal transmission through the material [43]. The main difference between glass and quartz lies in their atomic structure. Glass systems possess an amorphous structure, which allows the light to be transmitted without being scattered. On the other hand, quartz mineral has a crystalline structure, which creates planar crystalline plans where the light is scattered.

2.5. *Glass systems*

The selection of a suitable glass composition to create an optical glass fibre sensor is directly based on the glass parameters, such as the glass fibre structure, the maximum photon energy, the chemical durability, and the purity. Their composition will directly affect in light transmission and in their uses.

Glassy systems are split in two main groups. The first group consist on the glasses which contain silica, such as the silica-based glasses. The second group is the non-silica-based glasses, such as the phosphate, tellurite, fluoride ZBLAN and chalcogenides glasses.

2.5.1. *Silica based glasses*

Silica based glasses are the most common glasses and the most used around the world. Indeed, they are well widespread materials and intensively used in photonics and communications devices. In comparison to the others glass systems, they are cheap and easy to fabricate and for these reasons they are very welcome to be used.

Silicon dioxide (SiO_2) glasses exhibit high intrinsic absorption beyond $2.4 \mu\text{m}$. This absorption makes them ideally to be used in the visible and near infrared (NIR) spectra. SiO_2 based glass presents extremely low propagation loses, suitable to handle high temperatures, and presents high mechanical strength when they are pulled or bent [44]. Therefore, these properties make the silica glasses very interesting to produce sensor and photonic devices. For this reason and especially

for the cost-effectiveness, this project selected the silicon dioxide-based glass system to fabricate a new optical glass fibre sensor.

2.5.2. *Non-silicate oxide glasses*

Numerous important and essential photonic devices are based on non-silica oxide glasses compressing the phosphate, borate, germanate or tellurite systems. Even if they are not subjected to mass production due to their extremely higher cost manufacturing, poor chemical durability and very low mechanical strength, they hold exclusive properties that cannot be achieved by silicate glasses [44].

Phosphate based glasses are the most resistant to quenching concentration effect. Furthermore, they enable to dissolve larger amounts (compared to silicate) of rare earth (RE) elements in its composition ($\sim 10^{21}$ ions/cm³) compared to silicate ($\sim 10^{19}$ ions/cm³). For this reason, even if their fabrication has high costs, they are relevant for photonics devices such as lasers and amplifiers.

Tellurite based glasses exhibit low intrinsic absorption up to 5 μ m, which make them perfect for mid-IR spectral zone. Tellurite glasses have the higher chemical stability and corrosion resistance compared with other non-silica-based glasses. They are suitable to be stored in ambient air without becoming degraded. Furthermore, they present a high RE solubility ($\sim 10^{21}$ ions/cm³) like phosphates glasses [45], [46].

Nevertheless, these attributes did not feed the purpose of this project. The developed optical glass fibre sensors required an optical fibre suitable to be embedded in an epoxy and being chemically stable. Furthermore, it was required a OF able to handle some stress and fatigue during the fabrication of glass fibre reinforced composites, which the non-silicate glasses possess. Finally, the cost production for non-silicate oxide glasses is very important to consider since it was required to develop a low-cost optical glass fibre sensor.

2.5.3. *Fluoride ZBLAN*

Fluoride glass, such as the well-known ZBLAN (ZrF₄-BaF₂-LaF₃-AlF₃-NaF) is the most common heavy-metal fluoride glass. Before its discovery, the fluoride glasses were based on Na-F-NdF₃ systems. However, these were toxic and

hygroscopic making them very unsuitable for optical devices. In contrast, Zr-F₄ based glasses are not and become the interesting glasses for especial photonic applications.

ZBLAN fibres possess a transparent absorption until 6 μm [43], which make them appropriate for fibre laser devices in the mid-IR. This presents a great advantage versus the silicate and phosphorus fibres because SiO₂ and P based glasses struggle to reach the mid-infrared region. Furthermore, ZBLAN fibres are chemically stable. However, their fabrication has a high cost, more than the tellurite and phosphate-based glasses. Their high costs are because to produce the fluoride glass it is necessary to have ultra-pure raw materials must be ultra-pure and without absolute absence of water. Another important parameter that increases their cost is that they have low viscosity which makes the possibility to form crystals very easily. For these reasons, the ZBLAN glass fibre was also not preferable to elaborate the optical glass fibre sensors. Even having good mid-IR transparency, they were not suitable due to their cost of fabrication and extremely difficult manufacturing process.

2.5.4. *Chalcogenide*

Chalcogenide glasses have received increased interest during the recent years in many companies due to their unique features in sensing applications. This special glass is made from elements of the Periodic Table located in the III-V group, arsenic (As), selenium (Se), tellurium (Te), and germanium (Ge). One of the best properties is their suitability to produce optical glass fibre sensors that rely on an original spectroscopic technique called Fibre Evanescent Wave Spectroscopy (FEWS), [47].

Chalcogenide glasses have wide IR transparency, ranging from 2 to 25 μm . This presents the particularity capability to work in the middle and long IR range. They also present particularities of low optical losses and chemical stability as well as resistance to atmospheric moisture [48]. Nevertheless, to obtain a good chalcogenide glass with large IR transparency, it is crucial to manufacture the glass under the absence of oxygen, hydrogen, carbon and silicon [49]. For these reasons, this glass must be manufactured in a glovebox.

Chalcogenide glasses are widespread in industry. One of the most remarkable applications are lenses for thermal imaging. For example, the company UMICORE-

IR produces glasses with germanium, arsenic and selenium composition, commonly called GASIR glass. They are applied in the automobile market by companies such as BMW and TOYOTA. These glasses are specially designed for night vision devices, such as night cameras and night vision driving assistance [50]. Furthermore, they are used in electronics industries, in devices such as digital versatile disk (DVD) readers [49].

This project chose chalcogenide glasses to make a glass fibre sensor suitable to follow the cross-linking reactions of the resin and the detection of water and ethanol through the epoxy. Although expensive to produce, yet easy to fabricate, these optical fibres offered unique transmission properties to follow chemical reactions. With the fabricated fibre it was then possible to monitor the degree of conversion in polymers.

Table 2. 3. Comparison of selected glass fibre properties of the silica, phosphate tellurite, fluoride ZBLAN, and chalcogenide glasses [44], [51], [52], [53], [54], [55], [56], and [57]. These values may vary with changing the glass chemical compositions.

Glass property	Silica	Phosphate	Tellurite	Fluoride ZBLAN	Chalcogenide
Range transmission [μm]	0.2 ÷ 2.5	0.2 ÷ 4	0.4 ÷ 5.0	0.2 ÷ 6	0.8 ÷ 8
Glass transition temperature [$^{\circ}\text{C}$]	1000	461	300	260	300
Density [g/cm^3]	2.2	2.6	5.5	4.3	4.5
Young modulus [GPA]	70	47	34	58	22
Fibre loss [dB/Km]	0.2 @ 1.5 μm	15·10 ³ @ 1.05 μm	50 @ 1.2 μm	0.65 @ 2.59 μm	12 @ 3 μm
RE solubility	10 ¹⁹ ions/cm ³	10 ²¹ ions/cm ³	10 ²¹ ions/cm ³	10 ²¹ ions/cm ³	0.1 mol%
Abbe number	68	68	10 ÷ 20	76	NA

2.6. Introduction to optical fibres

2.6.1. Basic concepts about light propagating in optical fibres

Light is an electromagnetic radiation which plays the most important role in optical fibres. Light can be transported along the fibres and can be disturbed to produce new signals. In order to further understand how an optical glass fibre can be used as a sensor it is necessary to discuss what light is, how it works and why it can be altered.

Light is defined as an electromagnetic radiation having a spectral distribution (i.e. from one to several frequencies). The wavelength range of electromagnetic waves that is conventionally called “light” ranges from 10 nm to 1 mm and it is normally divided into three sub-ranges: ultraviolet light (UV), visible light (VIS), near infrared (NIR), and infra-red (IR) light. Figure 2. 8. shows the complete spectrum of the electromagnetic frequencies. UV light ranges from 10 nm to 400 nm. Visible light goes from 400 nm to 700 nm, and IR is found between 700 nm to 1 mm. Optical communication uses light as the carrier and uses the range between 850 to 1550 nm fall between the ultraviolet and microwave frequencies in the light spectrum [58].

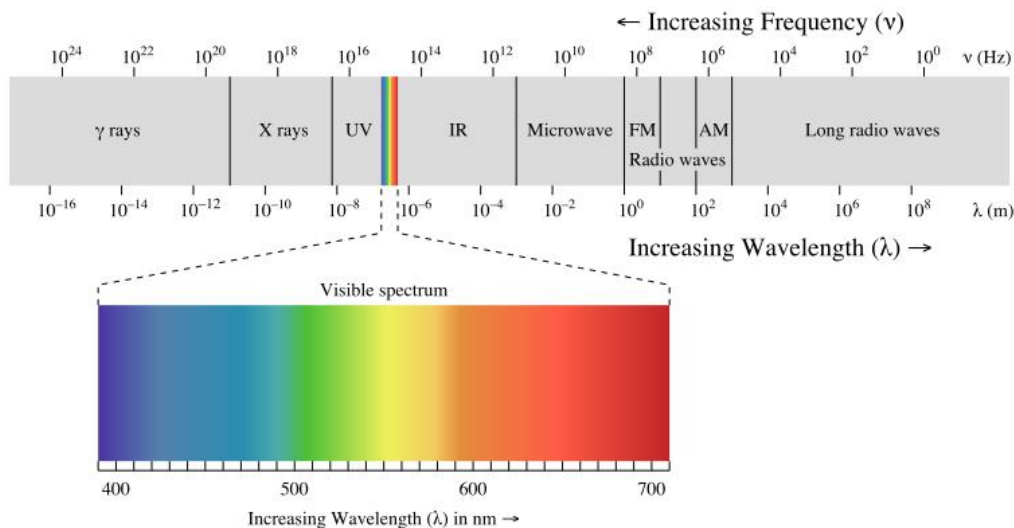


Figure 2. 8. Scheme of the full electromagnetic frequencies, where the light spectrum is found.

In optics, the refractive index describes the way light propagates through a medium. For this reason, the speed of light in a medium is minor than in vacuum

“ c ”, where there are not dipoles to interact. The ratio between speeds of light in the vacuum versus the medium “ v ” is called the refractive index “ n ”, (Eq. 1.1):

$$n = c/v \quad (1.1)$$

Thus, the electromagnetic wave velocity “ v ” in a dielectric medium is physically defined as, (Eq. 1.2):

$$v = 1/\sqrt{\epsilon_r \epsilon_0 \mu_0} \quad (1.2)$$

where ϵ_r is the electrical relative permittivity, ϵ_0 is the electrical permittivity and μ_0 is the magnetic permittivity.

If light travels in vacuum conditions, ϵ_r becomes 1, where (Eq. 1.3):

$$v = 1/\sqrt{\epsilon_0 \mu_0} = c = 3 \cdot 10^8 \text{ms}^{-1} \quad (1.3)$$

Hence, the refractive index can also be expressed as (Eq. 1.4):

$$n = \sqrt{\epsilon_r} \quad (1.4)$$

As the relative permittivity depends directly on the frequency of the wave, the refractive index also becomes dependent. This is called dispersion and it is expressed by the Abbe number, where a small Abbe number represents a high dispersion, (Eq. 1.5).

$$v_d = n_d - 1/n_f - n_c \quad (1.5)$$

where n_d is the Helium d-line (wavelength: 587,56 nm), n_f is the f-line of Hydrogen (wavelength 486.13 nm), and n_c is the H c-line (wavelength: 657.27 nm).

In a dielectric material, the electric field E presence causes, slightly, the bound charges in the material creating a local electric dipole moment. Hence, the electric displacement field D can be expressed (Eq. 1.6):

$$D \equiv \varepsilon_0 E + P \quad (1.6)$$

In a homogenous, linear and isotropic dielectric material, the polarization P is aligned and proportional to the electric field. Thus, (Eq. 1.7):

$$P = \chi^1 E^1 \quad (1.7)$$

where the proportionality coefficient χ^1 is called linear electrical susceptibility.

If the relation of the equation 1.5 is not linear, such as in a high-power laser beam, the expression becomes the summation of electric fields multiplied by each different polarization coefficient, (Eq. 1.8):

$$P = \chi^1 E^1 + \chi^2 E^2 + \chi^3 E^3 \quad (1.8)$$

where χ^2 and χ^3 are the second and the third susceptible nonlinear order, respectively.

In an isotropic material such as glass, the second order of the non-linearity, $\chi^2 E^2$, is equal to zero and the nonlinearity above the four becomes negligible and can be discarded, thus the eq. 1.7, becomes, (Eq. 1.9):

$$P = \chi^1 E^1 + \chi^3 E^3 \quad (1.9)$$

Therefore, in glass, the refractive index n varies with the intensity I of light, (Eq. 1.10):

$$n = n_0 + n_2 I \quad (1.10)$$

where n_0 is the linear refractive index when the relation in the expression (1.6) holds, and n_2 is the nonlinear reflective index, expressed in m^2/W [43].

The defined non-linear refractive index, introduced above, can have a huge contribution in high intensity applications. Nevertheless, in the presented sensors of this research the experiments were made with low-intensity signals and therefore the non-linearity of refractive index is negligible.

2.6.2. Refraction, reflection, critical angle, and total internal reflection

The phenomena of refraction, reflection and critical angle were firstly observed and described by the physician Ptolemy on 1021 in Egypt, but it was not until the mathematician Willebrod Snell in 1621 in Germany, that the relationship between the light beam crossing different media was. But it was not until 1621 by the Dutch mathematician and astronomer Willebrod Snell when the relationships of these phenomena were described. This is nowadays known as the Snell's law. In order to describe how the Snell law works, Figure 2. 9. shows an example of light travelling through water towards the boundary with another material such as air, which is a less dense material, which shows the three mentioned possibilities that can occur when the incident beam changes the material. The Snell's law describes the relationship between the incident and the refracted ray between two different media, [59], and it is expressed with the following (Eq. 1.11):

$$n_1 \sin \theta_1 = n_2 \sin \theta_2 \quad (1.11)$$

When a beam of light travels in a media with a refractive index n_1 and encounters a different media with different refractive index n_2 the light can be refracted or reflected. The incident ray changes the direction because the speed of light changes in different media. So, refraction can be defined as a change in direction of propagation of a wave when the wave changes the medium [60]. The refraction follows the Snell Law described in the equation 1.11.

Reflection occurs when the incident ray reaches the boundary and at least some part of the incoming ray remains in the same medium. Assume the incoming ray makes an angle of θ_i with the normal plane tangent to the boundary. This ray will make an angle θ_r with the normal tangent and lies on the same plane as the incident ray. Hence, it is produced the reflection (Eq. 1.12):

$$\theta_i = \theta_r \quad (1.12)$$

The critical angle occurs when the angle of incidence in water reaches a certain critical value, the refracted ray lies along the boundary, with an angle of refraction of 90-degrees. This is the largest angle of incidence for which refraction can still occur and the light will travel along the boundary interface [61]. Total internal reflection (TIR) occurs when the angle of incident θ_i is larger and no light escapes

from the medium [60]. This angle is then called the critical angle θ_c , and it can be described with the following (Eq. 1.13):

$$\sin\theta_c = n_2/n_1 \quad (1.13)$$

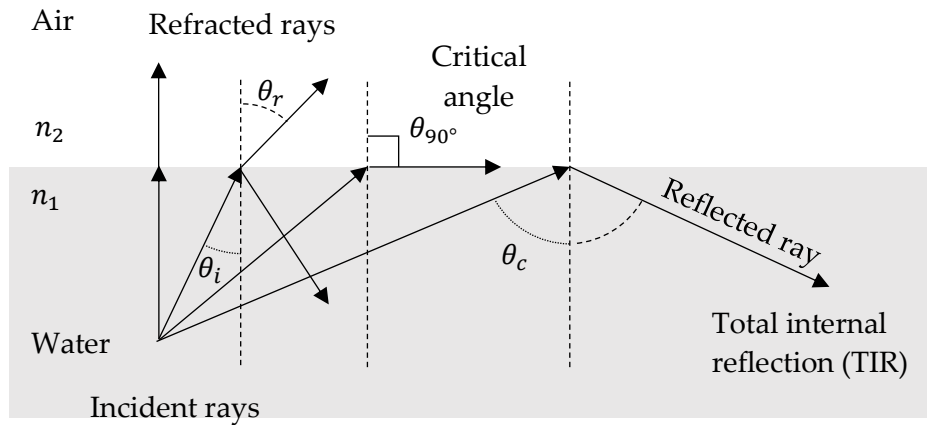


Figure 2. 9. Scheme of the refraction, critical angle, and reflection principles. The incoming ray is found in water, with a refractive index n_1 , and the out-coming ray in air with refractive index n_2 .

The total internal reflection is the simplest way to explain how an optical fibre works. Figure 2. 10. a scheme of one optical fibre where it operates on the principle of total internal reflection. This phenomenon has the property to keep the light confined inside the core and to guide light along the length of the optical fibre. OF cores have a higher refraction index, n_{core} , than claddings, $n_{cladding}$ ($n_{core} > n_{cladding}$, [62]).

However, there is always some part of the electromagnetic radiation that penetrates the boundary, which is explained using the mode theory of light.

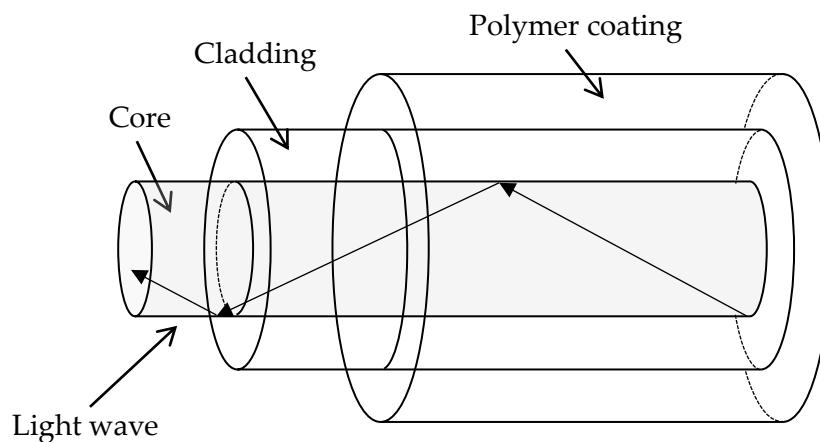


Figure 2. 10. Scheme of the refraction, critical angle, and reflection principles. The incoming ray is found in water, with a refractive index n_1 , and the out-coming ray in air with refractive index n_2 .

2.6.3. Basic structure of an optical fibre

Optical glass fibres are normally composed of three parts: the core, the cladding, and the polymer coating (Fig. 2.11.). The core and the cladding are made primarily of highly purified silicon dioxide (SiO_2), [63], often doped with different compounds to trim the refractive index and other optical properties. The high purity is obtained in the now-outmoded crucible manufacturing method. This consists of spread liquid silicon tetrachloride (SiCl_4) in a stream of pure gaseous oxygen (O_2). Furthermore, germanium tetrachloride (GeCl_4), and phosphorus oxychloride (POCl_3) can be used as other chemicals to produce the highly pure silicon dioxide, [64].

The degree of the manufacturing glass is strongly linked with the fibre losses. For this reason, it is crucial to have a very pure glass to have less losses.

The core, normally made of glass and formed by a cylindrical rod of dielectric material, is where light is confined and propagated. The cladding englobes the core, which has a lower refractive index to accomplish the condition explained above ($n_{core} > n_{cladding}$, [62]). Furthermore, the cladding has other function such as reduce light losses from the core to the surrounding environment, reduce the scattering loss at the boundary between the core and the cladding, protects the core for possible absorbing contaminates, provides mechanical strength. Finally, the

optical fibre is protected typically using a polymer coating. This has the finality of improve the mechanical strength, protect the optical fibre against moisture, and prevents the scattering losses produced by micro bends. Once the fibre is coated, it can be rolled in a buffer, which can be subsequently transported.

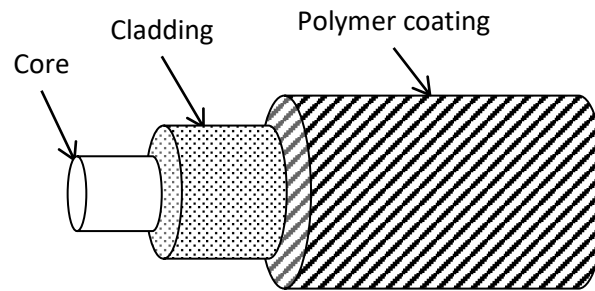


Figure 2. 11. Optical fibre scheme.

2.6.4. *Acceptance angle and numerical aperture*

Light propagates along inside the fibre by multiple TIRs at the core/cladding boundary. However, only the light rays that are launched with a certain angle can propagate. The angle at which the first refraction occurs is the most critical and it is special because it commands the subsequent internal reflections following the TIR principle. This angle is called the acceptance angle (Fig. 2.12.), [65], [66]. Hence, an incident light beam can only be guided in the OF if it is in the acceptance cone range. The acceptance angle, which is the half-angle of the cone, is called α_{max} . This value is directly linked with the fibre composition, the geometry of the fibre and the refractive index of the core and cladding. Figure 6 shows the conditions in which the ray is propagated or lost [67].

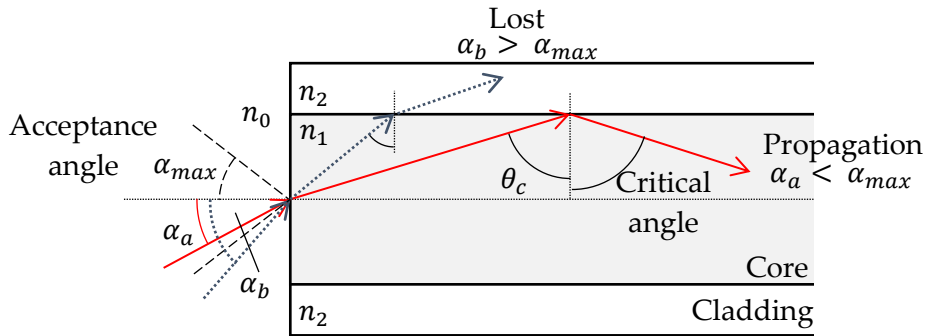


Figure 2. 12. Acceptance angle of an optical fibre where the light ray that accomplish the conditions of the $\alpha < \alpha_{max}$ is propagate by TIR.

The acceptance angle can be calculated with the following (Eq. 1.15).

$$\theta_x = \sin^{-1} \left(\frac{n_1}{n_x} \sin \left(\frac{\pi}{2} - \theta_c \right) \right) \quad (1.15)$$

Figure 2.13 shows an example of a planar illustration, but in reality, the optical system has an aperture like a cone, which can collect the light incident on it is called numerical aperture (NA) (Fig. 2.13), [68], [69].

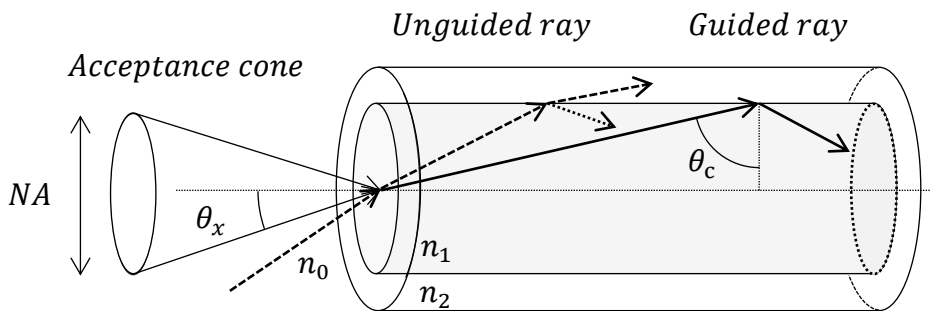


Figure 2. 13. Scheme of the numerical aperture of an optical fibre. Rays within the acceptance cone are guided by total internal reflection.

The maximum value of α defined as maximum angle, α_{max} , of acceptance, and $n_0 \cdot \sin \alpha_{max}$ is called numerical aperture (NA). When the condition in which $\theta_x = \theta_c$, the maximum value admitted for α is given. Therefore, applying the Snell law at the boundary between n_0 and n_1 , (Eq. 1.16):

$$n_0 \cdot \sin\alpha_{max} = n_1 \cdot \sin\left(\frac{\pi}{2} - \theta_c\right)$$

or

(1.16)

$$n_0 \cdot \sin\alpha_{max} = n_1 \cdot \cos\theta_c = n_1 \sqrt{1 - \sin^2\theta_c}$$

At these conditions, the TIR is given (Eq. 1.16) where the critical angle of incidence in denser medium (n_1) has an angle of refraction of $(\pi/2)$. Therefore (Eq. 1.17):

$$n_0 \cdot \sin\theta_c = n_2 \cdot \sin\left(\frac{\pi}{2}\right) \quad (1.17)$$

Thus, (Eq. 1.18):

$$\sin\theta_c = n_2/n_0 \quad (1.18)$$

Thus, substituting the angle θ_c , the numerical aperture NA, (Eq. 1.19) can be written:

$$NA = n_0 \cdot \sin\alpha_{max} = n_1 \sqrt{1 - \frac{n_2^2}{n_1^2}} ;$$

$$NA = n_0 \cdot \sin\alpha_{max} = (n_1^2 - n_2^2)^{\frac{1}{2}} ;$$

$$NA = (n_1^2 - n_2^2)^{\frac{1}{2}}$$

(1.19)

The importance of NA is that it promotes light propagation through the fibre, which is considered the light gathering capacity of fibres. The higher the value of $n_0 \cdot \sin\alpha_{max}$ or NA, the greater is the light which can be collected and propagated in the fibre.

2.7. *Light propagation, the optical fibre communications basics*

In his famous experiment Isaac Newton put a prism on a beam of light projected on his window, revealing the full visible light spectrum. He observed how white light can be disassembled and reassembled using a prism. This phenomenon was described in his book *Opticks*, [70]. The phenomena described by Newton holds the basics of reflection and refraction, which are based on the ray theory, or geometrical optics.

After the postulation of Newton in 1671, two theories can explain light propagation through glass fibres. These are ray theory, which describes light as a simple ray, and the Mode theory, which describes the propagation of light as an electromagnetic wave.

2.7.1. *Ray theory*

The ray theory, or geometrical optics, is explained with two types of rays, meridional rays and skew rays and follows the TIR principle. Figure 2. 14. shows a representation of meridional rays, which are defined as the rays that travel along the fibre crossing the symmetry axis, and skew rays, which propagate in a helical path [65].

Meridional and skew rays follow reflection and reflection theory, in which part of them remain reflected in the core and part of them are refracted and escape in the cladding of the OF. When the rays are in the cladding, two situations can occur. In the first situation, the ray becomes reflected again on the boundary between the cladding and the buffer, and the ray return into the core. This is an ideally situation where the core-cladding interface is completely perfect. In the second situation, the ray becomes refracted again and it is lost. Currently, this is more realistic situation where the core-cladding boundary is not perfect, and the formed imperfections refract out the light of the core. Normally, these rays are used to illustrate a light beam transmission in optical fibres [71], [72]. In general, meridional ray are subjected to the laws of reflection and refraction and for this reason, it is crucial to have the light ray well guided with a certain cone as the previous section explains.

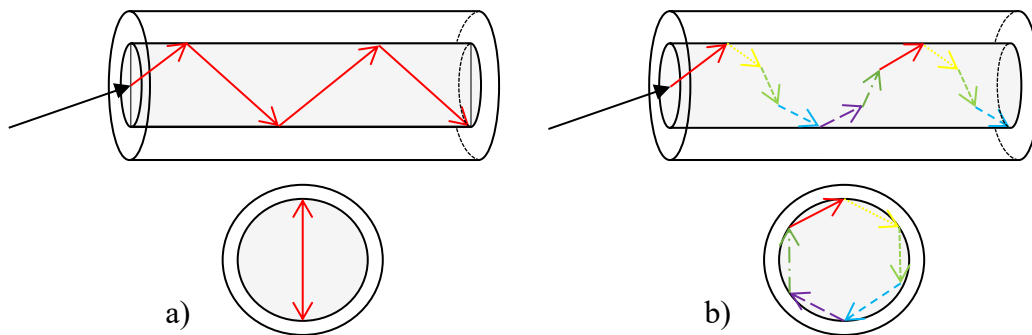


Figure 2. 14. a) Scheme of meridional rays, which travel along the fibre crossing the symmetry axis. b) Scheme of skew rays, which propagate in a helical path.

2.7.2. Mode theory

The mode theory describes the propagation of light into an optical fibre as an electromagnetic wave. This theory can describe light properties that the ray theory is unable to define because it can explain how light can be propagated and guided along the fibre.

In order to understand these modes, the mode theory views the light as a sum of plane waves. A plane wave compresses the light properties of direction, amplitude, and wavelength propagation. The plane wave is also defined as a wave whose surfaces of constant phase are infinite parallel planes normal to the direction of propagation. When the planes have the same phase, they called wavefronts, in which the wavelength (λ) is given by (Eq. 1.20):

$$\lambda = c/(f \cdot n) \quad (1.20)$$

where c is the light speed in the vacuum, f is the light frequency, and n is the refraction index of the medium where the plane wave propagates.

Figure 2. 15. shows an illustration of the direction and wavefront of plane-wave propagation. These propagate through the fibre like the light rays. Not all wavefront incidents on the fibre angles are being propagated, even if wavefronts have an acceptance angle less than or equal to the critical angle. The wavefront must be in phase in order to be transmitted along the fibre. If the propagating wavefronts are not in phase, they can create a destructive interference and disappear. This is the

explanation for why only a finite number of modes can propagate along the fibre [74], [75].

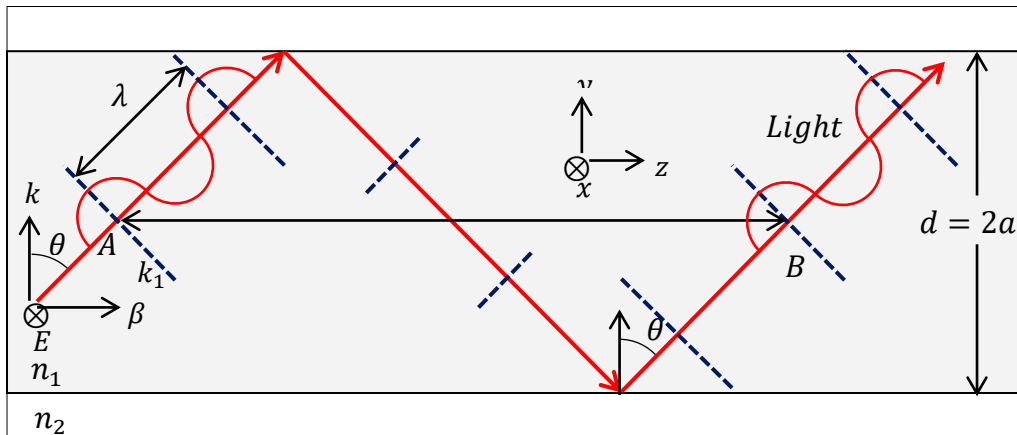


Figure 2. 15. Scheme of wavefront propagation along the fibre. In order to be propagated, the electromagnetic wave cannot be destructive.

When the plane waves travel along the fibre axis, they repeat themselves and these are assumed to be in z axis direction. The repetition distance of the plane wave (φ_z) is (Eq. 1.21):

$$\varphi_z = \lambda/\sin\theta \quad (1.21)$$

Hence, plane waves also repeat the periodic frequency, (Eq. 1.22):

$$\beta = 2\pi \cdot \sin\theta/\lambda \quad (1.22)$$

Thus, the constant propagation along the fibre axis I defined as a quantity of beta (β), where if the λ changes the propagation value.

When a mode is no longer bound to the fibre it is said to be cut off. For an optical fibre, the cut of angle of linear polarized (LP) mode sets the limitations of the mode propagation. Nevertheless, an optical fibre is always able to transmit one mode, which is called the fundamental mode. Fibre cut-off wavelength is the wavelength that inhibits the subsequent higher mode of propagation.

The electromagnetic waves or modes were described by Maxwell [75] and have two components. These are the electric field, $E_{x,y,z}$, and the magnetic field, $H_{x,y,z}$,

which are found at right angle ($E \perp H$). In an optical fibre, the modes propagate along the axis of the fibre and these are called transverse electric (TE) modes. TE modes are in perpendicular direction to the propagation path. Another type of transverse mode is the transverse magnetic (TM) mode, which is the opposite of TE modes.

TE mode fields set a pattern. This pattern is identified with a mode number $m=0, 1, 2$, etc. Figure 2. 16. shows the first three order modes field patterns travelling along the fibre. The order of each mode is described by the number of field maxima, TE. For instance, TE_0 has only one field maxima and is considered the fundamental mode. The maximum of E is found in the centre of the optical core and decays toward the cladding boundary. As higher the TE rises, higher-order modes are found. It can be observed that modes are not perfectly confined in the fibre core. Modes are partially extended in the fibre cladding. Low order mode slightly penetrates the cladding because E and H are concentrated near the fibre core centre. High order modes are more intense in the fibre cladding because the E and H are distributed in different parts of the fibre core. They are called cladding modes.

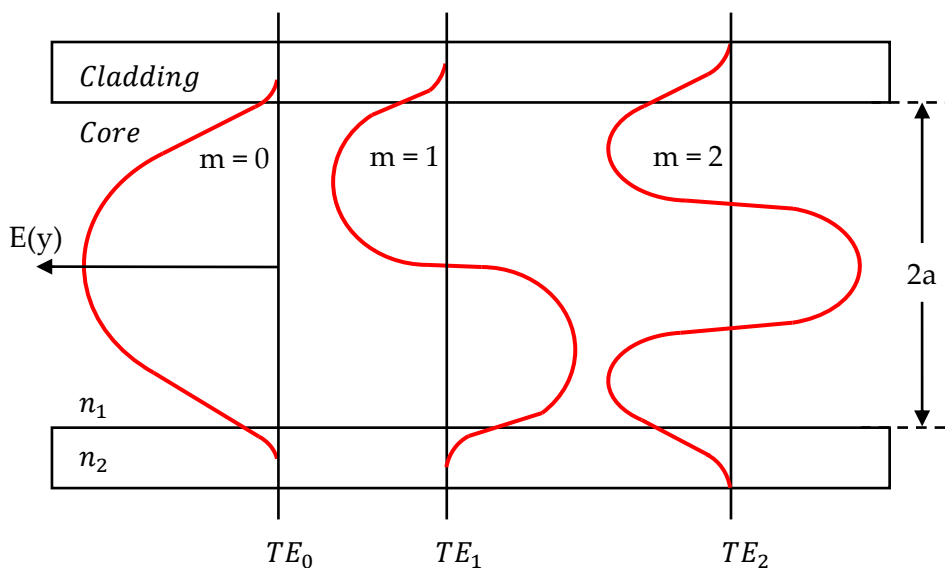


Figure 2. 16. Transverse electric (TE) mode field patterns.

Figure 2. 17. shows how the angle of the wavefront can also determine the order of modes. Higher order modes cross the axis with higher angle compared to lower modes, and the lowest mode travels nearly parallel to the fibre axis. Due to these modes, the light pulse that enters in the optical structure is broken into various

modes. Consequently, the modes propagate at different group velocity and emerge at the end with a broadened light pulse.

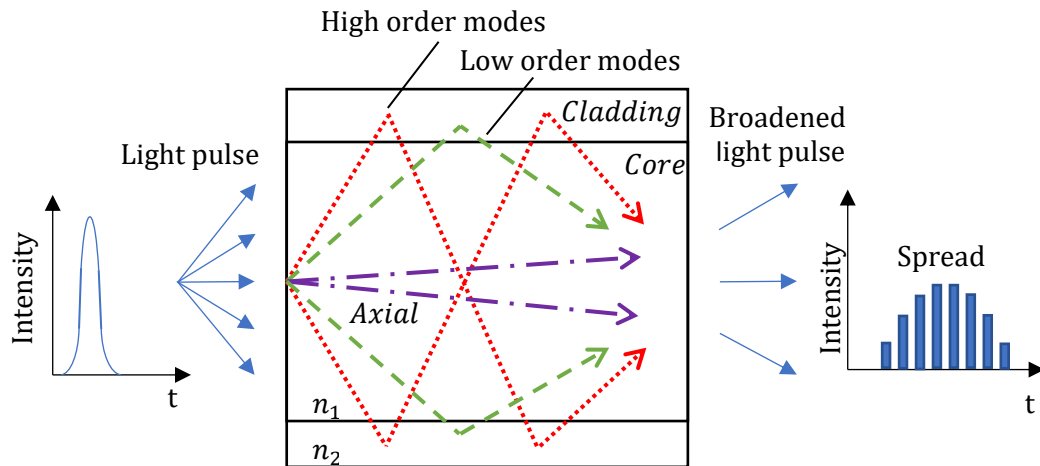


Figure 2. 17. Light pulse travelling in a waveguide optical structure where the initial signal is broken into various modes. The emerging signals is broadened [76].

Because of the modes travel through the fibre core and the fibre cladding, the mode coupling occurs. Mode coupling is the exchange of power between two modes, and results in a power loss of the core modes. Furthermore, leaky modes appear. Leaky modes lose power along the fibre propagation. Commonly, modes leaked in the cladding become lost in a few centimetres. Nevertheless, leaky modes possess a large amount of power in short fibres. A certain condition is necessary for a mode to remain within the core. A mode can remain bounded if the propagation constant, β , has the following boundary condition: (Eq. 1.23). When the propagation constant is small and becomes smaller than β the modes can leak out of the core and end up in the cladding, where they become lost, [73].

$$\frac{2\pi \cdot n_2}{\lambda} < \beta < \frac{2\pi \cdot n_1}{\lambda} \quad (1.23)$$

where n_1 and n_2 are the index of refraction for the core and the cladding, respectively.

The normalized frequency, V , is an important parameter that can describe the amount of modes that a fibre can support. The mode number increases when the value V increases [68], [77], [78]. V is a dimensionless quantity expressed by the (Eq. 1.24):

$$V = \frac{2\pi \cdot n \cdot a}{\lambda} \cdot NA; \quad (1.24)$$

$$V = \frac{2\pi \cdot n \cdot a}{\lambda} \cdot (n_1^2 - n_2^2)^{\frac{1}{2}}$$

where n_1 is the core index of refraction, n_2 is the cladding index of refraction, a is the core radius, and λ is the wavelength of light in air.

Geometry (a) and refracted index (n_1 and n_2) determine the V number in function of a given wavelength λ . Hence, this is a characteristic parameter of the optical fibre. For a value $V \leq 2.405$ only the fundamental mode can propagate, while high order modes are lost in the cladding. This behaviour is a typical property of the single mode (SM) fibre. The V value should remain near 2.405 for an effective propagation, otherwise, for low V values (≤ 1.0) the propagation ends in the cladding and is lost due to fibre bends, [79].

When the V value is higher than 2.405 the number of modes suddenly increases. This kind of fibres are called Multimode (MM) fibres. The number of modes M that a MM fibre can support can be calculated approximately as (Eq. 1.25):

$$M = \frac{4}{\pi^2} V^2 \quad (1.25)$$

2.7.3. *The single-mode SM fibres and the multi-mode MM fibres*

OF are basically split in two types, the optical single mode (SM) fibre and the optical multi-mode (MM) fibre. SM fibre normally has a diameter of 8.3 to 10 microns. It has only one mode of transmission, which typically propagates a wavelength between 1310 nm to 1550 nm [80]. SM carries higher bandwidths than the MM fibre, however it, requires a light source with a very narrow spectral width. Furthermore, SM provides a higher transmission rate and up to 50 times more distance than MM fibres. Unfortunately, SM fibres are more expensive than MM fibres. The small core and the single light wave eliminate the distortion produced from the overlapping light, which provides the lowest signal attenuation and the highest transmission speed of any kind of fibre. MM fibres have a bigger core size than SM fibres. They have a core diameter between 50 to 100 microns. The most

common size is 62.5 microns. MM fibres give a high bandwidth at high speeds over medium distances. The light waves are dispersed into numerous paths or modes, which typically travel from 850 to 1300 nm [81].

Nevertheless, in long fibre distances like one kilometre, the multiple paths can cause a signal distortion. This distortion can result in an unclear or missing data transmission.

The SM fibre and the MM fibre present two additional important characteristics, the cut-off wavelength and the feed mode diameter. The cut-off wavelength, for any mode, is defined as the maximum wavelength at which the mode will be propagated. In other words, it is the wavelength that the optical fibres can sustain. The wavelengths below the cut-off can only support one mode, and it is determined by the refractive index, geometry (a) and V . The feed mode diameter refers to the numerical aperture of the core size. The numerical aperture is the measure of the light angle range accepters and depends on the refractive index of the OF. The core diameter is the fundamental design of the MM fibre. The larger the core, the higher the amount of light that can be propagated, but the more distortion will appear.

2.7.4. *Step-index and graded-index fibres*

Figure 2. 18. shows a typical step-index profile with an optical fibre representation, where the x axis shows fibre radius and y axis represents refractive index. The refractive index of the fibre core (n_1) is higher than the refractive index of the cladding (n_2). So, the core has a high refractive index and step down to low refractive index of the cladding ($n_1 > n_2$). Therefore, it is called step-index. This is a typical structure of SM fibres, but it can be also found in MM fibres.

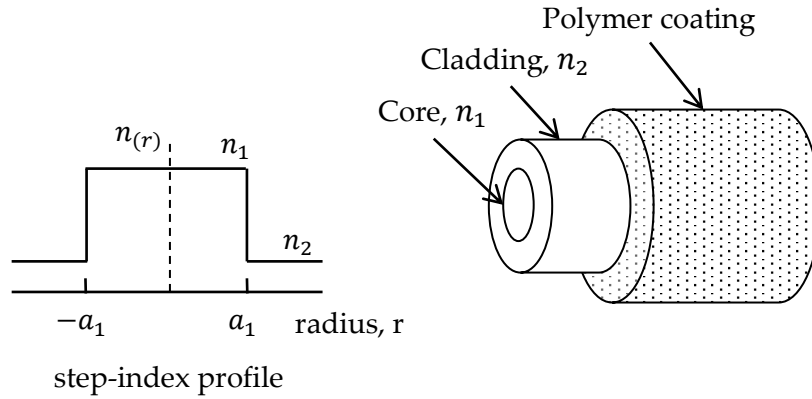


Figure 2. 18. Light pulse travelling in a waveguide optical structure where the initial signal is broken into various modes. The emerging signals is broadened [80].

In a step-index fibre, the modes (light ray travelling along the fibre with a particular angle) must have particular conditions, the normalized frequency (V) and the mode propagation constant, β_m , which depends on the mode and in general varies with the frequency or wavelength. This quantity is always between the plane propagation constant (wave number) of the core and the cladding media (Eq. 1.26), [76].

$$n_2 k < \beta_m(\omega) < n_1 k \quad (1.26)$$

At each frequency or wavelength, there exist only a finite number of guided or propagating modes that can carry light. Each of these modes can propagate in the fibre only if the frequency is above the cut-off frequency, ω_c , obtained for the cut-off condition (Eq. 1.27), [76].

$$\beta_m(\omega_c) = n_2 k \quad (1.27)$$

Solving the equations of the step-index fibres we can obtain the graph below (Fig. 2. 19. where the lines represent the different modes and V number is determined by the construction of the fibre such as the geometry, refractive index of core and cladding, and the wavelength (Eq. 1.28), [76].

$$\Delta = n_1^2 - n_2^2 / 2n_1^2 \approx n_1 - n_2 / n_1 \quad (1.28)$$

where Δ is the fractional change in the index of refraction.

From the graph it is seen that when the V number is less than 2.405 only one mode can propagate, while when it is higher more than one mode can propagate at the same time.

MM fibres typically have larger core sizes allowing more than one mode propagation. However, when more than one mode propagates occurs the dispersion and the light is spread since the different modes travel at different velocity. In order to solve this issue, the graded-index fibre was created [76]. This fibre forces the wavelength to converge in different points along the fibres avoiding the dispersion (Fig. 2. 20.).

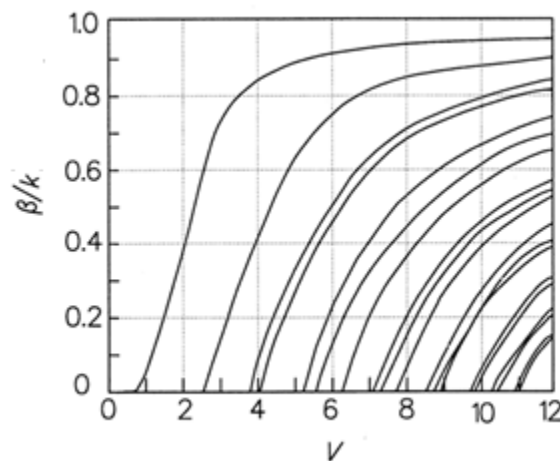


Figure 2. 19. V number graph example construction, (adapted from [76]).

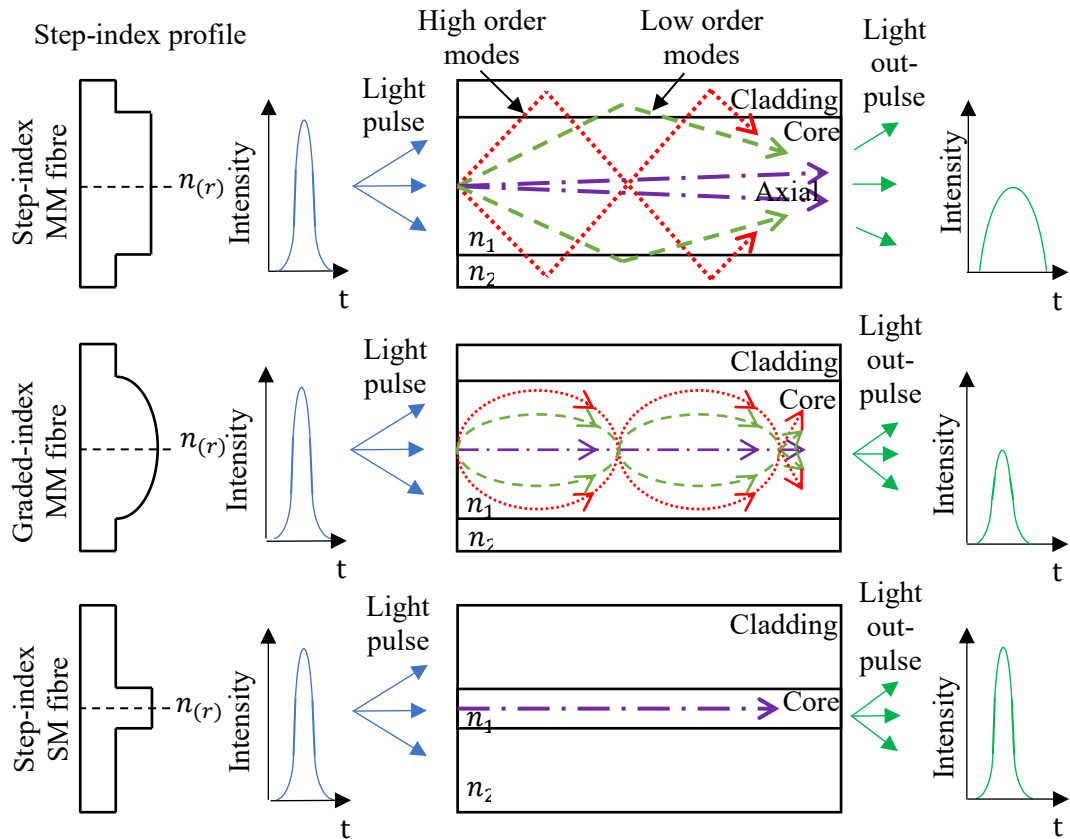


Figure 2. 20. Scheme illustration of the light pulse travelling in different fibre step-index profiles.

2.7.5. Optical fibres fabrication

In order to make an optical fibre, it is necessary to prepare the rod perform. This consist of a small cylinder, or rod, of ultra-pure silica, which will form the core of the future OF. This is inserted in a tube, the future cladding, which has 1 % of impurities as it was explained previously (Fig. 2. 21.).

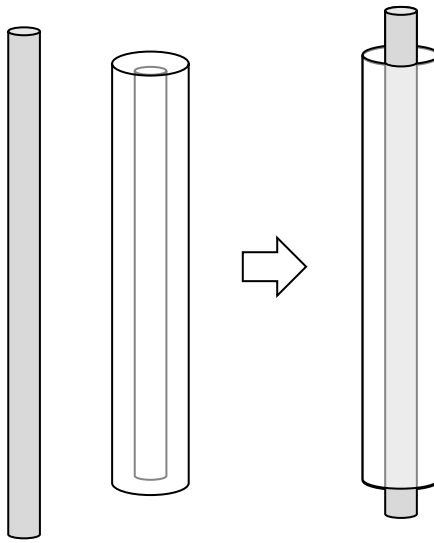


Figure 2. 21. Scheme of the rod-tube-technique. On the right, ultra-pure rod of silica represented on blue. In the middle, tube of the ultra-pure silica with 1% of impurities added. On the left, the perform rod.

Before heating the rod, an inert gas such as argon must be pumped in to create an inert atmosphere, which will prevent the formation of impurities. Most importantly, the impurities can undergo as formation of crystals at the edges of the fibre walls, which produce the scattering of the electromagnetic wave and reduce the transmission. Furthermore, the crystals effects on the mechanical integrity and robustness of the OFs.

The preform rod is then placed in the drawing tower where is heated until the glass reaches a viscosity of approximately $10^5 Pa$. When the heat is applied in inert conditions, the cladding tube collapses around the ultra-pure rod under effect of gravity and surface tension [82].

Then, the silica perform rod starts to draw producing a necked OF. The first filament, called noodle because it has a heavy end, is passed through the diameter controller and the tension-meter. This is the most difficult stage. The diameter and fibre structural control is the most difficult achievement and it can be controlled by tuning the speed and the preform feeding of the drawing tower. Thus, the fibre diameter, d_{fibre} , can be calculated by the following (Eq. 1.29). By controlling the temperature and the tension-meter accurately, the selected diameter of the fibre can be produced.

$$d_{fibre} = d_{preform} (v_{preform} / v_{fibre})^{1/2} \quad (1.29)$$

where $d_{preform}$ is the preform diameter, $v_{preform}$ is the preform feed speed and v_{fibre} is the pulling speed.

If a thin polymer coating of polyamide or acrylate is applied and the fibre becomes coated. An optical glass fibre without a polymer coating is extremely fragile and therefore unsuitable for most applications. Finally, the fibre is attached to the drum and rolled. Figure 2. 22. shows the advanced silica glass fibre technology drawing tower [82], in which the ultra-pure silica rod is placed in the sample holder.

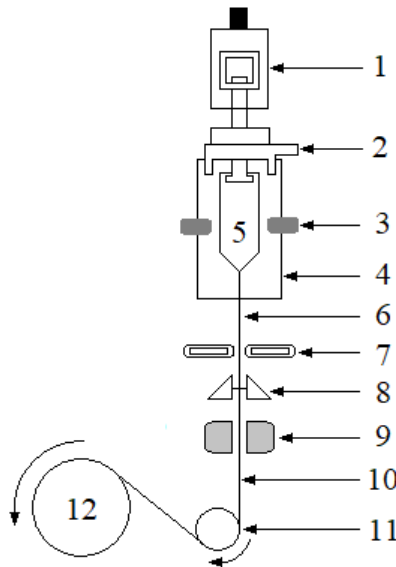


Figure 2. 22. Scheme of a drawing tower. 1: preform descent; 2: inert flux input; 3: ring furnace heater; 4: insulation air chamber protection; 5: specimen rod; 6: necked fibre; 7: diameter measurement; 8: polymer coating; 9: polymer heater; 10: coated fibre; 11: tension-meter; 12: drum

2.8. Conventional humidity sensing techniques

Focusing on the ageing of the GFRP produced by the moisture and humidity, traditional humidity sensors are briefly described in order to compare them with the new technologies' sensors.

2.8.1. *The chilled mirror hygrometer*

In the last forty years metrology laboratories and industries have used the chilled mirror hygrometer due to its high measurement precision. The device presents a standard deviation of ± 0.1 °C. It is employed to make standard calibrations of other humidity sensors [83]. This device works with an optical technique, which uses the dew point temperature phenomenon. It works by reading the signal in an optoelectronic module, or photodetector, from the reflected signal of the temperature-controlled reflective condensation mirror, also called thermoelectric cooler. The LED pump in a light beam on the mirror surface, in which light is then collected by the optoelectronic module. When the gas condenses on the mirror surface, the light intensity beam collected in the optoelectronic module decreases and indicates the percentage of humidity (Fig. 2. 23.). However, it requires high maintenance due to the possibility of surface mirror contamination and it is an expensive device.

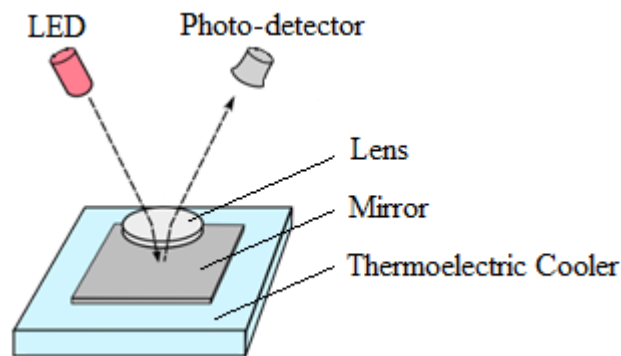


Figure 2. 23. Scheme representation of the chilled mirror hygrometer (adapted from [83]).

2.8.2. *The infrared optical absorption hygrometer*

Optical hygrometer detection and determination of the water vapour concentration is obtained by the absorption bands of water in the IR spectrum. Water has distinct absorption bands which can be detected by an IR analyser. This uses the dual-wavelength method principle based on the absorption of electromagnetic radiation. Furthermore, two transmittance measurements are required, one with dry air as a reference and the second with the sample with the water gas content (Fig. 2. 24.). The optical hygrometer method determines the attenuation of radiation in a waveband of the water vapour content along the path

between a source of radiation and a receiving device. This process is relatively expensive. The method is fast, it has good reproducibility, and presents a small standard deviation [84]. The sensitivity of the sensor depends on the instruments and the measurements are governed by the Beer-Lambert law [85] (Eq. 1.30), where the IR transmission through a transparent absorbing material is inversely proportional to the exponential function of the material concentration and the path length. However, this method cannot be used inside composites and a sample of the material must be extracted to analyse the water content of humidity or moisture.

$$\text{Absorbance } (A) = \log_{10} \frac{I_0}{I} = \epsilon lc \quad (1.30)$$

where I_0 is the intensity of the incident radiation, I is the variation of the intensity obtained, ϵ is the absorptivity, l is the pathway length and c is the concentration of the solution.

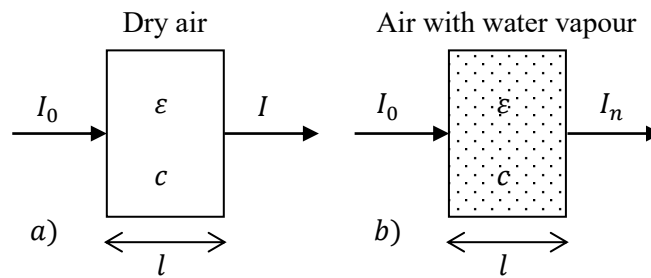


Figure 2. 24. Two transmittance measurements necessary for determining the concentration of water vapour [85].

2.8.3. Piezoelectric sensors

The high demand for small, reliable and low-cost sensors has led to the development of miniaturised electronic humidity sensors. These have the peculiarity of being compacted. They operate in capacitive, resistive and gravimetric methods. Lee and Lee [86] and Chen and Lu [87] have made reviews of these devices. Capacitive and resistive humidity sensors are the most frequent and represent approximately 75 % of the market of humidity sensors [88]. They basically operate using the changes given by a dielectric material. Resistivity based sensors operate on the changes of conductivity produced by the water absorption of the materials. These sensors are cheap and have low electricity consumption and

provide a good repeatability. However, they are susceptible to temperature changes and they can be chemically damaged through the water content impurities.

One of the most well-established testing techniques is the ultrasonic inspection. However, this technique requires a normal (perpendicular) interface between the transducer and the sample [89]. Giurgiutiu et al. [89] proposed an alternative is the use of active sensors. They are small, thin, and non-invasive. These can easily produce waves travelling in parallel to the surface sample and be detected by an ultrasonic detector. However, it is necessary to move the detector through the sample surface in order to obtain the data. For this reason, they are not suitable for buried or immersed pipelines.

The electro-mechanical (E/M) impedance method is a non-invasive sensor. This sensor consists on several piezoelectric active sensing points which produce an electrical field, which is read for the detector (Fig. 2. 25.). When the electrical field is compromised, a signal is produced giving the detection of the failure or corrosion. However, this technique is very susceptible to magnetic fields and temperature.

Yang et al. [90] fabricated a dielectric sensor by printing a circuit board were able to monitor the degree of cure of an epoxy and extrapolate the results to understand the epoxy ageing (Fig. 2. 26.). However, the sensor is not useful for long time due to it only register the degree of cure. It is also required to be connected in an electric system and need a parallel plate capacitor, which can become incompetent if the sensor and the capacitor are not in parallel.

Davis et al. [34] developed a sensor based on electrochemical impedance spectroscopy. This sensor was able to detect the diffusion through polymers. The moisture was detected by the electrical increment of the dielectric constant of the polymer because of the moisture absorption. However, this device is not suitable to be embedded while the curing of polymers is occurring due to the sensor must be put in completely dry conditions.

A big drawback of this device is that they can trigger fire, as they operate with electricity. They are electromagnetic, and therefore susceptible to electromagnetic fields. For these reasons industries such as petrochemicals refineries try to avoid these devices and do a great amount of research on OFSSs.

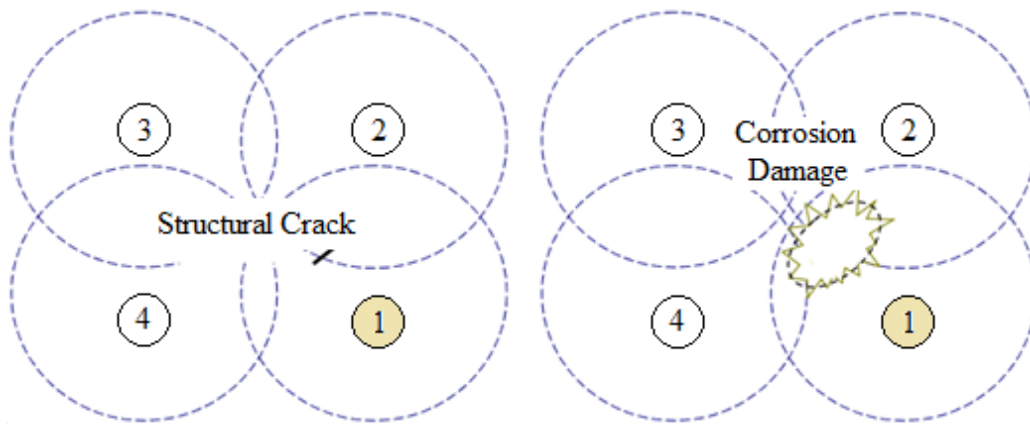


Figure 2. 25. Scheme of E/M impedance method of an array of 4 piezoelectric active sensors where a structural crack or corrosion damage can be detected (adapted from [34]).

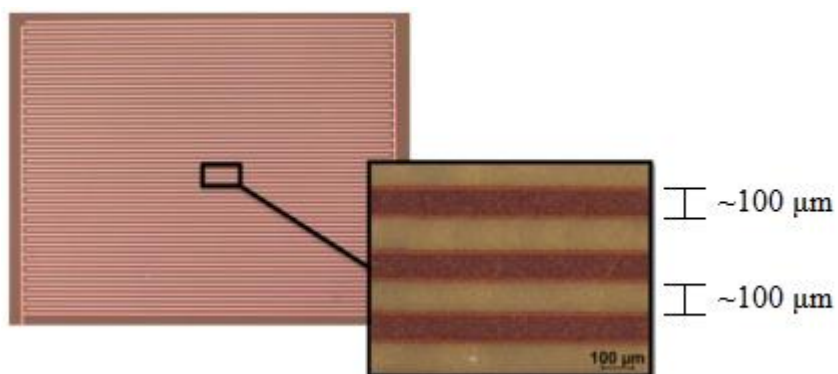


Figure 2. 26. Fabricated interdigital sensor (adapted from [91]).

Table 2. 4. Comparison of piezoelectric sensors.

Sensing method	Sensing approach	Ability to		Authors
		Moisture/humidity detection	Be embedded	
Capacitive and resistive	dielectric material	Yes	Yes	Lee and Lee [86]
Capacitive and resistive	dielectric material	Yes	Yes	Chen and Lu [87]
Electro-mechanical impedance	ultrasonic inspection	Yes	No	Giurgiutiu et al. [89]
Resistivity impedance	dielectric material	No	Yes	Yang et al. [90]
Electrochemical impedance spectroscopy	dielectric material	Yes	Yes	Davis et al. [34]

2.8.4. *Self-diagnosing fibre reinforced composites*

Self-diagnosing, or self-monitoring composites contain an electrically conductive phase such as carbon fibre, conductive fillers on their matrix or spread on their glass fibre plies. They are used for monitoring the stress, strain, temperature or moisture content in the material where they are embedded.

Neitzert et al. [91] engineered a self-diagnostic sensor for moisture detection mixing multi-wall carbon nanotubes (MWCNTs) with an epoxy resin. The smart material was immersed into distilled water in order to investigate the water resistance exposure and its mechanical stability, which were confirmed by more than 150 days. After the immersion, the authors registered a resistance increment around 5% as compared to the tested dry samples.

Tang et al. [92] created a very small non-invasive device to detect the water diffusion through polyimide/multiwall carbon nanotube (PI/MWNT) composite films (Fig. 2. 27.). The sensor works using the percolation phenomenon. The percolation results from the rapid appearance of electrical paths in a polymeric matrix when the percolation threshold is reached [93]. The increase of resistance of CNTs was analysed in terms of two main effects. The first one was related by the increment of the intrinsic resistance of the CNTs. The second one was explained by the so-called inter-tubes effect. CNTs can be separated into metallic (M) and semiconducting (S) type depending on their chirality. Thus, the result of the CNTs network outcomes from the barrier M/S types CNTs, which the tunnel effect plays a vital part for the electron transfer.

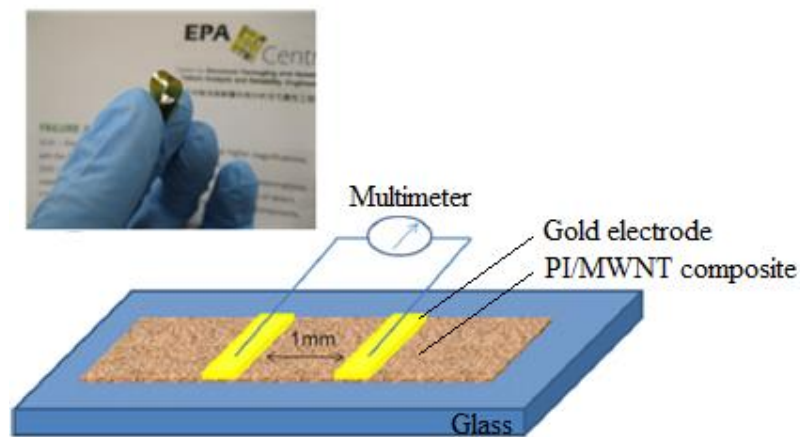


Figure 2. 27. Scheme of the sample PI/MWNT film. (adapted from [92]).

2.9. *Optical fibre sensors (OFSs)*

Optical glass fibres (OFs) is, without doubt, the crown jewel of 21st century telecommunications. It is thin, transparent, has flexible strength and is made from pure drawn silica, the optical glass fibre. Optical fibre is strong, flexible and reliable. It is stronger than steel and more durable than metallic copper. Fibre offers excellent signal performance over a wide range of environmental conditions. It can send video, voice and text data in the form of light signals at very high speeds. This revolutionary media is thinner than a human hair. It is composed by two basic elements of glass: the inner core and an outer cladding. The core, where the signal of light is transmitted and the cladding, which surrounds the core keeping the light confined and preventing its escape [94], [95].

After the invention of the OF technology, considerable research has been carried out in order to develop a low-cost optical fibre sensor (OFS). Because of advances and development, optical sensing has become a unique monitoring method in oil and gas industry. Optical sensing enables the transmission of large amounts of data over long distances. It has been widely employed in many sensing applications because of its immunity to radiofrequency interferences, able to work in harsh environments, and intrinsic fire safety. These features make the OFSs very attractive in the oil and gas industry, where conventional electric-based sensors may involve remarkable limitations in terms of remote operation, self-corrosion, and embedding complications. For instance, optical fibres can be used to monitor the water absorption of a GFRP pipes by monitoring the resistivity of the GFRP with low cost integrated circuits. However, their digital output must be readable within a few tens of cm, limiting remote operation. Moreover, embedded electric probes having ~ 1 mm in diameter may affect the mechanical properties of polymer composite structures.

The problem of continuous monitoring of the ageing/degradation of GFRPs occurs in real frameworks and is a challenging issue for companies that perform materials testing. They normally run the tests (e.g. diffusion of chemicals, pressure/thermal tests etc.) in dedicated machines where access to the sample is not allowed and changes of its characteristics can only be detected by subsequent inspections [96]. In these cases, it would be advisable to equip the sample with sensors that can be remotely interrogated:

- a. in real-time,
- b. without the need of power supply, visual or wireless access,
- c. reliably, withstanding the environmental conditions of the test.

Bare optical fibre sensors can be embedded into a GFRP composites without compromising its mechanical characteristics [97]. Furthermore, they can be interrogated remotely, in the range of kilometres or more. The scientific community has presented several applications where optical fibre sensors have been used to monitor physical and chemical properties in GFRP composites [97], [98]. Most of those applications are based on the well-established optical fibre sensors. These are the so-called fibre Bragg grating sensors [99].

There are two types of fibres. The first one is the single mode, which has a small core diameter designed to send light in only one direction in long distances.

It has high current information capacity and low attenuation and it is the most widely used in the world. The second is the multimode fibre. This has a larger core and allows light to travelling in multiple paths simultaneously. Typically, multimode fibres are used in local area networks and storage areas networks where it is more cost effective than single mode fibre [68].

Optical glass fibre sensors are one of the most remarkable sensing developments for communications and optoelectronics. Fundamentally, OFSs work by modulating the light properties such as, intensity, wave propagation, polarization, phase and wavelength. The capabilities of OFSs have been possible due to their production and fabrication, which has fallen during the last years. Photonics technology has become one of the primary sources of OFs. Nowadays, sensing applications of OFSs are replacing current electrical sensors, due to, the unique and particular approaches of the optic fibres [100].

OFSs run multiple sensing applications such as monitoring structures for strain sensing and damage detection in the field of oil & gas and infrastructures for buildings [101], [102]. They are also used for oxygen blood monitoring in the field of biomedicine [103]. They can also able to detect temperature, pressure, vibration, rotation, velocity, magnetic fields, acceleration and gyroscope [104], [105], [106]. Furthermore, in chemistry they also have contribution sensing to detect chemical species and their characteristics such as pH level [107], [108], [109].

Optical glass fibre principle operates in the total reflection in the inner core. This keeps the light in the inner core and guides the light along the length of the fibre. The principle of refraction refers to the bending of the light passing from one substance to the other. The glass used in the inner core has a higher reflective index than the glass used in the cladding. So, the light can be trapped in the core inner phase as it propagates along the fibre. OFSs may be defined by means of an interaction, which can be physical, chemical or biological, where the confined light in the fibre interacts with the environment. If the properties of the light become perturbed, they can produce a new different phase, intensity or propagation property in the light wavelength, which can be measured giving us a new outcome data. Figure 2. 28. illustrates a scheme which a light wavelength is propagated through an optical glass fibre and a light modulator of any species of interest, changes the wavelength function and modulates a new wavelength with a new phase. This new wavelength of interest is related to a target of interest which we can record.

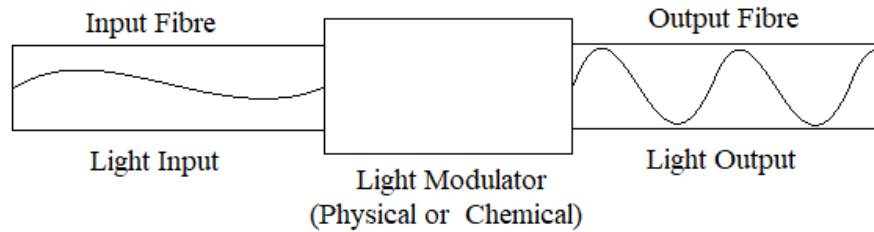


Figure 2. 28. Basic modulating arrangement of a basic optic sensor system.

These revolutionary sensors present advantages versus the conventional electric sensors because, compared to them, OFSs have distinct characteristics that the conventional sensors cannot achieve, such as:

- a. No electromagnetic interference susceptibility, due to its optics properties are not susceptible for electromagnetic fields;
- b. Inability to conduct electricity, because they are made of inorganic no metallic materials, which only allows the propagation of light along the fibre;
- c. Remote sensing. They make it possible to insert a segment of an optical fibre sensor gauge using another fibre or the same fibre and convey the sensing information to a remote section.
- d. No invasive systems. Due to their small dimensions they can be integrated in building infrastructures such as reinforced polymer composites, or aeronautics devices and they can be also embedded in polymeric matrix such as epoxies, silicones, and adhesives.
- e. Ability to work in hazardous environments. OFSs have been tested under extreme hazard conditions such as high and low temperatures and pressures, corrosive medias, radioactive zones, high electromagnetic fields and toxic environments;
- f. High sensitivity and wide sandwich. OFSs are sensitive to small perturbations due to their micro bending effects.
- g. Distributed measurement. Due to their line without significant loss, it is possible to measure data in different points.

2.9.1. Classification of OFSs

OFSs are classified in two types: optical fibres intrinsic sensors and optical fibres extrinsic sensors [110], [95]. They are characterized according their operation (Fig. 2. 29.). The extrinsic sensors are fundamentally distinguished because the sensing takes place outside the optical fibre. The optical fibre is only used to deliver and collect light. The propagation of the light can leave the optical fibre and be collected for another optical fibre to propagate the new wavelength or be directly collected by a detector. The most relevant sensors in this group are the Fabry-Perot interferometers which uses some advantages of optoelectronics over conventional technologies [111]. In an intrinsic sensor, the light does not have to leave the fibre to produce a propagating wave function. The optical fibre structure is modified and the optical fibre itself plays an active role in the sensing function. The most well-known intrinsic sensors are fibre Bragg gratings. Other intrinsic sensors, which compress the fibre optic gyroscope include long period gratings and micro bend and coated or doped fibre sensors.

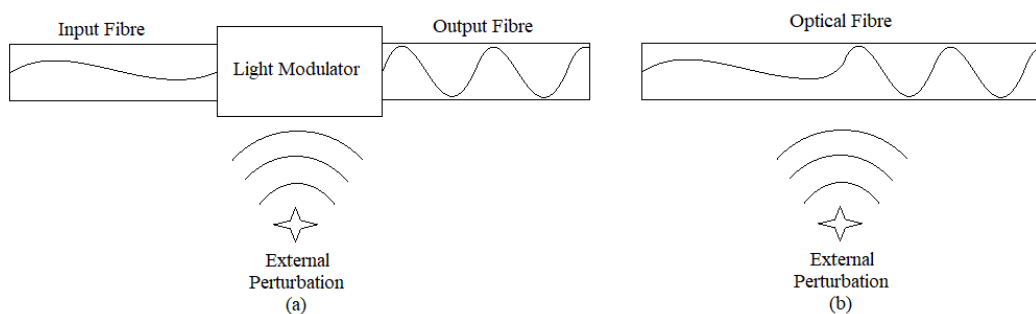


Figure 2. 29. Scheme of general optical glass fibre design of: (a) extrinsic sensor and (b) intrinsic sensor (adapted from [112]).

2.9.2. Modulation techniques

Optical glass fibres sensors can detect a perturbation based on intensity (amplitude), phase, wavelength (frequency) and polarization (Fig. 2. 30.). When a perturbation occurs in their surroundings at least one of these factors normally becomes perturbed and produce new outcome which can be detected.

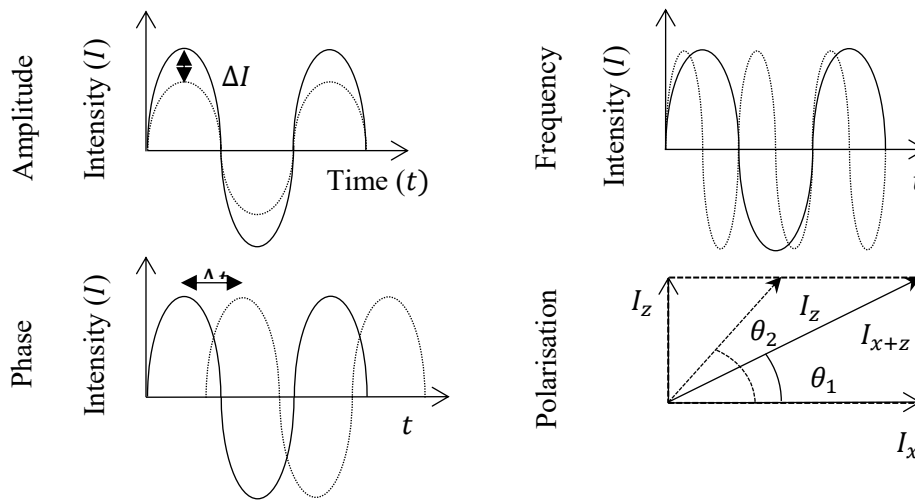


Figure 2. 30. Scheme of the basic modulation techniques.

2.9.2.1. Intensity modulated OFSs

The intensity modulated optical fibre sensor raises the measurement by measuring the amplitude. Normally, measuring the optical power is easier than measurements of optical properties such as phase, wavelength or polarization. Phenomena such as transmission, reflection, micro-bending, or other phenomena such as absorption, scattering, or fluorescence can be associated with light loss (Fig. 2.31.). For this reason, the intensity-based modulated OFS represents one of the most common optical fibre sensors. Furthermore, OFSs are usually made with multimode fibres [95], [112]. These have larger cores which allow simple configuration, low fabrication costs, robustness, the possibility of being multiplexed, and flexibility (because they do not require a special optical component). However, they have some limitations. One of the biggest limitations is that they can have losses in the systems which are not related to the environment effects. This occurs in the connectors and splices, micro and macro bending loss, misalignment and deterioration of the fibres and detectors [113], [11].

2.9.2.2. Phase modulated OFSs

Phase modulated OFS uses the phase of light rather than intensity for detection. This factor is intrinsically extremely sensitive to its surrounding which make the sensor highly sensitive to its environment modulation. This means that phase modulated OFS are very greatly sensitive and therefore they can have high

resolution (Fig. 2.31.). Furthermore, they are more sensitive than the intensity-based OFS. The light beam pass through the fibre is modulated by the field to be detected [100], [11]. This phase modulation is measured with an interferometer where the light is spliced in two light beams. One is exposed to the action of the measured and undergoes a phase shift. The second one is used as a reference. The Mach-Zehnder interferometer is the most commonly used due to their wide applications in science, engineering and technical phases such as to measuring pressure rotation and magnetic fields. Other commonly used phases modulated sensors are Michelson, Fabry-Pero, Sagnac, polarimetry, and grating interferometer.

2.9.2.3. *Polarization modulated OFSs*

Stress or strain can modify the refractive index in an optical fibre perfectly. This effect is common called a photo elastic effect. As the stress or strain can have different directions, the refractive index can change in different ways too. In other words, the polarization can obtain two different directions. This polarization would play an important role in a system using single mode fibres. This physical phenomenon comprises a variety of physical phenomena in the state of polarization of light, Fig. 2. 31. They are Faraday rotation, electro-gyration, the electro-optic effect and the photo elastic effect [105]. So, these sensors will be useful to measure magnetic fields caused by Faraday rotation of the plane polarized light by an angle to the strength of the magnetic field, electric field temperature and chemical species based on the polarization effect [114], [95].

2.9.2.4. *Wavelength modulated OFSs*

This type uses the change in the wavelength of the light for detection. They are most commonly used in fibre modulated gratings. A grating is a periodic structure that forces light to behave in a certain way which depends on the periodicity of the grating (Fig. 2.31.). Due to their wide range of applications, these sensors form part of another subcategory explained below.

2.10. Fibre optic techniques for humidity sensing

All the devices described above rely on the typical fundamental properties of water gas and their electrical, optical and mechanical effects on the devices, and provide a direct relative measurement. However, none of these sensors, except the optical waveguide sensors, are suitable to be embedded in composite materials.

2.10.1. Direct spectroscopy optical based humidity sensors

The spectroscopy method examines the optical signal obtained related to the absorption and fluorescence produced by the target analytes. Normally, this method compresses a fibre immersed in a cell for a direct spectroscopy measurement. Another common method is to configure a fibre opt-rode. This is an alternative where a reactive chemical layer is put on the fibre. This layer will react with the chemical target analyte producing an absorption or an emission of a light signal which can be read [115]. The most common direct spectroscopy optical based humidity sensors use the opt-rode approach, in which a chemical sensitive to the moisture is coated on the fibre.

Absorption based sensors present a variety of potentially suitable materials because they have good absorption when they are in contact with water. The most common materials are the cobalt chloride (CoCl_2) [116], Cobalt oxide (Co_3O_4) [117], Rhodamine B [118], crystal violet [119], electrochromic polymers [120], and bacteriorhodospin (BR) doped biochromic film [121]. The measurement is given by the variation of the absorption of light intensity due to the interaction of water and the chemicals reagent dyes.

Zhou et al. [122] demonstrated an in-line absorption sensor based on CoCl_2 . They doped a piece of porous glass fibre with the cobalt chloride which exhibits strong absorption on the wavelength region band between 550 and 750 nm. CoCl_2 changes from blue to pink when in contact with moisture or humidity. They create the sensing element using a borosilicate fibre with a pre-treated reaction to create a porous fibre (Fig. 2. 31.). Subsequently, the fibre was immersed in a solution of water and CoCl_2 and dried at room temperature. The authors experimented with the porous fibre because when the light was launched some light was absorbed by the cobalt chloride and some was scattered. This was taken into consideration for the subsequent experiments. The sensor was operative until a RH of 50% depending on the CoCl_2 solution concentration used for tailoring the fibre. The sensor had a

response signal around three minutes after had contact with the moisture. The sensor proved to be reversible.

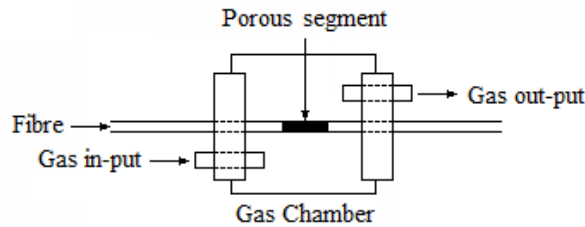


Figure 2. 31. Schematic diagram of the fibre setup used by Zhou et al. (adapted from [122]).

Tao et al. [116] used a similar technique using the same CoCl_2 reagent. The porous sensing element in this case was created using a sol-gel technique instead of pre-treating the fibre segment. The sensing element was mould-cast using a sol solution premixed with CoCl_2 . This approach proved to be more easily tailored compared to the sensors developed by Zhou et al. Tao et al. sensor was able to detect an RH level down to 2 %. However, the RH operating limit was around 10 %, which made the sensor only useful to determine low concentration of moisture.

Otsuki et al. [118] presented an air-gap design, which worked in an in-line absorption configuration. The sensor was created with an airgap of two sections of large core fibre positioned on the same axis. The end of one fibre was coated with Rhodamine B (RB) and hydroxypropyl cellulose (HPC). In order to measure the optical signal light, one fibre was couple to the other which contained the reactive coating (Fig. 2. 32.). The sensor was able to operate from 0% to 95 % of RH with a response time of around 2 minutes.

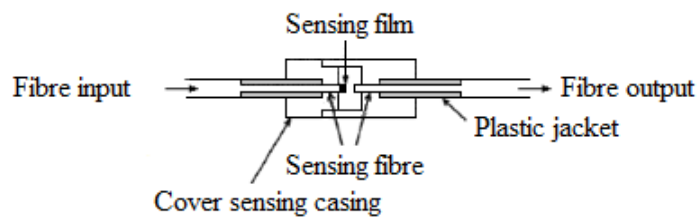


Figure 2. 32. Schematic diagram of the instrumentation used for Otsuki et al. (adapted from [118]).

Luminescence, or fluorescence, lifetime method can be another solution for humidity detection. This method is based on the intensity of the absorption of the

fibre. When humidity reaches the fluorescent material, this emits light which can be read by the spectrometer as a variation of the intensity.

Glen et al. [123] used a lifetime luminescent system based on a ruthenium complex immobilized with a membrane of Nafion®, which was mechanically attached on the fibre. The sensor was able to give a response for humidity and moisture diffusion. However, it could only be used once before restoring the luminescent coating, which makes it a single-use sensor if it is embedded in a polymeric matrix.

Bedoya et al. [124] created another luminescent sensor which presented more robustness and stability than the sensors developed by Glen et al. They used the same ruthenium complex, but they immobilized it in with a poly(tetrafluorethylene) (PTFE) membrane, which allowed a continuous monitoring of the humidity. The operation range was between 4 to 100 %RH. The authors were able to make the sensor operative at different temperatures using a commercially available lifetime-based humidity sensor instrument optode, Optosen®.

Table 2. 5. Overview of fibre humidity-based sensors using different chemical doping for humidity detection.

Sensing method	Sensing approach	Ability to		Author
		Moisture/humidity detection	Be embedded	
Direct in-line absorption	tailored of CoCl ₂ in an etched borosilicate optical fibre	Yes	No	Zhou et al. [122]
Direct in-line absorption	rhodamine B doped HPC	Yes	No	Otsuki et al. [118]
Direct in-line absorption	porous sol-gel fibre doped with CoCl ₂	Yes	No	Tao et al. [116]
Fluorescent lifetime	lithium-trated nafion membrane	Yes	Yes	Glen et al. [125]
Fluorescent lifetime	ruthenium-based complex doped PTEE membrane	Yes	Yes	Bedoya et al. [124]

2.10.2. *Evanescent wave spectroscopy optical based humidity sensors*

Light can travel along the fibre by reflection. Total internal reflection (TIR) occurs when the propagated waves strike the boundary with no light escaping from the core medium [60]. At this point light forms an extension beyond the core of the

optical fibre and penetrates the cladding producing the evanescent wave (EW). This wave does not propagate but it has a great amount of energy and only exists to satisfy the boundary condition.

To reach the evanescent field it is necessary to remove the cladding up to the boundary between the core and the cladding. The cladding can be polished or etched. Chemical reagents can be deposited on the necked core, also called de-clad optical fibre, and used as targets for reacting with humidity or moisture.

In comparison with the previously described sensors, EW based sensors present some advantages, such as having more configuration flexibility in terms of interaction length, time response and distributed sensing capability. However, they also present a high fragility and poor mechanical properties as the necked core is exposed. Furthermore, they are susceptible to chemical contamination and small deformations will affect light signal processing.

Kharaz et al. [119] immobilized a gelatine membrane of hydroxyethylcellulose (HEC) mixed with CoCl_2 in a U-bent fibre configuration of a silica-fibre (Fig. 2. 33.). They were able to detect moisture in a range of 40 to 80 %RH. and humidity in a range between 30 to 96 %RH. This EW sensor worked with an absorption produced by a colorimetric interaction of cobalt chloride.

Jindal et al. [126], further developed Kharaz et al. sensor using the same U-bent configuration but using Polyvinyl alcohol (PVA) instead of (HEC) in a core-plastic fibre. This approach made it possible to increase the %RH between 3 to 90 %RH.

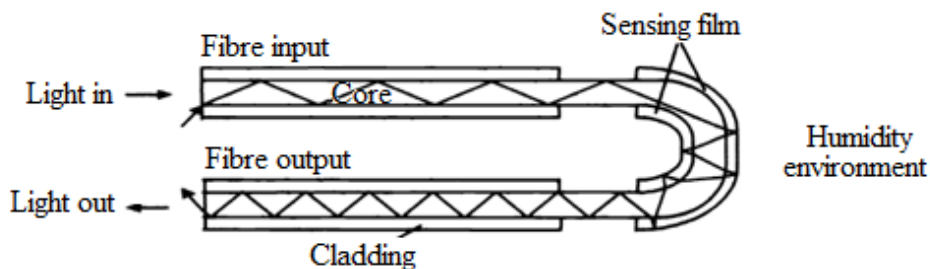


Figure 2. 33. U-bent fibre optic configuration tailored with HEC and CoCl_2 . (adapted from [126]).

Alvarez-Herrero et al. [127] demonstrated the possibility to use titanium oxide (TiO_2) for humidity detection in a side-polished fibre. They deposited a nano-film on the polished fibre using a technique of physical vapour deposition (PVD). The authors experimented with the refractive index changes, which consisted in monitoring the optical spectrum resonance bands. These resonance bands interacted with the coating, and when the humidity found the TiO_2 , a shift on the resonance bands was produced and gave a different signal. The shift showed a linear wavelength between 0 to 15 %RH and then became planar from 15 to 90 %Rh. The sensor showed good RH percentage detection and was suitable to be embedded in polymer composite materials. However, a PVD process was required, which is not a cheap instrument and not all laboratory facilities can afford it.

Xu et al. [128] used another approach to develop an EW sensor. It was based on ray-light scattering based humidity sensing. They used a U-bent fibre configuration and coated the sensor with a process of sol-gel silica film. Then, a light source in the near infrared (NIR) spectrum was employed and the ray-light scattering effect was evaluated when the water reaches the sensor (Fig. 2. 34.). They detected the moisture by an attenuation of the light intensity in a range of 3 to 90 %RH.

The developed sensor for the Xu et al. group is without doubt, the most suitable sensor based on humidity sensing. It was capable to be embedded in polymer composite materials and be tailored with other dyes to make it sensitive to other chemicals. Their sensor could be useful to monitor the lifetime of the polymer structures such as epoxies, adhesives, and polymer composites. However, the sol-gel process is not an easy technique, but it is feasible.

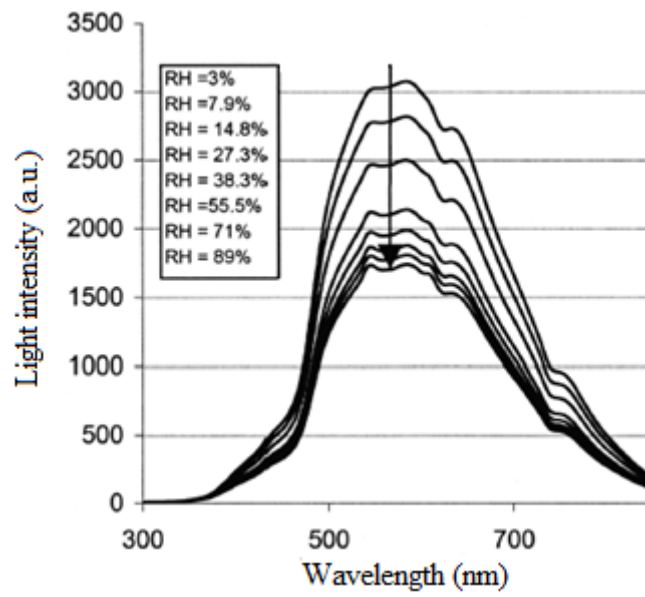


Figure 2. 34. Attenuation of the intensity spectrum of light guided in the U-bent configuration sensor coated with sol-gel silica film (adapted from [128]).

Table 2. 6. Overview of fibre humidity EW based sensors using different chemicals doping for humidity detection.

Sensing method	Sensing approach	Ability to		Author
		Moisture/humidity detection	Be embedded	
Absorption measurement using U-bent fibre configuration	CoCl ₂ doped with HEC	Yes	Yes	Kharaz et al. [129]
Absorption measurement using U-bent fibre configuration	CoCl ₂ doped PVA film	Yes	Yes	Jindal et al. [126]
Wavelength resonance shift using side-polished fibre	TiO ₂ nano-film	Yes	Yes	Alvarez-Herrero et al. [127]
Attenuation measurement	porous sol gel silica cladding	Yes	Yes	Xu et al. [128]

2.11. *Fibre grating based sensor*

The fibre grating sensor works by modulating the phase of the light, as wavelength modulators OFSs. A fibre grating sensor is made by creating a periodic refractive index perturbation along the length of the fibre core [130]. This induced defect allows coupling to propagate modes forward or backward, depending on the

grating period [131]. However, they present some problems associated with the fluctuation of the power source, coupler losses, micro and macro bending, losses in misalignment and absorption effects [104]. In order to overcome these factors one of the most promising sensors is fibre grating. Furthermore, they can be divided into two categories depending on the grating period and the type of mode coupling.

Fibre gratings are classified in fibre Bragg gratings (FBGs) and long-period gratings (LPGs), according to grating period. LPG typically presents a grating period range between 100 μm to 1 mm, while FBGs have a sub-micron period. The transmission spectrum of LPGs is based on the reflection of a range of the spectrum while the FBGs operates in transmission, where on part of the spectrum is reflected and it does not arrive to the detector [132] and [133].

2.11.1. Fibre Bragg gratings (FBGs)

In a fibre Bragg grating sensor commonly called short period gratings, the coupling takes place between two modes travelling in opposite directions, Fig. 2. 35. They are the most used and standardized optical sensors, due to their high sensitivity. Furthermore, nowadays, the huge demand in telecommunications has revolutionized a reasonable fabrication cost. However, they are difficult to produce and consequently they are still expensive. For example, a normal fibre grating can cost around 80 € and this phase-based sensor can be also compromised by temperature and vibration.

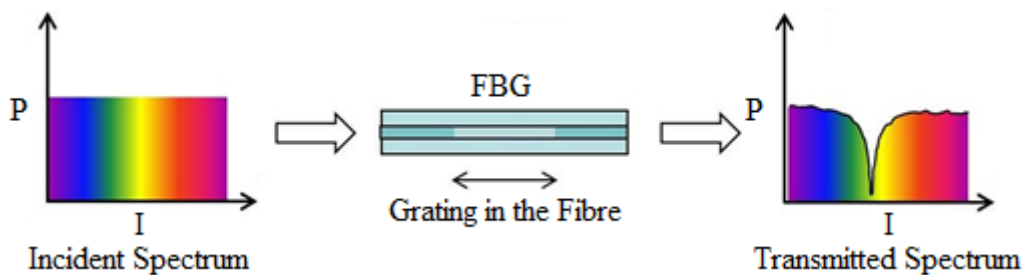


Figure 2. 35. Illustration of FBG sensor working principle. FBGs work in transmitted spectrum (adapted from [134]).

The principle of the Bragg grating sensors is based on the shift of the Bragg wavelength. For this reason, temperature and pressure are the two physical parameters that can directly tune the FBGs. Light coupling interacts with the pure

silica core modes and interacts with the surrounding refractive index. For this reason, they cannot be used as sensors for chemical and biological species.

2.11.1.1. Long period gratings (LPGs)

In a long period, grating sensor or commonly called transmission grating, coupling takes place between the core and the cladding modes that travel along the fibre in the same direction (Fig. 2. 36.). The different wavelength in the grating transmission spectrum becomes distinct due to the attenuation that occurs on the propagation of the cladding modes. LPGs are used as gain equalizers, dispersion compensators, optical switches, band rejection filters and mode converters [131]. LPG bands of attenuations are strongly related with external perturbations such as strain, temperature and surroundings refractive index. These affect the coupling strength between the core and the cladding modes, which can shift the attenuation bands.

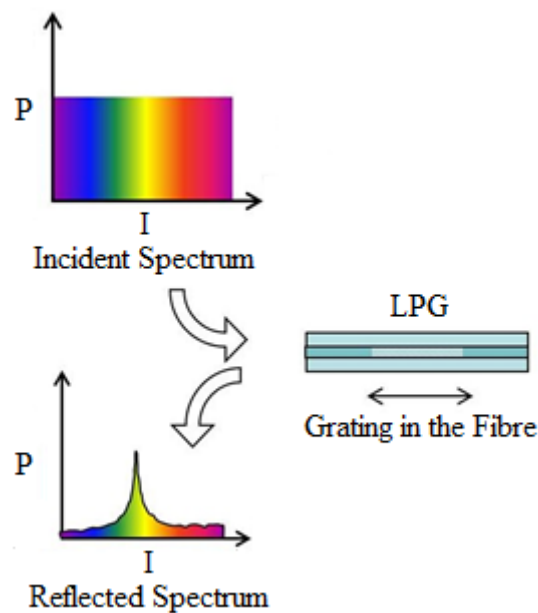


Figure 2. 36. Illustration of LBG sensor working principle. FBGs work in reflected spectrum (adapted from [134]).

LPGs have a high sensitivity to the refractive index in the ambient media. However, their multiple resonance peaks and broad transmission spectra produce some limitations for accurate measurements and multiplexing capabilities.

Refractive index in FBGs is problematic for their application as sensors. Normally, FBGs are less sensitive than LPGs because they are less sensitive for refractive index variations. In FBGs, it is normally required to etch the fibre with hydrofluoric acid in order to reach the evanescent field of the guided mode to be accessed. This process will reduce the fibre integrity, strength and durability, and therefore it would be easier and more susceptible to breaking in harsh conditions. In contrast, LPGs refractive index sensors retain their endurance as the integrity of the fibre is not violated.

2.11.1.2. Fibre Bragg grating sensors-based humidity sensors

Fibre Bragg grating sensors are described in the section on fibre grating based sensors above. FBGs sensors are more commonly used for physical detections but they also have room for chemical detection. LPG uses the refractive index phenomenon for chemical selective detection, which make them very attractive for detection of certain chemical species of interest in sectors such as environmental and health sensing.

FBG sensors are quite recent in chemical sensing. The first humidity FBG sensor was reported in 2001 by École polytechnique fédérale de Lausanne, Switzerland, [135]. This FBG was coated with polyimide polymer using the setup shown to investigate the humidity influence. The sensors had a linear response and were able to detect humidity between 10-90 % RH with good repeatability. Kunzler et al. [136] researched FBG sensors in harsh environments. They used the polyimide coating on the FBG it was possible to detect soil moisture. Sensors had to operate between 2 to 18 gravimetric soil moisture levels (Fig. 2. 37.). However, the sensors were only able to operate until soil gravimetric measurement of < 4 % level because of the 100 % saturation of RH.

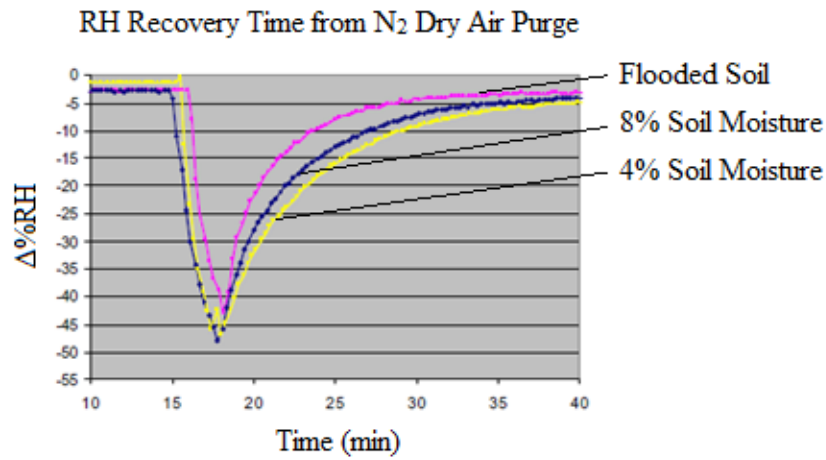


Figure 2. 37. FBG sensor tracks the evaporation rates for three soil moisture levels (adapted from [136]).

Yeo et al. [137] engineered some promising sensors to diagnose the structural robustness of the integration of moisture in various materials. This can be used as a powerful tool for civil, petrochemical and aeronautical engineering to detect the earlier ingress of moisture in composite materials. The moisture ingress was detected by a rapid change in the Bragg wavelength of the sensor.

Luo et al. [138] used a carboxymethylcellulose (CMC) hydrogel covalently attached to an LPG to fabricate the humidity-based sensor (Fig. 2. 38.). The sensor operated in a range between 0 to 95 %RH, with non-linear response dependency. However, it was unstable when it reached saturation at 100% RH.

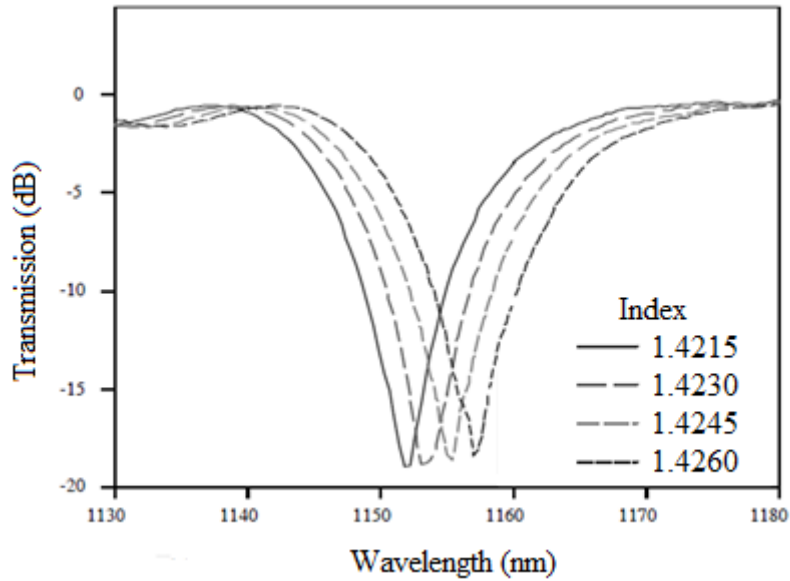


Figure 2. 38. LPG transmission spectrum on the refractive index of surrounding medium (adapted from [138]).

Tan et al. [139] used a gelatine-coated LPG humidity-based sensor and Konstantaki et al. [140] described an FBG coated with CoCl_2 and polyethylene oxide (PEO) (Fig. 2. 39.). However, both sensors showed poor operating humidity ranges.

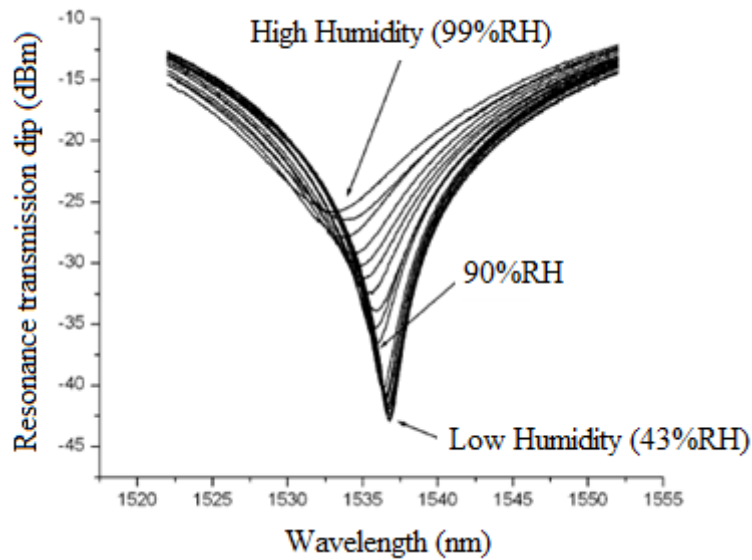


Figure 2. 39. LPG spectrum with %RH changes from 42.8 to 99 %RH (adapted from [140]).

Kelb et al. [141] developed a 2D optical strain sensors to integrate in polymer foils for health structural monitoring for buildings and aircraft applications. However, they use a grating fibre, and this is not able to detect any chemical diffusion.

Table 2. 7. Overview of fibre humidity grating based sensors using different chemical doping for humidity detection.

Sensing method	Sensing approach	Ability to		Author
		Moisture/humidity detection	Be embedded	
Strain induced Bragg wavelength measurement	polyimide	Yes	Yes	Kronenberg et al. [135]
LPG resonant band wavelength measurement	CMC	Yes	Yes	Luo et al. [138]
LPG resonant band intensity measurement	gelatine	Yes	Yes	Tan et al. [139]
LPG resonant band intensity and wavelength measurement	CoCl ₂ doped PEO film	Yes	Yes	Konstanki et al. [140]
LPG resonant band intensity and wavelength measurement	/	No	Yes	Kelb et al. [141]

2.11.2. *Interferometric sensors-based humidity sensors*

Optical interferometry sensors have been used because of their powerful, versatile, and high yield performance. They present unique advantages due to the OF physical property of phase modulation, which can be perturbed. They are widely used in research and industry for very small measurements that are not achievable any other way, changes in the refractive index, and the Luminiferous Aether.

Mitschke [142] proposed an interferometer sensor which a thin film Fabry-Perot interferometer fabricated on the tip of the fibre sensor. The Fabry-Perot captivity was created by depositing a layer of TiO₂ sandwiched between two partially reflective mirrors. As the refractive index depends on humidity variation, it can be recorded by a variation of the intensity measurement fixed at one wavelength.

Arregui et al. [143] and Yu et al. [144], designed an interferometric humidity sensor like Mitschke, with a submicron cavity length. Their interferometric sensors showed a fast response and operated over a wide humidity range.

Table 2. 8. Overview of fibre humidity interferometric based sensors using different chemical doping for humidity detection.

Sensing method	Sensing approach	Ability to		Author
		Moisture/ humidity detection	Be embedded	
Intensity measurement using Fabry-Perot configuration	SiO ₂ -TiO ₂ -SiO ₂ cavity	Yes	Yes	Mitschke [142]
Intensity measurement using Fabry-Perot configuration	SiO ₂ -[Au:PDDA+7PS S]-air cavity using ISAM technique	Yes	Yes	Arregui et al. [143]
Intensity measurement using Fabry-Perot configuration	SiO ₂ -[PDDA+7PS-119]-air cavity using ISAM technique	Yes	Yes	Yu et al. [144]

2.12. *Current available smart composites*

Various methods of self-sensing and self-healing have been developed in the last two decades [145]. These composites are well known as smart composites. Damage sensing using electrical resistance and optical intensity variation in GFRP materials have been demonstrated and implemented [146].

With the increment of GFRP in the petrochemical industry sector it is desirable to develop, to implement and to monitor smart composites systems. Smart composites allow the capacity of monitor and record mechanical damages such as cracks, partial or total ruptures, and degradation such as chemical ageing or

corrosion. For this reason, smart composites are defined as materials capable to self-heal. Additionally, these materials are well suited in petrochemical sectors due to their possible manufacturing improvement and implementation [147]. Table 2. 9. summarize some of the current available smart composites in the market, which are basically based on piezoelectric and glass fibre sensors.

Table 2. 9. Current commercially available smart composites.

Smart composite	Sensor detection approach	Company
Smart pipeline	Optical fibres	Huawei [148]
Printed and flexible sensors	Optical fibres Piezoelectric	IDTechEx [149]
Smart flexible materials	Self-diagnosing	Composites UK [150]
Smart pipeline	Optical fibres	Smartpipe [8]
Smart pipes	Piezoelectric	Smartpigs [151]
Smart pieces	Piezoelectric	Shell [152]
Smart pipelines	Optical fibres Foams	i2i Pipelines [153]
Smart pipes	Piezoelectric	Bodine, services of the Midwest [154]
Smart pipes and composites	Piezoelectric	T.D. Williamson, pipeline performance™ [155]

2.13. *Description of the work and partners objectives*

The main objective of this PhD dissertation is to develop new low-cost chemical sensors to be embedded in advanced composites without compromising its mechanical integrity. The developed sensors are aimed at to monitor the diffusion of corrosive media and degradation through the thickness of the protective polymer liner of petrochemical components. Furthermore, the novel sensors can assist with the development of a more reliable accelerated ageing test to assess the performance of composites in hostile environments.

With the support of the Marie Skłodowska-Curie grant and the European training network, the objectives are achieved between universities and industrial partners framework. These are Politecnico di Torino (Torino, Italy), Université de Rennes 1 (Rennes, France), Element Materials Technology (Hitchin, UK), Incubatore Imprese Innovative Politecnico Torino (Torino, Italy), and Nanoforce Ltd. (London, UK).

The main objectives consisted of design, manufacture, integration and testing of innovative silica-based optical glass fibre sensors for detecting ingress of chemicals in glass fibre reinforced composites in harsh environments, and the preparation of glass fibre reinforced polymer samples containing glass fibre sensors were developed at Politecnico di Torino and Element Materials Technology.

Design, optimisation and testing of alternative chalcogenide-based optical glass fibre sensors were produced at Université de Rennes 1, Rennes, France. Finally, the development, design and testing of alternative sensors based on nano-fillers were carried out in Nanoforce Ltd.

The great potential impact on the market was found with the new and low-cost optical glass fibre sensors to be placed in hostile environments. In collaboration with Incubatore Imprese Innovative Politecnico Torino it was studied the possible industrialization and commercialization of the sensors.

In summary, three different sensors are fabricated and investigated to be embedded in polymer composites for monitoring the chemicals diffusion and degradation through the GFRP samples thickness in order to accomplish the objectives.

Chapter 3

Materials & methods

The workflow of this section is split into nine experimental activities, namely:

1. The epoxy samples preparation and characterisation;
2. The fabrication of optical fibre sensors based on the evanescent field sensing that could work in reflection;
3. The fabrication of epoxy and GFRP samples containing the optical fibre;
4. The interrogation setup of the optical fibre;
5. The sensor response at high-pressure;
6. The fabrication optical glass fibre selective sensors;
7. The mechanical characterisation of the GFRP samples;
8. The fabrication of optical chalcogenide glass fibre sensors.
9. The fabrication of the samples containing carbon nanotubes sensors;

The first six tasks refer to the development of a proper technique to embed multiple sensors that could detect the water and hydrochloric acid diffusion through the thickness of the samples. The last two tasks refer to the development of alternative sensors that can be used as well to detect the water diffusion through the thickness of the samples.

3.1. Epoxy preparation and characterization

The epoxy resin selected for this project was the Ampreg 26. The data sheet of Ampreg 26 epoxy resin reveals that this is mainly composed of a mix of bisphenol-A-diglycidylether, bisphenol-F-diglycidylether and, 1,6-hexanediol diglycidylether) (Gurit, Switzerland, [156]). This is the same resin used to produce the glass fibre reinforced polymer (GFRP) composites in Element Materials

Technology laboratory (Hitchin, UK), which is involved in this project. This epoxy is also particularly suitable for manufacturing of large and high-performance composite structures.

The resin was crosslinked with the provided commercial amine, Ampreg 26 slow hardener (a mix of Polyoxyalkyleneamine, 2,2'-dimethyl-4,4'-methylenebis(cyclohexylamine), 4,4'-methylenebis(cyclohexylamine) and 2,2'-iminodiethylamine), in a weight ratio of 100:33, following the technical sheets. The resin was cured at different times and temperatures to obtain the best performing polymer concerning thermo-mechanical and viscoelastic properties. Samples were prepared by using custom silicone mould CS-25 [157]. Then, the best curing conditions were evaluated using different analytical polymer instruments. These were the Differential Scanning Calorimetry (DSC), (Mettler Toledo, Stare system DSC 1), the Fourier-Transform Infrared spectroscopy (FT-IR), (Thermo Scientific Nicolet 5700), in attenuated total reflectance mode from 500 to 4000 cm^{-1} (2.5 to 20 μm regarding of wavelength). The crosslinked materials were characterised by Dynamic Thermal Mechanical Analysis (DTMA), (Tryton Technology). A crosslinked epoxy sample with the dimensions of (110 x 80 x 50 mm) was sectioned into 15 pieces. Then, it was completely evaluated to check if there were variations in the thermal curing over the full sample. The thermal stability of the epoxy was characterised by a Thermogravimetric analysis (TGA), (Mettler Toledo, Stare system TGA). Diffusion coefficients of different chemicals were evaluated by performing gravimetric analysis. Finally, it was investigated the change in the Reflective Index (RI) (Metricon instrument) of the immersed samples with different reagents.

The resin was crosslinked in accordance with the following procedure: 1) degassing of the reagents (epoxy resin and amine cross-linker) at room temperature and 2) mixing epoxy with the hardener (both steps performed under vacuum); 3) pouring the mixture into a silicone mould in air; 4) leaving the mixture at room temperature for 24 hours in air and, finally, 5) thermal curing at 80 °C for 5 hours. The final curing temperature was assessed by taking into account the DSC, FT-IR, TGA and DMTA analysis.

The diffusion of different reagents such as artificial salty water [158], distilled water, ethanol, and HCl was investigated. Although the artificial sea water and distilled water were tested at 80 °C the other reagents were tested at room temperature. Furthermore, the gravimetric test using artificial salty water was subjected to high pressure and 80 °C to accelerate the diffusion and recreate harsh

conditions. Samples had dimensions of (20 x 20 x 5 mm). The diffusion coefficients of the reagents into the crosslinked epoxy were measured by soaking them (full immersion) and performing gravimetric measurements until reaching the saturation. The absorption curves and the diffusion coefficients were calculated with (Eq. 3.1):

$$D = \pi \left(\frac{h}{4M_{\infty}} \right)^2 \left(\frac{M_2 - M_1}{\sqrt{t_2} - \sqrt{t_1}} \right)^2 \quad (3.1)$$

where h is the sample thickness, M_{∞} is the weight gain at saturation expressed in percentage; M_1 and M_2 are two points on the linear section of the weight gain curve expressed in percentage, while t_1 , t_2 are the corresponding time spots in s [159].

Using the diffusion coefficient, it was then possible to calculate the diffusion penetration of the reagents through the epoxy matrix using the Fick's law, (Eq. 3.2):

$$d = 2\sqrt{Dt} \quad (3.2)$$

where “ d ” is the distance of the water diffusion, “ t ” is the time corresponding to the signal drop of the sensor and “ D ” is the diffusion constant [160].

Refractive index analyses of the epoxy, before and after the immersion into artificial salty water, and hydrochloric acid were carried out with METRICON instrument, which is based on the prism-coupling of light. Samples were mounted on a rotational stage and butt-coupled to a prism with high refractive index (RI of the prism ~ 1.9). The light from a laser source is incident on the prism with a defined angle, partially reflected at the prism-sample interface and finally collected by a photodetector. For a certain angle, defined critical angle, most of the light is coupled into the bulk sample and trapped there. Thus, the intensity measured by the detector drops. By trigonometric calculations (directly performed by the instrument's software), it was possible to calculate the unknown refractive indexes of the samples under test.

3.2. *Fabrication and optimization of the evanescent wave optical fibre sensors*

The evanescent field produced by the total internal reflection (TIR) of the light beams through the optical fibres is found in the interface of the core and the cladding. In order to make the optical fibre sensitive to changes in the surrounding environment (in this case for the chemicals diffusion through the composite materials where the optical fibre is embedded), a chemical etching to reduce the optical fibre diameter of the initial 125 μm down to $\sim 55 \mu\text{m}$ was produced. The etching modifies the optical properties of the fibre and the light travelling through it since the cladding is reduced. Light is normally confined into the core, and it extends to the surrounding medium as an evanescent wave. Removing the cladding of the fibre it is possible to make act the optical fibre working as an evanescent wave optical sensor (EWOS).

The optical fibre was chemically etched to expose the core, where the light is confined, to the surrounding environment [96]. Then, the fibres were cleaved with a diamond-blade cleaver to obtain a right angle cut on the fibre end tip. Finally, a silver coating using the Tollen's reaction [161], [162], was deposited on the end tip. Using this approach, it was possible then to make the sensors working in reflexion instead of transmission, which provides huge advantages in costs and fabrication. Furthermore, sensors were performed with different lengths (either 2, 6, 8, 10 or 14 cm) to check the reflectivity of the sensors.

For this reason, it was necessary to calculate the etching ratio of the optical fibres in hydrofluoric acid (HF). The etching rate was experimentally determined and optimised. Optical glass fibres (GIF 625 silica multimode fibre, Thorlabs) with a length of 150 mm were cut. Then, optical glass fibres were soaked into acetone for 2 minutes. The aim of immersing the optical fibres into acetone was to make the polymer coating of the optical fibres softer. Then, the polymer coating of the optical glass fibre was mechanically stripped without difficulties and without breaking the optical glass fibre or producing micro crack on this. The naked optical glass fibre of 125 μm was carefully cleaned with a wipe impregnated of isopropanol to remove and perfectly clean any possible remaining polymer impurity on the glass fibre stripped section. Then, the optical glass fibres were attached on a plastic holder and they were immersed in hydrofluoric acid. The hydrofluoric acid then produced the chemical etching. The chemical etching equation was obtained by etching a total of 10 samples at a different time.

Subsequently, after the etching, the optical glass fibres were rinsed with distilled water to remove any remaining HF on the optical fibres. Finally, the etched optical glass fibres were carefully inspected with an optical microscope to measure the etched diameter accurately. The inspection was performed to verify the required diameter approximately at 55 μm .

Then the optical fibre was perfectly cut in a right angle using a diamond- blade cleaver. The cut also represented a crucial point to produce the sensor. Small tilt cut affects the reflection of the light making favourable the light scattering. Afterwards, the optical fibres were immersed into the Tollen's reaction, and a silver mirror coating of approximately 2 mm was deposited on the extreme tip. Finally, the reflectivity of every OFSs was carefully checked and only the sensors which presented an excellent reflexion were used. The reflexion of the sensors was compared with the reflexion obtained from a commercial reference mirror, which represented the maximum of the total reflection.

To create the silver mirror, three different silver coatings were examined. The first one consisted of Tollen's reagent. The second one was with physical vapour deposition (PVD) and, the last one, was prepared using silver glue. This silver glue is the conventional glue used to attach the samples in the sample carrier for SEM.

Tollens' reagent is a chemical reaction which consists of a solution of silver nitrate and ammonia. This reaction produces the precipitation of elemental silver on the surface. Physical vapour deposition is a physical method to produce thin films, typically in the range of few nanometres. PVD uses a physical process of heating or sputtering in order to produce a vapour of material. Finally, the silver glue is a solution of silver micro particles mixed with a polymer linker which become solid when this is dried.

Some sensors were sputtered with copper in the sensitive section to annihilate their sensitivity to the surrounding environment. These sensors (referred to as Cu-OFS) were prepared by depositing a copper coating on the bare core by Radio Frequency magnetron sputtering (Microcoat). The purpose of using the Cu-OFSs was to prove that the information provided by the OFSs was not related to spurious phenomena (source fluctuation, mechanical stress, temperature change, and so on).

3.3. *Epoxy and glass reinforced fibre polymer fabrication*

Figure 3. 1. shows a scheme of an epoxy sample with embedded optical fibre sensors at different depths, along with a picture of a sample. A thermally-shrinking protection sleeve with a length of 40 mm was used to protect the insertion of the fibre into the epoxy due to the interface of the optical fibre with the epoxy becomes a fragile critical point.

The sample was cut in a cross-section, and the epoxy containing the OFSs was polished. SEM analysis to characterise the adhesion between the OFSs and the epoxy were performed. by scanning electron microscopy (Philips 525 M SW9100 EDAX).

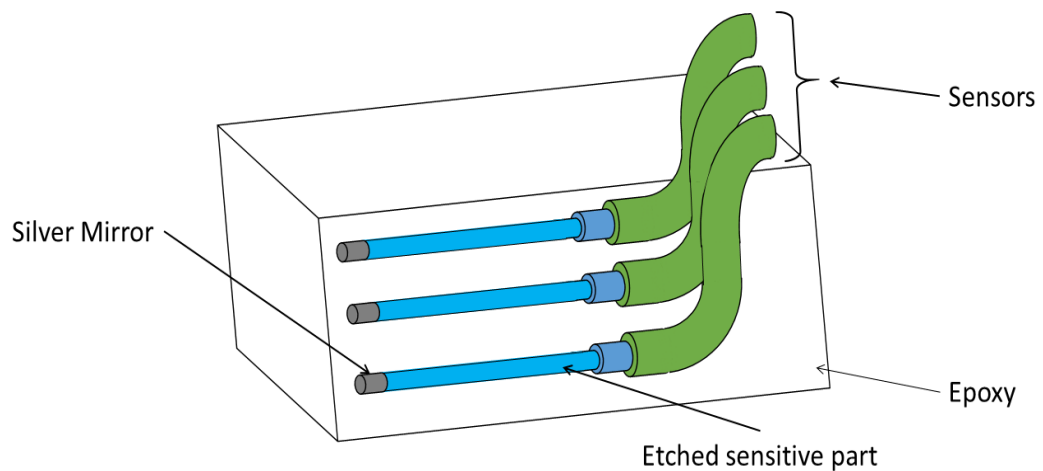


Figure 3. 1. Schematic of an epoxy sample with multiple optical fibre sensors (OFSs) with silver (Ag) coated tip that are embedded at different heights.

GFRP samples were fabricated by making vacuum moulding bag infusion. These samples were manufactured using the same Ampreg 26 resin with E-CR glass fibres fabric (Advantex). A metallic surface was spread with frekote NV 400. Then a glass fibre ply was deposited in 0° , and three optical glass fibres were deposited on that ply. These OFSs were parallel distributed, with a separation of 0.5 cm each. Then, another ply at 90° was put on the first ply to create the composite plies network of 0° - 90° direction. A peel ply and the diffusion mesh were put on the glass fibre plies. A plastic foil seal was used to cover all the plies, and butyl tape was used to seal the infusion. The epoxy resin was mixed using the ratio of 100:33

and degassed as described in section 3.1 and [14]. The reagents were weighted with Orma Scales, model BC with a tolerance of 0.001 g, and manually mixed. The mixture was subjected to a vacuum for 1 hour at -1 bar to degas the resin. Finally, it was infused and left for 24 hours at room temperature before proceeding with the thermal curing at 80 °C for 5 hours. The dimensions of the GFRP samples with embedded sensors are 100 × 15 × 5 mm (Fig. 3.2.).

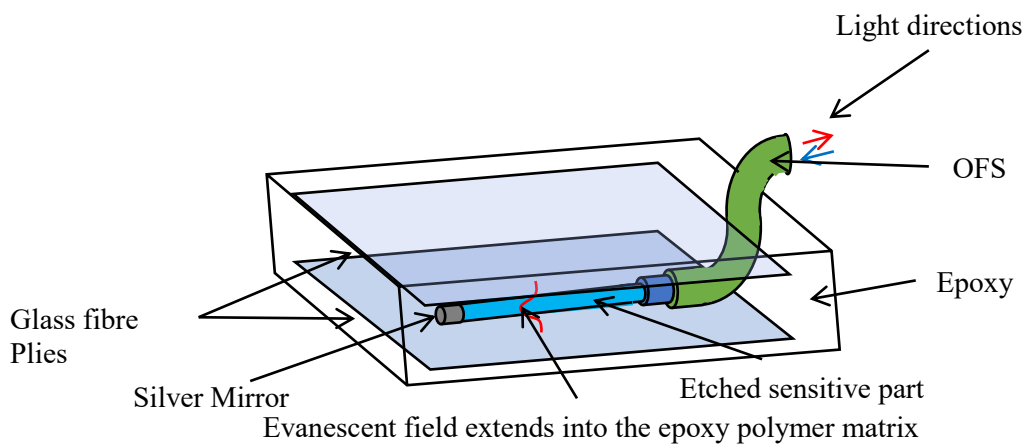


Figure 3. 2. Schematic of a GFRP sample with an optical fibre sensor (OFS) with silver (Ag) coated tip that is embedded between glass fibre plies.

3.4. Characterization of epoxy and glass fibre reinforced polymer samples equipped with OFSs

Samples containing multiple embedded fibre sensors were immersed into artificial salty water at room temperature and 80 °C and 80 °C at 50 bars. Samples were also tested with HCl and distilled water at room temperature. The sensors were interrogated with the setup depicted in Figure 3. 3. The equipment used to build this setup is off-the-shelf in the telecommunication industry and can be integrated into a self-standing measurement unit. The optical signal for the interrogation of the sensors is provided by a broadband source (Photonetics 3626BT) emitting a total power of 25 mW in the range 1500-1600 nm. The optical signal is addressed to multiple sensors employing a computer-controlled fibre optics switch (JDS Uniphase 2x16 SB series). The sensors are connected to the switch by movable connectors (Thorlabs BFT-1). Movable connectors represent an easy-handling

alternative to fusion-spliced pigtails because they introduce losses that are negligible in this application and can be easily replaced by cheap field-installable connectors [163], [164] in a manufacturing framework. A fibre optic coupler extracts the reflected signal from the sensor (that contains the sensing information) from the transmitted one. The reflected signal is processed and displayed by an optical spectrum analyser (Avantes AvaSpec-NIR256-1.7), capable of measuring spectra in the range 1100-1700 nm [165], [28], (Fig. 3. 4.). The system was designed for automatic logging of the spectra through a LabVIEW custom-developed program (Fig. 3.5.). The spectra could be recorded with a selectable sampling rate. In general, most of the experiments were carried out by recording spectra every 5 minutes and lasted from hours to days.

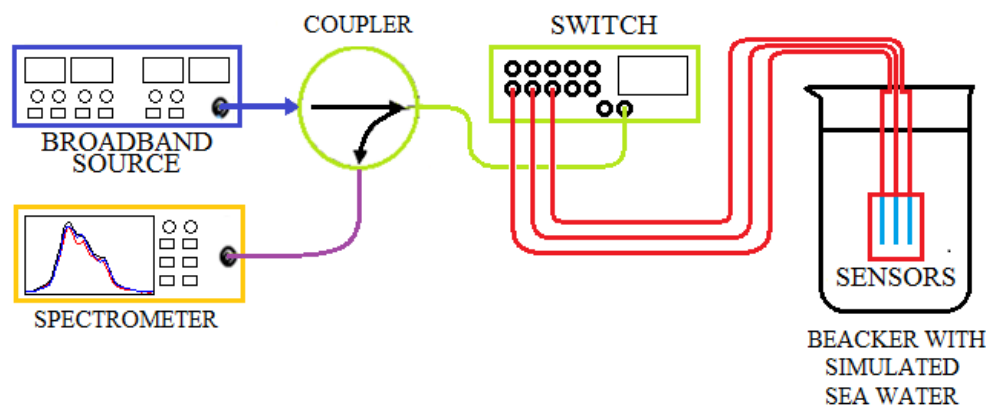


Figure 3. 3. Schematic of the interrogation setup for the OFSs.

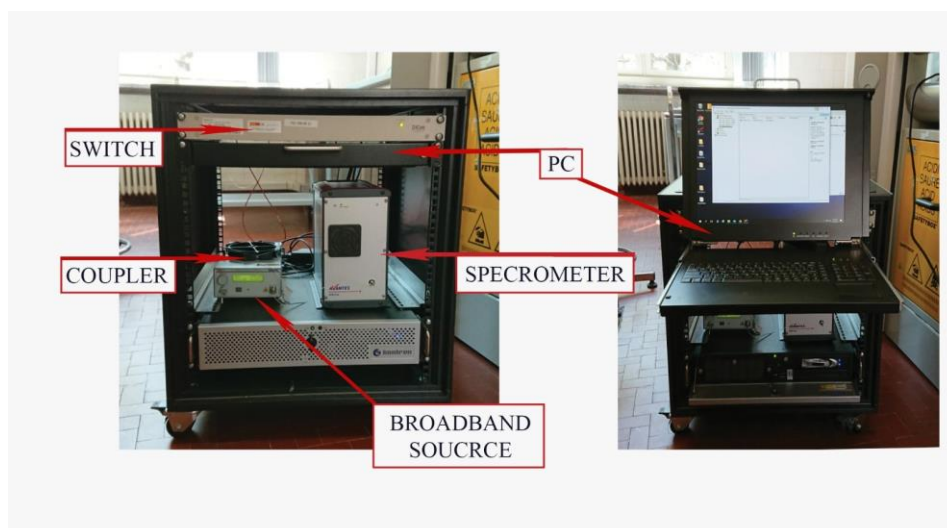


Figure 3. 4. Picture of the interrogator setup.

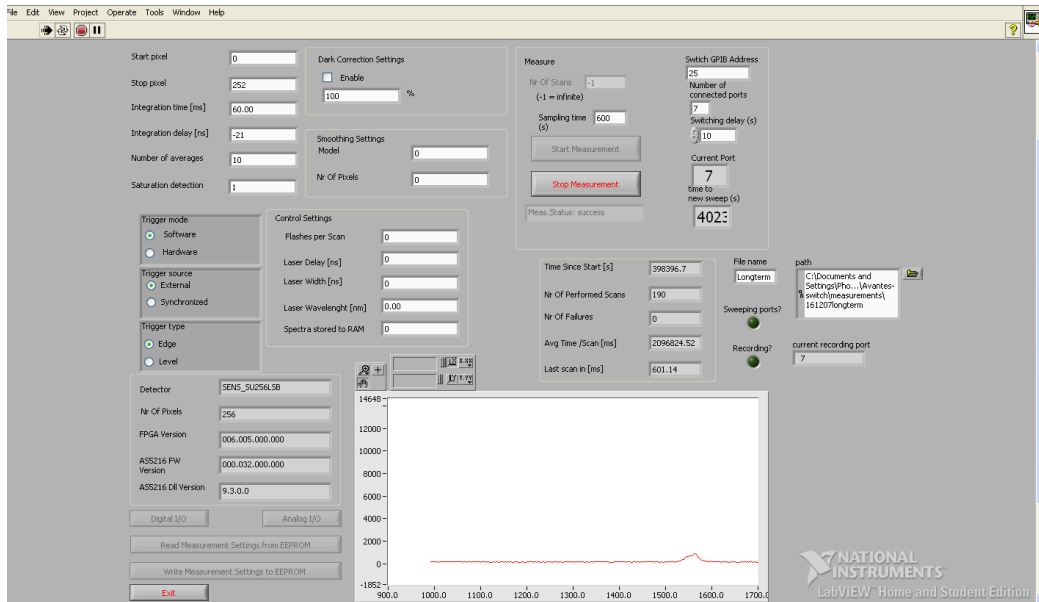


Figure 3. 5. Picture of the user interface of the custom LabView programme used to automatically control 16 OFSs.

3.5. *Interrogation setup for samples subjected at 50 bars and 80°C*

Figure 3. 6. shows the setup used in the experiment at high pressure (50 bars). The scope of this test was to expose the OFSs at working conditions. The vessel is placed in a separate room for safety conditions. The fibres, crossing the wall between the two rooms, run through a Conax adaptor sealant. This adaptor has two holes where up to four optical fibres per hole can be inserted. The adaptor was screwed directly to the vessel where nitrogen (N₂) air gas line was connected. Moreover, the vessel was connected to a network system to monitor the pressure and temperature during the experiments, carried out at Element Materials Technology laboratory (Hitchin, UK).

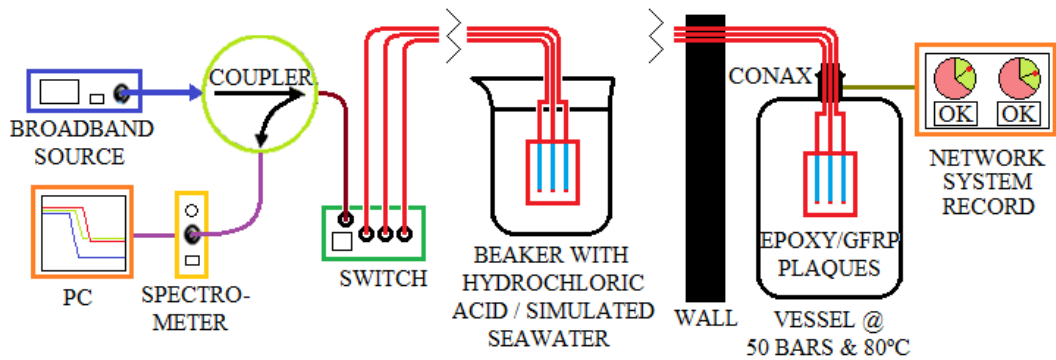


Figure 3. 6. Schematic of the interrogation setup where the samples were placed in another room.

Once the tests were performed, the samples were cut into five parts to measure the distance between the external surface and the embedded optical sensor. The cuts were made with an automatic cutting machine, (Brillant 220 ATA), using a diamond disc. Then, samples were polished using a Struers polishing machine. Finally, the samples were measured using an optical microscope.

3.6. *Selective optical fibre sensors*

In order to make the sensors selective to hydrochloric acid, some were sputtered with aluminium. Furthermore, some were sputtered with copper to compare their affinity. Both different sputtered sensors were coated in the sensitive section to annihilate their sensitivity to the surrounding environment. These sensors (referred to as Cu-OFS and Al-OFS) were prepared by depositing a copper coating or aluminium coating on the bare core of the etched OFS by Radio Frequency magnetron sputtering (Microcoat), (Fig. 3. 7.).

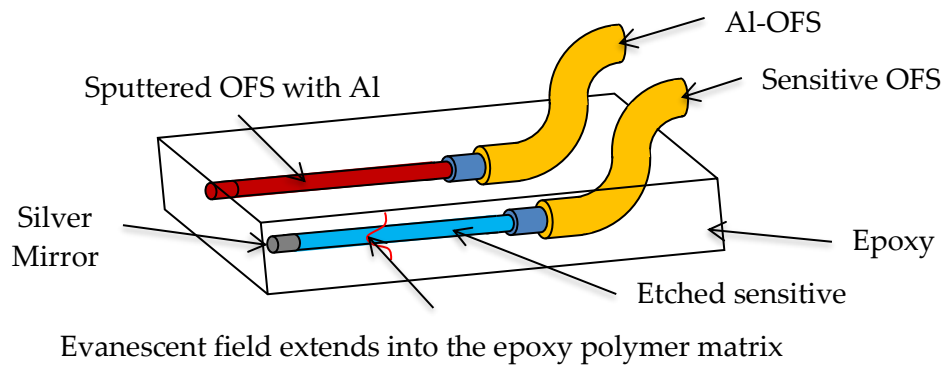


Figure 3. 7. Schematic of an embedded optical fibre sensor (OFS) and sputtered OFS with aluminium (Al-OFS) in an epoxy polymer matrix (adapted from [15]).

The purpose of using the Al-OFS was to prove that the information provided by the Al-OFSs was not related to the water detection. Al-OFSs make the sensors not sensitive to water but sensitive to HCl. In fact, HCl can quickly dissolve the nano-metric sputtered coating (~100 nm). When the coating is dissolved, the sensor sensitive part becomes exposed to the surrounding and can then react with the environment, in this case with the water.

3.7. *Mechanical testing*

Tensile test and three-point bending test were carried out on GFRP with and without embedded sensors to assess their mechanical properties and investigate the effect of optical fibre sensors embedded in the composite. Two sets of samples, 10 without OFSs and 10 with three embedded OFSs, were prepared. The distance between the embedded optical sensors was ~1 cm.

The tensile test was carried out according to the ASTM D3039/D3039M—17 [166] through a mechanical testing machine (ZwickRoell GmbH & Co., Ulm, Germany). The samples (25 0x 25 x 2 mm) were disposed in the middle of holding grips with a gauge length of 50 mm. The test speed was 2 mm/min.

Three-point bending samples (80 x 15 x 2 mm) were tested according to ISO 14125 standard [167] utilizing a mechanical testing machine (ZwickRoell GmbH

& Co., Ulm, Germany). The load was applied by moving the cross-head at a speed of 1.5 mm/min.

3.8. *Fabrication of chalcogenide TAS glass and fibre*

This activity was carried out at the “Verres et Céramiques, Institute of Université de Rennes 1”, Rennes, France. The fabrication of chalcogenide optical fibres consisted of three main steps. The first part started by weighting the ultra-pure elements Te, As and Se (TAS) (5N) in a glove box (Jacomex model) under argon atmosphere, in order to avoid atmosphere contamination such as oxygen and moisture. The powders would be later poured in a silica glass tube. This tube had previously been cleaned with hydrofluoric acid (HF) at 40 % (purchased from Sigma-Aldrich) to remove possible silica impurities, then rinsed with distilled water.

The tube was placed under the vacuum sealing, (Fig. 3. 8.), (Pfeifer vacuum Hi-Cube) for two hours at 10^{-5} bars to perfectly dry and avoid any kind of extra environmental impurity. Closing two valves, the glass tube was introduced in the glove box. The scaled elements were poured inside the glass tube. Then, it was connected again to the system and it was left for nearly 5 hours at 10^{-5} bars vacuum.

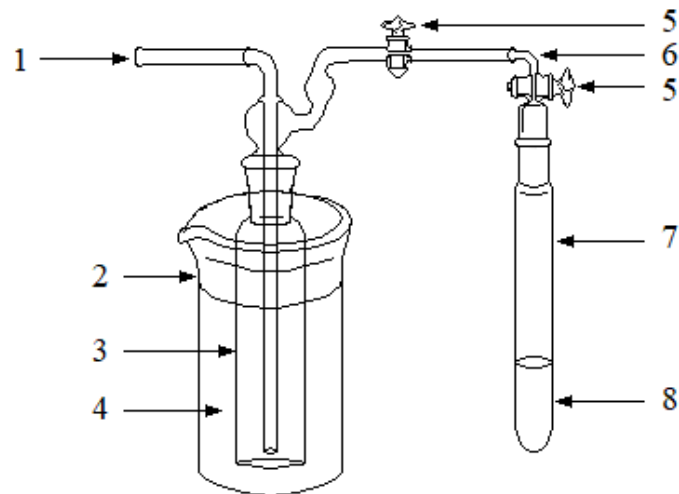


Figure 3. 8. Scheme of the vacuum sealing. 1: connection to the pump; 2: thermo to keep the liquid nitrogen and to hold the water trap inside; 3: water trap; 4: nitrogen; 5: valves; 6: glass connectors; 7: glass tube; 8: chalcogenide elements.

The tube was sealed by melting the edges. Then it was put for 14 hours in the rocking furnace (Pekly-Herrman-Moritz) using the following thermal treatment: heating from 450 to 750 °C with a heat ramp of 2 °C/min. It was kept for 2 hours at 750 °C and then cold down until 450 °C for 2 hours more. Then the tube was quenched in water to avoid the formation of crystals and put in an annealing furnace (Naberthern P320) at ~135 °C to remove the stresses induced by the quenching and the TAS rod was obtained.

The second step started by removing the TAS rod from the silica tube and placing it in the first sample holder inside the special distillation vacuum, (Fig. 3. 9.). The tube was sealed by melting the glass and the vacuum was switched on to reach a pressure of 10⁻⁵ bars. The glass was thermally treated from room temperature up to 450 °C for 8 hours and it was kept at 450 °C for two more hours. During this process, the glass was evaporated from the first sample holder and precipitated in the second sample holder due to the temperature difference. By evaporating the elements, the impurities were kept in the first sample holder. By sealing the edge between the second sample holder and the first sample holder the impurities were removed and as a plus the tube conserved the inert atmosphere.

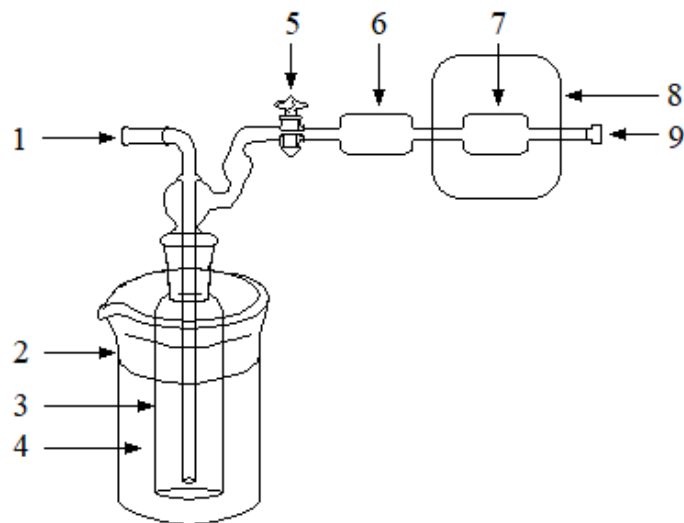


Figure 3. 9. Special distillation vacuum. 1; connection to the pump; 2: thermo beaker; 3: water trap; 4: nitrogen; 5: valve; 6: second sample holder; 7: first sample holder; 8: furnace; 9: sample insertion which was sealed by melting the silica glass.

The third step consisted in putting the sealed tube inside the furnace (Pekly Libelle Tubular). It was thematically treated from a starting temperature of 500 °C and heated until 580 °C during a period of 3 hours. This thermal method followed

the same principle of the second step. An Ultra-pure chalcogenide was obtained in the third sample holder. The glass evaporated and precipitated again, and the last impurities were kept in the second sample holder. The tube was sealed between the second sample holder and the third one, (Fig. 3. 10.). Then, another thermal treatment in the rocking furnace was required to well homogenise the TAS glass. In this part, the second heating treatment cycle in the rocking furnace consisted with a starting temperature of 450 to 650 °C with a heat ramp of 2 °C/min. Glass was kept at 650 °C for 6 hours and then it was cooled down to 500 °C for 2 hours. The sample was quenched again and put in the annealing furnace for 2 hours at 135 °C. Finally, the sample was removed from the silica glass tube and the chalcogenide rod was ready to be drawn in the drawing tower.

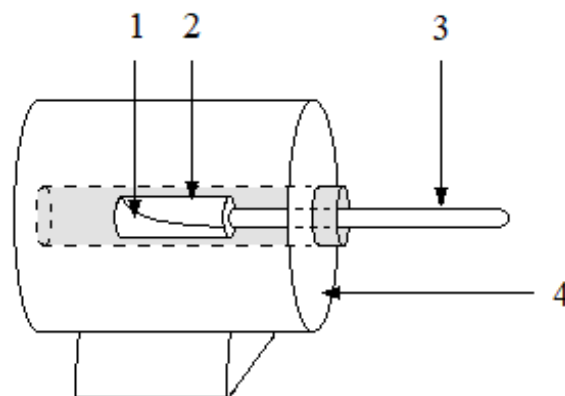


Figure 3. 10. Furnace pre-purification set up. 1: first purification sample; 2: second sample holder; 3: third sample holder; 4: furnace.

The chalcogenide rod was then placed in the sample holder of the drawing tower built in the Glass -CNRS group, (Fig. 3. 11.). Argon gas was pumped in the sample holder to create an inert atmosphere in order to avoid any kind of oxygen or carbon formation impurities on the surface of the glass when it was heated. The TAS rod was heated using the ring furnace heater and when the glass had a temperature nearly 135 °C, at which the viscosity of the TAS glass decreased, it started to melt. The primarily filament was passed through the diameter controller and the tension-meter and finally it was attached to a rotating drum for coiling. With a good control of the temperature and the tension, the selected diameter could be achieved. The fabricated TAS fibre had a diameter around 250 µm. Finally, the TAS fibre was rolled in the drum.

The TAS fibre was inspected under an optical microscope (Olympus BX41M-LED) in order to find microscopic crystal formations or dust inclusions. Furthermore, microscopic inspection was crucial to confirm the good quality of the process, assessed by a good, uniform and homogeneous fibre.

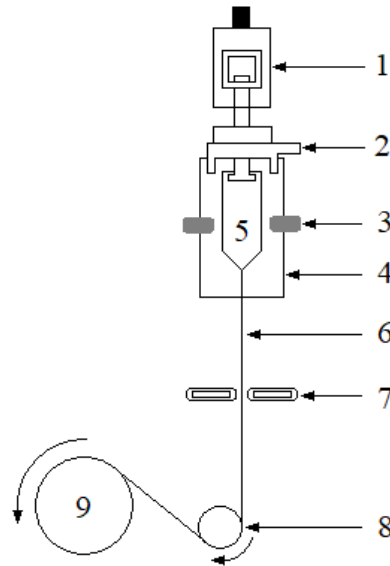


Figure 3. 11. Scheme of drawing tower. 1: preform descent; 2: He/Ar flux input; 3: ring furnace heater; 4: insulation air chamber protection; 5: TAS rod; 6: TAS necked fibre; 7: diameter measurement; 8: tension-meter; 9: drum.

3.8.1. Sample and instrumentation setup

The epoxy resin (Ampreg 26, Gurit) was prepared with the same procedure as described in section 3.1. The resin was poured in two different custom silicone moulds (CS-25 Condensation Cure Silicone Rubber purchased from Easy Composites [2]). One small with an inner a dimension of 20 x 10 x 20 mm, and one big mould with inner dimensions of 200 × 100 × 20 mm.

The diffusion coefficients were measured by immersing ten samples per test (25 x 25 x 5 mm) in distilled water at 80 °C and ethanol at room temperature up to 576 hours. Coefficients were calculated from the experimental absorption curves, and the expected diffusion length of the chemicals in the epoxy were evaluated assuming Fick's model and considering constant diffusion coefficients like in the section 3.1

The TAS fibre was passed through the custom silicone mould and connected to the IR analyser and to the detector. The resin was poured in the mold covering the TAS fibre. The sample was left for 24 hours at room temperature and thermally cured at 80 °C for 5 hours using a bath of silica sand with a hot plate. The epoxy cross-linking was monitored in situ and real-time. After register the epoxy cross-linking it was added on the cured epoxy surface the distilled water or ethanol. Their diffusion was also monitored in situ and real-time (Fig. 3. 12.).

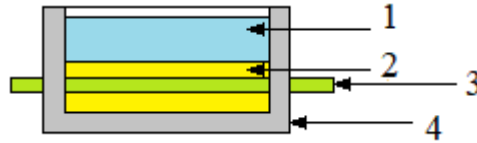


Figure 3. 12. Profile scheme of the TAS fibre embedded with the epoxy and with the water or ethanol on the top inside the mould. 1: distilled water or ethanol, 2: epoxy resin, 3 TAS fibre, 4: silicone custom mould.

Samples were sectioned in five parts and for each sectioned part a slide of 1 mm was cut to measure the distance between the epoxy surface to the embedded TAS fibre. Cuts were produced by a Precision Diamond Wire Saw, 3500. Samples were perfectly polished using polishing machine, Presi, Minitech 233. Finally, the samples were observed under an optical microscope Olympus BX41M-LED.

The transmission spectrum was obtained by dividing the two signals of classical transmission spectrum spectroscopy. In the same way, the absorbance spectrum was obtained by using (Eq. 3.3). The system is based on a FT-IR spectrometer. The input beam is produced by the black body source and is injected in the fibre. The output beam is collected on a mercury cadmium telluride (MCT) detector after focus by two parabolic mirrors. In order to avoid any kind of achromatism interference, the mirror is fixed in the IR range, (Fig. 3. 13.), [47]. Pristine measurement was recorded as reference spectra. This was carried out placing the necked TAS fibre through the mould without any extra contact to other materials or reagents.

$$A = \log \left(\frac{I_{ref}}{I_s} \right) \quad (3.3)$$

where I_{ref} is the intensity of pristine fibre and I_s is the intensity when the fibre is in contact with the sample.

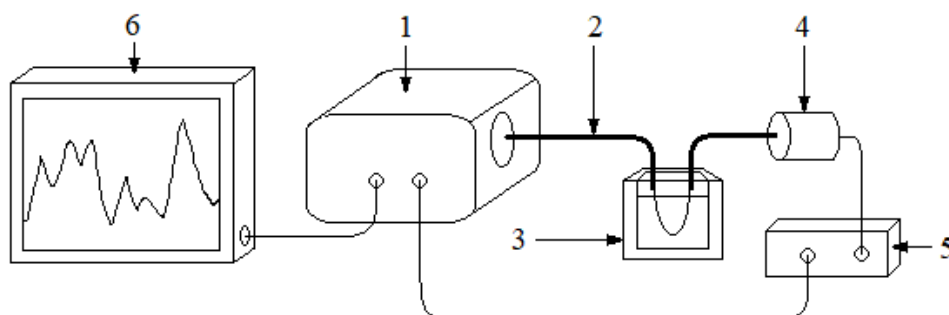


Figure 3. 13. Scheme of the principle of fibre wave spectroscopy (FEWS). 1: FTIR spectrometer, 2: chalcogenide fibre, 3: mould to hold the chemical to analyse, 4: MCT detector, 5: amplifier, 6: PC.

3.9. Epoxy containing CNTs samples fabrication

The epoxy resin (Ampreg 26, Gurit) was used and prepared with the same procedure as ascribed in the section 3.1. Precision scale (Balance technology explorer Ohaus with a precision of 0.0001 mg) placed inside a fume hood, was used to weight all the materials. CNTs (NC7000 Nanocyl CNTs) were weighed and manually mixed inside the fume hood with the epoxy resin. Afterwards, the mixture was thoroughly mixed using a three roll mill (TRM) instrument (80E EXAKT, GmbH, Germany) [168]. Moulds were fabricated using a CS-25 condensation cure silicone rubber purchased from Easy Composites [157].

Different CNTs filler content was used to generate the electrical percolation curve (1.50, 1.00, 0.75, 0.5, 0.25, 0.01 and 0.00 wt.%). Resin containing CNTs were prepared by TRM and degassed for 1 hour using a reduced pressure of -1 bar, before casting [169] into the silicone mould, where electrodes were already placed. Strips of aluminium foil, of dimension of 80 mm length, 3 mm width and 0.5 mm thickness, were used as electrodes. The epoxy resin was cured following the best curing conditions explored previously in ref. [14]. Artificial sea water was prepared following the ASTM D1141-93 (2003) procedure [170].

The percolation threshold of CNTs was calculated by the classical percolation theory equation, describing the conductivity change with filler content (Eq. 3.4.), [170]:

$$\sigma = \sigma_0(\varphi - \varphi_c)^t \quad (\text{Eq. 3. 4.})$$

where σ is the conductivity of the polymer containing CNTs, σ_0 is the scaling factor, φ is the filler content, φ_c is the percolation threshold, and t is a critical exponent which is expected to depend on the conductive system dimensionality only.

The diffusion coefficients of the epoxy and GFRP05 (GFRP samples containing spread CNTs on the plies fabrication) samples were evaluated and calculated with (Eq. 3.1). The absorption curves were obtained by immersing the samples in artificial sea water at 80 °C and performing gravimetric measurements until saturation was reached. Samples of epoxy containing CNTs and GFRP spray coated with CNTs on the plies had dimensions of (20 x 20 x 5 mm).

3.9.1. *GFRP samples containing spread CNTs on the plies (GFRP05)*

During the mixing of the CNTs with the epoxy resin, the viscosity was found to increase with the filler addition. For this reason, the cross-linking window of the epoxy was reduced from 2 hours to 30 minutes when the CNTs concentration was higher than 1 wt.% of CNTs. Furthermore, the filler tends to agglomerate, making it more difficult to obtain a good dispersion. To overcome the problem, CNTs were directly deposited on the Advantex E-CR glass fiber fabric (Owens Corning, USA) [172]. A solution of 0.01 g of CNTs with 100 ml of methanol (MeOH), purchased from Sigma Aldrich, was ultrasonicated at 5000 J energy with 20% of the maximum amplitude level for 15 min. After sonication, the suspension was sprayed with an airbrush on the E-CR plies. The GFRP composites s contained two fabrics; the two spray coated plies were assembled by positioning the spray coated face (0.50 wt.% of CNTs) of each ply in contact with each other (one ply at 90° respect to the other ply) [173]. The so manufactured GFRP composite is referred to as GFRP05.

3.9.2. *GFRP samples containing spread CNTs on the plies and embedded OFSs fabrication (SC-GFRP)*

The hybrid GFRP composite (H-GFRP) consisted of five optical fibre sensors and two plies spray coated with 0.50 wt.% CNTs. Figure 3. 14 shows a schematic of the H-GFRP cross-section where four OFSs are placed on the outer parts and the

one in the middle of the plies containing spread CNTs, as well as, a picture of the H-GFRP.

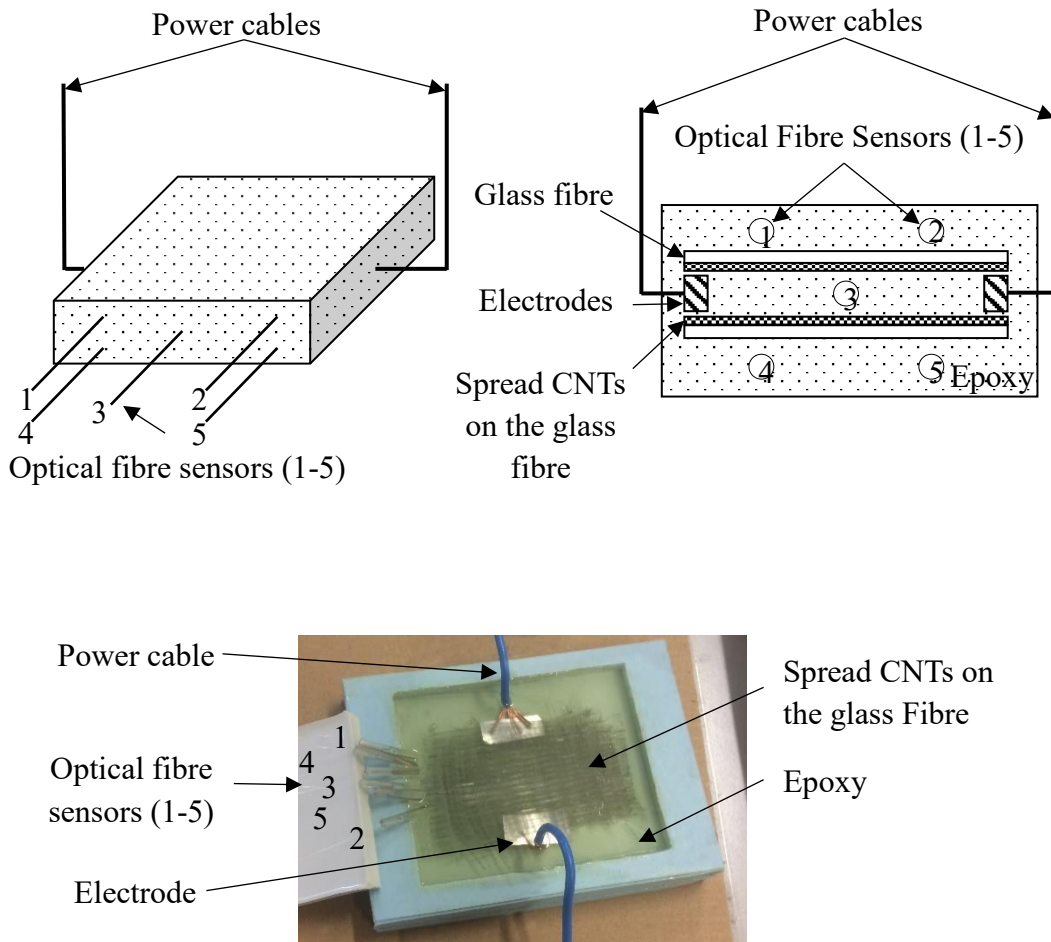


Figure 3. 14. Schematic, cross section representation and picture of the hybrid glass fibre reinforced polymer (H-GFRP) sample.

The H-GFRP was fabricated using a custom mould with inner dimensions of 50 x 80 x 110 mm. It was possible to calculate approximately the water diffusion distance, from the epoxy surface to fibres 1, 2, 4 and 5 in Fig. 3. 14., with Fick's law, (Eq. 3.2), [160] and using that the water diffusion coefficient in the epoxy measured [14], [15].

3.9.3. Optical fibre sensors fabrication and the interrogation setup

The optical glass fibre sensors were fabricated as described in the section 3.2. OFSs were interrogated using the interrogation setup explained in the section 3.5. Two-probes electrodes Keithley's Series 2400 source measure unit (SMU) instruments were used for the electrical resistance measurements. Samples were tested every 24 hours (Fig. 3. 15.).

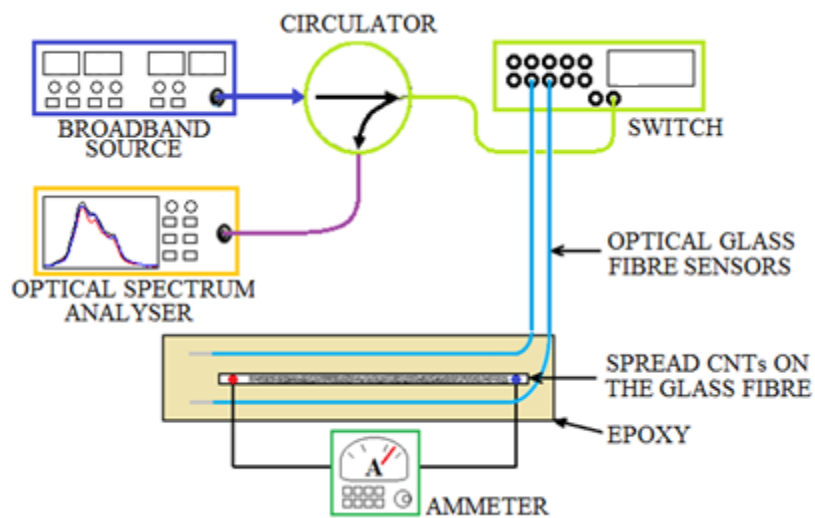


Figure 3. 15. Schematic of the interrogation set up of the combined sensors GFRP sample.

Chapter 4

Results & discussion

4.1. Epoxy, preparation and characterization results

4.1.1. Evaluation of the best curing conditions

The results and discussion from 4. 1. to 4. 7. are published and discussed by C. Marro Bellot et. al [14] and [15]. The curing conditions of the epoxy resin were determined by DSC and FT-IR analysis. DSC-dynamic analyses were initially performed to assess the heat released for a complete epoxy group conversion [174]. Figure 4. 1. shows the evaluation of the nonisothermal curve from 20 to 200 °C, which shows a single exothermic peak with excellent symmetry attributed due to the highly exothermic epoxy-amine addition. The total conversion of the epoxy resin is ΔH of $426 \pm 2 \text{ J/g}$. The DSC thermograms at different isothermal studies at 60, 80 and 100 °C, either for 3 or 5 hours at heating rate of 5 °C/min are given in the Fig: 4. 2. and 4. 3. The conversion data is represented in Figure 4. 4. As expected, by increasing the temperature a higher epoxy group conversion was achieved, since it was possible to delay the vitrification. As well, a longer curing time enhances the epoxy group conversion.

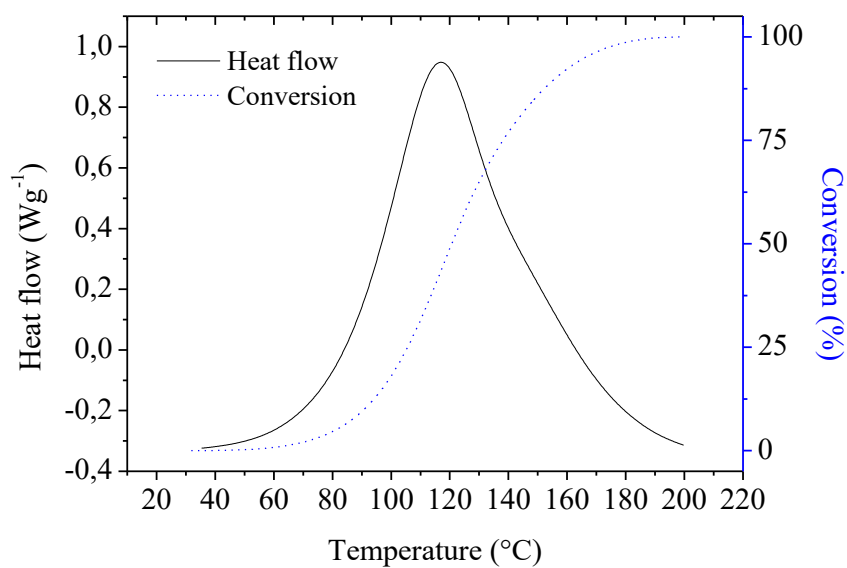


Figure 4. 1. DSC evaluation of the nonisothermal curve from 20 to 200 °C of the total ΔH study starting from 20 to 200 °C. The total ΔH is ($\Delta H_{\text{Total}} = 426 \text{ J/g}$).

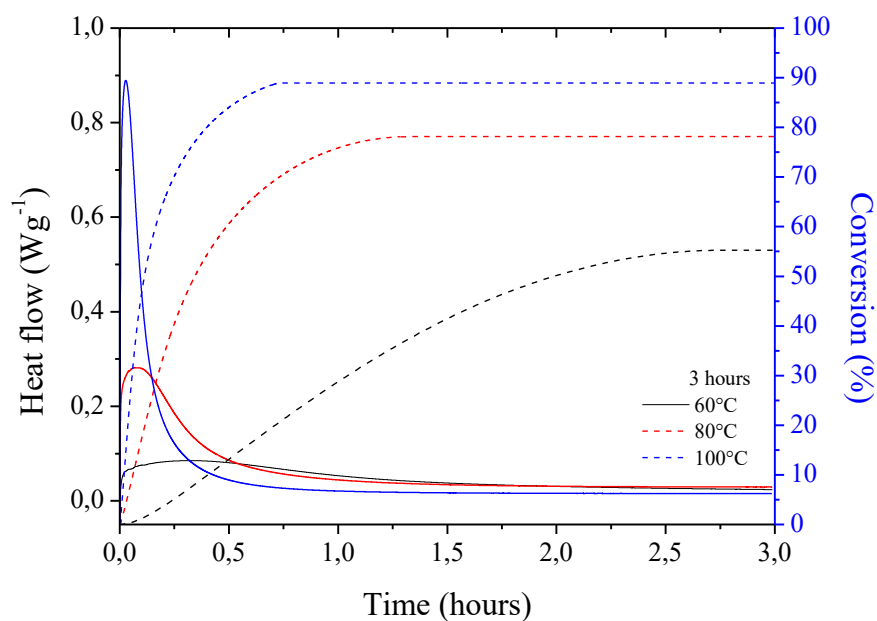


Figure 4. 2. DSC isothermals analysis at 60, 80, and 100 °C for 3 hours.

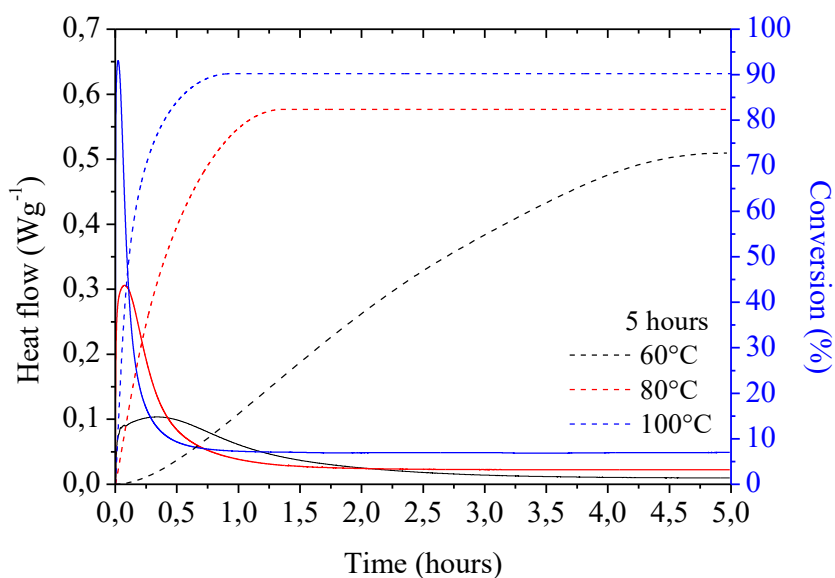


Figure 4. 3. DSC isothermals analysis at 60, 80, and 100 °C for 5 hours.

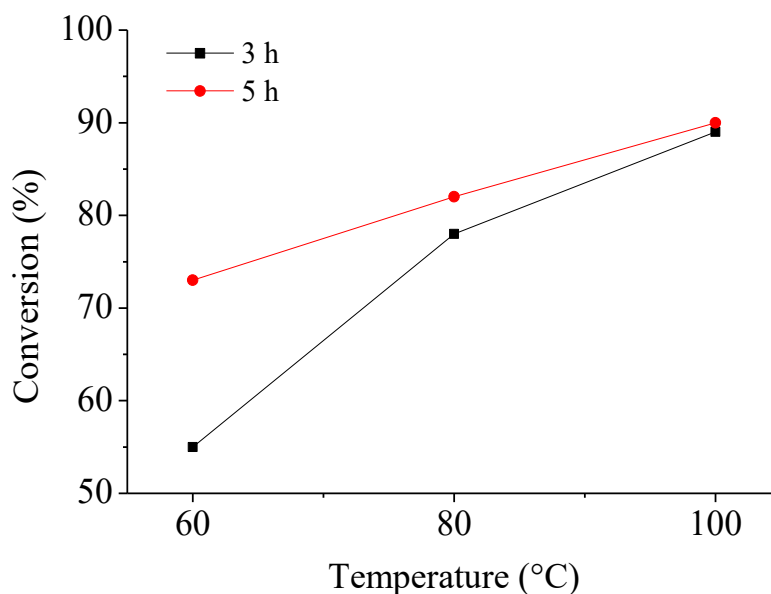


Figure 4. 4. DSC results at 60, 80, and 100 °C for 3 and 5 hours.

Epoxy group conversions were also measured by FT-IR analysis at 60, 80, and 100 °C, either for 3 or 5 hours. Epoxy group conversions were then evaluated by following the reduction of the peak area centred at 915 cm^{-1} . Figure 4. 5. shows the full FT-IR where the peak centred at 915 cm^{-1} decreases after the curing.

Furthermore, the centred epoxy group band peak is expanded inside Figure 4. 5. Table 4. 1. shows the conversions values calculated with the standard deviation by FT-IR analysis, which is in agreement with the values obtained by DSC experiments [175], [176], [177].

Table 4. 1. FT-IR conversion results at 60, 80, and 100 °C for 3 and 5 hours.

Temperature (°C)	Conversion (%) for 3 h	Conversion (%) for 5 h
60	86 ± 2	87 ± 1
80	88 ± 3	90 ± 2
100	92 ± 2	94 ± 3

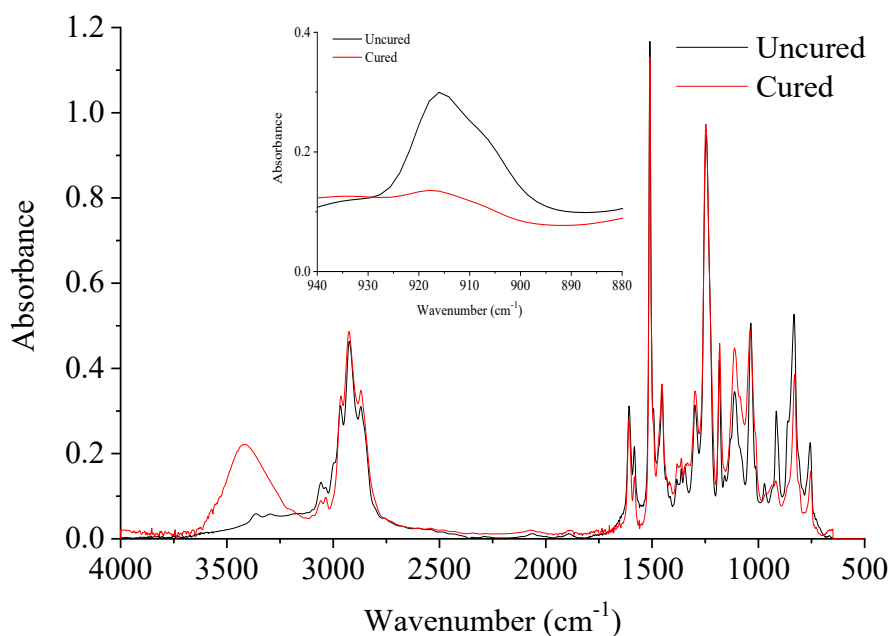


Figure 4. 5. FT-IR spectra for uncured epoxy (black) resin versus cured resin (red). The epoxy was treated for 24 hours at room temperature and 5 hours at 80 °C. The strong epoxy band appears between 930 to 890 cm^{-1} . Conversion is around 90 %.

4.1.2. Evaluation of the epoxy viscoelastic characteristics

The next analysis consisted of the study of the viscoelastic properties of the crosslinked epoxy. The viscoelastic properties of the crosslinked materials were evaluated by DMTA analysis. The values of the glass transition temperature (T_g) were measured as the maximum of $\tan\delta$ peak. The data, which compress the standard deviation, is summarized in Table 4. 2. As expected, by increasing the epoxy group conversion it was possible to achieve higher T_g values for the crosslinked materials due to a higher crosslinking density. By comparing the values obtained for the samples cured at 80 or 100 °C for 5 hours, it is evident that the T_g is not much different. Figure 4. 6. shows the $\tan\delta$ curves obtained from the DMTA analyses.

Table 4. 2. DMTA data results at 60, 80, and 100 °C for 3 and 5 hours.

T^a (°C)	Tg_{3h} (°C)	Tg_{5h} (°C)
60	88 ± 3	90 ± 2
80	94 ± 5	108 ± 3
100	108 ± 2	110 ± 3

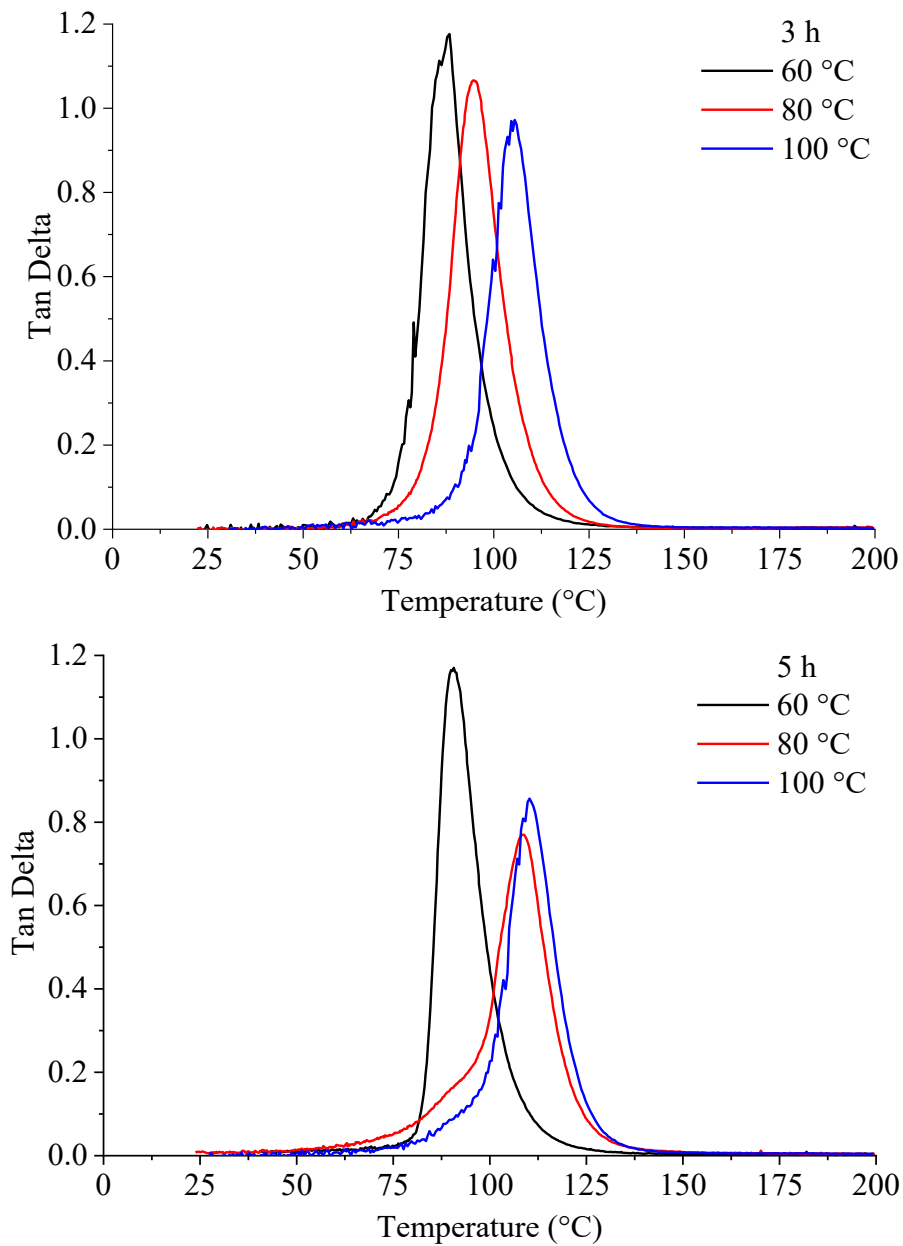


Figure 4. 6. DMTA $\tan\delta$ curves for the crosslinked epoxy at 60, 80, and 100 °C for 3 and 5 hours.

It was observed that the viscoelastic and thermal properties do not differ excessively for the crosslinked epoxy between 80 and 100 °C for 5 hours. For this reason, the curing conditions of the Ampreg 26 were established to be at 80 °C for 5 hours after characterising the viscoelastic and thermal properties, since these

allowed achieving an excellent conversion and a sufficiently high T_g of the crosslinked epoxy matrix.

Figure 4. 7. shows the results of the sectioned epoxy sample of 110 x 80 x 50 mm, cured at 80 °C for 5 hours, into 15 samples. The full characterization agreed with the excellent conversion and a sufficiently high T_g. It was demonstrated that the crosslinked epoxy was uniform giving in this case a T_g of 108 ± 1 °C. The small standard deviation in this case was attributed to the fact that the analysis was performed with the same epoxy sample instead of different samples. The high T_g of 108 °C was achieved for the full sample. Therefore, the selected curing conditions assure to obtain a crosslinked epoxy matrix characterized by high T_g and high thermal stability.

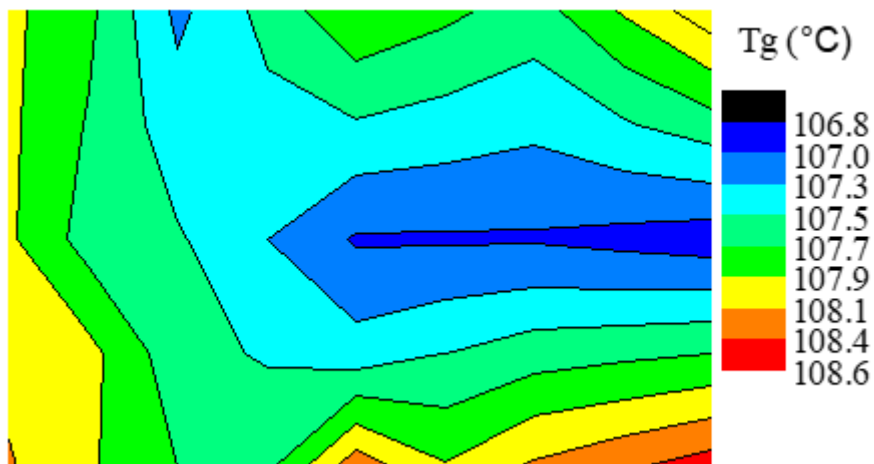


Figure 4. 7. DMTA characterisation of the sectioned into 15 pieces of an epoxy sample of 110 x 80 x 50 mm.

4.1.3. Evaluation of the thermal degradation temperature

Thermogravimetric analyses were performed to evaluate the thermal stability of the crosslinked material. The epoxy showed good thermal stability around 330 °C. It was observed the T_{5%} value around 333 ± 5 °C, which is a high enough temperature for the performance of the composites, Fig. 4. 8. After the temperature overpass the 300 °C, the mass losses start, and the epoxy resin decomposes. Within this temperature range, the chain scission of the epoxy resin networks yields the combustible gases, water, amines, and gaseous aromatic compounds, etc. [178].

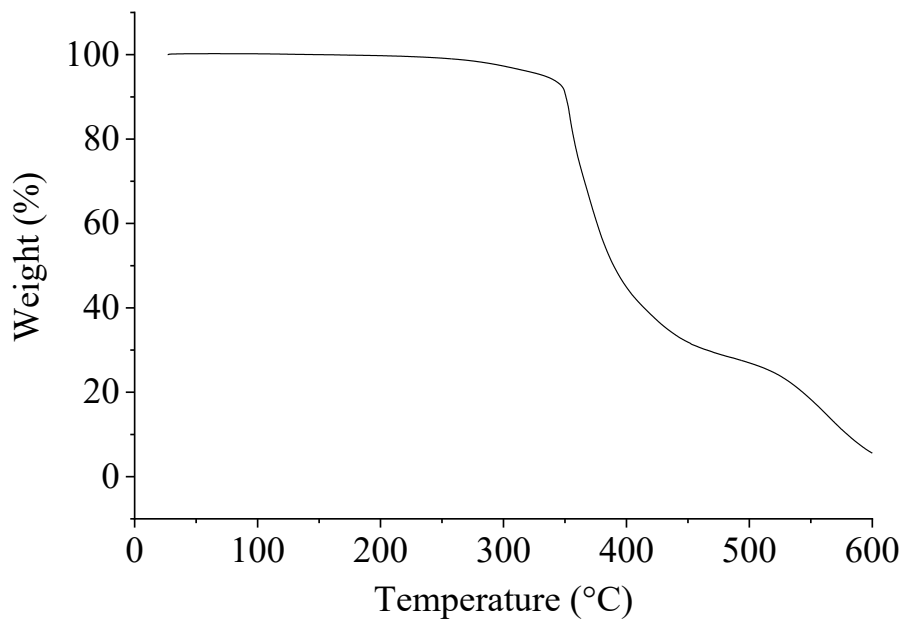


Figure 4. 8. TGA graphic analysis. The $T_{5\%}$ value occurs at around 333 ± 5 °C.

Since this is a commercial product, and it is not specified which are the exact percentages and compounds which forms the product, it is tricky to compare its physical properties with other epoxy resins. Assuming DGEBA and DGEBF are the mainly components in Ampreg 26 epoxy resin ($\geq 90\%$) and the Ampreg slow hardener is composed mainly with amines, the commercial product was compared with pure DGEBA and DGEBF, [179]. Ampreg 26 shows slightly better physical properties than the pure DGEBA and DGEBF. Furthermore, Ampreg 26 is a liquid substance at room temperature which allows an easy manufacture. The commercial resin presents a cost-effectiveness product while DGEBA and DGEBF are expensive.

4.1.4. Evaluation of the diffusion coefficients

The diffusion rates for the epoxy resin and glass fibre reinforced polymer (GFRP) samples were evaluated gravimetrically by immersing the samples into artificial sea water (ASW) under two different conditions: at 80 °C and at 80 °C under 50 bars of pressure. The diffusion values were also evaluated for the same samples, but this time immersed in HCl at room temperature. Figure 4. 9. reports the weight gain versus time; the calculated diffusion coefficients are reported in Table 4. 3. The diffusion coefficients were used to predict the diffusion time at a

given depth using (Eq. 3.1). It is apparent from this table that the hydrostatic pressure affects the diffusion coefficient of water at 80 °C. Several studies attempted to clarify the effect of hydrostatic pressure on water diffusion in composite materials [180], [181], [182], but the published results are contradictory. However, it is difficult to foresee, in general terms, the role of hydrostatic pressure, since the overall effect is due to a balance between the reduction free-volume (due to the increasing compression forces on the composites) and the increasing of the absorption driving force (due to the increasing chemical potential in the liquid phase). In accordance with our study, D. Choqueuse at al. [181] showed that increasing pressure results in faster water diffusion rates for epoxy-based materials.

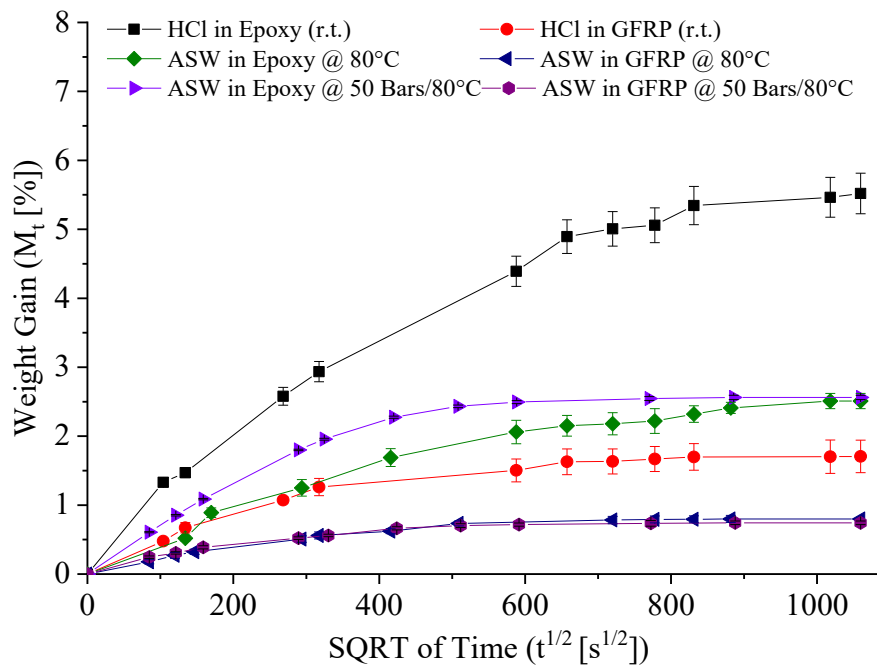


Figure 4. 9. Weight increment of the epoxy and GFRP samples immersed into artificial sea water (ASW at 80 °C, 80 °C under 50 bars of pressure and HCl at room temperature).

Table 4. 3. Diffusion coefficients calculated from Figure 4. 9. ASW = artificial sea water.

	<i>Epoxy</i>	<i>GFRP</i>
<i>ASW 80 °C</i>	$8.8 \pm 0.4 \times 10^{-12} \text{ m}^2/\text{s} *$	$4.9 \pm 0.1 \times 10^{-12} \text{ m}^2/\text{s} **$
<i>ASW 50 bars/80 °C</i>	$2.9 \pm 0.1 \times 10^{-11} \text{ m}^2/\text{s} **$	$8.9 \pm 0.1 \times 10^{-12} \text{ m}^2/\text{s} **$
<i>HCl r.t.</i>	$1.4 \pm 0.4 \times 10^{-11} \text{ m}^2/\text{s} **$	$4.5 \pm 0.2 \times 10^{-12} \text{ m}^2/\text{s} **$

*[11] **[12].

The diffusion coefficients rates of the epoxy and composites samples containing CNTs were also evaluated. These samples were tested by immersing epoxy containing 0.50 wt.% of CNTs (Epoxy05) and GFRP containing spread 0.50 wt.% of CNTs on the glass fibre plies (GFRP05) into artificial sea water (ASW) at 80 °C. They were prepared and evaluated in Nanoforce Ltd., (London, UK). Figure 4. 10. reports the weight gain versus time for the epoxy containing CNTs and GFRP containing spread CNTs on the ply samples water uptake. The calculated diffusion coefficients are reported in Table 4. 5. In comparison with the pristine samples (samples without CNTs) Epoxy05 and GFRP05 samples present a lower diffusion rate. This could be explained with the barrier properties of nanofillers which forms complicated paths, delaying the moisture diffusion and reducing the diffusion rate [183]. The results agreed with the research developed by Prolongo et al. [184] were the contrasted samples of an epoxy resin and epoxy resin containing CNTs present a similar behaviour and data agrees with the expected rates.

The diffusion rates for the epoxy resin were also evaluated gravimetrically by immersing the samples into distilled water (DW) at 80 °C and ethanol (EtOH) at room temperature. These tests were carried out at Université de Rennes 1, (Rennes, France). The calculated diffusion coefficients were used to approximately predict the diffusion time at a given depth using the (Eq. 3.2). Figure 4. 10. reports the weight gain versus time. The calculated diffusion coefficients are reported in Table 4. 4. Several studies attempted to clarify the effect of bounds interactions between these reagents when they diffuse in polymer matrix [185], [186]. The investigated results are in accordance by the investigated diffusion behaviour presented by M.

Sheng et al. (2016), [187]. The diffusion coefficients indicate that water diffusion has faster diffusion than ethanol diffusion due to the percolated free volume, or in other words, due to the water-accessible open space, in the epoxy structure. The paths of the water solute molecules display Brownian motion which can jump from pore to pore passing through the polymeric entanglement chain of the epoxy. The solute transport depends on both the Van der Waals interactions and on the size of the solute. For the ethanol solutes, the diffusion transport is lower because ethanol solutes have higher Van der Waals interactions when they diffuse in the epoxy and these solutes presents higher volume, which overcomes to less existing percolated free volume in the epoxy structure [187]. Furthermore, the distilled water diffusion agrees with the artificial salty water explained in the previous section.

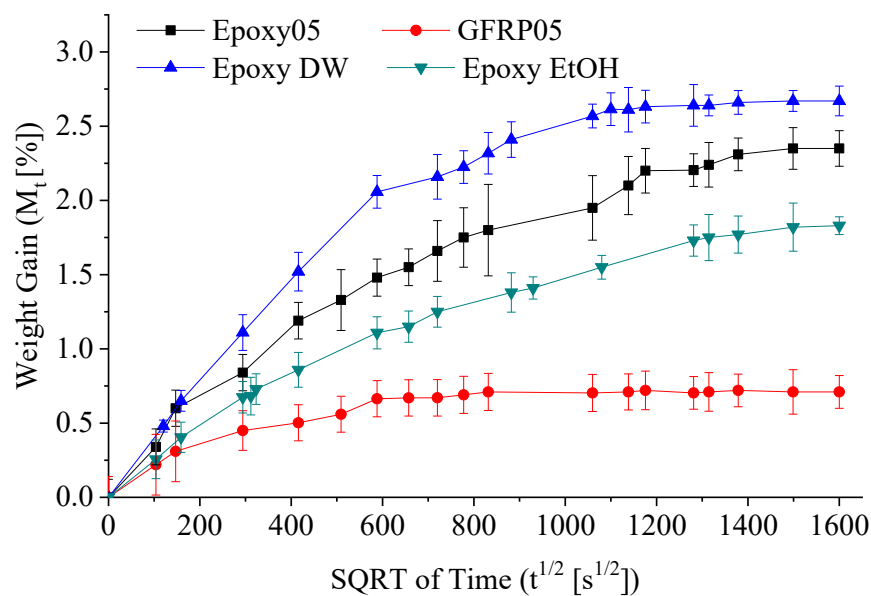


Figure 4. 10. Gravimetric experiment results of epoxy specimens full immersed into distilled water at 80 °C and ethanol at room temperature, and Epoxy05 and GFRP05 samples full immersed into artificial salty water at 80 °C. All samples were tested up to 712 hours.

Table 4. 4. Diffusion coefficients calculated from Figure 4.10.

	<i>Distilled water at 80 °C</i>	<i>Ethanol</i>
<i>Epoxy</i>	$8.4 \pm 0.3 \times 10^{-12} \text{ m}^2/\text{s}$	$5.7 \pm 0.2 \times 10^{-12} \text{ m}^2/\text{s}$

Table 4. 5. Diffusion coefficients calculated from Figure 4.10.

	<i>Epoxy05</i>	<i>GFRP05</i>
<i>ASW 80 °C</i>	$5.4 \pm 0.3 \times 10^{-12} \text{ m}^2/\text{s}$	$4.0 \pm 0.1 \times 10^{-12} \text{ m}^2/\text{s}$

4.1.5. Evaluation of the epoxy refractive index

Figure 4. 11. reports the evaluation of the refractive index (RI) of the pristine epoxy samples and epoxy samples after being immersed for two weeks into artificial salty water and hydrochloric acid. In order to investigate different possible absorptions, the wavelengths for the measurement were carried out in the range from 633 to 1533 nm. The given RIs by the RI instruments are summarized in Table 4. 6. As it was expected, it was observed that the epoxy RIs have not changed significantly. Furthermore, the pure epoxy samples agreed with the expected RI of 1.55 [179]. The RIs of the samples were always superior to the RI of the optical glass fibre, which is 1.47. This condition makes favourable the scattering of the light from the optical glass fibre sensors making them more sensitive for environmental surrounding changes.

On the other hand, the change of the absorption of the light can be directly observed by naked eye. The fresh cured epoxy samples show a yellow transparent colour. After their immersion in artificial salty water, the epoxy samples become yellowish. Finally, after their immersion in hydrochloric acid, the epoxy samples become reddish. Nevertheless, a change in the colour in the UV-Vis does not mean that the RI of the epoxy changes. The different tested epoxy samples confirmed that the absorptions on the UV-Vis did not produce changes in the infrared.

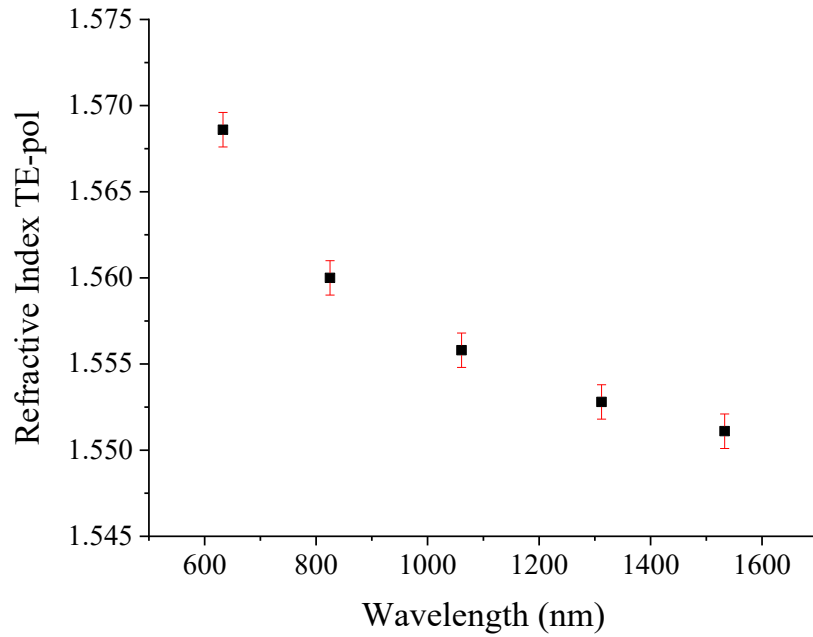


Figure 4. 11. The RI average measurements at the wavelengths from 633 to 1533 nm. The epoxy RI average is 1.55 ± 0.01 .

Table 4. 6. The RI of the epoxy after curing, the epoxy after being treated in artificial salty water and hydrochloric acid for two weeks.

<i>Sample</i>	<i>RI</i>
Epoxy	1.55 ± 0.01
Epoxy subjected to artificial salty water	1.55 ± 0.01
Epoxy subjected to hydrochloric acid	1.55 ± 0.01

4.2. *Fabrication of the optical fibre sensors*

4.2.1. *Etching of the optical fibres*

The optimisation of the etching was necessary to produce the optical glass fibre sensors with a good accuracy and reproducibility. It was expected to obtain a linear

curve such as Dennis et al. [188] presented in their patent. Figure 4. 12. shows the experimental etching curve obtained after the etching of the optical glass fibres. In comparison with the previous works by Milson et al. [28], [96] the etching rate was mostly the same. The etching follows a linear regression which allows the possibility to calculate the time necessary in order to obtain the desired diameter of approximately 55µm.

After the etching the optical glass fibres becomes extremely fragile since the protecting polymer coating is stripped and the cladding is etched.

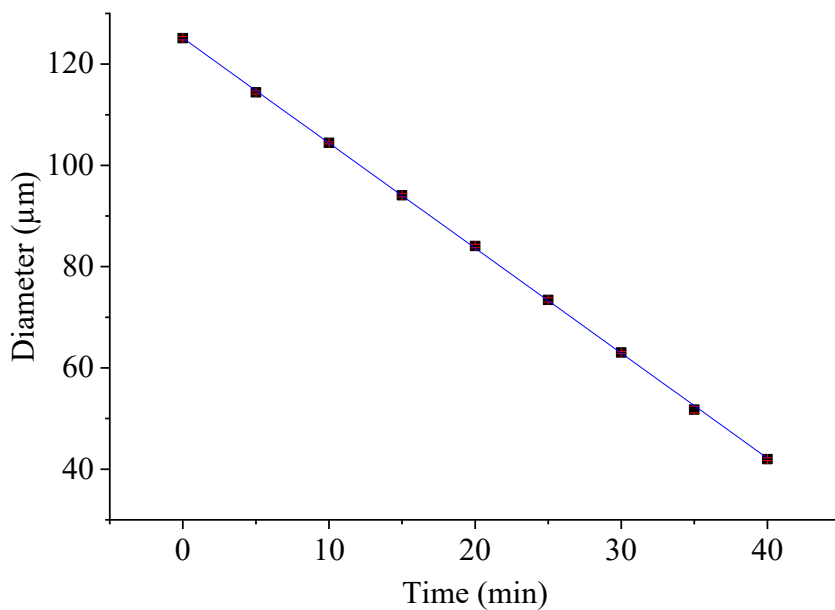


Figure 4. 12. Etching graph relation where the etching rate follows the equation $y = 125.1 - 2.1 \cdot t$ at room temperature.

Figure 4. 13. shows the typical images of the optical glass fibres during the etching process at different times. Furthermore, the cross-sectional image reveals the good and uniform etching of the fibre. The pictures reveal an excellent time-etched dependence following the etching rate calculated above of etching diameter = $125.1 - 2.1 \cdot t$. For the required application and in order to obtain a good, and reproducible sensor, the etching must be uniform. Otherwise, a uniform etched fibre could behave like a side- polished optical glass fibre and the sensitive part of the exposed etched core could be not sensitive at all. This situation would directly affect to the optical glass fibre sensor fabrication because light would not be well guided along the fibre.

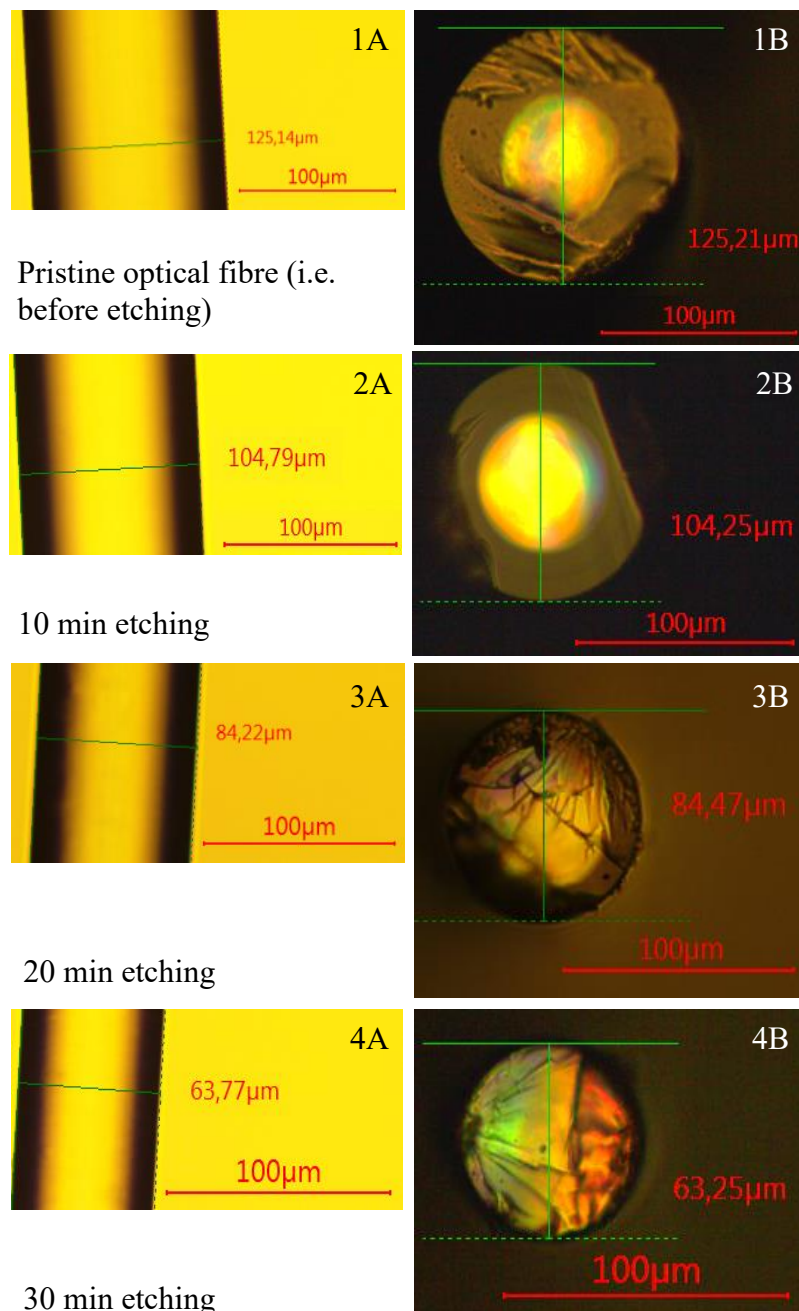


Figure 4. 13. Microscopy cross-section images taken during the etching process; 1: Pristine optical fibre (i.e. before etching); 2: 10 min etching; 3: 20 min etching; 4: 30 min etching; A: longitudinal image; B: cross-section image (bright inner circle is the core where the light is guided). From 1B to 4B it can be observed that the diameter is almost reduced to the core. Scratches, due to poor cleaving, are observable in all cross-section pictures.

4.2.2. Silver coating deposition and fabrication of the optical glass fibre sensor

Both Tollen's reagent and PVD showed excellent results producing the reflective mirror on the extreme tip of the optical glass fibre with an efficiency of 100% respecting on the commercial reference mirror. The silver glue had poor results and did not produce any reflective coating due to their big silver particles. It was observed an efficiency of less than 30 %.

Figure 4. 14 a) shows an example of one OFSs measured by an optical microscope. The pictures show an etched OF before producing the silver deposition using the Tollen's reagent. The OF shows a uniform etching and it does not present cracks or perturbations on the fibre. Furthermore, it can be observed the good cleaving of 90° at the extreme tip of the fibre. As it was discussed before, this is crucial in order to get an excellent reflected transmitted light. The fibre presents a diameter of roughly $55 \pm 1 \mu\text{m}$ after immersing it into HF for ~ 33 min. Figure 4. 14. b) shows the optical microscopy analysis after performing the Tollen's reagent. The picture shows an excellent silver attachment along the fibre. It can be also observed some silver flakes on the fibre wall, which could be produced due to some impurities on the chemical deposition. From the measured pictures the deposited silver thickness using the Tollen's reagent is $5 \pm 1 \mu\text{m}$. However, in order to obtain more precise measurements, the silver tips of the OFSs were evaluated using a Scanning Electron Microscope (SEM).

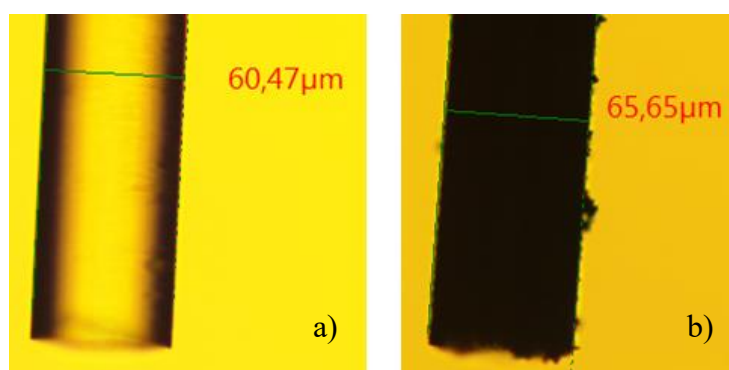


Figure 4. 14. a) Uncoated optical fibre perfectly cleaved at 90°, b) optical fibre after silver deposition using Tollens' reagent.

Figure 4.15. shows an example of one SEM image of the deposited silver coating on the extreme of the straight cleaved fibre tip using the Tollen's reagent. The image shows a silver coating thickness of $4 \pm 1 \mu\text{m}$. Furthermore, it can be observed an excellent adhesion and excellent uniform distribution of the deposited silver coating. In order to investigate the flakes attached on the wall observed by the optical microscope, a sectional SEM analysis of the OFS was made. Figure 4. 16. shows the sectional picture of the OFS where the previously observed flakes correspond to agglomeration of silver particles along the fibre. Since the silver coating is only produced to reflect the light, these thicker depositions do not affect the measurements.

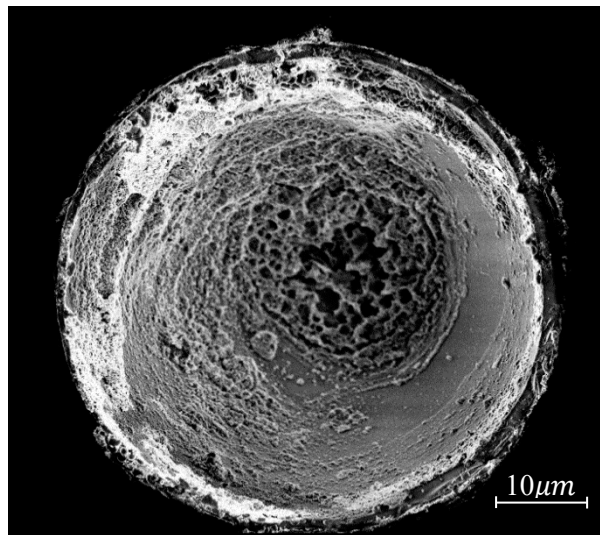


Figure 4. 15. SEM image of the extreme tip coated using Tollen's reagent.

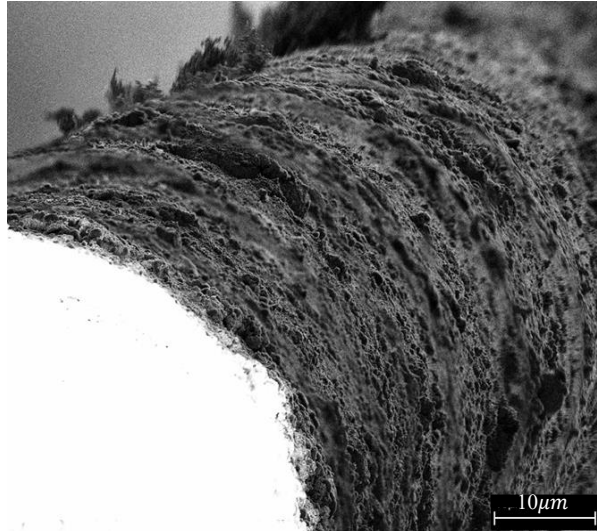


Figure 4. 16. Sectional SEM image of the extreme tip coated using Tollen's reagent.

H. H. Schroeder et al. [194], explored the excellent reflective properties of copper and gold to be used as a possible mirror due to these two metals can reflect extremely well in the infrared. These two materials could be taken into consideration as alternative reflective coatings. However, they require the PVD technique which is not commonly available in industrial R&D laboratories or facilities. For this reason, the chemical method was preferred due to the excellent results and easy performance.

4.2.3. *Optimization of the optical fibre sensor length*

The etched optical silica fibre acts as a sensor by leaking light into the epoxy. The attenuation of the light guided into the fibre changes because of a change in the optical properties of the epoxy surrounding the core of the fibre. A trade-off between the length of the sensor and the back-reflected signal exists: short sensors did exhibit low sensitivity, whereas long sensors did not provide enough back-scattered signals to be probed. For these reasons, the length of the optical fibres was optimised.

In order to optimise the sensitivity, sensors were produced with different lengths of the chemically-etched section (2, 6, 8, 10 and 14 cm). Figure 4. 17. shows the spectra reflected from sensors manufactured with different sensing lengths, when they are characterized in the same conditions (i.e. the same power of the source, same parameters of the spectrometer). These spectra are compared with the commercial reference fibre mirror. The reference fibre mirror is a commercial component devised to back-reflect 100% of the light coming from the source. An evanescent wave sensor provides the back reflection of a portion of the light of the source, since part of it is scattered in the surrounding environment (i.e. the epoxy sample).

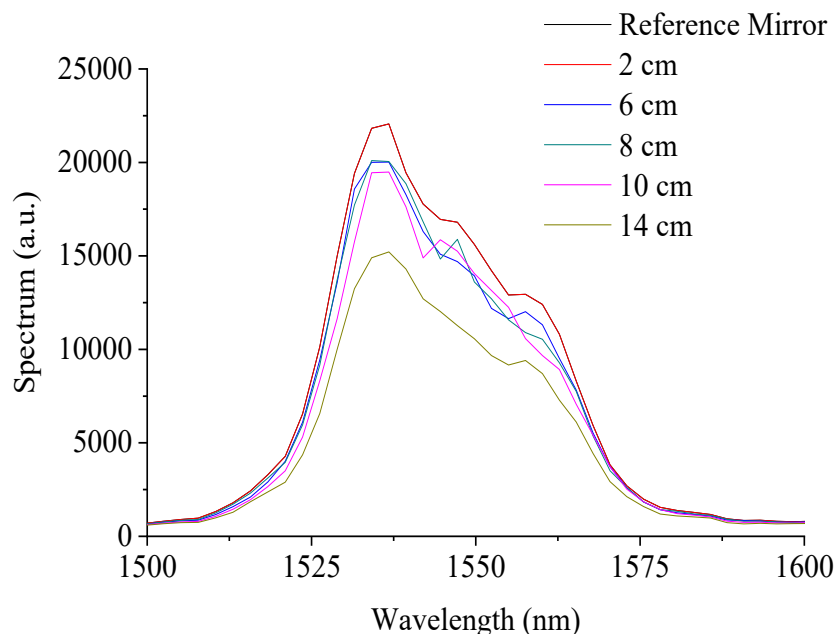


Figure 4. 17. Experimental optimization of the length of the optical fibre sensors embedded in an epoxy by comparing back-reflected spectrum with that of a reference fibre mirror.

Experimental optimisation of different sensors length showed that the sensors of 2 cm length embedded in the epoxy could not detect water diffusion when they were immersed in artificial salty water, due to their sensitive part were not enough. Whereas the embedded sensors of over 10 cm length did not provide a useful back-scattered signal, due to the light got scattered. Embedded sensors with lengths between 6 to 10 cm proved to yield a back-reflected signal close to that of the

reference mirror, yet exhibiting sensitivity to water diffusion. Therefore, the standard length for the subsequent water diffusion experiments was set to 8 cm.

After the fabrication and the length optimisation of the OFSs working reflectively, some sensors were sputtered with copper in their sensitive section to annihilate their sensitivity to the surrounding environment. These sputtered optical fibre sensors were prepared (referred to as Cu-OFS) by depositing a copper coating on the bare etched core by Physical Vapour Deposition (Radio Frequency magnetron sputtering, Microcoat). The purpose of using the Cu-OFSs was to prove that the information provided by the OFSs was not related to spurious phenomena such as for example a source fluctuation, mechanical stress, and temperature change.

Furthermore, the standard deviation of the fluctuation of the interrogation setup was also evaluated. It was used the purchased reference mirror to obtain the reference signal. The reference mirror was connected and disconnected several times using different movable and fix connectors. The spectres were also recorded for 24 hours to have an accurate fluctuation. Figure 4. 18. shows the reference signal with the standard deviation acquired for 24 hours. The calculated standard deviation can vary depending on which wavelength it is analysed. Figure 4. 18. depicts a small standard deviation in the range from 1500 to 1600 nm. These ranges show a standard deviation of less than 500 nm. In the middle range of the spectra, from 1526 to 1569 nm the variation reaches approximately 1000 nm.

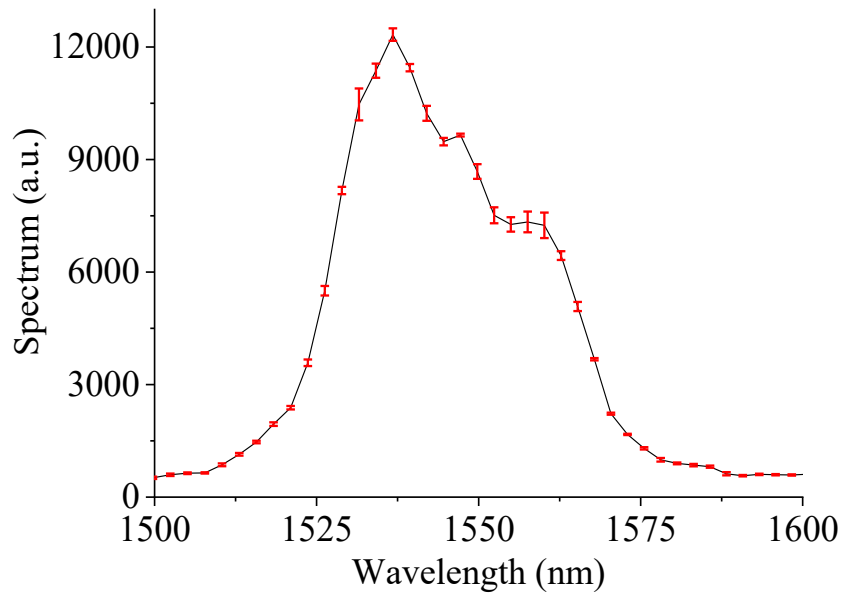


Figure 4. 18. Standard deviation fluctuation of the recorded spectra for 24 hours.

4.3. *Mechanical tests*

In order to demonstrate that the embedding of the OFSs do not affect the mechanical properties of the composites, the GFRPs were mechanically tested with and without embedded OFSs (in collaboration with Element Technology, UK). The results of the tensile and three-point bending tests are summarised in Table 4. 7. The results confirm that the optical fibres have no relevant effects on the mechanical properties of the composites and agree with early studies [97], though attention should be paid if the composites were subjected to fatigue load. Furthermore, more specific mechanical characterisations should be carried out to assess the possible effect of embedded OFSs on the final component properties.

Table 4. 7. Mechanical test results of the tensile test and three-point bending test of GFRPs with and without embedded OFSs.

	Tensile test		Three-point bending test	
	σ (MPa)	E (GPa)	σ (MPa)	E (GPa)
GFRP	367 ± 15	22 ± 5	364 ± 24	17 ± 1
GFRP + OFSs	356 ± 23	20 ± 3	368 ± 26	17 ± 1

4.4. *Characterization of the epoxy samples equipped with optical fibre sensors*

4.4.1. *Epoxy samples subjected to artificial salty water at 80 °C non-continuous monitoring*

Figure 4. 19. a) shows a real epoxy sample picture with the dimensions of (110 x 80 x 50 mm) where two OFSs are embedded. The OFSs tales are protected using an optical fiber heat shrinkable splice protection sleeves.



Figure 4. 19. a) Picture of epoxy sample where two OFSs are embedded.

Once the epoxy with an embedded sensor was fabricated, samples were immersed into artificial salty water. The temperature was fixed at 80 °C to accelerate the diffusion of the water through the epoxy and, moreover, to accelerate

the ageing of the sample. This temperature is also close to the Tg of the polymer, which makes favourable a faster diffusion. Furthermore, some samples contained both OFSs and a Cu-OFSs. These samples were tested following the same conditions of immersing them in artificial salty water at 80 °C until the signal decreased.

The aim of embedding these different sensors typology, one with the sensitive part exposed and one with the sensitive part sputtered with copper, was to demonstrate and corroborate the sensitivity of the optical sensors against the water. It was expected that only the optical fibre sensors with their sensitive etched part exposed to the surrounding environment would response when the water would reach their depth position. In contrast, the optical fibre sensors sputtered with copper would not due to their etched core sensitive parts were completely covered with the metal. Therefore, the sensors would be inert to water detection because now the water cannot interact with the etched sensitive part.

The first experiments were carried out in non-continuous mode. The epoxy samples had a dimension of (105 x 80 x 10 mm). The samples were immersed in the artificial salty water at 80 °C, and the reflected signal from the sensors was recorded every 5 min. Figure 4. 20. depicts an example of the response of the reflected signal from an OFS in the near-infrared spectrum (1500-1600 nm) recorded at different exposure times. A remarkable signal drop occurs at 48 hours. As discussed in [14], the spectral attenuation is probably due to a change in the optical properties, in particular, the absorption coefficient of the epoxy surrounding the exposed core. The absorption coefficient represents the imaginary part of the refractive index and it affects the attenuation of the sensing region of the embedded optical fibre. In previous works (e.g. [28] and [96]), it was demonstrated that the increment of absorption in the infrared region of the spectrum, observed after water diffusion, could be ascribed to -OH stretching. Furthermore, the real part of the refractive index measured on pristine and water saturated samples was about 1.55 ± 0.01 without a remarkable variation caused by water exposure, hence concluding that the attenuation of the optical signal is caused by an increment of the optical absorption of the epoxy in the recorded spectral range. This hypothesis is also supported by the calculated diffusion time to reach the depth corresponding to the sensor position, which occurs approximately after 48 hours.

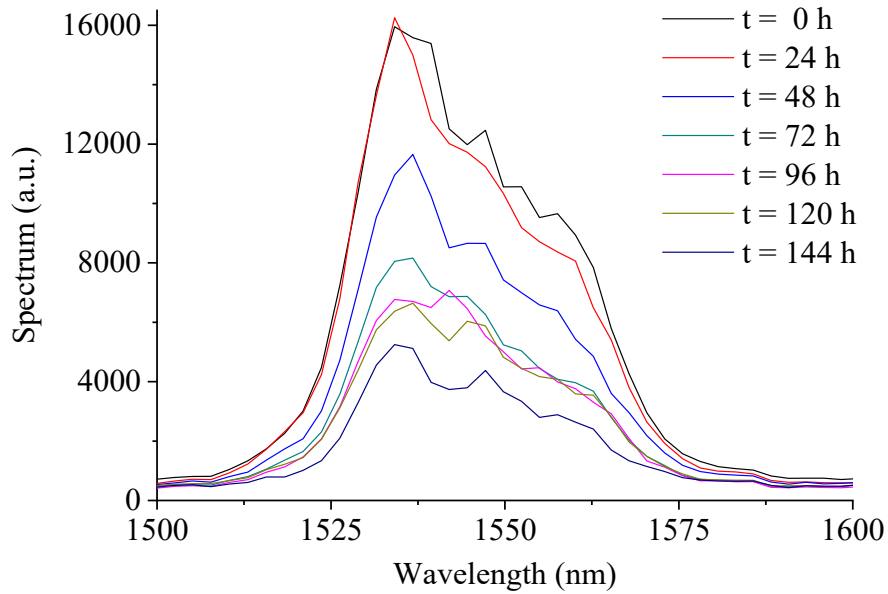


Figure 4. 20. Reflected spectra of an OFS embedded in the epoxy exposed to artificial salty water at 80 °C. Spectra were collected every 5 min, but only relevant curves are here reported.

Furthermore, the Cu-OFS sensor did not exhibit any changes within the measurement uncertainty (Fig. 4. 21.). Cu-OFS confirmed that diffusion of the water produced the information obtained from OFSs through the matrix rather than spurious effects such as thermal expansion, contraction or temperature change. The small decrease observed was correlated with the fluctuation of the signal produced by the broadband source and connectors.

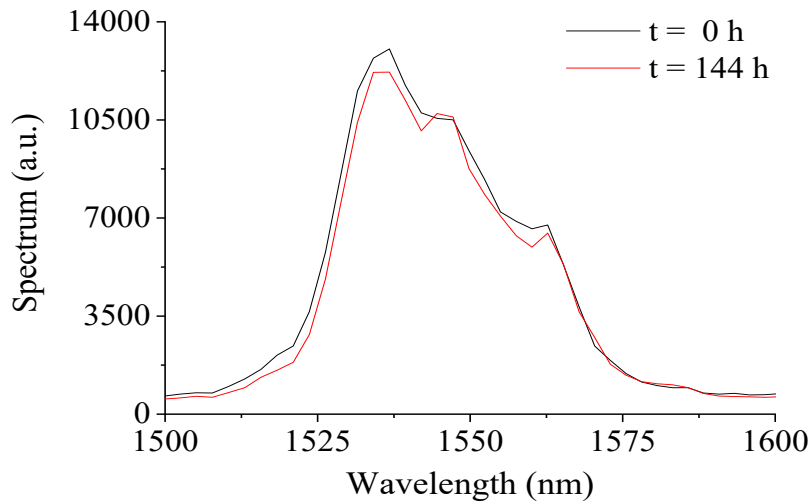


Figure 4. 21. Reflected spectra of a Cu-OFS embedded into the epoxy exposed to expose to artificial salty water at 80 °C.

The OFSs showed to be sensitive to moisture. So, it was checked if the sensors could be reversible by drying the samples after being immersed in the artificial salty water. Epoxies containing embedded optical glass fibre sensors samples were dried at 80 °C for two weeks after been exposed in artificial salty water for one week to study the reversibility. As shown in Figure 4. 22., the response of the embedded OFS is completely reversible: when the water is not present in the epoxy resin surrounding the sensitive region of the OFS, the signal intensity is comparable to the one before the ageing test.

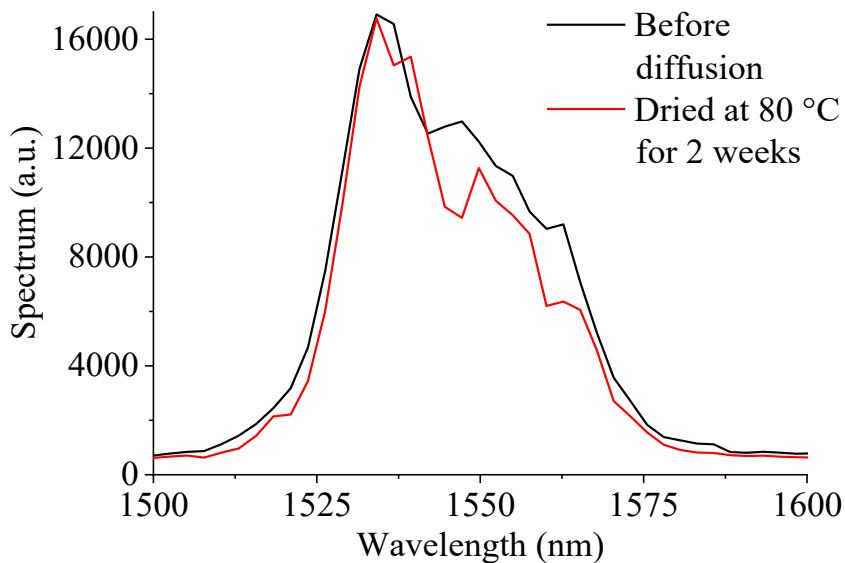


Figure 4. 22. Reflected spectra before water diffusion (black) and after the water-diffused sample was dried at 80 °C for two weeks (red).

4.4.2. *Epoxy samples subjected to artificial salty water at 80 °C continuous monitoring*

After obtaining the first promising data, further experiments were carried out in continuous monitoring for both sensors, the OFSs and Cu-OFSs. A custom LabView program in collaboration with the Mario Boella Institute, Torino, Italy, was developed. This software allowed the possibility to use a switch and automatically analyses the sensors.

Furthermore, a switch made possible to test a total number of 16 sensors at the simultaneously without human intervention. This approach represents a considerable advance in the sensing because it was not necessary to manipulate the sensors, connecting and disconnecting every time them to get the data. As the fibres were not continuously manipulated, the obtained data presented better stability. Therefore, the water diffusion through the epoxy was successfully registered in continuous and real time. Furthermore, it was possible to perfectly record at which point the signal of the reflected light of the optical sensors started to decrease.

Epoxy samples containing a total of three embedded sensors were immersed in artificial salty water at 80 °C for 48 hours. It was then possible to automatically

record the reflected light signal from the optical sensors using the custom LabView program. The data was recorded every 5 minutes in a range between 1500 to 1600 nm. The maximum intensity of the signal given by the spectrometer occurred at 1532 nm, which was then evaluated as a function of time. After the analyses, the samples were cut into five parts, and the distances from the surface to the optical sensor were measured.

Figure 4. 23. shows an example of the signal obtained from one optical glass fibre sensor embedded into an epoxy sample. The reflected light signal from the optical sensor dropped from around 17000 to near 5000 a.u. after 21 hours. The decrement of the reflected light signal was quite notable because it had a significant decrease of approximately 90% of the reflected light. The optical sensor was embedded in a measured depth distance of about 1.6 mm. According to the theoretically calculated D coefficient of the diffused water length the signal was expected to occur approximately at 20 ± 2 hours. As the graph below shows, the signal drop was recorded after 21 hours which means that the optical sensor can detect the water diffusion through the epoxy with a good approximation.

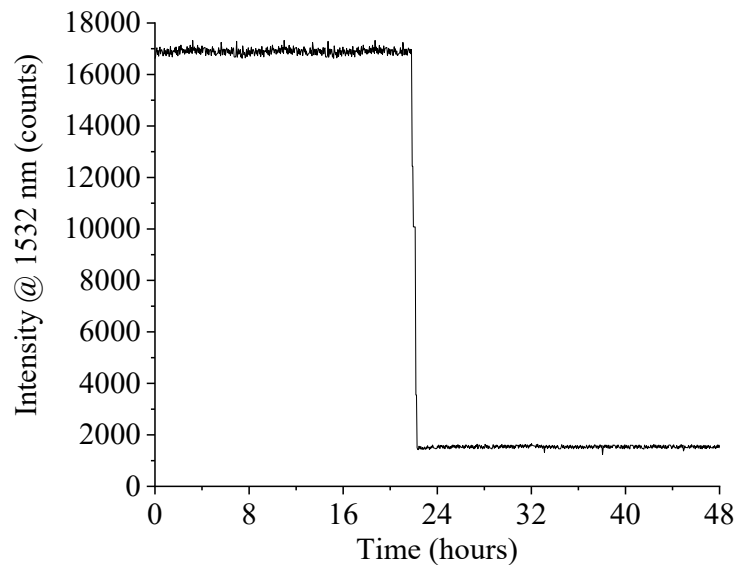


Figure 4. 23. Signal intensity, at wavelength of 1532 nm, from an optical glass sensor embedded in an epoxy sample at depth of 1.6 mm.

Figure 4. 24. shows the signal obtained from the copper sputtered optical sensor (Cu-OFS) embedded in an epoxy sample. The signals were constant with a smooth fluctuation of the signal for 24 hours. Once again, the experiments demonstrate that

the obtained signals from the OFSSs were produced from the moisture and not from spurious phenomena.

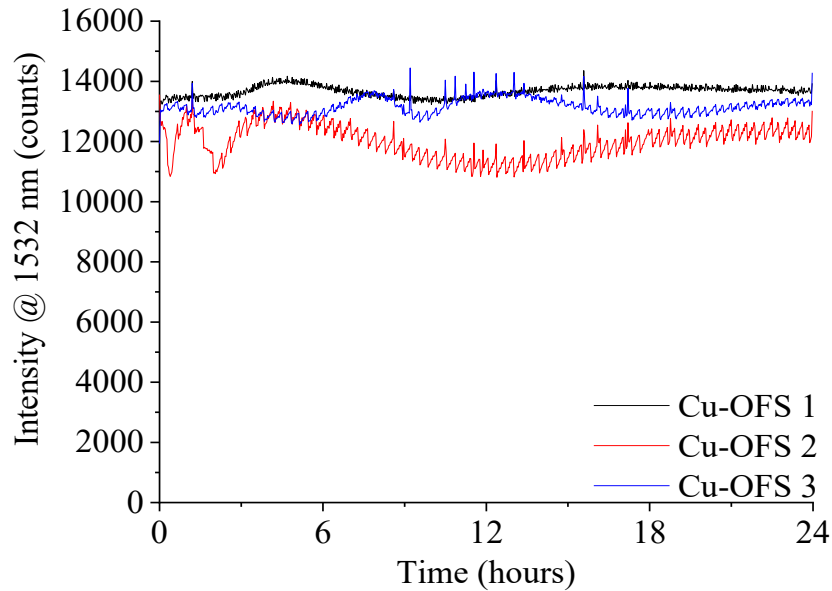


Figure 4. 24. Signal intensity at wavelength of 1532 nm from three embedded Cu-OFSs for 24 hours in continuous monitoring.

4.4.3. Epoxy samples subjected to artificial salty water at 80 °C with OFSSs embedded at different depths in the epoxy in continuous monitoring

The sensors showed to be able to produce a signal when the water diffuses through the epoxy matrix. It was then planned another experiment to detect the water diffusion through the epoxy. Figure 4. 25. shows the signal intensity at 1532 nm recorded from three different OFSSs embedded in the epoxy at different distances from the surface. The epoxy sample containing the three different OFSSs at different depths had a dimension of (105 x 80 x 15 mm). The epoxy sample was immersed in artificial sea water at 80 °C up to 96 hours. The signals from the optical sensors dropped at different times according to the depths of the sensors. The first sensor, located at a depth of 2.5 ± 0.1 mm, showed a drop in the signal after approximately 43 hours. The second sensor, located at a depth of 2.8 ± 0.1 mm, showed a drop in the signal after approximately 64 hours. Finally, the third sensor, located at a depth of 3.0 ± 0.1 mm, showed a drop in the signal after approximately 73 hours. The calculated diffusion time, related to the depth of the three sensors, was 44, 63 and

72 ± 1 hours, respectively Tab. 4. 8. Hence, the OFS were able to detect the water diffusion through the epoxy thickness with a good agreement with the calculated diffusion time.

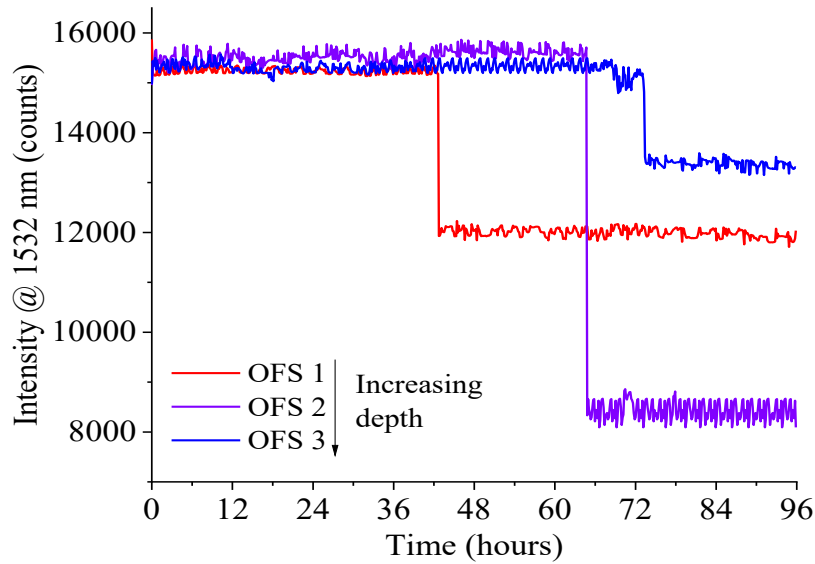


Figure 4. 25. Signal intensity, at a wavelength of 1532 nm, from three optical fibre sensors embedded in an epoxy at different depths. The sample was immersed in artificial sea water at 80 °C.

Table 4. 8. Calculated and measured diffusion heights.

OFSs	Distance (mm)*	Experimental time (h)**	Theoretical time (h)***
1	2.4 ± 0.1	43	44±1
2	2.7 ± 0.1	64	63±1
3	3.0 ± 0.1	73	72 ±1

* Measured by optical microscopy analysis; ** Experimentally measured; *** Determined by Fick's law applying the approximately calculated diffusion length.

As an example, the results of a sample containing eight sensors at depths ranging from 0.8 to 2.3 mm are summarized in Table 4. 9. This table compares the diffusion length estimated with Fick's law (Eq. 3.2) with the actual depth of the sensor that has detected the diffusion. Since the uncertainty on d is about ± 0.2 mm, a reasonably good agreement emerges between the columns, which demonstrates that the optical fibre sensors can detect the diffusion of water through the polymer with good temporal confidence. The overall monitoring process still requires improvements (reproducibility of the fabrication process of the sensors and positioning of the sensors into the sample). However, it demonstrates to be an effective diagnostic tool for pre-emptive maintenance and the results are expected to be easily extended to glass fibre reinforced polymers (GFRPs).

Table 4. 9. Calculated and measured diffusion heights.

OFSs	Distance (mm)*	Calculated distance (mm)**
1	0.5 ± 0.2	0.8
2	0.8 ± 0.2	0.9
3	0.9 ± 0.1	0.9
4	1.0 ± 0.2	1.4
5	1.2 ± 0.1	1.2
6	1.4 ± 0.1	1.1
7	1.5 ± 0.1	1.7
8	2.3 ± 0.1	2.3

* Measured by optical microscopy analysis; ** Determined by Fick's law applying the approximately calculated diffusion length.

4.4.4. Microscope analysis: optical microscope and SEM

Tested samples were cut and polished to measure the optical fibre sensor depth in the epoxy matrix. The measurements under an optical microscope were taken. Figure 4. 26. shows a typical microscope image of a cut and polished epoxy containing an embedded OFS sample. The image shows one embedded optical glass fibre sensor, white spot, in a perfectly polished epoxy surface. The picture reveals good adhesion between the fibre and the epoxy. In order to further investigate the adhesion, SEM analysis were made.

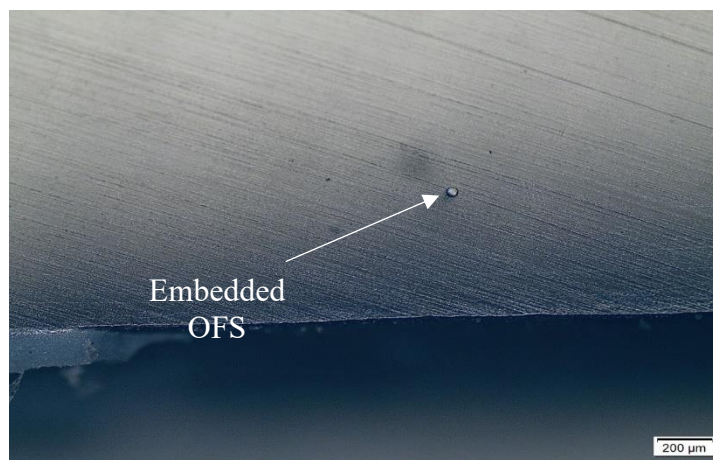


Figure 4. 26. Microscope image of the cut and polished epoxy sample section containing a cross-section cut of one OFS.

Figure 4. 27. a, b) show the SEM characterisation of the embedded sensors of a sensitive OFS and one copper sputtered OFS (Cu-OFS). a) Shows the cross-section of an OFS embedded in an epoxy matrix. The image highlights good adhesion between the optical fibre and the resin, without unbound sections. b) Shows the Cu-OFS embedded in the epoxy resin. The adhesion at the epoxy interface is excellent and the Cu coating is continuous and has adhered well to the silica fibre sensor.

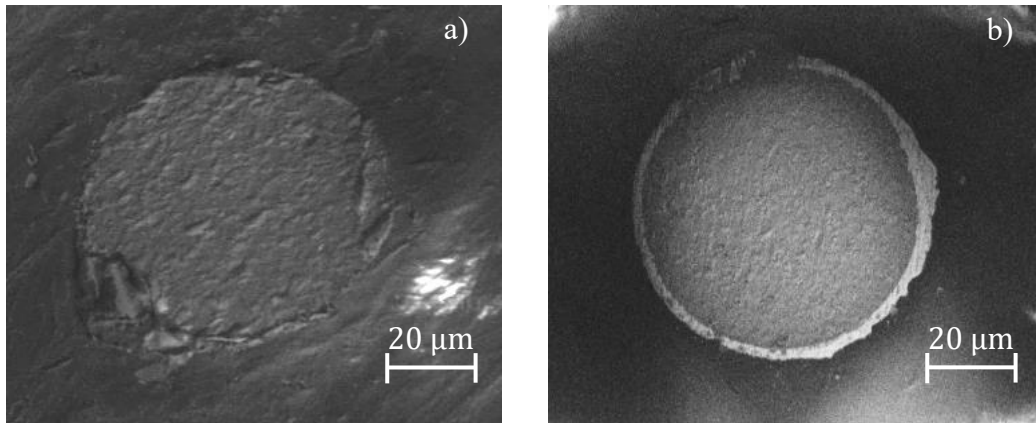


Figure 4. 27. SEM micrographs of the cross section of (a) an OFS and (b) a Cu-OFS embedded in the epoxy resin.

The next step was the preparation of the glass fibre reinforced polymers containing embedded OFSs. The results obtained at this point could be easily extended GFRPs, paving the way to the development of a new platform of smart GFRP artefacts for harsh environments. These have a huge relevance in companies such as oil & gas, aerospace, and energy, whose status can be remotely and continuously monitored with standard and cost-effective optical equipment. However, these companies normally use GFRP composites, and for this reason, the research proceeds with the development of the OFSs embedded in GFRP composites.

4.5. Characterization of GFRP samples equipped with optical fibre sensors results

4.5.1. GFRP samples equipped with embedded OFSs

Figure 4. 28. shows a real GFRP sample with the dimensions of (100 x 70 x 20 mm) with only one embedded OFS.



Figure 4. 28. Picture of epoxy sample where two OFSs are embedded. b) Picture of GFRP sample with one embedded OFS.

A GFRP with embedded sensors sample was fully immersed into artificial sea water at 80 °C in order to accelerate the water diffusion and ageing of the GFRP sample such as the epoxy samples. The reflected signal from the sensor was recorded every 5 minutes over a spectral range of between 1500 and 1600 nm. Figure 4. 29. shows the signal drop obtained from one optical fibre sensor embedded into a GFRP composite. The signal from the embedded optical fibre sensor in the GFRP sample dropped from around 11500 to near 5000 counts, and thus to a decrement of slightly 60% happened after approximately 32 hours. The optical fibre sensor was embedded in a depth distance of 1.5 ± 0.1 mm measured by using the optical microscope. According to the theoretically calculated D coefficient of the diffused water length the signal drop was expected approximately at 30 ± 2 hours. This first result demonstrated once again the suitable potential of the optical fibre sensors to be embedded and used in glass fibre reinforced polymer composites. Therefore, in order to improve the GFRP composites and get more realistic data, further samples were prepared by infusion instead of pouring the resin.

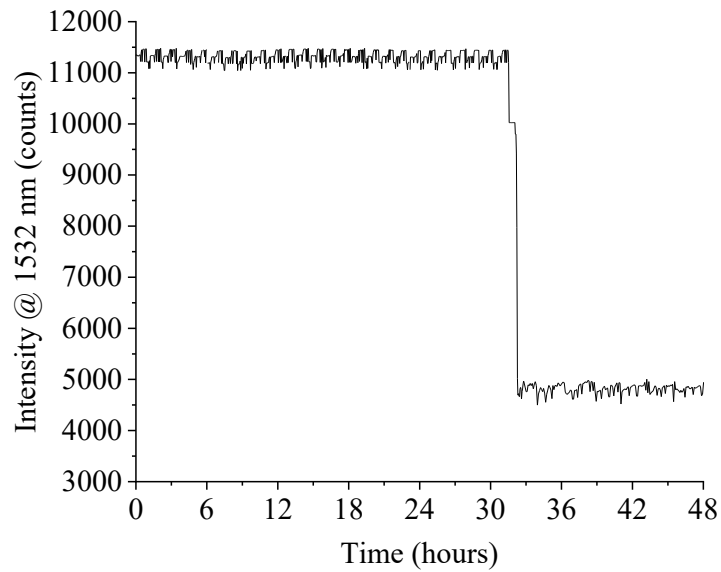


Figure 4. 29. Signal at intensity, at wavelength of 1532 nm, from an optical glass sensor embedded in an GFRP sample at depth of 1.6 mm. The sample was immersed in artificial sea water at 80 °C up to 48 hours.

Figure 4. 30. shows the signal intensity drop at 1532 nm from five different OFSs embedded in GFRP sample, all of which were at a distance of 0.9 ± 0.1 mm from the surface. The sample was tested by immersing it in artificial sea water at 80 °C with continuous monitoring. The maximum signal at the wavelength of 1532 nm given by the spectrometer as a function of time for 20 hours was evaluated. As the OFSs were positioned at the same depth, the drop in the signals occurred at nearly the same time, i.e. after approximately 14 hours. Assuming the approximation of a Fickian behaviour and, then, using the diffusion coefficient reported in Table 4. 3. in the section 4.1.4., the diffusion time for a thickness of 0.9 mm is 13 ± 1 hour. This result shows that the OFS also detected the water diffusion with a good accuracy when embedded in the composite.

Figure 4. 31. shows three embedded Cu-OFSs in a GFRP sample, all of which were at a distance of 0.9 ± 0.1 mm from the surface such as the OFSs resented above. The signals from the optical sputtered fibre sensors embedded in the GFRP sample are constant by the time, which are the expected behaviour because they are sputtered. Once again, the sputtered sensors demonstrated to be stable with the presence of water when their sensitive part is blocked by the copper. So, these results agree with the tested Cu-OFSs embedded in an epoxy sample.

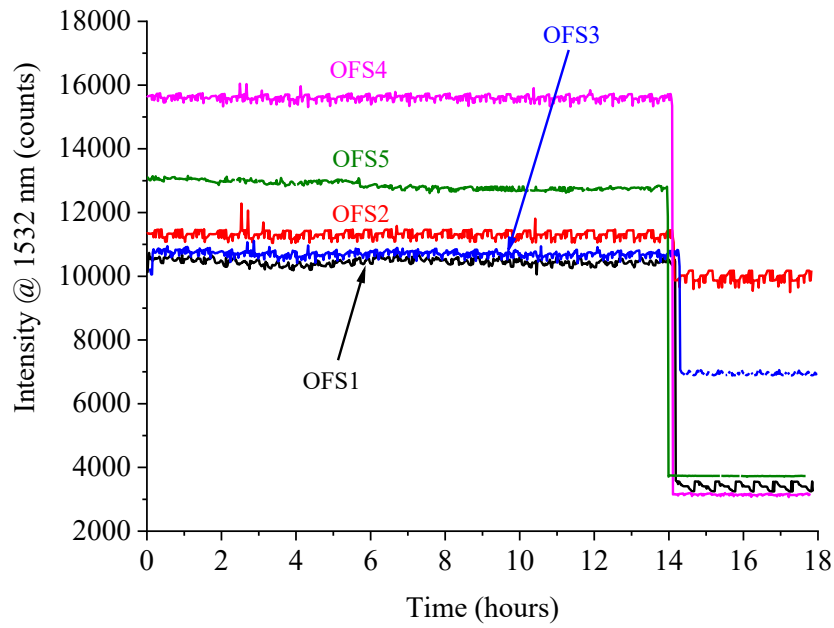


Figure 4. 30. Signal intensity, at a wavelength of 1532 nm, from the five different optical glass sensors embedded in GFRP sample at similar depths of nearly 0.9 ± 0.1 mm from the surface.

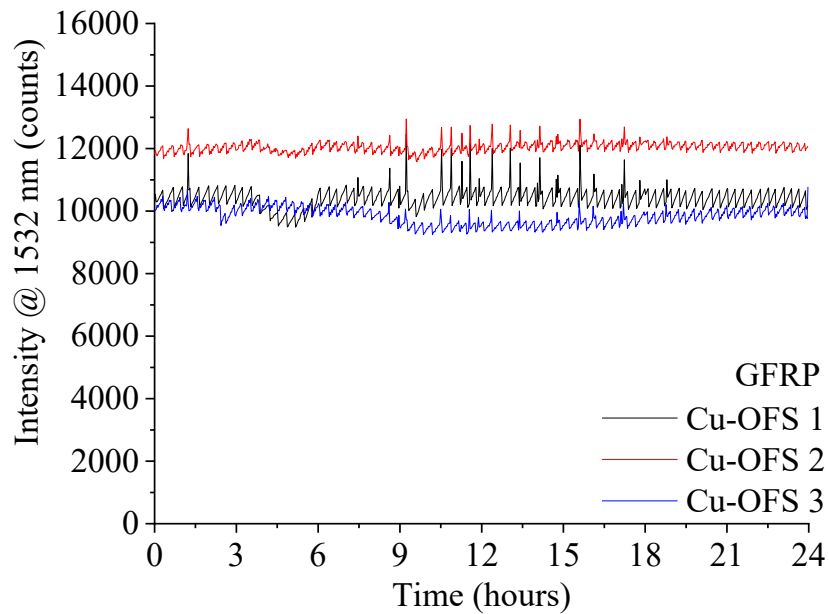


Figure 4. 31. Cu sputtered Optical Fibre Sensors (Cu-OFSs) were not able to detect the water diffusion through GFRP sample.

Figure 4. 32. shows a typical microscope image of a cut and polished GFRP containing two embedded OFSs. Image shows roughly in the middle the two embedded optical fibre sensors surrounded of epoxy. It is also appreciable the two EC-R plies in a perfectly cut polished GFRP surface sample section. The image reveals that the infusion of the epoxy through the plies was uniform and there was not found pores between the plies, which confirms the good procedure of the resin infusion to fabricate the GFRP sample containing embedded OFSs.

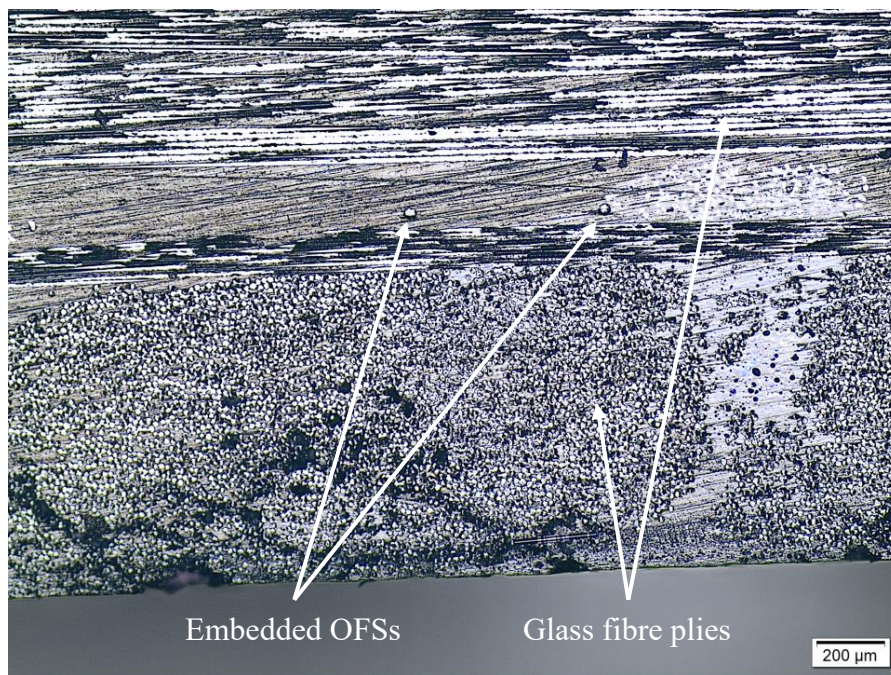


Figure 4. 32. Cross-section optical microscope image of GFRP sample containing two embedded OFSs.

At this point, it was possible to demonstrate the good potential of the OFSs to be used in petrochemical, aerospace and energy companies. They showed to be suitable to be embedded in epoxy and GFRP samples. It can be said that OFSs can be extended to be also embedded in other polymers such as silicones. However, all these tests were performed just applying temperature. To further extend the use of developed OFSs in a real workplace, it was also necessary to subject them in harsh environments. The OFSs embedded in epoxy and a GFRP subjected to high pressure.

4.6. Evaluation of samples subjected at harsh conditions of 50 bars and 80 °C

4.6.1. The vessel and the Conax adaptor for high pressure

This research activity was carried out at Element Materials Technology, Hitchin, UK. In order to investigate the use of the OFSs under harsh conditions, bare OFSs were subjected to high pressures. Figure 4. 33. shows the reflected signal continuously monitored by exposing the OFSs to pressures ranging from 1 up to 75 bars, with a ramp pressure of 5 bars per minute. The reflected signal from the sensors was recorded every 5 minutes over a spectral range of between 1500 and 1600 nm. No degradation of the response of the sensors was observed, thus showing that the OFSs could withstand high pressure conditions.

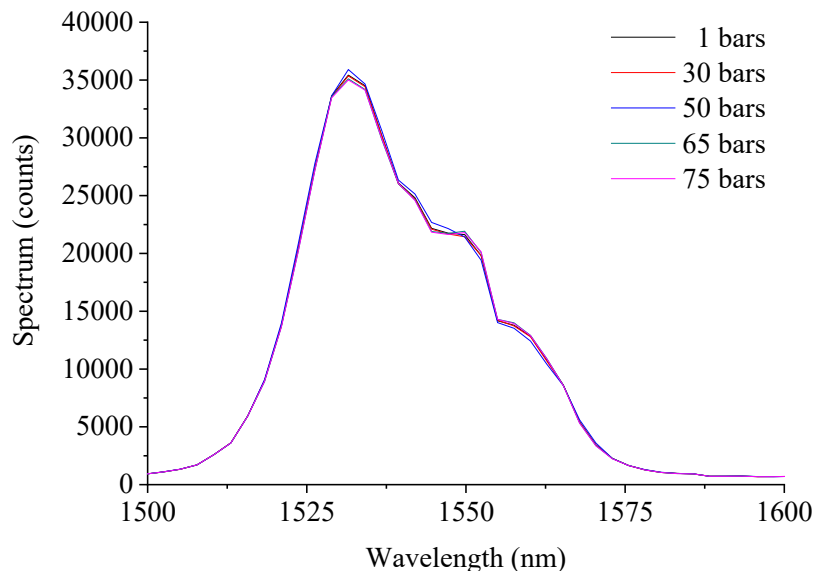


Figure 4. 33. Total reflection of the transmitted light spectra between 1500 and 1600 nm at different selected pressures. The data was recorded in continuous mode.

Once the OFSs showed excellent stability against the pressure, it was proceeded to check the Conax adaptor stability. This stability was another critical point to overpass before starting the high-pressure measurements. Figure 4. 34. shows the data recorded by the internal recording system of Element Technology for 90 hours where the vessel was pumped up to 75 bars at room temperature. The graph shows good pressure stability, which means that the adaptor can keep the pressure without leaks. The variation of ~12 bars variation was attributed to the ~2 °C variation. The optical spectrum of the reflected light form the OFSs was also monitored every 5

minutes up to 90 hours. The optical light spectrum did not show any variation which it means that optical fibres did not have any damage during the test at 75 bars for 90 hours. It was then decided to use the Conax adaptor for the following high-pressure experiments.

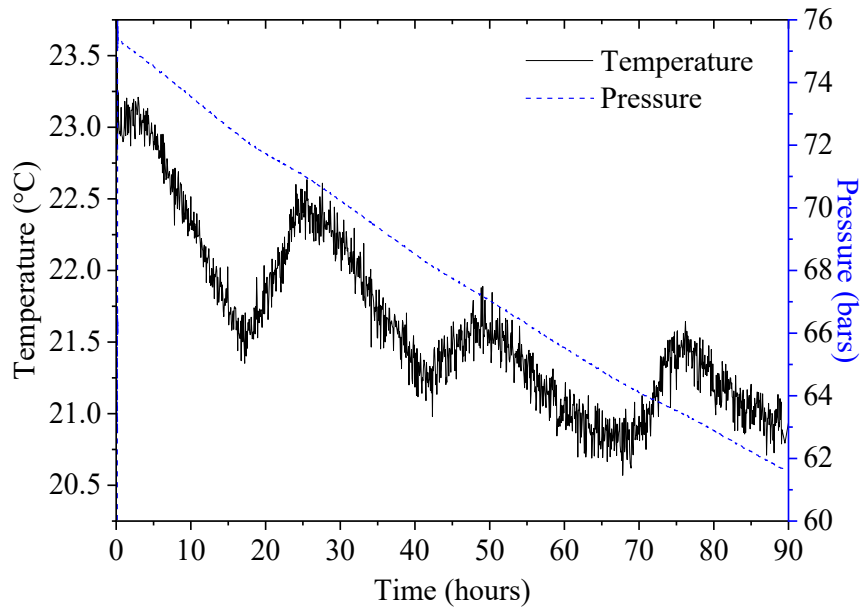


Figure 4. 34. Graph where on the left is represented the temperature and on the right is represented the pressure. Pressure agrees with the temperature.

Figure 4. 35. shows an optical microscope image of the section of the optical fibre, which corresponds to the part where the optical fibre was clamped in the Conax adaptor. The optical microscope analysis reveals the absence of damage of the optical fibre core integrity, which just presents a small stress on the polymer coating. To conclude, the Conax showed to be feasible to proceed with the high-pressure experiments with the required safety condition established at Element Materials Technology, Hitchin.

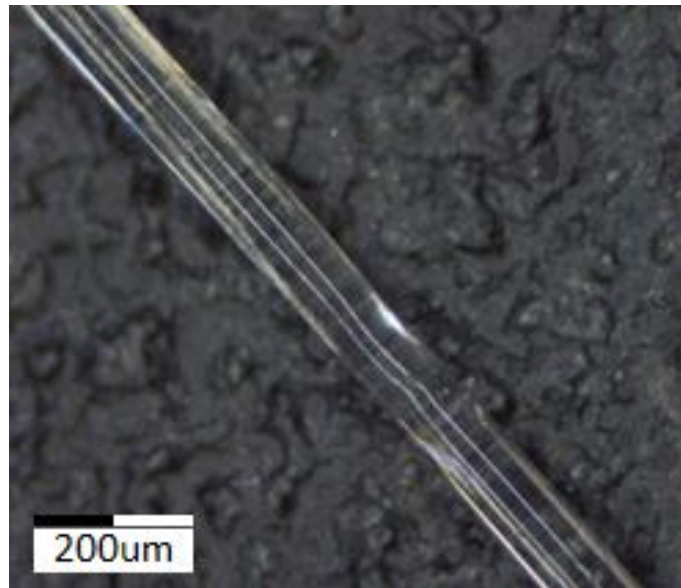


Figure 4. 35. Optical microscope image at (20 X) of the optical glass fibre after the pressure exposure test at 75 bars.

4.6.2. *Epoxy and GFRP samples equipped with OFSs tested in harsh conditions*

Based on this preliminary test, epoxy and GFRP samples containing OFSs were tested in artificial sea water at 80 °C under a pressure of 50 bars. The response of an OFS embedded in epoxy is reported in Figure 4. 36. as an example. In this case, the depth of the OFS, as measured with the microscope, was 0.9 ± 0.1 mm. The reflected light intensity at 1532 nm showed a sharp decrease after around 3h. This time was in accordance with the theoretical diffusion time calculated to reach a depth of 1.1 mm. Fig. 4. 36. also reports the signal recorded from an OFS embedded in GFRP and a drop is observed after about 4 hours. For this diffusion time, the expected diffusion depth was about 0.7 mm. The response of the OFSs in these tests are in rough agreement with the expected diffusion time, yet they prove the capability of non-destructive, real-time detection.

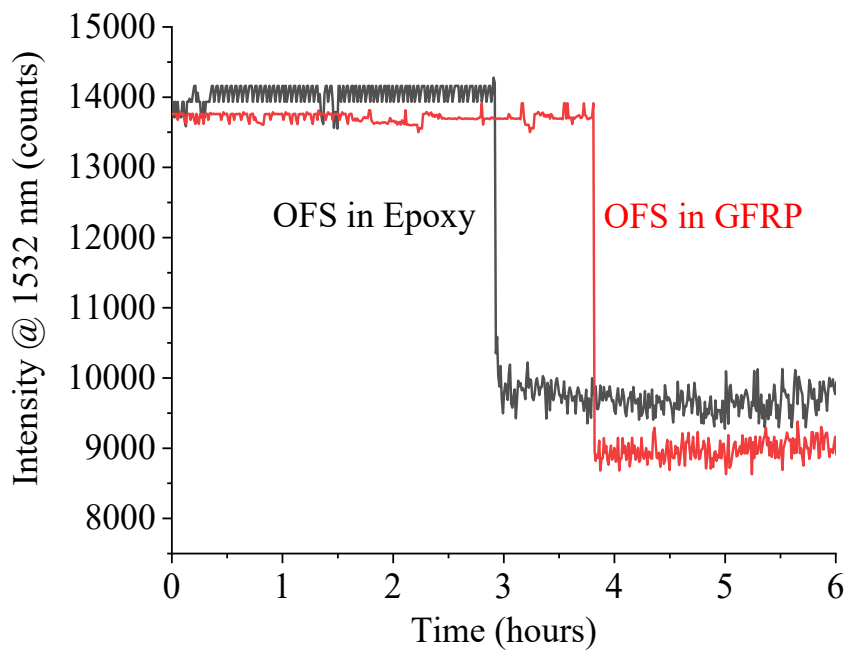


Figure 4. 36. Signal intensity at a wavelength of 1532 nm from an OFS embedded in an epoxy and in a GFRP at depths of 0.9 ± 0.1 mm and 0.8 ± 0.1 mm, respectively. The samples were immersed into artificial sea water at 80 °C and 50 bars.

OFSs experiments carried out at high pressure, by exploiting a special vessel container, confirmed the previously discussed results. Furthermore, these experiments yielded some knowledge about the installation of optical fibre sensors in harsh environments and hard-to-reach locations. On the other hand, pipelines used in oil & gas companies are sometimes subjected to convoy acids. It could be useful to have also a sensor capable of detecting acids such as hydrochloric acid. If a pipeline could be equipped with some sensors which can distinguish between moisture and acids the value of OFSs will increase.

4.7. *Selective Sensors*

OFSs, conceived to be selectively sensitive to HCl, were fabricated as described in sect. 2.1, but the exposed core was then coated with a ~100 nm layer of aluminium. These sensors are here referred to as Al-OFSs.

4.7.1. *Epoxy and GFRP samples containing OFSs subjected to hydrochloric acid at room temperature in continuous monitoring*

The calculated diffusion coefficients of HCl at room temperature in the pristine epoxy were measured by means of a gravimetric test, as reported in Figure 4. 9. and Table 4. 3. Furthermore, epoxy samples containing both standard OFSs and Al-OFSs were immersed into artificial sea water and HCl, respectively, at room temperature, for up to 24 hours.

The results of the diffusion experiment are shown in Figure 4. 37. a) reports the signal intensity recorded at 1532 nm, as a function of time, for the sensitive epoxy sample immersed in artificial sea water. On the other hand, Figure 4. 37. b) depicts the outcome for the sensitive sample subjected to HCl. It can be observed that the standard OFSs detect both water and HCl diffusion, whereas the Al-OFSs are only responsive to HCl, since HCl can solubilise the thin Al-layer, thus enabling the core to be sensitive to changes in the refractive index and absorption of the epoxy. This is a proof-of-concept that the integration of OFSs and Al-OFSs can be exploited to selectively detect the diffusion of water and acid.

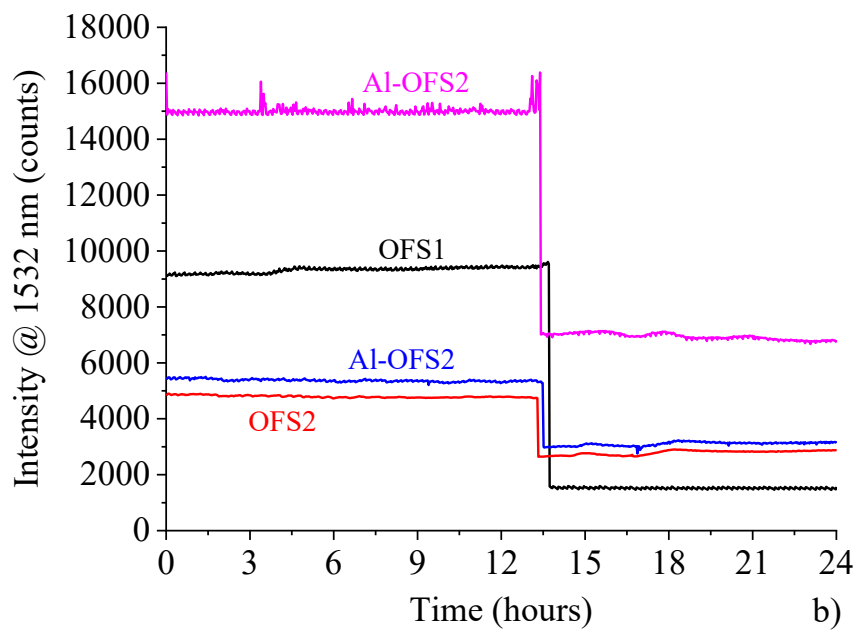
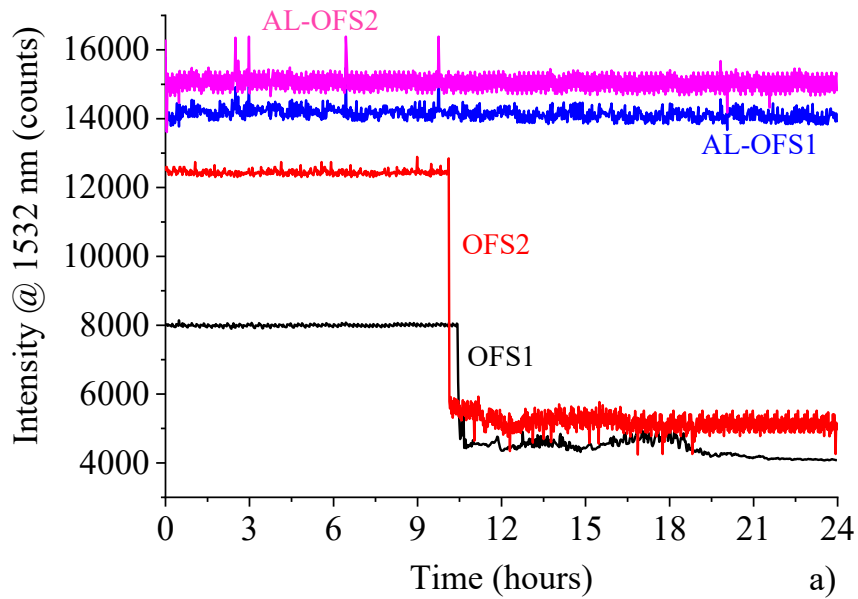


Figure 4. 37. Signal intensity at a wavelength of 1532 nm from sensors embedded in the epoxy exposed to a) artificial sea water and b) HCl. The AI-OFS are sensitive to HCl, whereas they do not exhibit any response to artificial sea water.

Analogous experiments were then performed with GFRP samples. Figure 4. 38. reports the response of two sensitive samples exposed to artificial sea water and

HCl at room temperature. Although the signal drop was not the same for all the sensors, they exhibited the same behaviour as when in epoxy. The standard OFSs detected the diffusion of both water and HCl, whereas the Al-OFS were only effective in sensing the diffusion of HCl. The time response was once more in agreement with that expected from Fick's diffusion model.

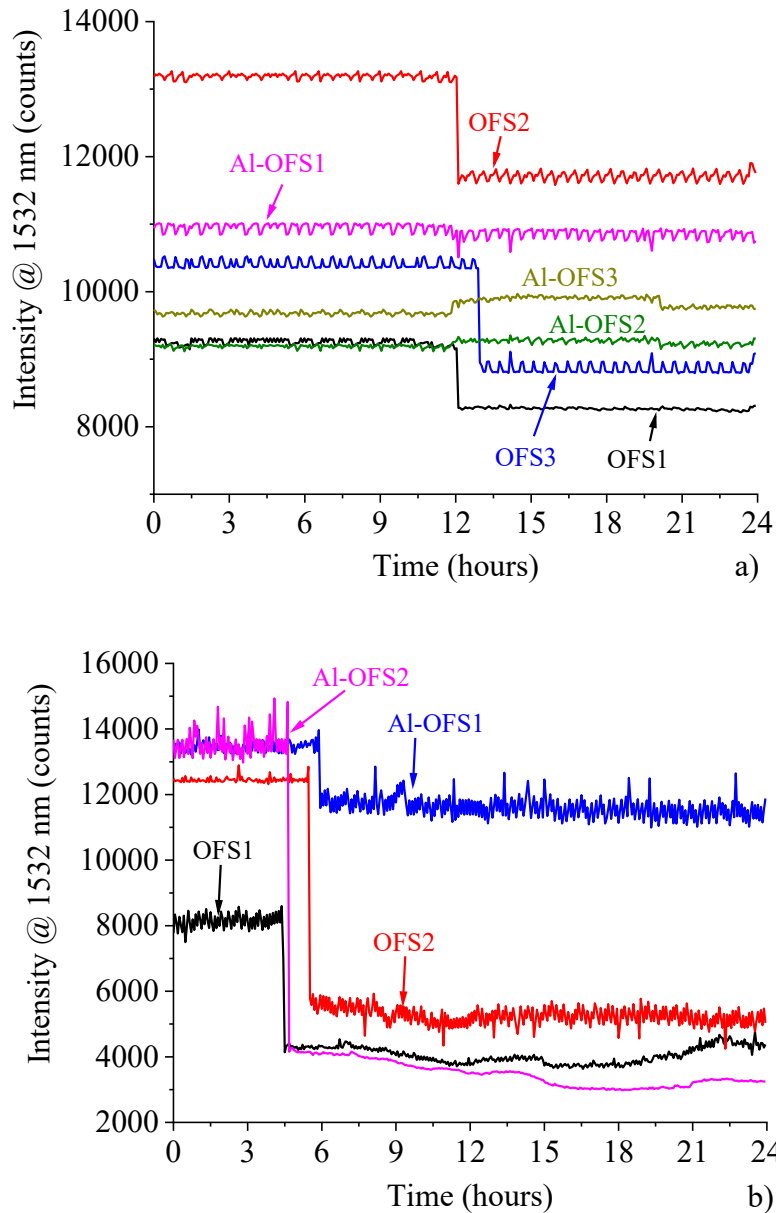


Figure 4. 38. Signal intensity at a wavelength of 1532 nm from sensors embedded in GFRP exposed to (a) artificial sea water and (b) HCl. The Al-OFS are sensitive to HCl, whereas they do not exhibit any response to artificial sea water.

The fabrication process reproducibility of these sensors still demands for some improvements, as it can be observed by comparing the initial and final intensity levels of the signals collected from the different experiments (Figs. 4. 24 to 4. 38.). The initial reflectivity (i.e. the initial recorded signal) is strongly dependent on the quality of the mirror realised on the fibre's tip as well as on the connection to the interrogation unit. Furthermore, the variation observed on the final levels could be ascribed to the effective length of the sensing region, that is not perfectly controlled during fabrication.

4.8. Chalcogenide fibre sensors

4.8.1. Cross-linking and diffusion monitoring using TAS fibre

This research activity was carried out at Université de Rennes 1, Rennes, France. Figure 4. 39. shows the cross-linking reactions of the epoxy resin using a TAS fibre. The reaction was successfully and completely recorded in situ and in real-time using the chalcogenide fibre with a yield of nearly 97% of conversion. Once again, it was demonstrated the possibility of using TAS fibres to monitor the crosslinking reactions as M. L. Anne et al., [190], reported the monitoring of a chemical reaction of an industrial resin, which opened up the possibility of using chalcogenide glass fibre to follow and monitor the manufacturing of polymer composites fabrication. However, while the small mould gave good signal response for the absorbance of the chemical groups, the large mould had an overload response. This means that it was not necessary to embed a long section of TAS fibre in order to follow the cross-linking reactions. In fact, two centimetres of TAS fibre were enough to follow the cross-linking reactions. In contrast, the epoxy group conversions were also measured by FT-IR and compared with the TAS fibre results (Fig. 4. 40.). Unfortunately, due to the limitations of the instrument the FT-IR analysis was not carried out in situ and real-time. In any case, in both experiments the epoxy group conversions were evaluated by following the reduction of the epoxy peak area, centred at 915 cm^{-1} with a yield of nearly 96% of conversion.

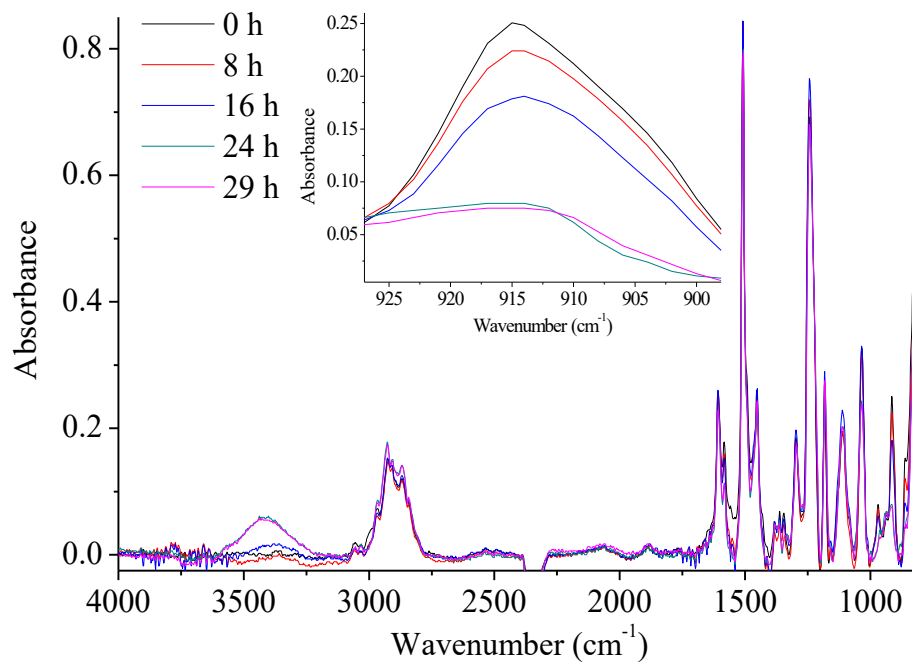


Figure 4. 39. FT-IR spectra for uncured epoxy (0 hours) resin versus cured resin (29 hours) where the epoxy groups conversion is zoomed. The registration was produced every half an hour and the selected: 0, 8, 16, 24, 29 hours, are represented. The first 24 hours corresponds to the cross-linking of the resin at room temperature and the last 5 hours corresponds to the thermal curing of the epoxy.

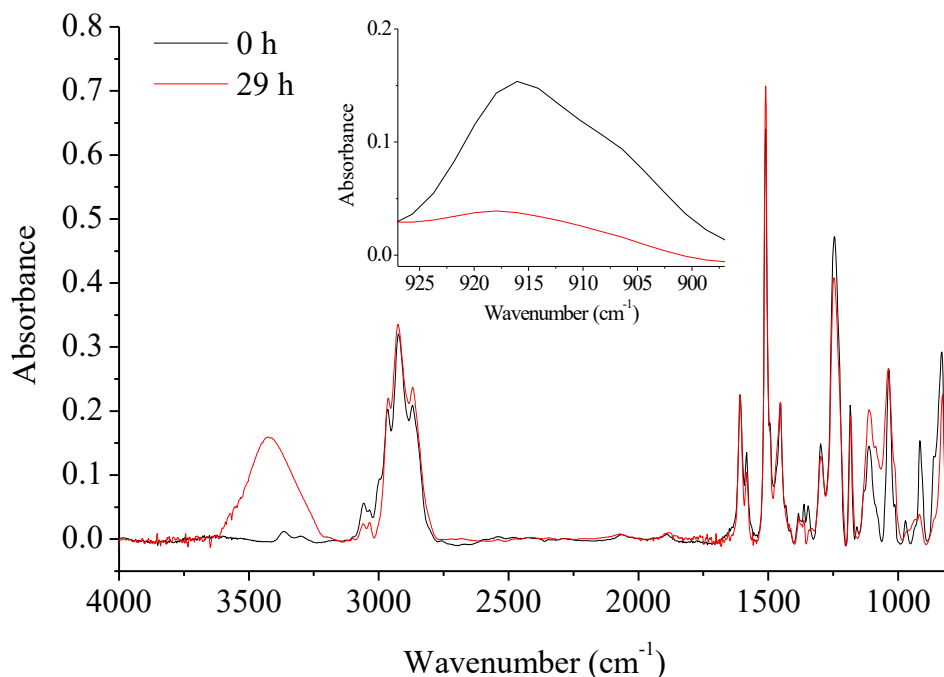


Figure 4. 40. FT-IR spectrum for uncured epoxy at 0 hours (black) resin versus cured resin at 29 hours (red) of the same epoxy where the registration was not in continuous. The epoxy group conversion is zoomed.

4.8.2. *Samples subjected to distilled water at 80 °C in continuous monitoring*

Figure 4. 41. shows the FT-IR spectrum obtained by the distilled water diffusion through the epoxy matrix using the TAS fibre. The graph shows a drop between 3652 and 3756 cm^{-1} corresponding to the symmetrical and asymmetrical stretching of the water, and at 1596 cm^{-1} corresponding to the symmetrical bending between the hydrogens of the water molecule [191]. The sample was kept at 80 °C to accelerate the distilled water diffusion through the epoxy using a heat plate. The TAS fibre was located at a depth of 0.25 ± 0.02 mm and recorded a drop signal after 0.25 hours. Assuming the estimation of a Fickian behaviour and, then using the calculated diffusion coefficient of the distilled water at 80 °C, the diffusion time for a depth of 0.25 mm is 0.51 ± 0.07 hours. For this diffusion time, the expected diffusion depth was about 0.18 mm. The response of the TAS fibre in this test is in estimated agreement with the expected diffusion time, yet they demonstrate the

capability of non-destructive, in situ, and rea-time detection using an embedded TAS fibre with at least a length superior of 20 mm.

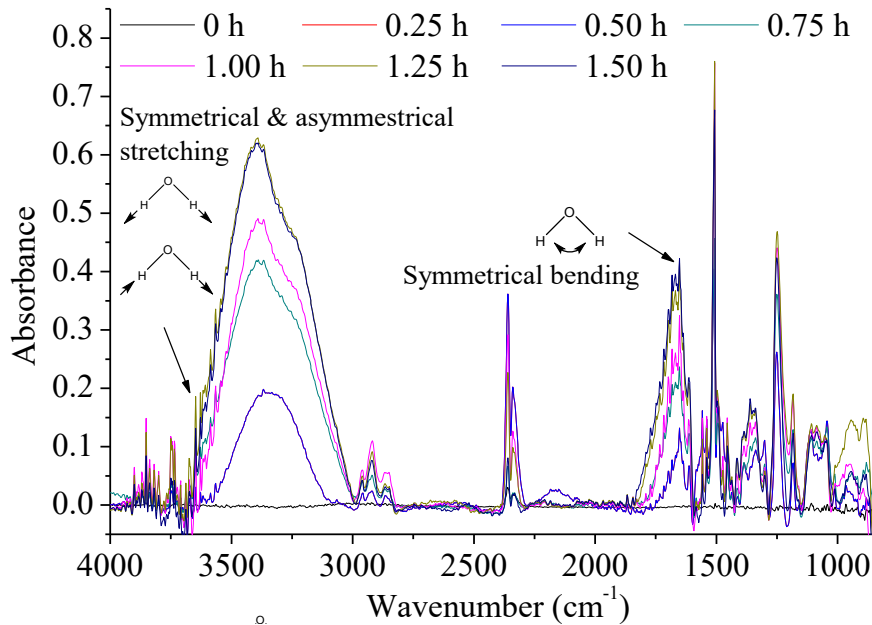


Figure 4. 41. FT-IR spectra of the detection of water using TAS fibre in a large mould. Water was detected by observing an absorbance increment in the spectra between 3652 to 3756 cm^{-1} and at 1596 cm^{-1} .

4.8.3. Samples subjected to ethanol at room temperature in continuous monitoring

Figure 4. 42. shows the FT-IR spectra when the ethanol was added on the surface of the epoxy. The ethanol diffusion was monitored in situ and real time up to three hours. The drops were associated to the stretching and bending signals produced by the alcohol groups [191]. However, the C-C-O asymmetric stretching groups at 1050 cm^{-1} were not well observed. Furthermore, the C-C-O symmetric stretching groups at 881 cm^{-1} were produced at the limit of the detector and for this reason were discarded. This last signal could become an outlier and give a false positive.

The distance measured between the epoxy surface and the embedded TAS fibre was obtained using an optical microscope. This distance was at 0.20 ± 0.01 mm. Assuming the approximation of the Fickian behaviour and, then using the calculated diffusion coefficient reported in Table 4. 4., it was expected to record a drop approximately at 0.43 ± 0.08 hours. This result shows that it was possible to

detect the ethanol diffusion with an acceptable accuracy when the TAS fibre is embedded in an epoxy. As Le et al. [192] proved the possibility of following the manufacturing process of the alcoholic fermentation of grape juice, the TAS fibre can be also used as a sensor to detect the alcoholic groups of ethanol diffusion through the polymer matrix. This opens the further investigation to use the TAS fibre as a consumable to detect the degradation of polymers when they are exposed in harsh environments.

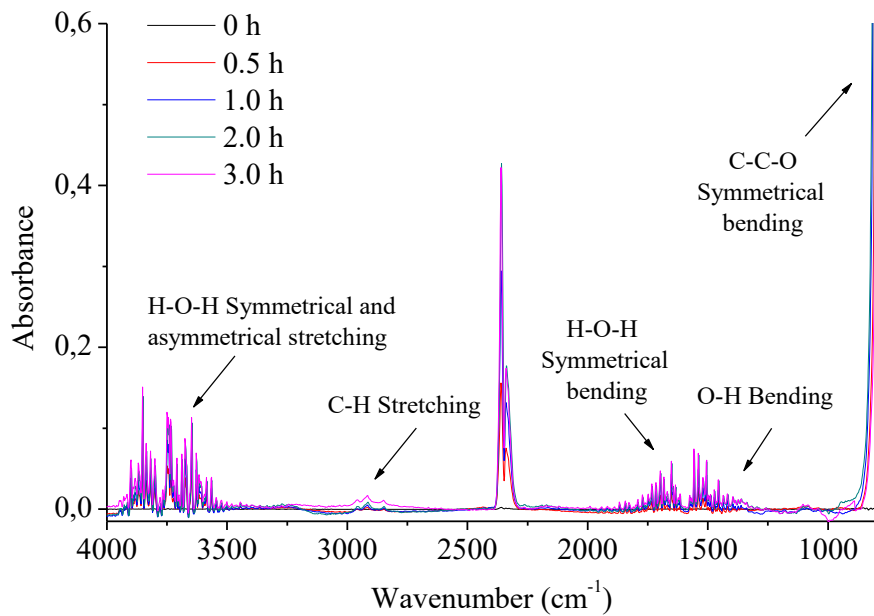


Figure 4. 42. FT-IR spectra of the detection of ethanol using TAS fibre. The spectra display water and alcohol groups. Water symmetrical and asymmetrical stretching groups are at 3652 and 3756 cm^{-1} , respectively. Water symmetrical bending is at 1596 cm^{-1} , C-H stretching is weakly detected at 2970 cm^{-1} , O-H bending is pointed out at 1330 cm^{-1} , and C-C-O symmetrical bending is at 881 cm^{-1} .

Figure 4. 43. shows a typical optical microscope image of one TAS fibre embedded in an epoxy. The image reveals the good adhesion between the TAS fibre and the epoxy. Furthermore, it can be observed the absence of crystal formations inside the TAS fibre which verify its excellent purity.

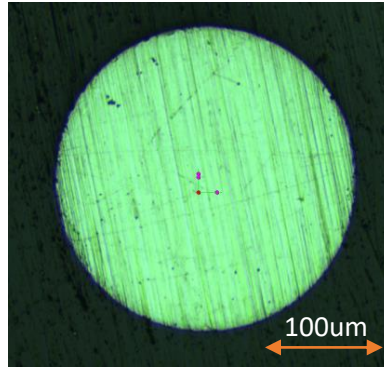


Figure 4. 43. Optical microscope image (10x) of a TAS fibre in the middle embedded with an epoxy resin. It shows a good adhesion between the fibre and the epoxy.

4.9. *Electrical sensors using carbon nanotubes*

4.9.1. *Evaluation of the percolation curve*

This research activity was carried out at Nanoforce Ltd., London, UK. Figure 4. 44. shows the percolation curve calculated using the Eq. 3.4. explained in section 3.9. The epoxy samples containing 0.01 wt.% of filler were not conductive and show a conductivity six orders of magnitude lower than the epoxy samples containing 0.25 wt.% of CNTs. Using Eq. 3.4., it was found a percolation threshold of 0.50 wt.%: above this concentration, the conductivity reaches the plateau.

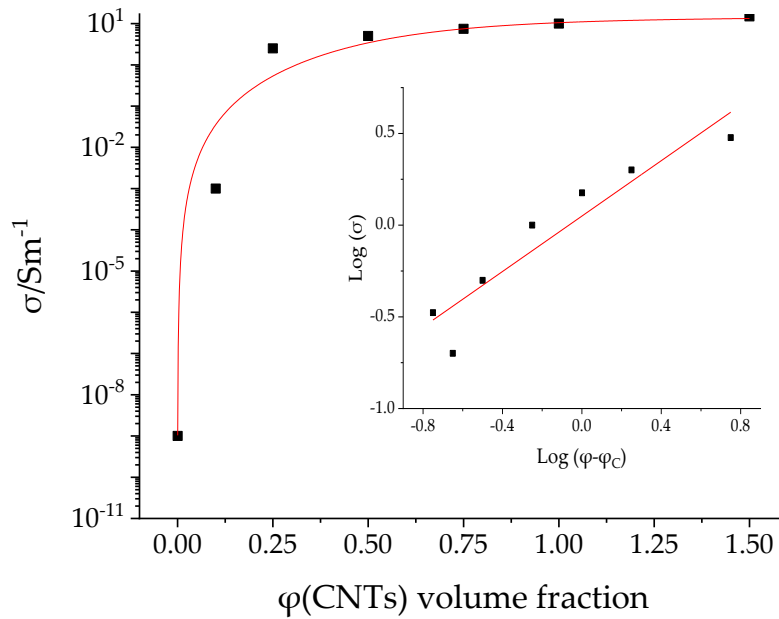


Figure 4. 44. Electrical conductivity of epoxy samples with the different percentage of fille.

4.9.2. Conductivity evaluation of epoxy and GFRP samples containing embedded CNTs

In order to compare the percolation curve obtained previously and further investigate the influence of the CNT fillers, the electrical conductivity of epoxy samples containing 0.00, 0.25, 0.50, and 0.75 wt.% of CNTs was also measured. These measurements were also performed because it is known that CNTs can easily agglomerate, depending on the fabrication method, thus affecting the electrical properties of the samples

In this work, the sensors were developed to detect the diffusion of sea water, one of the several corrosion agents in the oil and gas industry. For this reason, the electrical conductivity of all the fabricated samples at different ratios of epoxy containing CNTs was also measured during an accelerated ageing in artificial sea water at 80 °C [92].

The tested samples showed a remarkable conductivity increment with time (Fig. 4. 45.). The increase of the conductivity of epoxy samples containing CNTs and GFRP05 composites as a result of the moisture ingress is still under

investigation. The response was analysed in terms of the presence of ions in the artificial sea water contributing positively to the conductivity. For this reason, the increment of conductivity could be explained by the moisture diffusion through the samples, which bridges the CNTs and creates more effective conductive network. All the samples, independently from the filler content, showed an increase in electrical conductivity, except for pristine samples (samples without filler content).

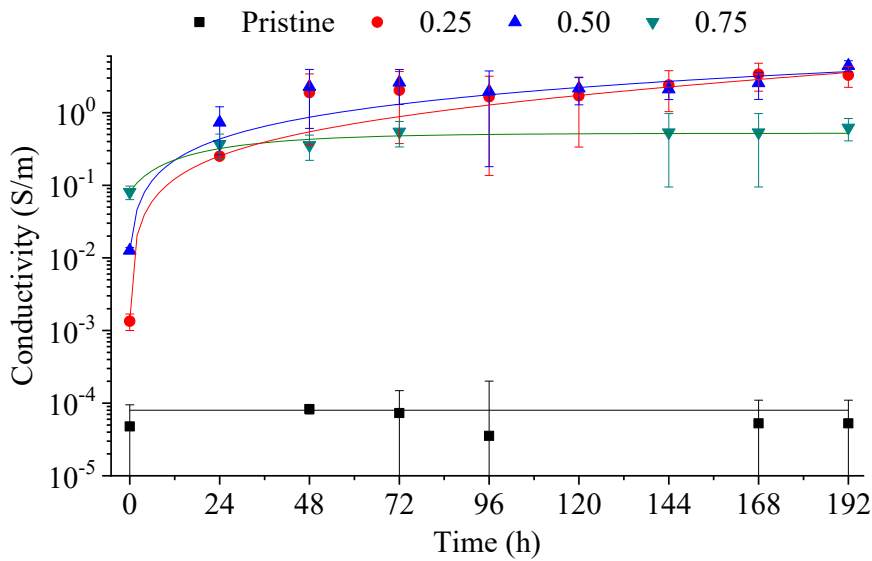


Figure 4. 45. Electrical conductivity graph of 4 different epoxy samples with different concentrations of CNTs immersed in artificial sea water at 80 °C. Data was reordered every 24 hours (non-continuous monitoring).

4.9.3. Evaluation of the conductivity of GFRP05

GFRPs with 0.5 wt.% of CNTs (GFRP05) were prepared as described in section 2.3, tested, and compared with pristine GFRP composites (GFRP without CNTs). The GFRP05s were tested under the same conditions as the epoxy containing CNT samples (full samples immersion in artificial sea water at 80 °C). Figure 4. 46. the electrical conductivity response during the first two weeks of immersion. Although, the conductivity increment presents less than one order of magnitude increment, it was enough to produce a clear detection.

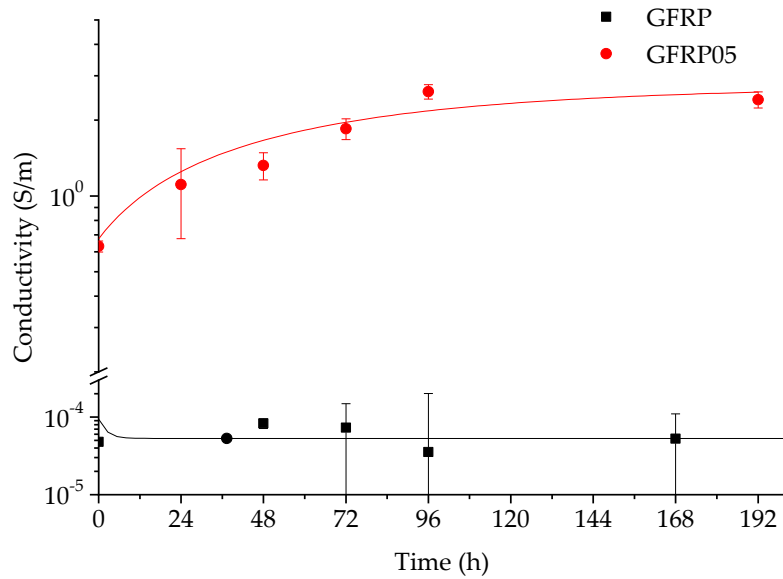


Figure 4. 46. Conductivity graph pristine GFRP composite and GFRP05 composites. Both immersed with in artificial sea water at 80 °C.

4.9.4. Evaluation of the OFS and CNT

The last experiment consisted in combining the different sensors, the optical fibre sensor and electrical sensor. in-situ and in real time the diffusion of sea water through the epoxy matrix of the composite was monitored by means of both the sensors in the so-called H-GFRP (preparation details in section 3. 9. 2.).

The H-GFRP was immersed in artificial sea water at 80 °C for 7 days. The reflected signal from the OFSs was recorded every 5 min in the spectral range of 1500 to 1600 nm. The shape of the spectra did not show any change, whereas it showed a sharp decrement in the maximum intensity signal at 1532 nm (the maximum intensity signal provided by the source) which was attributed to moisture diffusion. Because of the wavelength of 1532 nm represents the maximum intensity, only this wavelength was analysed in long-term experiments assuming a reasonable representation of the full spectrum. As already discussed in [28], [15], [14], the spectral attenuation could be determined by the change in the optical properties of the epoxy surrounding the core of the fibre, due to the moisture diffusion. In particular, the attenuation of the optical signal was caused by an increment of the optical absorption of the epoxy in the recorded spectral range.

Figure 4. 47. shows the signal intensities at 1532 nm recorded from the 5 OFSs embedded in the H-GFRP. The signals from the different OFSs dropped at different times because they were at different distance from the surface (measured by means of an optical microscope). Sensors 1, 4 and 5 were located at depth of 1.4 ± 0.2 mm and showed a signal drop after approximately 21, 18 and 19 hours, respectively. Sensor 2 was located at a depth of 1.3 ± 0.2 mm and showed a signal drop after nearly 13 hours. Table 4. 10. shows the diffusion times calculated taking into account the OFS measured distance from the surface and the water diffusion coefficient [14]: for OFSs 1, 4, 5 and OFS 2 were 16 ± 4 and 13 ± 4 , hours, respectively. shows the diffusion times calculated taking into account the OFS measured distance from the surface and the water diffusion coefficient [14]: for OFSs 1, 4, 5 and OFS 2 were 16 ± 4 and 13 ± 4 hours, respectively. Hence, OFSs were able to detect the water diffusion with acceptable time accuracy, in accordance to with the calculated diffusion time (Tab. 4. 4.).

OFS 3 was located between the plies at a depth of about 2.2 ± 0.2 mm and showed a signal drop after 43 hours. Due to its position, the diffusion time could not be calculated for this OFS using Eq. 3.1. and the water diffusion coefficient measured for the pristine epoxy.

On the other hand, Figure 4. 48 displays the increment of the conductivity after nearly 48 hours of the spread CNT plies. The CNTs recorded a signal by means of an increment of electrical conductivity. The CNTs were located close to OFS 2 at a depth of 2.2 ± 0.3 mm. The response of the CNTs in this test agrees with the response of the OFSs (in this test, OFS 2). Nevertheless, both typologies of sensors prove another time the potential capability of non-destructive and real-time monitoring detection, but further research is still needed.

Taking into consideration that the uncertainty of the measurement of d by microscope is about ± 0.2 mm, an acceptable agreement between experimental and theoretical data was found, which demonstrates that both sensors can detect by continuously monitoring the diffusion of water through the composite polymer matrix.

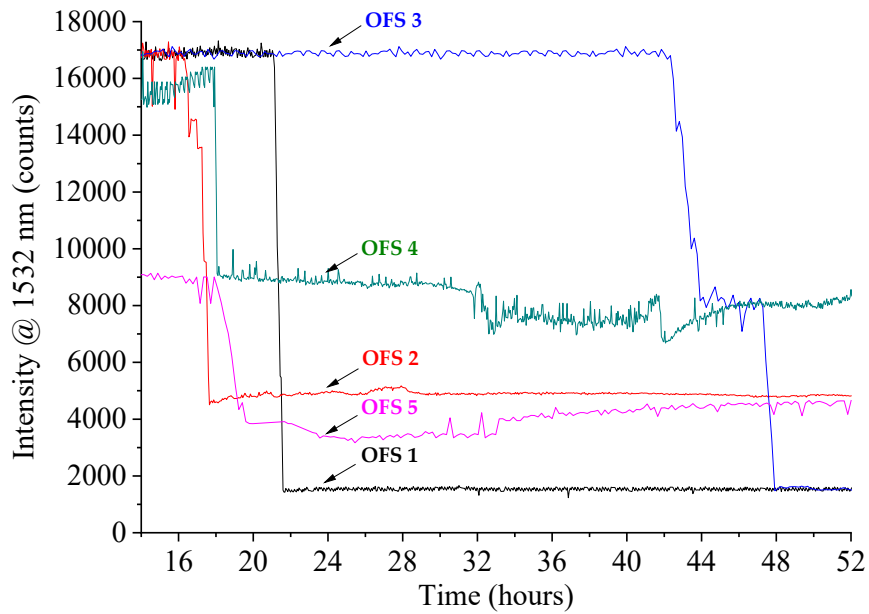


Figure 4. 47. Signal intensities at a wavelength of 1532 nm from the OFSs in continuous monitoring. The sample was immersed in artificial sea water at 80 °C for 7 days.

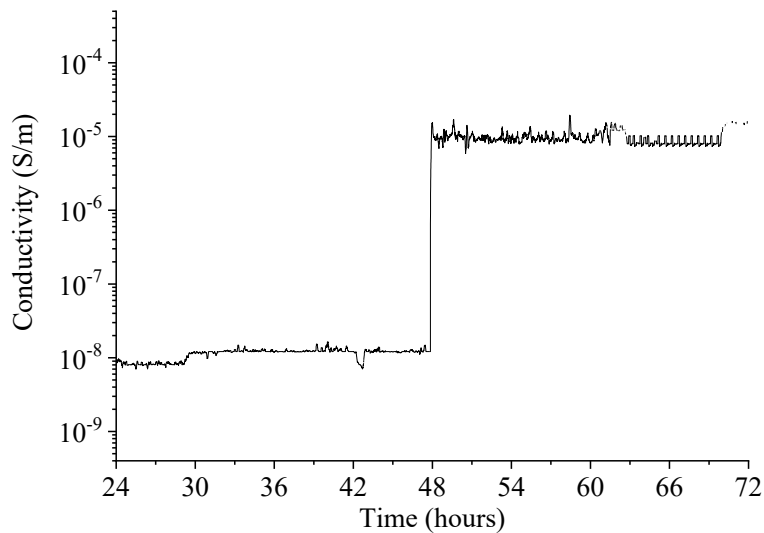


Figure 4. 48. Conductivity signal of the spread CNT on the plies at depth of 2.2 ± 0.3 mm, signal increased after 48 hours. All sensors embedded in the H-GFRP composite.

Table 4. 1. Summarized drop signals of the embedded optical fibre sensors and the spread CNTs on the plies in the H-GFRP.

Sensor type		Experimental distance (mm)	Experimental time (h)	Theoretical time (h)
Optical Glass Fibre Sensors	1	1.4 ± 0.2	21	16 ± 4
	2	1.3 ± 0.2	16	13 ± 4
	3	2.2 ± 0.2	43	NCD
	4	1.4 ± 0.2	18	16 ± 4
	5	1.4 ± 0.2	19	16 ± 4
CNTs	Plies	2.2 ± 0.3	48	NCD
NCD = No Corresponding Detection				

The experiments demonstrated the possibility of using either CNTs or OFSs to approximately detect water diffusion through a GFRP matrix. Also, CNTs and OFSs demonstrated the possibility of working together. The interaction to produce a combined effect greater than their separate signal effects was found. When the OFS was placed between spread plies with CNTs the signal drop was not corresponding to the expected. Furthermore, CNTs were able to detect the moisture but the conductivity increment was not corresponding to the expected signal as well as the OFS. This could be explained because when there are CNTs placed on the plies the water diffusion through the composite must face the hydrophobicity of the CNTs producing a delay a synergism effect. These results agree with the measured diffusions of the pristine samples and the samples containing CNTs where CNTs demonstrated to possess lower diffusion coefficients.

The possibility of creating a composite with more spray coated plies, positioned at different depths, to monitor the water diffusion through the GFRP was contemplated. However, as there is a low amount of resin between the plies, it could

be the case that the agglomeration of plies behaves as a unique ply because the diffusion in 3D objects does not follow a uniform line. This means that when the water is diffused inside the composite, the plies become wet at different points and they can provide a false positive signal. So, they could present challenges for carefully detecting water diffusion at different depths.

Chapter 5

Exploitation plan

5.1. *Relevant results after research activities*

5.1.1. *Target solutions*

The target solution of this project is to develop innovative low-cost optical fibre sensors (OFSs) for monitoring the diffusion of corrosive media and degradation through the thickness of GFRP epoxy matrices. Glass Fibre Reinforced Polymers (GFRPs) are largely used in oil pipes as middle-layer materials. They are cheaper to produce than steel pipes due to lower processing temperatures and materials costs. Since the pipes are installed in harsh environments such as the seabed, they are subjected to severe environmental conditions in terms of temperature, humidity, and so on. Additionally, GFRPs composites are being promoted as the materials of the 21st century because of their superior corrosion resistance, excellent thermo-mechanical properties, and high strength-to-weight ratio. An area that remains challenging is the diffusion of salty water and moisture through the pipe thickness.

In order to further incorporate GFRPs into the petrochemical industry, it is necessary to give accurate, non-invasive data on the degradation rate and lifetime of these materials. This can be achieved through the implementation of monitoring sensors for the GFRPs conditions.

5.1.2. *Main features*

These sensors can detect the water diffusion through an epoxy matrix and can help predict possible failures within pipelines.

These sensors are defined evanescent wave optical sensors (EWOSs), since they rely on light “leaking” from the fibre to interact with the surrounding material. These are embedded into the GFRP sample and tested. Owing to their small dimension, they can preserve the mechanical properties of the GFRP. The diffusion of water or other corrosive chemicals is probed by recording the spectral attenuation of the fibre sensor, as detailed in the following sections.

These sensors are fabricated by chemically etching a standard silicate glass fibre to remove its cladding and make it sensitive to the surrounding environment. A silver mirror is deposited on the fibre tip, in order to produce a total reflection of the transmitted light so that the OF sensors can be used as pinpoint single-ended probes. The sensors are embedded into the polymer matrix during the composite preparation.

Experiments to sense sea water diffusion were carried out at 80 °C in continuous monitoring. The temperature was imposed in order to accelerate the composite aging process and the diffusion of the water through the resin. Preliminary results showed that the sensors were able to detect water diffusion through the polymer matrix by exhibiting an increment of their transmission loss.

5.1.3. Benefits and fields of application

Optical fibres sensors (OFSs) are preferred in sensing applications due to their immunity to electromagnetic interferences and intrinsic fire safety. These features have become attractive for the oil and gas industry, where conventional electric-based sensors present notable limitations. Additionally, OFSs are very cost effective in terms of production. The breadth of developments in optical fibre sensor technology has been reflected in several books and many review papers. Moreover, OFSs can present a non-invasive structure in the host composite and the early stage detection of water diffusion should be accomplished by a continuous-monitoring system that exhibits some specific features: remote operation, safety and minimum invasiveness, among others.

In general, the possible target markets are oil & gas companies. Besides oil & gas, they can be also applied in fields such as aerospace, automotive and chemical industry in general, where there is an extensive use of composite materials that are facing harsh environments. Currently, the sensors have been tested in a long term and harsh conditions testing performed in Element Materials, Hitchin.

The pipeline infrastructure in the United States is extensive, including 259.409 km of liquid fuel pipelines, 495.371 km of natural gas transmission pipelines, 1.771.654 km of natural gas distribution pipelines in service, and 2.414.016 km of large water and sewage pipes. Figure 5. 1., 2., and 3. show the total amount of incidents, fatalities and total costs occurred in pipeline incidents from 1997 to 2017,

[193]. This indicates the importance for companies to ensure the safety of the materials used.

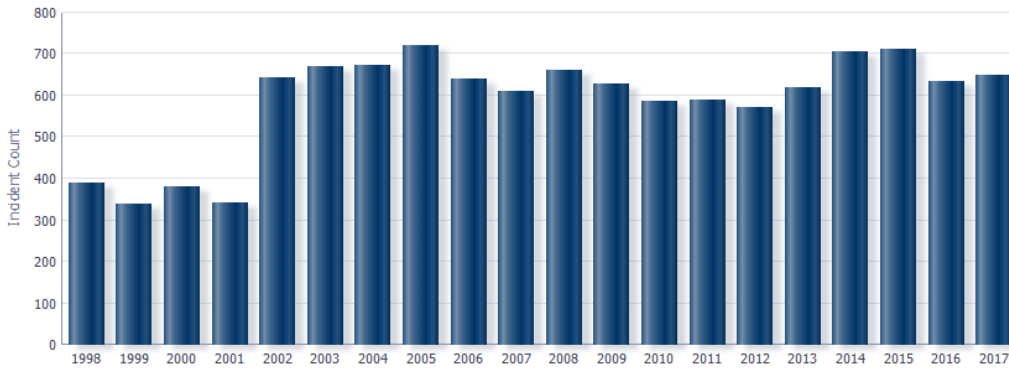


Figure 5. 1. Pipeline Incident: Count (1997-2017), (adapted graph from [193]).

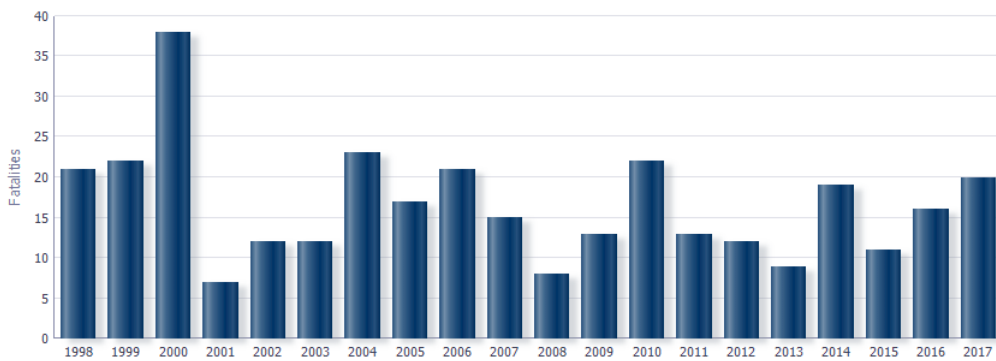


Figure 5. 2. Pipeline Incidents: Fatalities (1997-2017), (adapted graph from [193]).

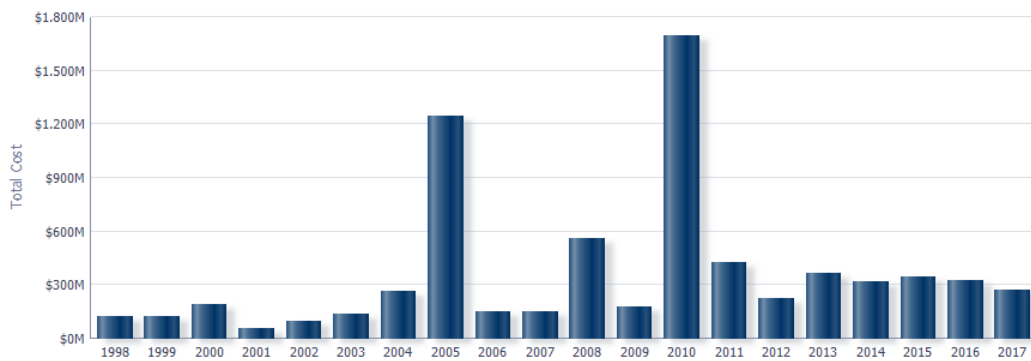


Figure 5. 3. Pipeline Incidents: Total costs (1997-2017), (adapted graph from [193]).

5.2. *Main players*

This technology could be relevant for the following companies

- First Sensor AG
- CMOSIS
- Banner engineering Belgium
- Sterkelec – Automatismes et Electronique

Furthermore, companies that can use the technology:

- Element
- ENI
- Repsol
- BASF
- Agip
- Shell

5.3. *Most relevant costs for industrialization*

Optical fibre sensors require special equipment. Costs for industrialization are the acquisition of all the setup needed in order to run the sensors. The designed setup costs are approximately: the computer €2K, a portable spectrometer €15K, a Switch €8K, a Circulator €1K, a Broadband Source €5K and the optical fibre connectors €2K. Furthermore, it is necessary to account the sensor production. This is estimated to no overpass more than 1€. To sum up, the total costs will rise approximately €33K for the first time. After the acquisition of the setup, is not necessary to buy new instrumentation. Currently, with the current configuration setup, it is possible to analyse 16 sensors simultaneously. Then, the only remaining cost will be the costs of fabrication.

5.4. Strategic choices

The key strategic choices concern the definition of relationships with industrial players, the management of intellectual property rights and finally the will to build a spin off or to simply license the technology rights. These choices allow us to have a clearer view of the strategy to undertake in defining the business model and therefore of the implementation plan.

The designed optical fibre sensors are currently in patent-pending, which is a key in the definition of the business model. If the investors or an industrial player who wants to make a strategic partnership are interested, one good option would be a business entrepreneur because it could be a great business opportunity. Fiber optic sensors, which have immunity to electromagnetic fields and can implement distributed sensing, have legitimate opportunities for market acceptance and success in diverse sectors.

The benefits that drive business as a start-up are numerous. The first is linked to the size of the market, as there are no rival sensors on the current market. Moreover, licensing of patents causes the loss of most of the value generated in the value chain, by the industrialization of the innovative Optical fiber sensors (OFSs). Finally, the sensors are easy to manufacture. They are economic and they can be produced in a normal laboratory without expensive instrumentation, thus any barrier to entry created by the amount of investment needed. The goal of the entrepreneurial team is to extract the maximum economic value possible from the product. For this, it is necessary to sell the processing data and alert service as a turnkey service, rather than the sensor. The value of the technology lies in the ability to detect and process the data detected daily by the sensors distributed along the pipeline under control. Therefore, the idea is to set up a business model based on the sale of turnkey service, in which the end customer will be alerted in case of loss of oils pipelines flows or if the customer needs information about the degradation status of the pipeline.






Furthermore, the technology is very innovative, and it is necessary to completely develop a market and a value chain, integrating it vertically, within the supply chain in the initial phase. This factor supports the willingness to create a university spin-off, that independently manages the value generated for customers. Table 5. 1. represents the main factors which influenced our choice.





Table 5. 1. Criteria and Alternatives in strategic choices: in yellow the strategic choices that concern for the companies in terms of intellectual property / spin-off / start-up.

	ALTERNATIVES		
CRITERIA	<i>Building a Spin-off or a Start-Up</i>	<i>Selling IP and R&D services</i>	<i>Selling IP</i>
Entrepreneurial team	<i>We have or we can obtain entrepreneurial skills and we are committed to becoming entrepreneurs</i>	<i>We want to continue to work in R&D on this subject, but not as entrepreneurs</i>	<i>We want to approach other challenges not related with this subject</i>
Development process nature	<i>Very risky and/or complicated activity with no other established player interested to complete the mission</i>	<i>Activity which requires strong scientific skills to be completed</i>	<i>Activity which does not require strong scientific skills to be completed</i>
Relations with other players in this consortium	<i>There are not agreements on the R&D results, or if there are agreements, they are compatible with a start-up initiative</i>	<i>There are not agreements on the R&D results or if there are agreements, they are compatible with a licensing and R&D services selling</i>	<i>There are not agreements on the R&D results or if there are agreements, they are compatible with a licensing</i>
Value chain and market	<i>If there is not a value chain or a developed market, it is possible to create them</i>	<i>There is a value chain and an eligible market</i>	<i>There is a value chain and an eligible market</i>

Product technologies	<i>Barriers to entry are surmountable for a new company</i>	<i>Barriers to entry are not surmountable for a new company</i>	<i>Barriers to entry are not surmountable for a new company</i>
Process technologies	<i>The technology can be incorporated in a service or in a product</i>	<i>The technology can be incorporated as part of an internal process in, or can developed as products among the portfolio of an existing company</i>	<i>The technology can be incorporated as part of an internal process in, or can developed as products among the portfolio of an existing company</i>
Funds	<i>Funds can be obtained by VC, Business Angels or industrial partners</i>	<i>Cost of money is compatible with that one of an existing company</i>	<i>Cost of money is compatible with that one of an existing company</i>
IPR	<i>There is the opportunity to obtain a patent and it's really strategic for the business of a hypothetical new company</i>	<i>IP and researchers' know how are both essential for complete the task</i>	<i>Researchers' know how is not so crucial to continue the implementation task</i>
Product life cycle stage	<i>Our technology will impact on a product in its initial phase of life (maybe never seen in the market)</i>	<i>Our technology will impact on a product in its maturity (also developed and sold)</i>	<i>Our technology will impact on a product in its maturity (also developed and sold)</i>

5.5. *How the business model works*

Key Partners 	Key Activities 	Value Propositions 	Customer Relationship 	Customer Segments 
<ul style="list-style-type: none"> • Research Center. • University. • Companies to make a direct test in real samples. • Supplier. 	<ul style="list-style-type: none"> • IP Management. • R&D. • Certification. • Sales & Marketing. • Customer training. • Production process. • Engineering, Procurement, Construction e control activities. 	<ul style="list-style-type: none"> • Prevent and/or reduce environmental disaster, industry fires, human lives and bring safety and security in the companies. • Reduction of control costs. • Reduction of maintenance costs. • Flat rate • Exploitation of the know-how 	<ul style="list-style-type: none"> • Communication and training, trough workshop and experimental activities. • Assistance and maintenance service. • Publication of information in trade and scientific publications. 	<ul style="list-style-type: none"> • Element, • ENI, • Repsol, • Shell, • Air bus, • Water plants, • Pipelines manufacturing. <p>In general, all the companies interested in check the degradation of their polymer tubes or scaffolds.</p>

	<p>Key Resources </p> <ul style="list-style-type: none"> • IP. • Human (technicians, vendor). • Know-how. • Software application for data and alert management. 		<p>Channels </p> <ul style="list-style-type: none"> • Direct sales. 	
<p>Cost Structure </p> <ul style="list-style-type: none"> • Patent maintenance and extension. • Human. 		<p>Revenue Streams </p> <ul style="list-style-type: none"> • Turnkey alert system (Engineering, Procurement, Construction, Alert System). 		

5.6. *Operations*

The search results can be protected using a patent filing, a key resource in business development. Currently, the research team has successfully carried out a patent application to cover the innovative and distinctive aspects of technology. The team wants to exploit its monopolistic rights by producing the sensor based on the patent if it has the necessary organizational and financial resources to develop, produce, distribute and serve the product successfully. The ease of production and the reduced value of the investments, necessary to start the production process, mean that the company will direct its efforts in the distribution and in commercial activities.

IP management is becoming a very complex field, requiring skills and competencies that go beyond the capabilities of most firms. Together with undeniable advantages, the choice of patenting an invention also has a number of drawbacks, which must be carefully considered. Patenting is quite expensive, especially for individuals and small firms. An initial cost comes from administrative fees due for filing the patent application and for renewing the validity of the patent over time (maintenance fees). An additional cost comes from hiring a good patent attorney, who will have to spend time and effort writing a strong patent application. In fact, the application must have carefully worded claims that might make it through the examination procedure and—most of all—hold up well in court, should someone challenge the validity of the patent and/or should the inventor decide to sue infringers.

Once the preliminary activities related to the management of IP have been defined, it is necessary to estimate the resources needed to complete the R & D activities to obtain the first 100% performing product. Currently, the first prototype is in the early stage where it is being produced in the laboratory and tested.

The European patent is currently the simplest, quickest and cheapest solution for protection not only in the European Union but also in almost in all Europe, as well as in non-European countries such as USA and Asia. It is good to bear in mind that the European patent does not represent a unitary title but is rather a single procedure for granting a number of national patents that will have to be made effective after the granting through the validation phases. The idea is to support the validation costs for the main European regional markets in which the start-up operates: Germany, Switzerland, Finland, Greece, Poland, Austria and Italy; USA and Asia for a total of €25K, (Tab. 5. 2.). The patent costs will be borne by the

research hosting institution, in particular, with the collaboration of TRIN (Politecnico di Torino technological transfer). Clearly, the IP must be reacquired to fulfil its monopoly rights.

Table 5. 2. Cost item table.

Cost item	Total (€)
Intellectual property advice	30.000
Patent filing	20.000
Validation Costs (7 Countries)	25.000
TOT (€)	75.500

Parallel to the strategic business activities it will be necessary to complete the R & D activities in order to obtain the first prototype that uses optical glass fibre sensors embedded into an epoxy matrix. Work Breakdown Structure (WBS) is split in two main activities. The first activity consists on the deposition processes, and the second activity is related to chemistry and material science studies, (Fig. 5. 4.).

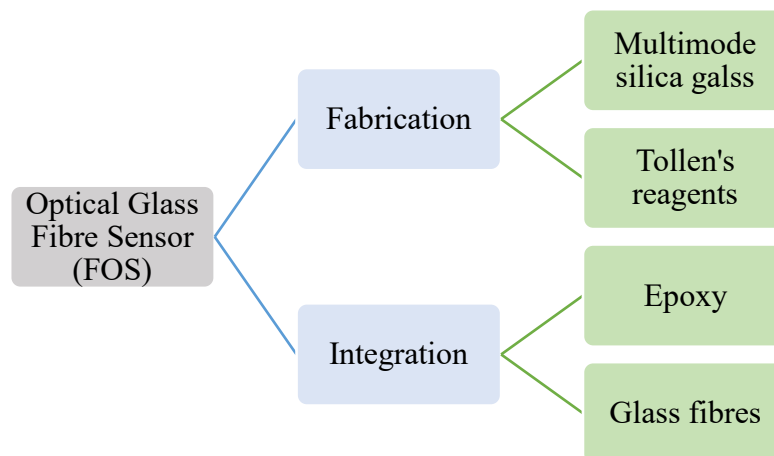


Figure 5. 4. Project R&D WBS.

As indicated in Fig. 5. 4., the deposition of silver must be further developed. Furthermore, in the same way, it will be necessary to test the possibility of depositing other metals by using physical vapour deposition. Given the strategic need IP, the activities of integration will be parallel to the embedding process. For this reason, it will be necessary to increase the number of technical resources used in R&D activities. Epoxy and Fibre optics studies are a very important part of the project. The two main activities will be to test mechanical properties and degradation lifetime. Other studies may be useful. R&D activities will last for a total of 2 months, (Tab. 5. 3.).

Table 5. 3. R&D activities budget.

Cost item	Effort/Quantity	Total (€)
HR techniques (2 resources)	40 day/man	5.000
Research laboratory contracts		35.000
Reagents		2.000
Substrates		1.000
<i>TOT (€)</i>		43.000

Since this solution is related to its possible use in the aerospace field, some other tests are needed such as in-situ real monitoring test. An external consultancy of doctors and valuation of people who are directly linked with the potential user will also be necessary. The technical implementation requires a period of 5 months, (Tab. 5. 4.).

Table 5. 4. Technical solution implementation budget.

Type	Effort/Quantity	Total (€)
HR techniques	100 day/man	50.000
In situ real monitoring Test		40.000
Prototyping and Testing		80.000
Consulting		60.000
<i>TOT (€)</i>		300.000 €

This first series of activities will produce the first series of prototypes, in the various application fields described. Therefore, the budget necessary to complete R&D activities, test, obtain the first series of prototypes and file a European patent are a total of € 418.500. Once these activities have been performed, the product must be certified, engineered, the production line must be set up and marketed. The quantification of the cost items is seen from month 7 to month 24, when the sale of the product begins. The budget of the first R&D stage has already been increased, Tab. 5. 5.

Table 5. 5. Exploitation Plan budget.

Marketing & Sales & Assistance.

Cost item	Total (€)
HR M&S	
Senior (1)	100.000
Junior (2)	70.000
HR Assistance	
Junior	35.000
Trade fairs	
Total (2)	50.000
Publication, brochure, and presentation material	35.000
Business Trips	75.000
TOT (€)	365.000

R & D

Cost item	Total (€)
HR techniques	
Senior (1)	100.000
Junior (2)	60.000
Research laboratory contracts	50.500
Research laboratory testing contracts	50.000
Consulting	20.000
Certification	50.000
TOT (€)	380.000

Investments in production

Cost item	Total (€)
Laboratory investment(instrumentation)	25.000
Production line (Machines, equipment)	150.000
Logistic Equipment	25.000
PC e SW	10.000
TOT (€)	210.000

Another technical HR

Cost item	Total (€)
HR purchasing office	
Junior	35.000
HR production techniques	
4 resources (first 3 productive months)	25.000
TOT (€)	60.000

The total investment to complete the R&D activities, start production of the first lots and launch the product on the market it is assumed equal to 1.19 million of €.

The following page summarizes the project operational roadmap in the form of a Gantt.

5.6.1. Implementation Plan

The Implementation Plan has been divided into two macro categories that can be summarized as follows:

- R&D;
- Patent;
- Prototyping and test;
- Certification;
- Engineering;
- Communication and trading;
- Marketing & sales;
- Production process.

The implementation of the eight macro-categories is expected to take place over a period of 24 months, as summarized in the figure below (the red line indicates the current reference period), (Tab. 5. 6.).

Table 5. 6. Implementation plan for two years.

Activity	Description	1st year												2nd year											
		1	2	3	4	5	6	7	8	9	10	11	12	1	2	3	4	5	6	7	8	9	10	11	12
1	R&D: Fabrication process	█	█																						
2	Technical product development: Prototype realization			█	█	█																			
3	Test Prototypes and tuning						█	█																	
4	Patent filing	█	█	█	█	█																			
5	Certification								█	█	█	█													
6	Search for industrial partners and suppliers								█	█	█	█													

5.7. *How much value can we obtain?*

The economic-financial plan, reported in this section, is at a preliminary stage of analysis and further investigations are needed both in terms of costs and turnover growth and market share. The hypotheses underlying the model of extraction of value, for the Spin-off and for IP owner property are the following:

- Spin-off revenue growth, in line with the growth rates of Global sensor water detection market by end users (oil & gas, Aerospace & defence, Chemicals and petrochemicals);
- Product portfolio share and growth, according to sensor water detection market;
- Start of new product sales from the end of 2019;
- Growth rate proportional to the commercial effort applied by the sales force

Variable costs have a low impact on costs and consist only of the cost of the material needed for the production of the fibre sensor. Costs of raw material and consumable account for only around 15% of the total operational costs incurred, while most of the cost refers to external expenses and personnel. After the launch of the product, in 2020 the Earnings before Interest, Taxes, Depreciation and Amortization (EBITDA) will be around 23%, guaranteeing the company an increase in operating margins, due to new products marketed. The graph is a snapshot of the company's economic results in the next 5 years of activity (Fig. 5. 5.).

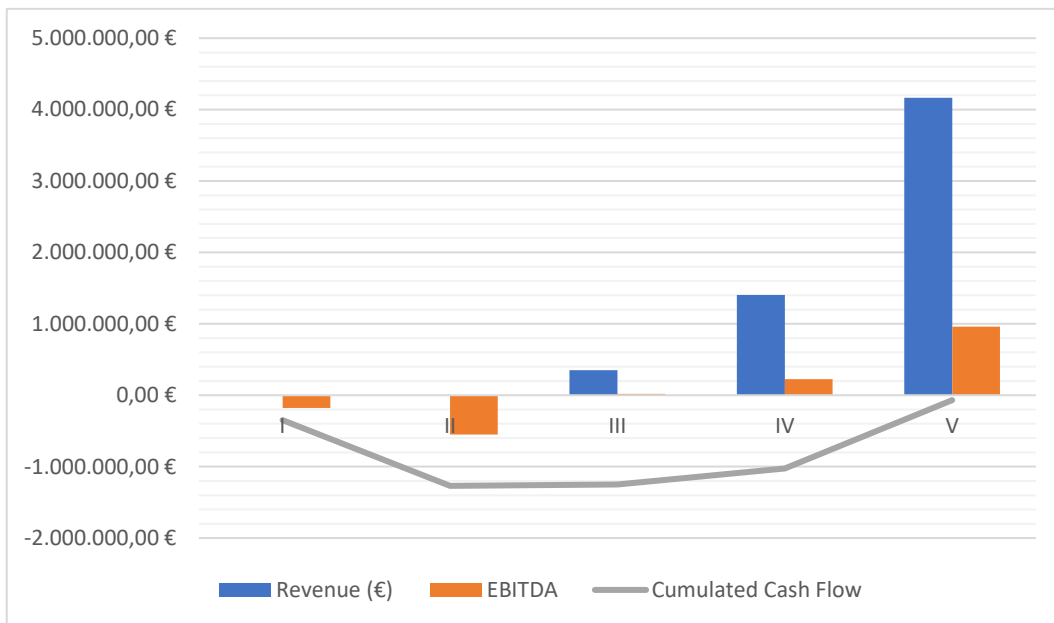


Figure 5. 5. Financial Highlights.

The maximum financial requirement is about € 1.3 million reached in the second year, when the structure grows to sustain the expected volume of business. In the first year, the maximum requirement is approximately equal to € 400k. The break even, including the full recovery of investments, is assumed at the end of the sixth year, although not directly shown in the diagram. Table 5. 7. shows the model of the economic and financial plan for the new company, which will complete the R&D activities, engineer, produce and market the new product.

Table 5. 7. Business Plan Model of the economic and financial plan for five years.

	2018	2019	2020	2021	2022
TAM (Total Addressable Market)					
Global Sensor Market (€ Million)	145.438	162.361	181.195	202.939	228.103
Growth Rate	11,20%	11,60%	12%	12,40%	12,80%
Target segment market share					
<i>Aerospace & Defense (%)</i>	5,46%				
<i>Chemicals & Petrochemicals (%)</i>	11,47%				
<i>Oil & gas (%)</i>	6,13%				
Tot	23,06%				
SAM (Serviceable Available Market)					
<i>€ Million</i>	33.538	37.440	41.783	46.797	52.601
SOM (Serviceable Obtainable Market)					
<i>Water in Fuel (WIF) Sensors (%)</i>	0,12%				
<i>€ Million</i>	40,25	44,93	50,14	56,16	63,12
<i>Market Share (%)</i>			0,70%	2,50%	6,60%
Revenue (€)	-	-	350.983	1.403.932	4.165.971
Cost (€)					

<i>Raw material and consumable</i>	3.000		50.015	176.895	481.170
<i>Other external expenses</i>	95.000	150.500	83.358	294.825	801.950
<i>Personnel costs</i>	80.000	400.000	200.060	707.581	1.924.679
Investment (€)					
<i>IP</i>	75.500				
<i>Prototyping and testing</i>	40.000	40.000			
<i>In situ real monitoring test</i>	20.000	20.000			
<i>Trade Fairs</i>		50.000			
<i>Publication and brochure</i>	5.000	30.000			
<i>Certification</i>		50.000			
<i>Laboratory investment</i>	25.000				
<i>Production line (Machines, equipment)</i>		150.000			
<i>Logistic Equipment</i>		25.000			
<i>PC e SW</i>	5.000	5.000			
<i>EBITDA</i>	-178.000	-550.500	17.549	224.629	958.173
<i>EBITDA (%)</i>	-	-	5,00%	16,00%	23,00%
Cash Flow Analysis (€)					
<i>Cash Flow</i>	-348.500	-920.500	17.549	224.629	958.173
<i>Cumulated Cash Flow</i>	-348.500	-1.269.000	-1.251.450	-1.026.821	-68.648

To sum up, this exploitation plan shows a feasible hypothetically possibility of building a start-up company. The need of make big investments in R&D to produce the final product and the financial requirement for the first years make a financial need of €70K and subsequently the negative cash. For this reason, the financial need of €70K until the third year, included, produce the fact the start-up does not have immediately earnings. As a good proof of concept, the sensors have been deposited in a patent process. They are currently in a patent pending process [195].

Finally, this project won the funding of the competition in Politecnico di Torino called Proof-Of-Concept (POC) that yielded a grant of €40K. Thanks to POC it has been also possible the acquisition of new material and modern instrumentation. Thanks to the funding from the European Union's Horizon 2020 research and innovation programme under the Marie Skłodowska-Curie grant agreement No. 642557, this project opens new ways of research on optical fibre sensors to detect the earlier degradation in polymer composites.

Chapter 6

Conclusions

The best curing conditions of the Epoxy Ampreg 26 were investigated to obtain the best performing polymer, in terms of thermo-mechanical and viscoelastic properties. The final curing temperature was assessed by means of DSC, FT-IR and DMTA analysis.

The gravimetric test was shown to have a strong influence on the difference between the diffusion coefficients of the epoxy and GFRP samples. The different epoxy samples exposure to artificial salty water and HCl did not affect the RI.

Embedding optical glass fibres into the GFRP composites did not influenced their mechanical properties, as shown by a tensile test and three point bending test, which demonstrated the negligible variance of the maximum stress and flexural stress between the specimens.

Novel, single-ended, optical fiber sensors for the detection of chemicals have been fabricated, embedded, and tested in an epoxy resin and glass fiber-reinforced polymers. These sensors, which rely on evanescent field sensing, have the additional advantages of being single-ended and of being able to work as probes. A procedure to embed the optical fiber sensors has been developed and experimentally optimized. A setup for the continuous monitoring of the sensors has been designed to remotely track the embedded sensors. The recorded optical data of samples immersed in artificial sea water at 80 °C showed that it is possible to detect water diffusion by observing decreases in the spectral reflection from the sensors. The results were then corroborated by means of gravimetric measurements and a Fickian diffusion model. Tests conducted for up to 100 hours showed that the response of the sensors embedded at increasing depths in the samples was in full agreement with the expected diffusion time. Experiments at high pressure, carried out in a special vessel, also exhibited acceptable agreement between the experimental data and the calculated diffusion time.

By tailoring the sensors, it was possible to selectively detect the diffusion of hydrochloric acid. To implement this feature, the standard fabrication process was upgraded by coating the etched fiber with a 100-nm aluminium layer, which reacted to the hydrochloric acid.

An alternative optical fibre sensor was also fabricated and tested. An ultra-pure TAS fibre was successfully fabricated and tested starting from the bulk materials. The TAS fibre was carefully inspected using an optical microscope and corroborating the absence of crystal formations or dust inclusions along the fibre. Distilled water and ethanol diffusion coefficients were calculated assuming the Fickian approximation and performing gravimetric tests. It was possible to use the TAS fibre to follow the cross-linking reactions in situ and in real-time. Parallel FT-IR analysis tests were produced to compare a good epoxy conversion using TAS fibres which results in an excellent matching. Both analyses showed a high epoxy conversion of 97% and 96%, respectively. The chalcogenide fibre was able to approximately detect the distilled water and ethanol diffusion through the polymer matrix in its early diffusion step. Finally, a good adhesion between the fibre and the epoxy was found using an optical microscope. These results open up for the first time the possibility of using TAS fibre to be used as sensors to monitor the polymer crosslinking reactions and later on the diffusion of chemicals for earlier stage detection of the possible degradation of polymer composites.

The percolation threshold was investigated by mixing different CNTs concentrations with epoxy. Experimental results showed that the threshold was at approximately 0.50 wt% of mixed CNTs. Subsequently, 0.50 wt% of filler mixed with an epoxy was chosen to make a water sensitive sensor based on CNTs. The same percentage filler of 0.50 wt% was chosen to be spray coated on the glass fibre plies to produce the smart GFRP composite. Smart composites showed a good electrical conductivity response in distilled and artificial salty water.

The smart GFRP composite, GFRP05, was successfully fabricated and tested. This had one sensing part provided by CNTs by means of an increment of conductivity and the other part with OFSs by means of a drop in the intensity of the reflected light. OFS could present an advantage versus CNTs in oil and gas companies because they do not require a white room to manufacture the polymer composites.

Both sensors were able to detect approximately the diffusion through the H-GFRP composite. It would depend on the company facilities to choose between OFSs or CNTs to detect approximately the moisture diffusion through the polymer matrix. Finally, this research on new moisture sensors yields a preliminary experimental proof of their possible feasibility to implement these sensors in harsh environments, whose structural integrity can be remotely monitored.

Overall, this work yields a preliminary experimental proof of the feasibility of glass fibre reinforced polymers equipped with optical sensors, that can find applications in harsh environments (such as pipes exposed to sea water diffusion), whose structural integrity can be remotely monitored with a simple, electric-free system, and possible failures can be detected at early stages. Furthermore, tailoring the sensors opens up a wide range of new applications for sensing, of great and relevant interest to petrochemical companies.

In short, this research has provided a proof-of-concept of a sensitive GFRP composite that could be used, for example, in a pipeline to monitor the diffusion of chemicals in real time and provide information in order to reduce maintenance services.

Future research

These preliminary results show the huge potential of the OFSs as revolutionary sensors for GFRP composites. However, due to the time limitations of this project, some research on different points remains to be done in future works.

First of all, an automatization of the OFSs fabrication is still needed. A more precise etching process with a standard procedure would make the reproducibility of the sensors more accurate. Furthermore, an automatic cleaver could be used to cut the OF more accurately.

Another future work could investigate functionalizing the OFSs through a sol-gel process and incorporating CoCl_2 along the sensitive exposed core to make the OFSs more sensitive to moisture diffusion.

Several organic dyes were proposed to detect chemicals such as H_2S . Unfortunately, these were not able to resist the curing conditions of the Ampreg 26. For this reason, an epoxy with a lower curing temperature (below $55\text{ }^\circ\text{C}$) could have great potential for use with organic dyes for chemicals detection. Currently, OFSs can be tailored with different coatings to make them sensitive to other chemicals. For example, tailoring OFSs with Cu can make them selective to basic species such as NH_4OH .

OFSs have been employed in various companies, leading to the identification of some problematic issues. For example, “Ente Nazionale Idrocarburi” ENI S.p.A. identified a problem with leakage in their tanks. Research into resolving this leakage problem could make OFSs become highly valuable sensors in oil & gas companies.

Another interesting task, which it was not possible to perform due to the limitations of time and mobility in this project, would be to compare the signal provided by OFSs with the signal of TAS fibre sensors. It could be investigated whether these two different glasses can work in synergy and provide some valuable information.

Appendix A

List of acronyms and symbols

Acronyms

ASW Artificial Salty Water

Al-OFS Aluminium sputtered optical fibre sensors

ASTM American Society for Testing and Materials

ASME American Society of Mechanical Engineers

BS British Standard

CNT Carbon Nanotube

Cu-OFS Copper sputtered optical fibre sensors

DIS Draft International Standard

DTMA Dynamic Thermal Mechanical Analysis

DSC Differential Scanning Calorimetry

DVD Digital Versatile Disk

E/M Electro-Mechanical

EW Evanescent Wave

EWOS Evanescent Wave Optical Sensor

FEWS Fibre Evanescent Wave Spectroscopy

FBG Fibre Bragg Grating

FRP Fibre Reinforced Polymers

FTIR Fourier-Transform Infrared spectroscopy

H-GFRP Hybrid GFRP: GFRP sample containing spread CNTs on the plies and embedded OFSs

IR Infrared

IFP Institut Français du Pétrole

IPD Isophorone Diamine

ISO International Organization for Standardization

GIF Graded-Index Multimode Fiber

GRE Glass Fibre Reinforced Epoxy

GFRP Glass Fibre Reinforced Polymers

GFRP05 GFRP samples containing spread CNTs on the plies

LP Linear Polarized

LPG Long-Period Gratings

MDA Mentane Diamine

MM Multi-Mode

MCT Mercury Cadmium Telluride

NA numerical aperture

NIR Near Infrared

OF Optical Fibre

OFS Optical Fibre Sensors

POC Proof of Concept

PVD Physical Vapour Deposition

RE Rare Earth

RH Relative Humidity

RI Reflective Index

RTP Thermoplastic Pipework

SM Single-Mode

SEM Scanning Electro-Microscope

TAS Tellurium-Arsenic-Selenium

TE Transverse Electric

TGA Thermogravimetric analysis

TM Transverse Magnetic

TIR Total Internal Reflection

UV Ultra-Violet

VIS Visible

Symbols

α_{max} Maximum angle of acceptance

β Quantity of beta

β_m Mode propagation constant

c Speed of light

D Diffusion coefficient

d Distance

D Electric displacement field

$d_{preform}$ Preform diameter

E Electric field

ϵ_r Electrical relative permittivity

ϵ_0 Electrical permittivity

ϵ Absorptivity

f Light frequency

H Magnetic field

h Thickness

λ Wavelength

I Intensity

M_∞ Weight gain at saturation

M_n Weight gain

m Mode number

μ_0 Magnetic permittivity

n_d Helium d-line

n_f Hydrogen f-line

n_c Hydrogen c-line

n Refractive index

θ_i Angle of incident

θ_c Critical angle

P Polarization

σ Conductivity of the polymer containing CNTs

σ_0 Scaling factor

φ Filler content

φ_c Percolation threshold

φ_z Plane wave

τ critical exponent

t_n Time

V Normalized frequency

$v_{preform}$ Preform feed speed

v_{fibre} Pulling speed

v Medium

v Velocity

ω_c Cut-off frequency

χ^n Linear electrical susceptibility

Appendix B

Publications resulting from this thesis

Papers

C. Marro Bellot, M. Olivero, M. Sangermano, M. Salvo, Towards smart polymer composites: detection of moisture diffusion through epoxy by evanescent wave optical fibre sensors, *Polym. Test.* 71 (2018) 248–254.

C. Marro Bellot, M. Sangermano, M. Olivero, M. Salvo, Optical Fiber Sensors for the Detection of Hydrochloric Acid and Sea Water in Epoxy and Glass Fiber-Reinforced Polymer Composites, *Materials (Basel)*. 12 (2019) 379.

M. Sangermano, A. D’Anna, C. Marro Bellot, N. Klikovits, and R. Liska, “UV-activated frontal polymerization of glass fibre reinforced epoxy composites,” *Compos. Part B Eng.*, 143, (2018) 168–171.

Patents

M. Salvo, M. Sangermano, C. Marro Bellot, M. Olivero, Optical Sensor, Process for Making Such Sensors and Evaluation System Comprising at Least One of Such Sensors, 2018WO–IT00059, 2017.

Conferences

The AIDAA 2015 Conference on Aeronautics and Astronautics, Torino, Italy, from 17/11/2015 to 19/11/2015.

ICCE-25, The 25th annual International Conference on Composites or nano Engineering (ICCE), Roma, Italy, from 16/07/2017 to 22/07/2017.

ECCM-18, the 18th European Conference on Composite Materials (ECCM), Athens, Greece, from 24/06/2018 to 29/06/2018.

OFS-26 The 26th International Conference on Optical Fibre Sensors (OFS), Lausanne, Switzerland, from 24/09/2018 to 28/09/2018.

Research stays

Nanoforce, London, UK, Nanoforce, London, from 13/02/2017 to 13/05/2017.



Element Technology Materials, Hitchin, UK, Element Technology Materials, Hitchin, from 28/08/2017 to 03/11/2017.



Université de Rennes 1 | UR1, Université de Rennes 1 | UR1, Rennes, from 05/03/2018 to 30/03/2018.



Funding

The research leading to these results received funding from the European Union's Horizon 2020 research and innovation programme under the Marie Skłodowska-Curie grant agreement No. 642557.



References

- [1] B. Boyd, “Grayline: Energy and Natural Resources: Powering Societies.” [Online]. Available: <https://graylinegroup.com/energy-natural-resources-industry/>. [Accessed: 30-Jan-2019].
- [2] “Organic Hydrocarbons,” 2006. [Online]. Available: <https://opentextbc.ca/chemistry/chapter/20-1-hydrocarbons/>. [Accessed: 30-Jan-2019].
- [3] J. Awalt, “Global Pipeline Construction Outlook,” *Pipeline Gas J.*, vol. 246, no. 1, 2019.
- [4] L. D’Angelo, S. Furtado, O. Fyrileiv, and L. Collberg, “Ultra-deep water depth pipelines: design creteria review for new frontier applications,” *Pipeline Technol. J.*, no. 4, 2018.
- [5] C. Leif, J. K. Mork, and M. J. Marley, “Inherent Safety Level in Different Pressure Containment Criteria,” in *International Offshore and Polar Engineering Conference*, 2001.
- [6] M. Islam, T. Aravinthan, A. Manalo, and K. Lau, “Effectiveness of using fibre-reinforced polymer composites for underwater steel pipeline repairs,” *Compos. Struct.*, vol. 100, pp. 40–54, 2013.
- [7] M. E. Orazem, *Underground Pipeline Corrosion*. 2014.
- [8] Smartpipe, “Pipeline Replacement Technology,” 2018. [Online]. Available: <http://smart-pipe.com/>. [Accessed: 02-Aug-2018].
- [9] C. E. P. A. (CEPA), “About Pipelines,” 2016. [Online]. Available: <https://www.aboutpipelines.com/en/safety/pipeline-integrity/>. [Accessed: 31-Jan-2019].
- [10] C. Kassel, A. Liessem, T. Gjedrem, “Challanges of the large offshore project from a line pipe manufacturers view,” *Pipeline Technol. Journal*2, no. 4, p. 50, 2018.
- [11] A. Barrias, J. R. Casas, and S. Villalba, “A Review of Distributed Optical Fiber Sensors for Civil Engineering Applications,” *Sensors*, vol. 16, no. 748, p. 35, 2016.

- [12] M. Assarar, D. Scida, A. El Mahi, C. Poilâne, and R. Ayad, "Influence of water ageing on mechanical properties and damage events of two reinforced composite materials: Flax-fibres and glass-fibres," *Mater. Des.*, vol. 32, no. 2, pp. 788–795, 2011.
- [13] B. Milsom, M. Olivero, D. Milanese, S. Giannis, R. H. Martin, A. Terenzi, J. Kenny, M. Ferraris, G. Perrone, and M. Salvo, "Glass optical fibre sensors for detection of through thickness moisture diffusion in glass reinforced composites under hostile environments," *Adv. Appl. Ceram.*, vol. 6753, no. February 2017, 2015.
- [14] C. Marro Bellot, M. Olivero, M. Sangermano, and M. Salvo, "Towards smart polymer composites: detection of moisture diffusion through epoxy by evanescent wave optical fibre sensors," *Polym. Test.*, vol. 71, pp. 248–254, 2018.
- [15] C. Marro Bellot, M. Sangermano, M. Olivero, and M. Salvo, "Optical Fiber Sensors for the Detection of Hydrochloric Acid and Sea Water in Epoxy and Glass Fiber-Reinforced Polymer Composites," *Materials (Basel)*, vol. 12, no. 3, p. 379, 2019.
- [16] R. Chandra, S. P. Singh, and K. Gupta, "Damping studies in fibre-reinforced composites: a review," *Compos. Struct.*, vol. 46, no. 1, pp. 41–51, 1999.
- [17] C. E. Bakis, L. C. Bank, V. L. Brown, and E. Cosenza, "Fiber-Reinforced Polymer Composites for Construction - State-of-the-Art Review-," *Compos. Constr.*, vol. 6, no. May, pp. 73–87, 2002.
- [18] H. Ku, H. Wang, N. Pattarachaiyakoop, and M. Trada, "A review on the tensile properties of natural fiber reinforced polymer composites," *Compos. Part B*, vol. 42, no. 2, pp. 856–873, 2011.
- [19] P. K. Mallick, *Fibre-Reinforced Composites*, 3rd ed. London: CRC Press, 2007.
- [20] M. Koch and D. Lupton, "Design and Manufacture of Bushings for Glass Fibre Production," *Prod. Prop. Appl. Refract. Platin. Gr. Met. Contact with Glas. Melts*, no. October, 2006.
- [21] N. B. O. C. and Engineers, *The Complete Technology Book on Fibre Glass, Optical Glass and Reinforced Plastics*, 1st ed. Asia Pacific Business Press Inc., 2007.
- [22] A. R. Bunsell, *Fibre Reinforcements for Composite Materials*, vol. 1. Tokyo: Elsevier, 1988.

- [23] F. T. Wallenberger and P. A. Bingham, *Fiberglass and Glass Technology: Energy-Friendly Compositions and Applications*, 1st ed. Birmingham: Springer Science & Business Media, 2009.
- [24] “Glass Fiber Differences and Properties,” *Prince Engineering: Build on Prince*. [Online]. Available: <https://www.build-on-prince.com/glass-fiber.html>. [Accessed: 18-Jul-2018].
- [25] “Composites World,” 2018. [Online]. Available: <https://www.compositesworld.com/articles/fabrication-methods>. [Accessed: 23-Aug-2018].
- [26] P. J. Honka, “Method and Apparatus for Vacuum Bag Moulding of Composite Materials,” 5.106.658, 1994.
- [27] Compression molding [Online]. Available: <https://nptel.ac.in/courses/112107085/module5/lecture6/lecture6.pdf>. [Accessed: 23-Aug-2018]
- [28] B. Milsom, M. Olivero, D. Milanese, S. Giannis, R. H. Martin, A. Terenzi, J. Kenny, M. Ferraris, G. Perrone, and M. Salvo, “Glass optical fibre sensors for detection of through thickness moisture diffusion in glass reinforced composites under hostile environments,” *Adv. Appl. Ceram.*, vol. 114, no. sup1, pp. S76–S83, Sep. 2015.
- [29] A. G. Gibson, “The cost effective use of fibre reinforced composites offshore,” in *Health and Safety Executive*, Newcastle: HSE Books, 2003, p. 140.
- [30] “What is Duplex and Super Duplex Stainless Steel?,” 2017. [Online]. Available: <https://masteel.co.uk/news/what-is-duplex-and-super-duplex-stainless-steel/>.
- [31] “Difference Between Duplex and Super Duplex Steel,” *Oshwin Overseas*, 2016. [Online]. Available: <http://www.duplex2205.net/difference-between-duplex-and-super-duplex-steel/>.
- [32] P. Trifunović, “Use of composite materials in oil industry,” *Undergr. Min. Eng.*, vol. 19, pp. 157–164, 2011.
- [33] T. W. L. M. R. S. Research and Markets, “Global Forecasts to 2021,” 2018. [Online]. Available: <https://globenewswire.com/news-release/2016/09/22/873799/0/en/1-98-Billion-Composites-in-Oil-and-Gas-Industry-Market-by-Resin-Type-Fiber-Type-Application-and-Region-Global-Forecasts-to-2021.html>. [Accessed: 03-Aug-2018].

- [34] G. D. Davis, L. A. Krebs, and C. M. Dacre, “Sensor to detect moisture/degradation of composites and adhesive bonds,” in *International SAMPE symposium and Exhibition*, 2001, p. 20.
- [35] “Twaron®.” [Online]. Available: <http://www.directindustry.es/prod/teijin-aramid/product-18087-1219369.html>.
- [36] R. Sen and G. Mullins, “Application of FRP composites for underwater piles repair,” *Compos. Part B Eng.*, vol. 38, no. 5–6, pp. 751–758, 2007.
- [37] “Clock Spring Compan, INC,” 2018. [Online]. Available: <https://www.clockspring.com/product/clock-spring/>. [Accessed: 27-Aug-2018].
- [38] Sealxpert(R), “Oil&Gas industry,” 2018. [Online]. Available: <https://www.sealxpert.com/oil-gas>. [Accessed: 03-Aug-2018].
- [39] “RES-Q® Composite Wrap,” 2018. [Online]. Available: <http://www.tdwilliamson.com/solutions/hot-tapping-and-plugging/repair/res-q-wrap>. [Accessed: 27-Aug-2018].
- [40] T. Yeo, T. Sun, and K. Grattan, “Fibre-optic sensor technologies for humidity and moisture measurement,” *Sensors Actuators, A Phys.*, vol. 144, pp. 280–295, 2008.
- [41] R. Ramaswami, N. Kumar, and G. Sivarajan, *Optical Networks: A practical Perspective*, Third. USA: Morgan Kaufmann, 2015.
- [42] K. . Kao and G. . Hockham, “Dielectric-fibre surface waveguides for optical frequencies,” vol. 133, no. 3, pp. 191–198, 1986.
- [43] M. Yamane and Y. Asahara, *Glasses for Photonics*, 1st ed. United Kingdom: Cambridge University Press, 2009.
- [44] J. Lousteau, N. G. Boetti, D. Negro, E. Mura, G. C. Scarpignato, G. Perrone, D. Milanese, and S. Abrate, “Photonic glasses for IR and mid-IR spectral range,” in *SPIE*, 2017, p. 6.
- [45] B. Richards, A. Jha, Y. Tsang, D. Binks, J. Lousteau, F. Fusari, A. Lagatsky, C. Brown, and W. Sibbett, “Tellurite glass lasers operating close to 2 μ m,” *Laser Phys. Lett.*, vol. 3, pp. 177–193, 2010.
- [46] L. Gomes, D. Milanese, J. Lousteau, N. Boetti, and S. D. Jackson, “Energy level decay processes in Ho³⁺ -doped tellurite glass relevant to the 3 μ m transition,” *Appl. Phys.*, vol. 109, pp. 1–7, 2011.

- [47] A. Jean-Luc and X. Zhang, “Chalcogenide Waveguides for infrared sensing,” in *Chalcogenide glasses: Preparation, properties and applications*, Woodhead, 2004, pp. 381–383.
- [48] M. F. Churbanov and V. G. Plotnichenko, “Optical fibres from high-purity arsenic chalcogenide glasses,” in *Semiconducting Chalcogenide Glass. III. Application of Chalcogenide fibres. Glasses Semiconductor ans Semimetals*, 1st ed., vol. 80, UK: Academic Press, 2004, pp. 209–230.
- [49] B. Bureau, C. Boussard-pledel, P. Lucas, and X. Zhang, “Forming Glasses from Se and Te,” *Molecules*, vol. 14, no. Dvd, pp. 4337–4350, 2009.
- [50] L. Calvez, P. Lucas, M. Rozé, H. L. MA, J. Lucas, and X. H. Zhang, “Influence of gallium and alkali halide addition on the optical and thermo-mechanical properties of GeSe₂-Ga₂Se₃ glass,” *Appl. Phys. A*, vol. 89, pp. 183–188, 2007.
- [51] C. Harris, *Materials for Infrared Windows and Domes: Properties and Performance*, 2nd ed. Bellingham, WA: SPIE Optical Engineering Press, 1999.
- [52] X. Zhu and N. Peyghambarian, “High-Power ZBLAN Glass Fiber Lasers: Review and Prospect,” *Adv. Optoelectron.*, p. 23, 2010.
- [53] M. F. Churbanov, G. E. Snopatin, V. S. Shiryayev, V. G. Plotnichenko, and E. M. Dianov, “Recent advances in preparation of high-purity glasses based on arsenic chalcogenides for fiber optics,” *J. Non. Cryst. Solids*, vol. 357, no. 11–13, pp. 2352–2357, 2011.
- [54] T. Sorokina and L. Konstantin, *Solid-State Mid-Infrared Laser Sources*, Vol. 2. Berlin, Heidelberg: Topics in Applied Physics, 2003.
- [55] A. Zakery and S. R. Elliott, “Optical properties and applications of chalcogenide glasses: a review,” *Non-Crystal. Solids*, vol. 330, pp. 1–12, 2003.
- [56] V. . Dorofeev, A. . Moiseev, M. . Churbanov, G. . Snopatin, A. . Chilyasov, I. A. Kraev, A. S. Lobanov, T. . Kotereva, L. . Ketkova, A. . Pushkin, V. . Gerasimenko, V. . Plotnichenko, A. . Kosolapov, and E. . Dianov, “High-purity TeO₂-WO₃-(La₂O₃,Bi₂O₃) glasses for fiber-optics,” *Opt. Mater. (Amst)*, vol. 33, pp. 1911–1915, 2011.
- [57] A. B. Seddon, “Chalcogenide glasses: a review of their preparation, properties and applications,” *Non-Crystal. Solids*, vol. 184, pp. 44–50, 1995.

- [58] V. Maguire, “The fundamentals of optical light sources and transmission.” [Online]. Available: <https://www.cablinginstall.com/articles/2010/05/the-fundamentals-of.html>. [Accessed: 21-Feb-2019].
- [59] “The Physics classroom: Snell’s Law.” [Online]. Available: <http://www.physicsclassroom.com/Class/refrn/u1412b.cfm>. [Accessed: 22-Jun-2018].
- [60] “The Physics Classroom: Total Internal Reflection.” [Online]. Available: <http://www.physicsclassroom.com/Class/refrn/u1413b.cfm>. [Accessed: 22-Jun-2018].
- [61] “The Physics Classroom,” 2018. [Online]. Available: <http://www.physicsclassroom.com/class/refrn/Lesson-3/The-Critical-Angle>. [Accessed: 23-Jun-2018].
- [62] K. Okamoto, *Fundamentals of Optical Waveguides*, 2nd ed. Burlington, MA, USA: Elsevier, 2005.
- [63] “Fabrication of optical fibres.” [Online]. Available: <http://www.tpub.com/neets/tm/107-5.htm>. [Accessed: 01-Jul-2018].
- [64] “Manufacturing of Optical Fibers.” [Online]. Available: <https://wiki.metropolia.fi/display/Physics/Manufacturing+of+Optical+Fibers>. [Accessed: 01-Jul-2018].
- [65] Technobyte, “Optical Fiber Communication Basics – Ray theory of light.” [Online]. Available: <https://www.technobyte.org/2016/11/ray-theory-light>. [Accessed: 27-Jun-2018].
- [66] D. Milanese, J. Lousteau, A. Chavez-pirson, D. Pugliese, A. Chavez-pirson, D. Pugliese, N. G. Boetti, N. Peyghambarian, N. G. Boetti, and N. Peyghambarian, “Nonsilica Oxide Glass Fiber Laser Sources: Part I,” *Open access peer-reviewed chapter*, 2018. [Online]. Available: <https://www.intechopen.com/books/advances-in-glass-science-and-technology/nonsilica-oxide-glass-fiber-laser-sources-part-i>. [Accessed: 06-Jun-2018].
- [67] “Thorlabs: Guiding Light in an Optical Fiber.” [Online]. Available: <https://www.thorlabs.com/tutorials.cfm?tabID=789B6970-20AC-47C3-81A9-838CD7594644>. [Accessed: 21-Feb-2019].
- [68] B. D. Gupta, “Basic Fibre Optics,” in *Fibre Optic Sensors: Principles and Applications*, New Delhi, India: New India Publishing, 2006, pp. 11–26.

- [69] E. Stijns and H. Thienpont, "Fundamentals of Photonics," in *Optical and Digital Image Processing: Fundamentals and Applications*, vol. 5, J. W. & Sons, Ed. 2011, pp. 25–48.
- [70] I. Newton, "Opticks: Or, A treatise of the Reflections, Refractions, Inflexions and Colours of Light. Also Two treatises of the Species and Magnitude of Curvilinear Figures," *Opticks*, 1701. [Online]. Available: <http://www.newtonproject.ox.ac.uk/view/texts/normalized/NATP00034>. [Accessed: 26-Jun-2018].
- [71] N. G. Boetti, "Nd 3+ doped phosphate glass optical fibre lasers," Politecnico di Torino, 2014.
- [72] "Meridional and skew rays". [Online]. Available: <https://www.technobyte.org/user/umairhussaini/>. [Accessed: 24-Jun-2018].
- [73] U. Hussaini, "Optical Fiber Communication Basics – Mode theory of light," 2018. [Online]. Available: <https://www.technobyte.org/user/umairhussaini/>. [Accessed: 24-Jun-2018].
- [74] H. Volland, "Comparison Between Mode Theory and Ray Theory of VLF Propagation," *Research*, vol. 65, no. 4, pp. 357–361, 1961.
- [75] R. R. A. Syms and J. R. Cozens, "Electromagnetic fields and plane waves: Chapter two," in *Optical Guided Waves and Devices*, USA: McGraw-Hill Publishing Co., 1992, pp. 1–27.
- [76] "Basic optics for optical fiber." [Online]. Available: <https://www.fiberoptics4sale.com/blogs/archive-posts/95048070-basic-optics-for-optical-fiber>. [Accessed: 21-Feb-2019].
- [77] K. T. V. G. and B. T. Meggit, *Optical Fibre Sensor Technology*. London: Elsevier, 2000.
- [78] C.-A. Bunge, T. Gries, and M. Beckers, *Optical Fiber Technology: Basics of Fibers Principle*. UK: Woodhead Publishing, 2016.
- [79] S. O. Kasap, *Optoelectronics and Photonics: Principles and Practices*, 2nd ed. USA: Prentice Hall, 2013.
- [80] *Single Mode fibres*. *Integrated Publishing, Inc.* [Online]. Available: <http://www.tpub.com/neets/tm/106-12.htm>. [Accessed: 01-Jul-2018].
- [81] "Multimode fibres," *Integrated Publishing, Inc.* [Online]. Available: <http://www.tpub.com/neets/tm/106-12.htm>. [Accessed: 01-Jul-2018].

- [82] K. Oh and U.-C. Paek, *Silica Optical Fiber Technology for Devices and Components: Design, Fabrication, and International Standards*, 1st ed. Ho. NJ, USA, 2012.
- [83] J. D. Beaubien, “The Chilled Mirror hygrometer: How It Works, Where It Works-and Where It Doesn’t,” *Sensors Online*. [Online]. Available: <https://www.sensorsmag.com/components/chilled-mirror-hygrometer-how-it-works-where-it-works-and-where-it-doesn-t>. [Accessed: 09-Jul-2018].
- [84] G. Korotcenkov, “Optical Hygrometers,” in *Handbook of Humidity Measurement Methods, Materials and Technologies: Spectroscopic Methods of Humidity Measurement*, C. Press, Ed. London, 2018, pp. 49–82.
- [85] J. Clark, “The Beer-Lambert Law,” *chemistry Libre Texts*, 2017. [Online]. Available: [https://chem.libretexts.org/Textbook_Maps/Physical_and_Theoretical_Chemistry_Textbook_Maps/Supplemental_Modules_\(Physical_and_Theoretical_Chemistry\)/Spectroscopy/Electronic_Spectroscopy/Electronic_Spectroscopy_Basics/The_Beer-Lambert_Law](https://chem.libretexts.org/Textbook_Maps/Physical_and_Theoretical_Chemistry_Textbook_Maps/Supplemental_Modules_(Physical_and_Theoretical_Chemistry)/Spectroscopy/Electronic_Spectroscopy/Electronic_Spectroscopy_Basics/The_Beer-Lambert_Law). [Accessed: 10-Jul-2018].
- [86] C.-Y. Lee and G.-B. Lee, “Humidity Sensors: A Review,” *Sens. Lett.*, vol. 3, no. 1, pp. 1–15, 2005.
- [87] Z. Chen and C. Lu, “Humidity Sensors: A Review of Materials and Mechanisms,” *Sens. Lett.*, vol. 3, no. 4, pp. 274–295, 2005.
- [88] Z. M. Rittersma, “Recent achievements in miniaturised humidity sensors - A review of transduction techniques,” *Sensors Actuators, A Phys.*, vol. 96, no. 2–3, pp. 196–210, 2002.
- [89] V. Giurgiutiu, J. Redmond, D. Roach, and K. Rackow, “Active Sensors for Health Monitoring of Aging Aerospace Structures,” in *SPIE’s 7th Annual International Symposium on Smart Structures and Materials*, 2000, vol. 3985, pp. 294–305.
- [90] Y. Yang, G. Chiesura, G. Luyckx, T. Vervust, F. Bossuyt, M. Kaufmann, J. Degrieck, and J. Vanfleteren, “Development of a Dielectric Sensor System for the On-line Cure Monitoring of Composites,” *Procedia Technol.*, vol. 15, pp. 631–637, 2014.
- [91] H. C. Neitzert, A. Sorrentino, and L. Vertuccio, “Humidity sensing of an epoxy/MWCNT composite by electrical conductivity measurements,” *Proc. SPIE - Int. Soc. Opt. Eng.*, vol. 8766, p. 87660D, 2013.
- [92] Q. Y. Tang, Y. C. Chan, and K. Zhang, “Fast response resistive humidity sensitivity of polyimide/multiwall carbon nanotube composite films,” *Sensors Actuators, B Chem.*, vol. 152, no. 1, pp. 99–106, 2011.

- [93] S. L. Gao, R. C. Zhuang, J. Zhang, J. W. Liu, and E. Mäder, “Glass fibers with carbon nanotube networks as multifunctional sensors,” *Adv. Funct. Mater.*, vol. 20, no. 12, pp. 1885–1893, 2010.
- [94] B. Culshaw and A. Kersey, “Fiber-Optic Sensing: A Historical Perspective,” *Light. Technol.*, vol. 26, no. 9, pp. 1064–1078, 2008.
- [95] B. D. Gupta, “Optical Fibre Sensors,” in *Fibre Optic Sensors: Principles and Applications*, New India Publishing, 2006, pp. 1–9.
- [96] B. Milsom, M. Olivero, D. Milanese, M. Roseman, S. Giannis, R. Martin, and A. Terenzi, “Development and integration of innovative glass fibre sensors into advanced composites for applications in hostile environments,” in *Proceedings of the European conference on Composites Materials*, 2014.
- [97] D. C. Lee, J. J. Lee, and S. J. Yun, “The mechanical characteristics of smart composite structures with embedded optical fiber sensors,” *Compos. Struct.*, vol. 32, no. 1–4, pp. 39–50, Jan. 1995.
- [98] T. J. Young, M. J. Lodeiro, M. R. L. Gower, and M. B. Sassi, “Systematic approach for the calibration of humidity sensitive polyimide recoated fibre Bragg gratings for measuring humidity and temperature and their application for measuring moisture absorption in polymers,” *Meas. Sci. Technol.*, vol. 24, no. 8, p. 085101, Aug. 2013.
- [99] M. Olivero, G. Perrone, A. Vallan, and D. Tosi, “Comparative Study of Fiber Bragg Gratings and Fiber Polarimetric Sensors for Structural Health Monitoring of Carbon Composites,” *Adv. Opt. Technol.*, vol. 2014, pp. 1–8, Nov. 2014.
- [100] E. Udd, “Chapter 1: Overview of Fiber Optic Sensors,” in *Fibre Optic Sensors*, 2nd ed., 2011, p. 496.
- [101] S. Villalba and J. R. Casas, “Application of optical fiber distributed sensing to health monitoring of concrete structures,” *Mech. Syst. Signal Process.*, vol. 39, no. 1–2, pp. 441–451, 2013.
- [102] K. Hotate and S. S. . Ong, “Distributed Dynamic Strain Measurement Using a Correlation-Based Brillouin Sensing System,” *IEEE Photonics Technol. Lett.*, vol. 15, no. 2, pp. 272–274, 2003.
- [103] J. R. Griffiths and S. P. Robinson, “The OxyLite: a Fiber-Optic oxygen Sensor,” *Br. J. Radiol.*, vol. 72, no. 859, pp. 627–630, 1999.
- [104] J. Eric Udd, William B. Spillman, *Fiber Optic Sensors: An Introduction for Engineers and Scientists*, 2nd ed. 2011.

- [105] P. B. Ruffin, "Chapter 8: Fiber Optic Gyroscope Sensors," in *Fiber Optic Sensors, Second Edition*, 2008.
- [106] Y. Dong, X. Bao, and L. Chen, "Distributed temperature sensing based on birefringence effect on transient Brillouin grating in a polarization-maintaining photonic crystal fiber," *Opt. Lett.*, vol. 34, no. 17, pp. 2590–2592, 2009.
- [107] G. Stewart, W. Jin, and B. Culshaw, "Prospects for fibre-optic evanescent-field gas sensors using absorption in the near-infrared," *Sensors Actuators B. Chem.*, vol. 39, pp. 42–47, 1997.
- [108] H. Jiang, R. Yang, X. Tang, A. Burnett, X. Lan, and H. Xiao, "Multilayer fiber optic sensors for in situ gas monitoring in harsh environments," *Sensors Actuators B. Chem.*, vol. 177, pp. 205–212, 2013.
- [109] O. Wolfbeis, "Fiber-Optic Chemical Sensors and Biosensors," *Anal. Chem.*, vol. 80, pp. 4269–4283, 2008.
- [110] M. Archenault, H. Gagnaire, and J. P. Goure, "A simple intrinsic optical fibre refractometer," *Sensors Actuators B. Chem.*, vol. 5, pp. 173–179, 1991.
- [111] H. Hanada, "Characteristics of a Fabry—Perot interferometer with two retroreflectors and two beam splitters," *J. Opt. Soc. Am. A*, vol. 9, no. 12, p. 2167, 1992.
- [112] K. Fidanboyly and H. . Efendioglu, "Fibre Optic Sensors and Their Applications," in *5th International Advanced Technologies Symposium (IATS'09)*, 2015, pp. 1–6.
- [113] L. Deng and C. . Cai, "Applications of fiber optic sensors in civil engineering," *Struct. Eng. Mech.*, vol. 25, no. 5, pp. 577–596, 2007.
- [114] Y.-G. Han, "Temperature-insensitive strain measurement using a birefringent interferometer based on a polarization-maintaining photonic crystal fiber," *Appl. Phys. B*, vol. 95, pp. 383–387, 2009.
- [115] K. T. V. G. and Z. Y. Zhang, "Fibre optic luminescence thermometry," in *Optical Fiber Sensor Technology*, 1st ed., K.T.V. Grattan and B.T. Meggitt, Ed. London, UK: Klumer Academic, 2010, p. 336.
- [116] S. Tao, C. . Winstead, R. Jindal, and J. . Singh, "Optical-Fiber Sensor Using Tailored Porous Sol-Gel Fiber Core," *IEEE Sens. J.*, vol. 4, no. 3, pp. 322–328, 2004.

- [117] M. Ando, T. Kobayashi, and M. Haruta, "Humidity-sensitive optical absorption of Co₃O₄ film," *Sensors Actuators, B Chem.*, vol. 32, no. 2, pp. 157–160, 1996.
- [118] S. O. Tsuki, K. A. Dachi, and T. T. Aguchi, "A Novel Fiber-Optic Gas Sensing Arrangement Based on an Air Gap Design and an Application to Optical Detection of Humidity," *Anal. Chem.*, vol. 14, no. June, pp. 633–635, 1998.
- [119] T. E. Brook, M. N. Taib, and R. Narayanaswamy, "Extending the range of a fibre-optic relative-humidity sensor," *Sensors Actuators, B Chem.*, vol. 39, no. 1–3, pp. 272–276, 1997.
- [120] B. Kondratowicz, R. Narayanaswamy, and K. C. Persaud, "An investigation into the use of electrochromic polymers in optical fibre gas sensors," *Sensors Actuators, B Chem.*, vol. 74, no. 1–3, pp. 138–144, 2001.
- [121] J. P. Sharkany, S. O. Korposh, Z. I. Batori-Tarci, I. I. Trikur, and J. J. Ramsden, "Bacteriorhodopsin-based biochromic films for chemical sensors," *Sensors Actuators, B Chem.*, vol. 107, no. 1 SPEC. ISS., pp. 77–81, 2005.
- [122] Q. Zhou, M. R. Shahriari, D. Kritz, and G. H. Sigel, "Porous Fiber-Optic Sensor for High-Sensitivity Humidity Measurements," *Anal. Chem.*, vol. 60, no. 20, pp. 2317–2320, 1988.
- [123] S. J. Glenn, B. M. Cullum, R. B. Nair, D. A. Nivens, C. J. Murphy, and S. M. Angel, "Lifetime-based fiber-optic water sensor using a luminescent complex in a lithium-treated NafionTM membrane," *Anal. Chim. Acta*, vol. 448, no. 1–2, pp. 1–8, 2001.
- [124] M. Bedoya, M. T. Díez, M. C. Moreno-Bondi, and G. Orellana, "Humidity sensing with a luminescent Ru(II) complex and phase-sensitive detection," *Sensors Actuators, B Chem.*, vol. 113, no. 2, pp. 573–581, 2006.
- [125] S. Glenn, B. Cullum, R. Nair, D. Nivens, C. Murphy, and S. Angel, "Lifetime-based fiber-optic water sensor using a luminescent complex in a lithium-treated NafionTM membrane," *Anal. Chim. Acta*, vol. 448, no. 1–2, pp. 1–8, 2001.
- [126] R. Jindal, S. Tao, J. P. Singh, and P. S. Gaikwad, "High dynamic range fiber optic relative humidity sensor," *Opt. Eng.*, vol. 41, no. 5, p. 1093, 2002.
- [127] A. Alvarez-Herrero, H. Guerrero, and D. Levy, "High-Sensitivity Sensor of Low Relative Humidity Based on Overlay on Side-Polished Fibers," *IEEE Sens. J.*, vol. 4, no. 1, pp. 52–56, 2004.

- [128] L. Xu, J. C. Fanguy, K. Soni, and S. Tao, "Optical fiber humidity sensor based on evanescent-wave scattering.," *Opt. Lett.*, vol. 29, no. 11, pp. 1191–3, 2004.
- [129] A. Kharaz, B. E. Jones, K. F. Hale, L. Roche, and K. Bromley, "Optical fibre relative humidity sensor using a spectrally absorptive material," vol. 418555, no. November 2000, pp. 370-373 SRC-GoogleScholar FG-0, 2000.
- [130] R. Kashyap, *Fiber Bragg Gratings*, 2nd ed. Academic Press, 2009.
- [131] P. Ferdinand, S. Magne, V. Dewynter-marty, S. Rougeault, and L. Maurin, "Applications of Fiber Bragg Grating Sensors in the Composite Industry," in *The International Union of Materials Research Societies (IUMRS®)*, 2002, pp. 400–407.
- [132] H. Tsuda and K. Urabe, "Characterization of long-period grating refractive index sensors and their applications," *Sensors*, vol. 9, pp. 4559–4571, 2009.
- [133] T. Allsop, A. Gillooly, V. Mezentsev, T. Earthgrowl-Gould, R. Neal, D. J. Webb, and I. Bennion, "Bending and orientational characteristics of long period gratings written in D-shaped optical fiber," *IEEE Trans. Instrum. Meas.*, vol. 53, no. 1, pp. 130–135, 2004.
- [134] "Fibre Bragg Grating (FBG) Sensor Principle." [Online]. Available: <https://www.fbgs.com/technology/fbg-principle/>. [Accessed: 17-Jul-2018].
- [135] P. Kronenberg, P. K. Rastogi, P. Giaccari, and H. G. Limberger, "Relative humidity sensor with optical fiber Bragg gratings," *Opt. Lett.*, vol. 27, no. 16, pp. 1385–1387, 2002.
- [136] W. Kunzler, S. G. Calvert, and M. Laylor, "Measuring humidity and moisture with fiber optic sensors," in *Sixth Pacific Northwest Fiber Optic Sensor Workshop*, 2003, pp. 86–93.
- [137] T. L. Yeo, M. A. C. Cox, L. F. Boswell, T. Sun, and K. . V. Grattan, "Optical fiber sensors for monitoring ingress of moisture in structural concrete," *Rev. Sci. Instrum.*, vol. 77, no. 5, pp. 193–204, 2006.
- [138] S. Luo, Y. Liu, A. Sucheta, M. K. Evans, and R. Van Tassell, "Applications of LPG fiber optical sensors for relative humidity and chemical-warfare-agents monitoring," *Adv. Sens. Syst. Appl.*, vol. 4920, pp. 193–204, 2003.
- [139] K. M. Tan, C. M. Tay, S. C. Tjin, C. C. Chan, and H. Rahardjo, "High relative humidity measurements using gelatin coated long-period grating sensors," *Sensors Actuators, B Chem.*, vol. 110, no. 2, pp. 335–341, 2005.

- [140] M. Konstantaki, S. Pissadakis, S. Pispas, N. Madamopoulos, and N. A. Vainos, "Optical fiber long-period grating humidity sensor with poly(ethylene oxide)/cobalt chloride coating," *Appl. Opt.*, vol. 45, no. 19, pp. 4567–4571, 2006.
- [141] C. Kelb, E. Reithmeier, and B. Roth, "Foil-integrated 2D optical strain sensors," *Procedia Technol.*, vol. 15, pp. 710–715, 2014.
- [142] F. Mitschke, "Fiber-optic sensor for humidity," *Opt. Lett.*, vol. 14, no. 17, pp. 967–9, 1989.
- [143] F. J. Arregui, Y. Liu, I. R. Matias, and R. O. Claus, "Optical fiber humidity sensor using a nano Fabry-Perot cavity formed by the ionic self-assembly method," *Sensors Actuators, B Chem.*, vol. 59, no. 1, pp. 54–59, 1999.
- [144] H. Yu, L. Yao, L. Wang, and D. Hu.W, "Fibre optic humidity sensor based on self-assembled polyelectrolyte multilayers," *J. Wuhan Univ. Technol.*, vol. 16, no. 3, pp. 65–69, 2001.
- [145] Y. Redutskiy, "Conceptualization Conceptualization of of smart smart solutions solutions in in oil oil and and gas gas industry industry," *Procedia Comput. Sci.*, vol. 109, pp. 745–753, 2017.
- [146] T. J. Swait, A. Rauf, R. Grainger, P. B. S. Bailey, A. D. Lafferty, E. J. Fleet, R. J. Hand, and S. A. Hayes, "Smart composite materials for self-sensing and self-healing," *Plast. Rubber Compos.*, vol. 41, no. 4–5, pp. 215–224, 2012.
- [147] A. Kalamkarov, "The use of Smart Composite Materials and Structures and Nano-composites in everyday life," 2016. [Online]. Available: <http://www.isa.unibo.it/en/events/lectures/the-use-of-smart-composite-materials-and-structures-and-nano-composites-in-everyday-life>. [Accessed: 05-Apr-2018].
- [148] HUAWEI, "Smart Pipeline, Effective Communication," 2018. [Online]. Available: <http://e.huawei.com/en/material/onLineView?MaterialID=697c891cc16a48d28046bf1c2dfb3c88>. [Accessed: 02-Aug-2018].
- [149] IDTechEx, "Printed and Flexible Sensors 2017-2027: Technologies, Players, Forecasts," 2018. [Online]. Available: <https://www.idtechex.com/research/reports/printed-and-flexible-sensors-2017-2027-technologies-players-forecasts-000504.asp>. [Accessed: 02-Aug-2018].
- [150] C. UK, "Supporting UK Composites." [Online]. Available: <https://compositesuk.co.uk/communication/news/cristex-partner-saertex-develops-unique-defect-control-system>. [Accessed: 02-Aug-2018].

- [151] “Smart pigs,” 2018. [Online]. Available: <https://smartpigs.net/index.html>.
- [152] Shell, “Predecctive maintenance,” 2018. [Online]. Available: <https://www.shell.com/business-customers/lubricants-for-business/industry-insights.html>. [Accessed: 02-Aug-2018].
- [153] I. Pipelines, “Samart pipelines,” 2018. [Online]. Available: <http://www.i2ipipelines.com/>. [Accessed: 02-Aug-2018].
- [154] “Smart pig cecontamination,” 2018. [Online]. Available: <https://www.bodineservices.com/environmental-contracting/smart-pig-decontamination/>. [Accessed: 02-Aug-2018].
- [155] T. D. Williamson, “Solutions for non.intrusive inline isolation,” 2018. [Online]. Available: <http://www.tdwilliamson.com/>. [Accessed: 02-Aug-2018].
- [156] “Gurit, SP-High.” [Online]. Available: <http://www.gurit.com/Our-Business/Composite-Materials/Other-Products/Laminating-Infusion-Systems/Ampreg-26>. [Accessed: 17-Feb-2017].
- [157] “CS25 Condensation Cure Silicone Rubber.” [Online]. Available: <http://www.easycomposites.co.uk/#!/resin-gel-silicone-adhesive/rtv-silicone-rubber/condensation-cure-mould-making-silicone-rubber-rtv.html>. [Accessed: 09-Apr-2017].
- [158] “ASTM D1141 - 98(2013) Standard Practice for the Preparation of Substitute Ocean Water.” .
- [159] S. . Grammatikos, B. Zafari, M. . Evernden, J. . Mottram, and J. . Mitchels, “Moisture uptake characteristics of a pultruded fibre reinforced polymer flat sheet subjected to hot/wet aging,” *Polym. Degrad. Stab.*, vol. 121, pp. 407–419, Nov. 2015.
- [160] “Fick’s Laws,” *Comsol*, 2015. [Online]. Available: <https://www.comsol.com/multiphysics/diffusion-equation>. [Accessed: 14-Jul-2018].
- [161] M. Montazer, F. Alimohammadi, A. Shamei, and M. Karim, “In situ synthesis of nano silver on cotton using Tollens ’ reagent,” *Carbohydr. Polym.*, vol. 87, no. 2, pp. 1706–1712, 2012.
- [162] P. Dhara, V. K. Singh, M. Olivero, and G. Perrone, “Reflectance-based low-cost disposable optical fiber surface plasmon resonance probe with enhanced biochemical sensitivity,” *Opt. Eng.*, vol. 55, no. 4, p. 046114, Apr. 2016.

- [163] “NoFAST-SC-APC Connector,” 2009. [Online]. Available: <https://www.thorlabs.com/thorproduct.cfm?partnumber=30126J1>. [Accessed: 11-Oct-2017].
- [164] “Lynx CustomFit Splice-On SC Connector datasheet,” 2010. [Online]. Available: <https://www.sumitomoelectric.com/product/lynx2-customfit-splice-on-connectors-sc-lc-fc-and-st-2/>.
- [165] “Avantes.” [Online]. Available: <https://www.avantes.com/products/spectrometers/nirline/item/328-avaspec-nir256-1-7-tec>. [Accessed: 20-Feb-2017].
- [166] A. D3039/D3039M, “Standard Test Method for Tensile Properties of Polymer Matrix Composite Materials.” .
- [167] “ISO 14125,” 1998.
- [168] Y. Li, H. Zhang, E. Bilotti, and T. Peijs, “Optimization of Three-Roll Mill Parameters for In-Situ Exfoliation of Graphene,” *Nanomater. Synth.*, vol. 1, no. 19, pp. 1389–1394, 2016.
- [169] Y. Li, H. Zhang, M. Crespo, H. Porwal, O. Picot, G. Santagiuliana, Z. Huang, E. Barbieri, N. M. Pugno, T. Peijs, and E. Bilotti, “In Situ Exfoliation of Graphene in Epoxy Resins: A Facile Strategy to Efficient and Large Scale Graphene Nanocomposites,” *ACS Appl. Mater. Interfaces*, vol. 8, no. 36, pp. 24112–24122, 2016.
- [170] K. Zakowski, M. Narozny, and M. Szocinski, “Influence of water salinity on corrosion risk — the case of the southern Baltic Sea coast,” *Environ. Monit. Assess*, 2014.
- [171] Y. Liu, H. Zhang, H. Porwal, W. Tu, J. Evans, M. Newton, J. J. C. Busfield, T. Peijs, and E. Bilotti, “Universal Control on Pyroresistive Behavior of Flexible Self-Regulating Heating Devices,” *Adv. Funct. Mater.*, vol. 27, no. 39, pp. 1–9, 2017.
- [172] A. L. Efros and B. I. Shklovskii, “Critical Behaviour of Conductivity and Dielectric Constant near the Metal-Non-Metal Transition Threshold,” *Phys. Status Solidi B.*, vol. 76, pp. 475–485, 1976.
- [173] H. Zhang, Y. Liu, M. Kuwata, E. Bilotti, and T. Peijs, “Improved fracture toughness and integrated damage sensing capability by spray coated CNTs on carbon fibre prepreg,” *Compos. Part A Appl. Sci. Manuf.*, vol. 70, pp. 102–110, 2015.

- [174] L. Boger, M. H. . Wichmann, L. O. Meyer, and K. Schulte, “Load and health monitoring in glass fibre reinforced composites with an electrically conductive nanocomposite epoxy matrix,” *Compos. Sci. Technol.*, vol. 68, pp. 1886–1894, 2008.
- [175] A. Rigail-Cedeño and C. S. P. Sung, “Fluorescence and IR characterization of epoxy cured with aliphatic amines,” *Polymer (Guildf.)*, vol. 46, no. 22, pp. 9378–9384, 2005.
- [176] N. Poisson, G. Lachenal, and H. Sautereau, “Near- and mid-infrared spectroscopy studies of an epoxy reactive system,” *Vib. Spectrosc.*, vol. 12, pp. 237–247, 1996.
- [177] G. Lachenal, A. Pierre, and N. Poisson, “FT-NIR spectroscopy: Trends and application to the kinetic study of epoxy/triamine system (Comparison with DSC and SEC results),” *Micron*, vol. 27, no. 5, pp. 329–334, 1996.
- [178] E. D. W. S.V. Levchik, “Thermal decomposition, combustion and flame-retardancy of epoxy resins – a review of the recent literature,” *Polym. Int.*, vol. 53, pp. 1901–1929, 2004.
- [179] “Polymer data base.” [Online]. Available: <https://polymerdatabase.com/polymers/polybis-adiglycidylether-alt-hexanediamine.html>. [Accessed: 25-Feb-2019].
- [180] D. Grogan, M. Flanagan, M. Walls, S. Leen, A. Doyle, N. Harrison, D. Mamalis, and J. Goggins, “Influence of microstructural defects and hydrostatic pressure on water absorption in composite materials for tidal energy,” *J. Compos. Mater.*, vol. 52, no. 21, pp. 2899–2917, Sep. 2018.
- [181] D. Choqueuse and P. Davies, “Ageing of composites in underwater applications,” *Ageing Compos.*, pp. 467–498, Jan. 2008.
- [182] P.-Y. Le Gac, P. Davies, and D. Choqueuse, “Evaluation of Long Term Behaviour of Polymers for Offshore Oil and Gas Applications,” *Oil Gas Sci. Technol. – Rev. d’IFP Energies Nouv.*, vol. 70, no. 2, pp. 279–289, Jun. 2015.
- [183] V. Guadagno, L; Vertuccio, L; Sorrentino, A; Raimondo, M; Naddeo, C; Vittoria, “Mechanical and barrier properties of epoxy resin filled with multiwalled carbon nanotubes,” *Carbon N. Y.*, vol. 47, pp. 2419–2430, 2009.
- [184] S. G. Prolongo, M. R. Gude, and A. Ureña, “Water uptake of epoxy composites reinforced with carbon nanofillers,” *Compos. Part A Appl. Sci. Manuf.*, vol. 43, no. 12, pp. 2169–2175, 2012.
- [185] D. A. Powers, “Interaction of Water with Epoxy,” vol. 91, no. 12. Sandia Corporation, Albuquerque, New Mexico, pp. 1805–1811, 1995.

- [186] V. Freger, E. Korin, J. Wisniak, E. Korngold, M. Ise, and K. D. Kreuer, "Diffusion of water and ethanol in ion-exchange membranes: limits of the geometric approach," *J. Memb. Sci.*, vol. 160, no. 2, pp. 213–224, Jul. 1999.
- [187] M. Shen, S. Keten, and R. M. Lueptow, "Dynamics of water and solute transport in polymeric reverse osmosis membranes via molecular dynamics simulations," *J. Memb. Sci.*, vol. 506, pp. 95–108, 2016.
- [188] C. Dennis R. Turner and N. J. Township, Morris County, "Etch procedure for optical fibres," 4.469.554, 1984.
- [189] H. H. Schroeder and A. F. Turner, "Mirror Coatings for Low Visible and High Infrared Reflectance," *J. Opt. Soc. Am.*, vol. 228, no. January, pp. 31–35, 1956.
- [190] M.-L. Anne, J. Keirsse, V. Nazabal, K. Hyodo, S. Inoue, C. Boussard-Plédel, H. Lhermite, J. Charrier, K. Yanakata, O. Loreal, J. Le Person, F. Colas, C. Compère, and B. Bureau, "Chalcogenide Glass Optical Waveguides for Infrared Biosensing," *Sensors*, vol. 9, pp. 7398–7411, 2009.
- [191] S. Burikov, T. Dolenko, S. Patsaeva, Y. Starokurov, and V. Yuzhakov, "Raman and IR spectroscopy research on hydrogen bonding in water – ethanol systems," *Mol. Phys.*, vol. 108, no. 18, pp. 2427–2436, 2010.
- [192] D. Le Coq, K. Michel, J. Keirsse, C. Boussard-Plédel, G. Fontenau, B. Bureau, J. M. Le Quere, O. Sire, and J. Lucas, "Infrared glass fibers for in-situ sensing, chemical and biochemical reactions," *Comptes Rendus Chim.*, vol. 5, no. 12, pp. 907–913, 2002.
- [193] "United States Department of Transportation." [Online]. Available: <https://www.phmsa.dot.gov/hazmat-program-management-data-and-statistics/data-operations/incident-statistics>. [Accessed: 05-Feb-2018].
- [194] "Pipeline Incident 20-Years Trend." [Online]. Available: <https://hip.phmsa.dot.gov/analyticsSOAP/saw.dll?Portalpages>. [Accessed: 08-Jan-2018].
- [195] M. Salvo, M. Sangermano, C. Marro Bellot, and M. Olivero, "Optical sensor, process for making such sensor and evaluation system comprising at least one of such sensors," Application number 102017000053268, 2017.